

UNIVERSITY OF OKLAHOMA

GRADUATE COLLEGE

ELECTROCHEMICAL CHARACTERIZATION OF PHOTOCURABLE AND  
LAYER-BY-LAYER ASSEMBLED FERROCENE-MODIFIED LINEAR  
POLY(ETHYLENIMINE) BIOELECTRODES

A DISSERTATION

SUBMITTED TO THE GRADUATE FACULTY

in partial fulfillment of the requirements for the

Degree of

DOCTOR OF PHILOSOPHY

By

NICHOLAS PAUL GODMAN

Norman, Oklahoma

2015

ELECTROCHEMICAL CHARACTERIZATION OF PHOTOCURABLE AND  
LAYER-BY-LAYER ASSEMBLED FERROCENE-MODIFIED LINEAR  
POLY(ETHYLENIMINE) BIOELECTRODES

A DISSERTATION APPROVED FOR THE  
DEPARTMENT OF CHEMISTRY AND BIOCHEMISTRY

BY

---

Dr. Daniel Glatzhofer, Chair

---

Dr. Kenneth Nicholas

---

Dr. Wai Tak Yip

---

Dr. Robert Thomson

---

Dr. Stephen Crossley

© Copyright by NICHOLAS P. GODMAN 2015  
All Rights Reserved.

## **Acknowledgements**

First and foremost, I need to thank my wonderful wife Lindsay for being there for me throughout the last five years. She keeps me grounded and focused on what is truly important in life, and I am eternally grateful for her love and support. I also need to thank my parents for their supportive encouragement throughout this stage of life, and their love never ceases to amaze me.

I also feel it is necessary to thank all of the wonderful people I have met at McFarlin United Methodist Church. Being a Student Ministries Intern for the better part of two years helped to balance the stress of graduate school by reminding me that there is life beyond the lab bench. I am also proud to have been a part of the Young Adult Ministries and serve beside some wonderful, life-loving people. McFarlin has been a place for me to grow and mature, and I will always treasure the time I got to spend there.

I want to thank the members of my committee: Dr. Glatzhofer, Dr. Nicholas, Dr. Yip, Dr. Thomson, and Dr. Crossley. I would also like to thank Dr. Schmidtke for his valuable advice over the years as our groups have collaborated on various projects. Finally, I want to thank all the members of the Glatzhofer and Schmidtke labs who put up with me and helped me to grow as a scientist: Dr. Matt Czaplá, Dr. Rahul Kadam, Dr. Sachin Chavan, Dr. Anna J, Dr. Farid Ismail, Dr. David Hickey, Dr. Jie Chen, Dan Bamper, Abby Halmes, Matt Houck, Robin Christensen, Logan Branscum, and Jared DeLuca.

# Table of Contents

Acknowledgements .....	iv
List of Tables .....	ix
List of Figures.....	x
Chapter 1. Introduction and Background.....	1
1.1 General Introduction to Enzymatic Biosensors and Biofuel Cells.....	1
1.2 Redox Mediators and Enzyme Immobilization.....	4
1.2.1 Methods of Signal Transduction .....	4
1.2.2 Enzyme Immobilization Techniques .....	9
1.3 Fabrication Methods.....	12
1.3.1 Introduction to Photolithography .....	12
1.3.2 Layer-by-Layer Assembly.....	16
1.4 Project Goals and Background.....	20
1.4.1 Bioelectrode Fabrication Methods .....	20
1.4.2 Sulfur: Thermal Properties and Inverse Vulcanization .....	26
1.5 References .....	29
Chapter 2. Photocurable Redox Polymers Based on Ferrocene-Modified Linear Poly(ethylenimine) .....	36
2.1 Introduction .....	36
2.2 Results and Discussion.....	38
2.2.1 Development of the Synthetic Methodology for Redox-Active Photoresists.....	38
2.2.2 Proposed Mechanisms of Fc-C <sub>3</sub> -LP AEI Crosslinking .....	43

2.2.3	Cyclic Voltammetric Studies of Photochemically Crosslinked Films ...	45
2.2.4	Effect of Photochemical Crosslinking on Electron Diffusion .....	51
2.2.5	Enzymatic Properties of Photochemically Generated Biosensors.....	54
2.2.6	Effect of Photochemical Crosslinking on Biosensor Efficiency .....	56
2.2.7	Optimization of 25% TEG-N <sub>3</sub> Containing Films .....	60
2.2.8	Literature Comparison .....	62
2.3	Conclusions .....	65
2.4	Experimental.....	66
2.5	References .....	68
Chapter 3. Electrochemical Characterization of Layer-By-Layer Assembled		
	Ferrocene-Modified Linear Poly(ethylenimine)/Enzyme Composites for	
	Biosensor and Biofuel Cell Applications .....	72
3.1	Introduction .....	72
3.2	Results and Discussion .....	74
3.2.1	LBL Assembly of Films .....	76
3.2.2	Electrochemical Response of LBL Assembled Bioanodes .....	77
3.2.3	Electrochemical Stability of LBL Assembled Biosensors .....	86
3.2.4	Enzymatic Response of LBL Assembled Biosensors .....	89
3.2.5	Performance of LBL Assembled Anodes in a Biofuel Cell .....	95
3.3	Methylated Ferrocene Polymers and Preliminary Nanotube Incorporation.	99
3.3.1	Single Walled Nanotube Modified Glassy Carbon Electrodes .....	100
3.3.2	Effect of Methylation of LBL Assembled Bioanodes .....	102
3.4	Conclusion.....	104

3.5	Experimental.....	106
3.6	References .....	107
Chapter 4. Development and Characterization of Layer-By-Layer Assembled		
	Chloroferrocene-Modified Poly(ethylenimine)/Laccase Biocathodes .....	111
4.1	Introduction .....	111
4.2	Results and Discussion .....	113
4.2.1	LBL assembly of Films .....	113
4.2.2	Planar Gold Electrodes: Optimization of Fabrication Parameters.....	114
4.2.3	Planar Gold Electrodes: Electrochemical Characterization .....	119
4.2.4	Planar Gold Electrodes: Enzymatic Response .....	126
4.2.5	Carbon Paper Electrodes: Optimization of Fabrication Parameters.....	127
<b>4.2.6</b>	<b>Carbon Paper Electrodes: Electrochemically Active Surface Area .....</b>	<b>132</b>
4.2.7	Carbon Paper Electrodes: Electrochemical Characterization.....	136
4.2.8	Carbon Paper Electrodes: Enzymatic Response.....	141
4.2.9	LBL Assembled Biocathode Literature Comparison .....	142
4.3	Conclusions .....	144
4.4	Experimental.....	145
4.5	References .....	146
Chapter 5. Calorimetric Analysis of Sulfur/Paracyclophane Copolymerization ...		
5.1	Introduction .....	150
5.2	Results and Discussion .....	152
5.2.1	Thermal Analysis of Equal Mass Mixtures .....	152
5.2.2	Variable Sulfur Content Materials.....	155

5.2.3	Polymerization Scale-Up.....	156
5.2.4	Dichloroparacyclophane Incorporation .....	162
5.3	Conclusions .....	166
5.4	Experimental.....	167
5.5	References .....	168
Chapter 6.	Conclusions and Future Directions .....	171
6.1	Conclusions .....	171
6.2	Future Directions .....	174
Chapter 7.	Appendices .....	176
7.1	NMR Data .....	176
7.2	DSC Thermograms .....	184



## List of Tables

Table 2.2.1: Literature summary of photochemically generated glucose biosensors.....	64
Table 3.2.1: Effect of Fc-C <sub>n</sub> -LPEI biosensor fabrication method on electrochemical and enzymatic response.....	92
Table 3.2.2: Comparison of glucose/oxygen biofuel cells fabricated using LBL assembly .....	98
Table 4.2.1: Concentration dependence of $\Gamma_{\text{FcCl}}$ (nmol/cm <sup>2</sup> ) for (FcCl-C <sub>3</sub> -LPEI/laccase) <sub>4</sub> . 50 mM citrate buffer, pH 4.5.....	115
Table 4.2.2: Concentration dependence of $J_{\text{max}}$ (μA/cm <sup>2</sup> ) for (FcCl-C <sub>3</sub> -LPEI/laccase) <sub>4</sub> . 50mM citrate buffer, pH 4.5.....	117
Table 4.2.3: Summary of electrochemical data for (FcCl-C <sub>3</sub> -LPEI/laccase) <sub>4</sub> films constructed on various electrode materials. 50 mM citrate buffer, pH 4.5 .....	130
Table 4.2.4: Summary of calculated EASA and electrochemical measurements for various carbon electrodes. ....	134
Table 4.2.5: Summary of electrochemical and enzymatic data taking EASA into account .....	135
Table 4.2.6: Literature summary of LBL assembled oxygen biosensors .....	143
Table 5.2.1: Summary of physical characteristics for S:PCP with increasing amounts of PCP .....	156
Table 5.2.2: Summary of the physical characteristics of 1:1 (mol) S:PCP at increasing amounts of time at 300 °C. ....	157

## List of Figures

Figure 1.1.1 Graphical example of an oxidoreductase catalytic cycle: blue circle = electron donor, green octagon = electron acceptor, grey cloud = oxidoreductase. ....	1
Figure 1.2.1 Schematic representations of the different generations of biosensors: A) first, B) second, and C) third generation. ....	5
Figure 1.2.2 Reaction scheme of the oxidation of glucose using FAD in the active site of glucose oxidase. ....	7
Figure 1.2.3 Second generation redox polymer based on organoosmium modified poly(vinylpyridine) used by Heller in the mediation of glucose oxidase. ....	8
Figure 1.2.4 Generic representation of the four main types of enzyme immobilization: A) adsorption, B) covalent binding, C) membrane confinement, and D) polymer entrapment. ....	9
Figure 1.3.1 Simplified procedure for the production and development of photocurable materials. ....	13
Figure 1.3.2 Reaction scheme of both exposed and masked portions of Novolac photoresist. Where R is another unit containing a diazoketone. ....	14
Figure 1.3.3 Examples of common reactions used to photocrosslink negative photoresists: A) [2+2] cycloaddition, B) acid catalyzed epoxide opening, C) nitrene addition to alkenes. ....	15
Figure 1.3.4 Generic scheme for the layer-by-layer adsorption of polyelectrolytes onto a charged surface. ....	17
Figure 1.3.5 Successive adsorption of charged enzymes and polyelectrolyte on a surface modified electrode. ....	19

Figure 1.4.1 Proposed reaction scheme for the crosslinking of Fc-C <sub>n</sub> -LPEI with EGDGE to form a water insoluble hydrogel. Ferrocene mediator omitted from product for clarity.....	21
Figure 1.4.2 One possible mechanism for the radical crosslinking of allylated LPEI. Radical shown only at secondary carbon, but some portion of the primary radical may react as well. ....	22
Figure 1.4.3 Covalent layer-by-layer assembly process between Fc-C <sub>6</sub> -LPEI and p-GOX as proposed by DeLuca et al. <sup>105</sup> .....	25
Figure 1.4.4 DSC thermogram for elemental sulfur.....	27
Figure 1.4.5 Inverse vulcanization of sulfur using 1,3-diisopropenylbenzene as proposed by the Pyun group.....	28
Figure 1.4.6 Desired sulfur/paracyclophane polymer. R= H, Cl.....	28
Figure 2.2.1: Synthetic route and structure of LPCEI.....	39
Figure 2.2.2: Summary of synthetic routes of LPAEI and Fc-C <sub>3</sub> -LPAEI.....	40
Figure 2.2.3: Molecular structures of V50 (1) and TEG-N <sub>3</sub> (2).....	43
Figure 2.2.4: Proposed mechanisms for the crosslinking of LPAEI: (A) radical coupling, and (B) aziridine formation. ....	44
Figure 2.2.5: Possible products resulting from the photolysis of TEG-N <sub>3</sub> : desired dinitrene (3) and undesired diimine (4).....	44
Figure 2.2.6: Effect of irradiation time and crosslinking agent on the anodic peak current ( <i>i<sub>pa</sub></i> ) of Fc-C <sub>3</sub> -LPAEI/GOX films. ....	46
Figure 2.2.7: Representative CVs for Fc-C <sub>3</sub> -LPAEI/GOX control films fabricated without an added crosslinking agent. PBS pH 7.4. Scan rate = 50 mV/s.....	47

Figure 2.2.8: Representative CVs for Fc-C <sub>3</sub> -LPAEI/GOX films fabricated with radical initiator V50: (A) 10 mol% (B) 25 mol%. PBS pH 7.4. Scan rate = 50 mV/s.....	49
Figure 2.2.9: Representative CVs for Fc-C <sub>3</sub> -LPAEI/GOX films fabricated with diazide crosslinker TEG-N <sub>3</sub> : (A) 10 mol% (B) 25 mol%. PBS pH 7.4. Scan rate = 50 mV/s. ..	50
Figure 2.2.10: Representative CVs for Fc-C <sub>3</sub> -LPAEI/GOX films fabricated with diazide crosslinker 35 mol% TEG-N <sub>3</sub> . PBS pH 7.4. Scan rate = 50 mV/s. ....	50
Figure 2.2.11: Effect of irradiation time and radical crosslinking agent V50 on $cD_e^{1/2}$ for Fc-C <sub>3</sub> -LPAEI/GOX films. ....	52
Figure 2.2.12: Effect of irradiation time and a quantity of diazide crosslinker TEG-N <sub>3</sub> on $cD_e^{1/2}$ for Fc-C <sub>3</sub> -LPAEI/GOX films. ....	53
Figure 2.2.13: (A) Effect of irradiation time and crosslinking agent on the catalytic current density ( $J_{max}$ ) in response to glucose for Fc-C <sub>3</sub> -LPAEI/GOX films. (B) Example Michael-Menten curve for 25% TEG-N <sub>3</sub> at three hours irradiation. PBS pH 7.4.....	54
Figure 2.2.14: Effect of irradiation time and crosslinking agent on the apparent Michaelis constant ( $K_M^*$ ) in response to glucose for Fc-C <sub>3</sub> -LPAEI/GOX films. ....	58
Figure 2.2.15: Effect of irradiation time on the anodic peak current ( $i_{pa}$ ) of Fc-C <sub>3</sub> -LPAEI/GOX films fabricated with 25 mol% TEG-N <sub>3</sub> .....	60
Figure 2.2.16: Effect of irradiation time on the (A) catalytic current density ( $J_{max}$ ) and (B) the apparent Michaelis constant ( $K_M^*$ ) in response to glucose for Fc-C <sub>3</sub> -LPAEI/GOX films fabricated with 25 mol% TEG-N <sub>3</sub> . PBS pH 7.4.....	62
Figure 3.2.1: Synthetic scheme for Fc-C <sub>6</sub> -LPEI and Fc-C <sub>3</sub> -LPEI.....	76
Figure 3.2.2: Periodate modification of glucose oxidase and presumed attachment to Fc-C <sub>n</sub> -LPEI. Ferrocene omitted in final structure for clarity. ....	77

Figure 3.2.3: Representative CVs for (Fc-C<sub>n</sub>-LPEI/p-GOX)<sub>x</sub> films assembled with increasing numbers of bilayers (x = 1, 2, 4, 8, 12, 16) and the long wash method. A) Fc-C<sub>6</sub>-LPEI. B) Fc-C<sub>3</sub>-LPEI. 50 mM phosphate buffer, pH 7.0. Scan rate = 50 mV/s. .... 79

Figure 3.2.4: Representative CVs for (Fc-C<sub>n</sub>-LPEI/p-GOX)<sub>x</sub> films assembled with increasing numbers of bilayers (x = 1, 2, 4, 8, 12, 16) and the short wash method. A) Fc-C<sub>6</sub>-LPEI. B) Fc-C<sub>3</sub>-LPEI. 50 mM phosphate buffer, pH 7.0. Scan rate = 50 mV/s. .... 80

Figure 3.2.5: (A) Plot of ferrocene surface coverage ( $\Gamma_{Fc}$ ), obtained by integration of the anodic wave of the cyclic voltammogram, against the number of assembled bilayers. Fc-C<sub>3</sub>-LPEI, short wash (black triangle). Fc-C<sub>3</sub>-LPEI, long wash (black circle). Fc-C<sub>6</sub>-LPEI, short wash (white triangle). Fc-C<sub>6</sub>-LPEI, long wash (white circle). (B) Simplified layer-by-layer deposition of enzymes with a polyelectrolyte..... 81

Figure 3.2.6: Plot of ferrocene surface coverage ( $\Gamma_{Fc}$ ), obtained by integration of the anodic wave of the CV, against the potential separation between the anodic and cathodic peaks ( $\Delta E$ ) of the CV. (A) Comparison of long wash (white circle) and the short wash (black circle) fabrication for Fc-C<sub>3</sub>-LPEI/p-GOX films. (B) Comparison of long wash (white triangle) and the short wash (black triangle) fabrication for Fc-C<sub>6</sub>-LPEI/p-GOX films. .... 83

Figure 3.2.7: Plot of the changes in charge for LBL assembled (Fc-C<sub>n</sub>-LPEI/p-GOX)<sub>12</sub> films obtained by cycling the applied potential between 0.0 and 0.5 V vs SCE. Scan rate = 50 mV/s. 50 mM phosphate buffer (pH 7.0, T = 25 °C). .... 87

Figure 3.2.8: Plot of the changes in charge for LBL assembled (Fc-C<sub>3</sub>-LPEI/p-GOX)<sub>x</sub> films obtained by cycling the applied potential between 0.0 and 0.5 V vs SCE in 50 mM phosphate buffer (pH 7.0, T = 25 °C). .... 87

Figure 3.2.9: Plot of the changes in charge for LBL assembled (Fc-C<sub>3</sub>-LPEI/p-GOX)<sub>x</sub> films after acrolein vapor deposition. Obtained by cycling the applied potential between 0.0 and 0.5 V vs SCE in 50 mM phosphate buffer (pH 7.0, T = 25 °C). ..... 89

Figure 3.2.10: Effect of mediator tether length on glucose response for (Fc-C<sub>n</sub>-LPEI/p-GOX)<sub>x</sub> films assembled with increasing number of bilayers (x = 1, 2, 4, 8, 12, 16) and the long wash method. A) Fc-C<sub>6</sub>-LPEI. B) Fc-C<sub>3</sub>-LPEI. .... 90

Figure 3.2.11: Effect of mediator tether length on glucose response for (Fc-C<sub>n</sub>-LPEI/p-GOX)<sub>x</sub> films assembled with increasing number of bilayers (x = 1, 2, 4, 8, 12, 16) and the short wash method. A) Fc-C<sub>6</sub>-LPEI. B) Fc-C<sub>3</sub>-LPEI..... 91

Figure 3.2.12: Plot of biosensor sensitivity at 5 mM glucose against the number of assembled bilayers. Fc-C<sub>3</sub>-LPEI, short wash (black triangle). Fc-C<sub>3</sub>-LPEI, long wash (black circle). Fc-C<sub>6</sub>-LPEI, short wash (white triangle). Fc-C<sub>6</sub>-LPEI, long wash (white circle). ..... 93

Figure 3.2.13: Effect of mediator tether length and fabrication wash time on K<sub>M</sub><sup>\*</sup> for Fc-C<sub>n</sub>-LPEI/p-GOX films assembled with increasing number of bilayers (1, 2, 4, 8, 12, 16). Fc-C<sub>6</sub>-LPEI, long wash (light gray). Fc-C<sub>6</sub>-LPEI, short wash (dark gray). Fc-C<sub>3</sub>-LPEI, long wash (white). Fc-C<sub>3</sub>-LPEI, short wash (black)..... 95

Figure 3.2.14: Effect of electrolyte pH on (Fc-C<sub>3</sub>-LPEI/p-GOX)<sub>8</sub> bioanode performance: pH 7.0 (solid), pH 5.0 (dotted). (A) Representative power curves obtained by poisoning the potential against an air-breathing Pt cathode. Scan rate = 2 mVs<sup>-1</sup>. (B) Constant potential, steady state glucose calibration curves. E = 0.35 V. .... 97

Figure 3.3.1: Representative CVs for (Fc-C <sub>3</sub> -LPEI/p-GOX) <sub>1</sub> films assembled using the short wash method on both planar gold electrodes and SWNT-GCEs. Inset graph depicts the CV for gold electrodes to more accurately depict shape.....	101
Figure 3.3.2: Constant amperometry glucose response curves for (Fc-C <sub>3</sub> -LPEI/p-GOX) <sub>1</sub> films assembled using the short wash method on both planar gold electrodes and SWNT-GCEs. Inset graph depicts the results for gold electrodes to more accurately depict response. ....	102
Figure 3.3.3: Representative CVs for (Fc-C <sub>3</sub> -LPEI/p-GOX) <sub>1</sub> , (FcMe <sub>2</sub> -C <sub>3</sub> -LPEI/p-GOX) <sub>1</sub> , and (FcMe <sub>4</sub> -C <sub>3</sub> -LPEI/p-GOX) <sub>1</sub> films assembled using the short wash method on SWNT-GCEs. ....	103
Figure 3.3.4: Constant amperometry glucose response curves for (Fc-C <sub>3</sub> -LPEI/p-GOX) <sub>1</sub> , (FcMe <sub>2</sub> -C <sub>3</sub> -LPEI/p-GOX) <sub>1</sub> , and (FcMe <sub>4</sub> -C <sub>3</sub> -LPEI/p-GOX) <sub>1</sub> films assembled using the short wash method on SWNT-GCEs.....	104
Figure 4.1.1: Synthesis of FcCl-C <sub>3</sub> -LPEI.....	112
Figure 4.1.2: Schematic representation of a glucose/oxygen biofuel cell using tetramethylferrocene at the anode and chloroferrocene at the cathode .....	113
Figure 4.2.1: Representative amperometric response curve by (FcCl-C <sub>3</sub> -LPEI/laccase) <sub>4</sub> films to air after first purging the solution with nitrogen. ....	116
Figure 4.2.2: Redox polymer fabrication solution pH dependence of A) $\Gamma_{\text{FcCl}}$ and B) $J_{\text{max}}$ for (FcCl-C <sub>3</sub> -LPEI/laccase) <sub>4</sub> . Electrochemical experiments run in 50 mM citrate buffer, pH 4.5. ....	118
Figure 4.2.3: Representative CVs for (FcCl-C <sub>3</sub> -LPEI/laccase) <sub>x</sub> films assembled on planar gold electrodes with increasing numbers of bilayers. ....	119

Figure 4.2.4: Relationship between half wave potential ( $E_{1/2}$ ) and the peak separation ( $\Delta E$ ) for (FcCl-C <sub>3</sub> -LPEI/laccase) <sub>x</sub> films assembled on planar gold electrodes. ....	120
Figure 4.2.5: Plots of ferrocene surface coverage ( $\Gamma_{Fc}$ ) and chloroferrocene surface coverage ( $\Gamma_{FcCl}$ ), obtained by integration of the anodic wave of the cyclic voltammogram, against the number of assembled bilayers.....	122
Figure 4.2.6: Plot of chloroferrocene surface coverage ( $\Gamma_{FcCl}$ ), obtained by integration of the anodic wave of the CV, against the potential separation between the anodic and cathodic peaks ( $\Delta E$ ) of the CV for (FcCl-C <sub>3</sub> -LPEI/laccase) <sub>x</sub> films.....	125
Figure 4.2.7: Plot of the effect of FcCl-C <sub>3</sub> -LPEI/laccase bilayers on maximum catalytic current density ( $J_{max}$ ) for films assembled on planar gold electrodes.....	126
Figure 4.2.8: Representative CVs of (FcCl-C <sub>3</sub> -LPEI/laccase) <sub>4</sub> films constructed on various electrode materials. ....	128
Figure 4.2.9: Effect of electrode material on maximum current ( $I_{max}$ ) for (FcCl-C <sub>3</sub> -LPEI/laccase) <sub>4</sub> films .....	131
Figure 4.2.10: Representative CVs of compound 1 (5 mM) obtained using various carbon electrodes. PBS pH 7.4. Scan rate = 50 mV/s. ....	134
Figure 4.2.11: Representative CVs for (FcCl-C <sub>3</sub> -LPEI/laccase) <sub>x</sub> films assembled on planar gold electrodes with increasing numbers of bilayers. ....	136
Figure 4.2.12: Relationship between half wave potential ( $E_{1/2}$ ) and the peak separation ( $\Delta E$ ) for (FcCl-C <sub>3</sub> -LPEI/laccase) <sub>x</sub> films assembled on nitric acid oxidized carbon paper electrodes. ....	137
Figure 4.2.13: Plot of relative electron diffusion coefficient ( $cDe_{1/2}$ ) as a function of FcCl-C <sub>3</sub> -LPEI/laccase bilayers. ....	139



Figure 4.2.14: Relationship between chloroferrocene surface coverage ( $\Gamma_{\text{FcCl}}$ ) and the number of FcCl-C <sub>3</sub> -LPEI/laccase bilayers for films assembled on both gold and nitric acid oxidized carbon paper electrodes.....	140
Figure 4.2.15: Relationship between moles of chloroferrocene and the number of FcCl-C <sub>3</sub> -LPEI/laccase bilayers for films assembled on both gold and nitric acid oxidized carbon .....	140
Figure 4.2.16: Plot of the effect of FcCl-C <sub>3</sub> -LPEI/laccase bilayers on maximum catalytic current density ( $J_{\text{max}}$ ) for films assembled on both planar gold electrodes and nitric acid oxidized carbon paper electrodes. ....	142
Figure 5.1.1: Thermal ring opening and subsequent polymerization of sulfur .....	150
Figure 5.1.2: Proposed copolymerization scheme between sulfur and paracyclophane. ....	151
Figure 5.2.1: Overlaid DSC thermograms for sulfur and paracyclophane.....	152
Figure 5.2.2: Overlaid DSC thermograms for 1:1 (weight) S:PCP, i.e. 13.3 mol% PCP, both the first run and the reheat seven days later .....	153
Figure 5.2.3: (A) Overlaid DSC thermograms for S:PCP and (B) plot of exothermic peak temperatures with relation to increasing mole percentage of PCP .....	155
Figure 5.2.4: S-PCP-50 before and after heating at 300 °C for 90 minutes .....	158
Figure 5.2.5: Thermal decomposition of dibenzyl sulfide into stilbene and conversion of stilbene into tetraphenylthiophene.....	158
Figure 5.2.6: Proposed crosslinking of poly(p-xylylene) in the presence of excess sulfur. ....	159
Figure 5.2.7: Visual depiction of S-PCP-50 with continued heating on a hot plate.....	160

Figure 5.2.8: S-PCP-50 pellet after two hours heating at 300 °C in stainless steel die: (A) before and (B) after extraction with carbon disulfide.....	161
Figure 5.2.9: S-PCP-50 heated at 300 °C furnace for five hours. Top: die immediately after removal from furnace. Bottom: foamed material remaining inside the die. ....	162
Figure 5.2.10: DSC thermogram for dichloroparacyclophane. ....	163
Figure 5.2.11: Overlaid DSC thermograms for S-PCPCl <sub>2</sub> at 13.3 and 50 mol% PCPCl <sub>2</sub> . .....	164
Figure 5.2.12: S-PCPCl <sub>2</sub> -50 after heating at 300 °C for two hours. (A) Immediately after removal from furnace and (B) after cooling to room temperature .....	164
Figure 5.2.13: <sup>1</sup> H-NMR spectrum (top) and <sup>1</sup> H- <sup>13</sup> C HSQC spectrum (bottom) for S- PCPCl <sub>2</sub> -50.....	165
Figure 7.1.1: LPCEI .....	176
Figure 7.1.2: LPAEI .....	177
Figure 7.1.3: Fc-C <sub>3</sub> -LPAEI.....	178
Figure 7.1.4: Fc-C <sub>3</sub> -LPEI .....	179
Figure 7.1.5: Fc-C <sub>6</sub> -LPEI .....	180
Figure 7.1.6: FcCl-C <sub>3</sub> -LPEI.....	181
Figure 7.1.7: S-PCPCl <sub>2</sub> -50 after two hours heating at 300 °C.....	182
Figure 7.1.8: HSQC S-PCPCl <sub>2</sub> -50 after two hours heating at 300 °C.....	183

## Abstract

New methods of constructing enzymatic bioelectrodes based on ferrocene-modified linear poly(ethylenimine) (LPEI) were explored with the intent of lowering device fabrication times. Redox polymers were synthesized and characterized for usage as both anode and cathode materials.

Photolithography was used to form patterned films based on ferrocenylpropyl-modified linear poly(ethylenimine-co-allylethylenimine) (Fc-C<sub>3</sub>-LPAEI). Fc-C<sub>3</sub>-LPAEI (50% allylated, 5% ferrocene) films were crosslinked in the presence of glucose oxidase (GOX) using both photogenerated radicals and nitrenes. Biosensor efficiency was found to be a function of both polymer connectivity and enzyme stability. Fc-C<sub>3</sub>-LPAEI/GOX bioanodes were capable of generating  $44.9 \pm 1.3 \mu\text{Acm}^{-2}$  after five hours irradiation using a photogenerated dinitrene from 1,2-bis(2-azidoethoxy)ethane.

Both electrostatic and covalent layer-by-layer assembly were used for the fabrication of polymer/enzyme composite thin films. Ferrocenylhexyl- and ferrocenylpropyl- modified LPEI (Fc-C<sub>6</sub>-LPEI, Fc-C<sub>3</sub>-LPEI, 17-20% ferrocene) were used with periodate modified glucose oxidase (p-GOX) for the construction of enzymatic bioanodes capable of generating up to  $381 \pm 3$  and  $1417 \pm 63 \mu\text{Acm}^{-2}$ , respectively. Fc-C<sub>3</sub>-LPEI/p-GOX biofuel cells generated  $86 \pm 3 \mu\text{Wcm}^{-2}$  at pH 7 when poised against an air-breathing Pt cathode. A chloroferrocene-modified redox polymer (FcCl-C<sub>3</sub>-LPEI, 17-20% chloroferrocene) was assembled with laccase to construct biocathodes capable of generating up to  $5.75 \pm 0.14 \mu\text{Acm}^{-2}$  on planar gold electrodes and  $32.3 \pm 3.2 \mu\text{Acm}^{-2}$  on nitric acid oxidized carbon paper.

Lastly, sulfur and paracyclophane derivatives were copolymerized via inverse vulcanization to afford materials with the possibility of being incorporated in lithium-sulfur batteries. Differential scanning calorimetry was used to monitor the exothermic polymerization between the reactants, and the reaction parameters were optimized by varying the ratios of the starting materials.

# Chapter 1. Introduction and Background

## 1.1 General Introduction to Enzymatic Biosensors and Biofuel Cells

Enzymes are protein macromolecules that catalyze a specific biochemical reaction. These proteins are produced by living organisms and the key catalytic portion of the cell can often be extracted, isolated, and purified. While there are a whole host of enzyme types, the class known as oxidoreductases are unique in that they catalyze the transfer of electrons from one molecule (reductant) to another (oxidant).<sup>1</sup> A simple illustration of the electron transfer process is shown in **Figure 1.1.1**. First, an enzyme specific substrate (blue circle) transfers electrons to the enzyme (grey cloud) to create an oxidized product and the reduced form of the enzyme. Next, an electron accepting cosubstrate (green octagon) receives electrons from the reduced enzyme to form a reduced product and regenerate the active form of the enzyme. The opposite reaction—reduction followed by oxidation—is also possible depending on the enzyme used.

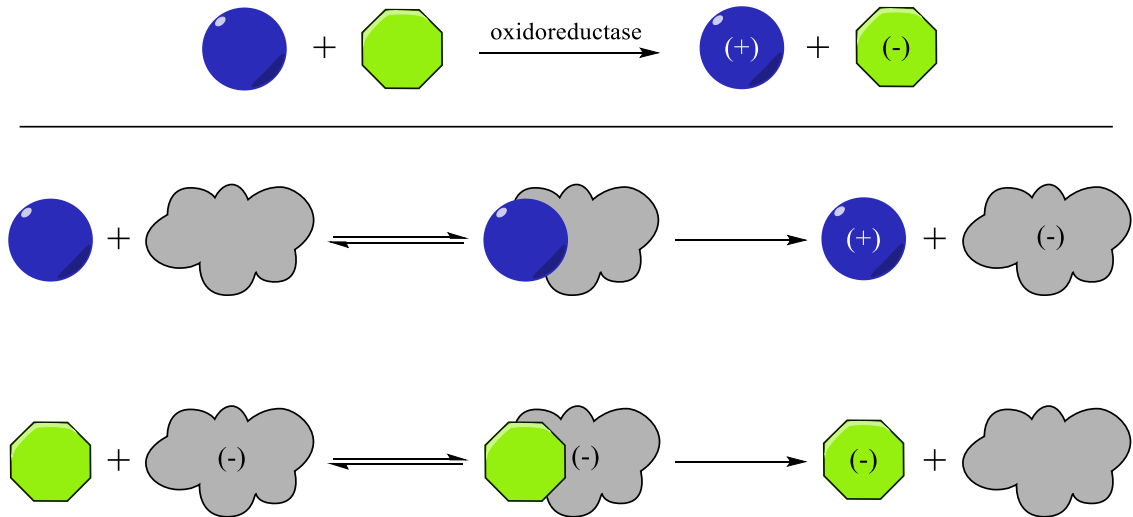


**Figure 1.1.1** Graphical example of an oxidoreductase catalytic cycle: blue circle = electron donor, green octagon = electron acceptor, grey cloud = oxidoreductase.

By understanding the redox chemistry involved with a particular enzyme, it is possible to harness electrons from these reactions. This can be done by choosing an electroactive compound with an electrochemical potential similar to that at which the enzyme naturally operates. This external electron mediator can take the place of either the electron acceptor or donor, as described above, which makes it possible to electrochemically measure the enzymatic process. Two applications of redox enzymes that have garnered a lot of attention in recent years are enzymatic biosensors and biofuel cells. The *Encyclopedia of Microfluidics and Nanofluidics*, published by Springer, defines these terms: “A biosensor is a device for the detection of an analyte that combines a biological component with a physicochemical detector component,<sup>2</sup>” and “A biofuel cell mimics electrochemical processes occurring in nature to harvest a useful electrical current, without the use of precious electrocatalysts such as platinum.<sup>3</sup>” The key feature central to these devices is the incorporation of a biological element that recognizes a specific analyte. It is important to note that this definition of a biosensor is not solely restricted to electrochemical detection; other methods that have been reported in the literature include optical,<sup>4</sup> gravimetric,<sup>5</sup> and calorimetric.<sup>6</sup> Additionally, the biologically derived portion of these devices are not limited to enzymes as the sensing component. Biosensors and biofuel cells constructed using microbes,<sup>7</sup> antibodies,<sup>8</sup> and DNA<sup>9</sup> have all been reported.

Enzymatic biosensors utilize the natural catalytic reaction of an enzyme to monitor the presence or concentration of a specific small molecule. The amount of substrate conversion catalyzed by the enzyme is converted to a measurable electrochemical signal through the use of a transducer.<sup>10</sup> When using an oxidoreductase,

an electron mediator is needed to act as an intermediate between the biological catalyst and the electrochemical detector.<sup>11</sup> Much research has been done to fine-tune the electronic properties of organometallic complexes to efficiently mediate the flow of electrons between enzymes and an electrode.<sup>12</sup> The electron mediator can be either dispersed in solution or contained within a matrix deposited directly onto an electrode.<sup>12</sup> Techniques related to the immobilization of enzymes will be discussed later in this chapter.

Biofuel cells represent an important stride forward in the way we traditionally think of power sources. According to the Institute for Energy Research's website, the combustion of fossil fuels provides approximately 82% of the United States' overall energy consumption. This fact, coupled with the mounting evidence in support of global warming, makes it clear that new methods of generating energy in an environmentally benign fashion are growing increasingly important. Enzymatic biofuel cells are of particular interest because they *generate* useful electrical current by taking advantage of catalytic processes found in redox enzymes, rather than merely store energy like a battery. In a biofuel cell, a biological fuel source is oxidized at the anode and an oxidant is reduced at the cathode.<sup>13,14</sup> Fuel sources for enzymatic biofuel cells are typically small sugar molecules,<sup>15,16</sup> and the oxidant is often molecular oxygen.<sup>17,18</sup>

The most well studied enzymatic biosensors and biofuel cells are those involving the oxidation of glucose.<sup>19,20</sup> The interest surrounding such systems is twofold: (1) the increasing diabetes epidemic in the United States and (2) the powering of small, implantable electronic devices. As of 2014, the CDC reports that 9.3% of the U.S. population, 29.1 million people, suffer from diabetes.<sup>21</sup> While there is still work to be

done on the actual treatment of this disease, new and more efficient methods of glucose detection are also in great demand. Better detection methods are important for patients to be able to monitor their condition, and the ultimate goal of glucose research is the development of highly sensitive, implantable, and long lasting glucose monitors. The advantage of an enzymatic biofuel cell is that it can potentially monitor and draw power from the body's own blood sugar. This would allow for a device to be powered without the need for an additional battery, and could potentially be less invasive.

## **1.2 Redox Mediators and Enzyme Immobilization**

### *1.2.1 Methods of Signal Transduction*

As mentioned above, a mediator is often needed to transduce the enzymatic electrocatalysis into a detectable electrical signal. This can be done through either direct electron transfer or by the “wiring” of electroactive small molecules in a polymer matrix<sup>22</sup>. The type of mediation required is often dependent on the enzyme under investigation, and similar types are grouped into three different “generations.” This nomenclature was first used to describe the stages of biosensor development, but has more recently been used to distinguish the various methods of signal transfer between a redox enzyme and an electrode. **Figure 1.2.1** gives an example of the three types of detection associated with each generation.

First generation systems detect either the disappearance of a substrate or the generation of product as it occurs from the enzymatically catalyzed reaction.<sup>23,24</sup> In either case it is necessary that the compound being monitored be electrochemically active. A common example is the detection of hydrogen peroxide formed from the reduction of molecular oxygen.<sup>25</sup> Oxygen is often a cosubstrate in enzymatic catalysis,<sup>26</sup> and both it



and hydrogen peroxide can be detected electrochemically. However, these systems are typically not optimal due to interferences of other biological compounds—i.e. ascorbic acid<sup>27,28</sup> or dopamine<sup>29</sup>—that have similar electrochemical potentials. Since first generation systems monitor product or substrate it is usually necessary to immobilize the enzyme near the electrode surface to limit diffusion away from the enzyme.

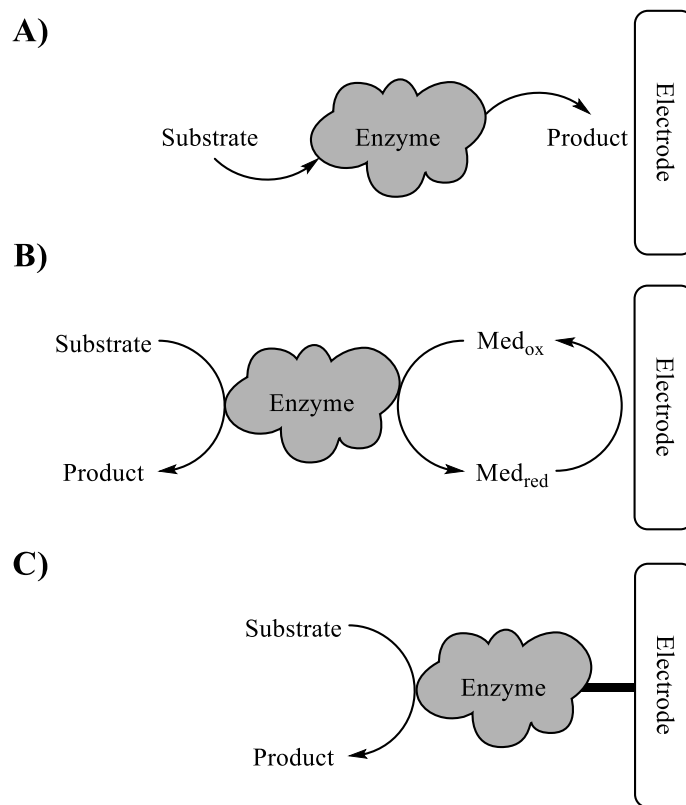


**Figure 1.2.1** Schematic representations of the different generations of biosensors: A) first, B) second, and C) third generation.

In the second generation, the enzymatic reaction is artificially mediated between the enzyme and the electrode through the usage of electroactive small molecules.<sup>30</sup> These electroactive compounds take the place of a cosubstrate, i.e. O<sub>2</sub>, to regenerate the active form of the enzyme and shuttle electrons to or from the electrode. In this method, the

three components—enzyme, mediator, and electrode—are essentially distinct systems that work in conjunction to detect and transduce an electrochemical reaction.

Third generation systems are fabricated such that the enzyme is in direct electronic communication with the electrode.<sup>31</sup> In this method, the enzymatic redox process is coupled directly to the electrode without the need for an external mediator. These so called “reagentless biosensors” can be operated at potentials closer to that of the enzyme and are less prone to interference.<sup>32,33</sup> The biggest hindrance in the development of third generation systems lies in the fact that most enzymes cannot undergo direct electron transfer with normal electrodes.<sup>34</sup> There has been much research in modifying electrodes and enzymes to orient them in such a way to enhance electronic communication without denaturation of the protein.<sup>35,36,37</sup> As such, this method can be cost prohibitive and difficult to process on a large scale.

Glucose biosensors of each generation, with varying degrees of success, have been reported in the literature.<sup>19,37</sup> The most abundant, and arguably fruitful, advancements have centered on the second generation. Glucose/O<sub>2</sub> biofuel cells that use second generation methods at the anode, and second or third generation methods at the cathode, have been reported in the literature<sup>20</sup>. The most commonly used enzymes in glucose biosensors and glucose/O<sub>2</sub> biofuel cells are glucose oxidase (GOX) and laccase because of their high turnover rates and overall robustness. While both of these enzymes are oxidoreductases, they differ in the reactions they catalyze and their electrocatalytic active sites. The type and location of the active site often determines the viability of using one generation of signal transduction over the other.

GOX is a large glycoprotein that contains a flavin adenine dinucleotide (FAD) redox cofactor buried deep within the interior of the enzyme.<sup>38,39</sup> When glucose is oxidized to gluconolactone, the FAD center is reduced to FADH<sub>2</sub> (**Figure 1.2.2**). Because the electroactive portion of GOX is tightly bound inside the enzyme, third generation direct electron transfer (DET) is almost impossible.<sup>37</sup> For GOX to undergo DET, electrons would have to tunnel from the active site to the outside of the enzyme, a distance of ca. 15 Å.<sup>40</sup> The critical distance for electron tunneling is ca. 20 Å,<sup>41</sup> making DET for GOX difficult as the rate for electron tunneling exponentially decays with distance.

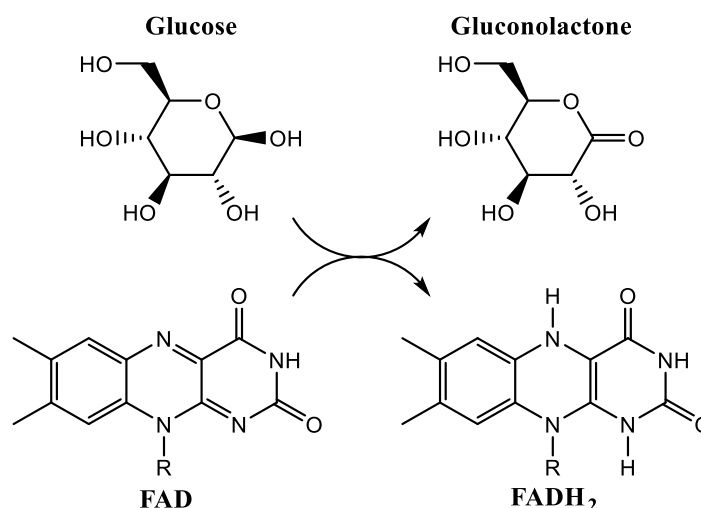


**Figure 1.2.2** Reaction scheme of the oxidation of glucose using FAD in the active site of glucose oxidase.

Since the active site for GOX is buried deep within the enzyme, electron mediation is typically achieved by small redox active molecules penetrating into the active site. Once electron transfer occurs, the mediator can diffuse out of the active site and transfer electrons through Marcus-type collisions.<sup>42,43,44</sup> This makes second generation mediation ideal for glucose bioanodes. A variety of conjugated polymers and redox polymers have been used as mediators for GOX.<sup>16,19,30</sup> One of the biggest

breakthroughs in this type of mediation came when Adam Heller's research group used organoosmium (**Figure 1.2.3**) complexes attached to a polymer backbone to effectively "wire" the enzyme to an electrode.<sup>45</sup> Since this discovery there have been many advancements in the design and type of organometallic compounds used for mediation. As will be discussed in **Section 1.4**, our group in particular has made use of ferrocene containing polymers for efficient election mediation.

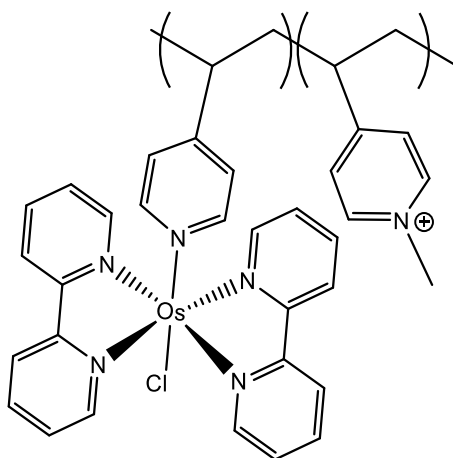


**Figure 1.2.3** Second generation redox polymer based on organoosmium modified poly(vinylpyridine) used by Heller in the mediation of glucose oxidase.

The enzyme laccase is a blue copper oxidase that catalyzes the reduction of molecular oxygen to water.<sup>46</sup> Laccase has a three copper cluster at its active site with an additional type-1 copper (T-1 Cu) center near the surface of the enzyme.<sup>46</sup> The T-1 Cu helps to aid in electron transfer and is located next to a hydrophobic region where organic compounds can be bound.<sup>46</sup> By having an electroactive compound near the surface, laccase is able to be used in both second and third generation electron mediation. Laccase has been shown to be effectively undergo direct electron transfer when coupled with anthracene-modified carbon nanotubes,<sup>35</sup> and it is also capable of being mediated by Heller-type organometallic redox polymers.<sup>47,48,49</sup>

For the purpose of this work, the focus from here on out will be on second generation electron mediation. For this type of signal transduction, the enzyme is typically immobilized at or near the electrode's surface

### 1.2.2 Enzyme Immobilization Techniques

Immobilizing an enzyme onto an electrode surface keeps it from diffusing away into solution. While enzymes in solution can still be mediated by redox active molecules, they cannot be easily recovered and it is generally a wasteful technique. Keeping enzymes confined to a specific area allows for more controlled electron capture, and increases the enzymatic lifetime, allowing for extended usage. There are four principal methods used for the immobilization of enzymes: adsorption, covalent binding, membrane confinement, and entrapment (**Figure 1.2.4**).<sup>50</sup>

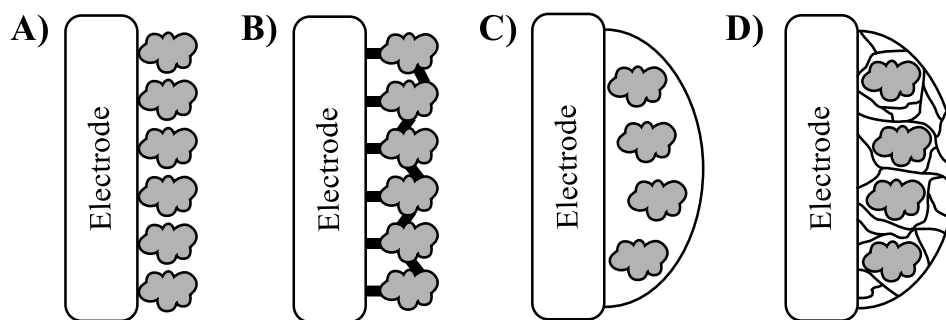


**Figure 1.2.4** Generic representation of the four main types of enzyme immobilization: A) adsorption, B) covalent binding, C) membrane confinement, and D) polymer entrapment.

The simplest method to immobilize an enzyme is through adsorption: the adhesion of a thin layer of material onto a solid surface.<sup>51,52</sup> Adsorption relies on non-covalent interactions and is therefore reversible under certain conditions. There are three general types of adsorption immobilization: nonspecific, ionic, and hydrophobic.

The first usage of this technique was reported by Nelson and Griffin in 1916 when they adsorbed invertase onto activated carbon without any change in enzymatic activity.<sup>53</sup>

The basic method of enzyme adsorption involves immersion of a solid support into an enzyme containing solution. After incubation in the solution, material is deposited onto the surface in a self-assembled monolayer. Depending on the support being used, the specificity of adsorption can be controlled. Nonspecific adsorption uses an inert support and relies on physical interactions such as hydrogen bonding or van der Waals forces for material deposition.<sup>52</sup> Ionic adsorption relies on the fact that most enzymes have a net surface charge.<sup>54,55</sup> By modifying the support structure with an ionic charge that is opposite that of the enzyme, it is possible to selectively adsorb the protein onto the surface. Unlike the previous methods, hydrophobic adsorption is an entropically driven process based on the minimization of surface area.<sup>56,57</sup> If the protein and the solid support being used are sufficiently hydrophobic, then the two will want to interact to minimize the interaction with the aqueous media. The resulting expulsion of water helps compensate for the loss in free energy once the two combine.<sup>58</sup> Adsorption is an attractive method due to it being mild, simple, and cost effective, but the enzymes can easily desorb with changes in pH, ionic strength or concentration.

Covalent immobilization of enzymes involves the formation of bonds directly to the enzyme to render it insoluble.<sup>59</sup> This is done by either crosslinking multiple enzyme units together or by attaching the enzyme directly to a surface. This technique takes advantage of the naturally occurring amino groups that are present on the enzyme. Since amines are good nucleophiles, most covalent binding methods involve the addition of electrophilic crosslinkers such as glutaraldehyde,<sup>60</sup> epichlorohydrin,<sup>61</sup> or cyanogen bromide<sup>50,62</sup> While this technique results in very little desorption, the enzyme can be

deactivated due to conformational change if amines in the active site participate in the crosslinking.<sup>61</sup>

Membrane confinement is a simple technique that isolates the enzyme behind a semipermeable membrane.<sup>50</sup> Ideally this technique allows for free movement of substrate and product in and out of the membrane while keeping the enzyme in a secured location. Since there are no direct linkages to the protein, this method keeps the enzyme in a natural state. While a seemingly simple and cost effective immobilization technique, membrane confined enzymes typically suffer from poor mass transport of material through the membrane, which lowers the effectiveness of the sensor.<sup>50</sup>

Entrapment describes the method of localizing an enzyme within the interstitial spaces of a water insoluble polymer matrix.<sup>50,63</sup> The entrapment is ideally performed in such a way as to retain the activity of the protein, while keeping it in a defined location. The polymer in use must be able to swell to some degree so substrate can diffuse into, and product can diffuse out of, the matrix. This is typically achieved by using amine, ether, alcohol, or carboxylate containing materials that allows for a high degree of hydration.<sup>64,65,66</sup> The polymer network must also be sufficiently crosslinked enough to keep the film from dissolving into the solution, but not so tightly crosslinked to constrict the enzyme and affect its activity. Because enzymes change state upon binding to a substrate,<sup>67</sup> too tight a crosslinked system can spatially inhibit the enzyme and lower its overall effectiveness. This, coupled with decreased substrate diffusion into a tightly bound matrix, makes the degree of crosslinking an important function in film formation.

The polymer for entrapping the enzyme can be crosslinked by two different methods: chemical and physical. Chemical crosslinking involves the formation of

covalent bonds between polymer strands to render the network water insoluble. This can be achieved either through the addition of external crosslinkers<sup>68</sup> or through coupling of reactive moieties on the polymer itself.<sup>69</sup> Chemical crosslinking is typically an irreversible process because the newly formed bonds are difficult to break. Some common examples of chemical crosslinking are: sol-gels,<sup>70</sup> coupling of epoxides with amines,<sup>71</sup> radical polymerization of monomers,<sup>72</sup> and photochemical crosslinking.<sup>69</sup>

Physical crosslinking is based on intermolecular attractions between polymer strands and is similar to the previously described adsorption methods. These attractive forces include hydrogen bonding, ionic interactions, and electrostatic coupling.<sup>63,73,74</sup> Common examples of physical crosslinking include chitosan<sup>75</sup> gels and layer-by-layer assembled films.<sup>76</sup> While these do not include covalent bonds between polymer strands, there are still sufficient interactions present that allow for a stable matrix to be formed.

While there are many possible methods of immobilization available, the two that were investigated in this work involve photochemical crosslinking and layer-by-layer self-assembly. These were chosen specifically for the fast nature of their fabrication, as the current method of crosslinking employed in our group requires 24-48 hours of curing to form cohesive films.

### **1.3 Fabrication Methods**

#### *1.3.1 Introduction to Photolithography*

The polymer network with which an enzyme is immobilized needs to be sufficiently crosslinked to allow for effective electronic communication throughout the film. One potential method for producing such crosslinked film production is photolithography, which literally translates from Latin to “light-stone-writing.” This



method of fabrication uses light to transfer a pattern from an opaque photomask onto a light sensitive material, called a photoresist. A photoresist is an uncrosslinked polymer film that, upon irradiation, becomes either more or less soluble in a developing solution. These two types of photoresists are designated as positive or negative, respectively.

**Figure 1.3.1** diagrams the general process for developing a photoresist.

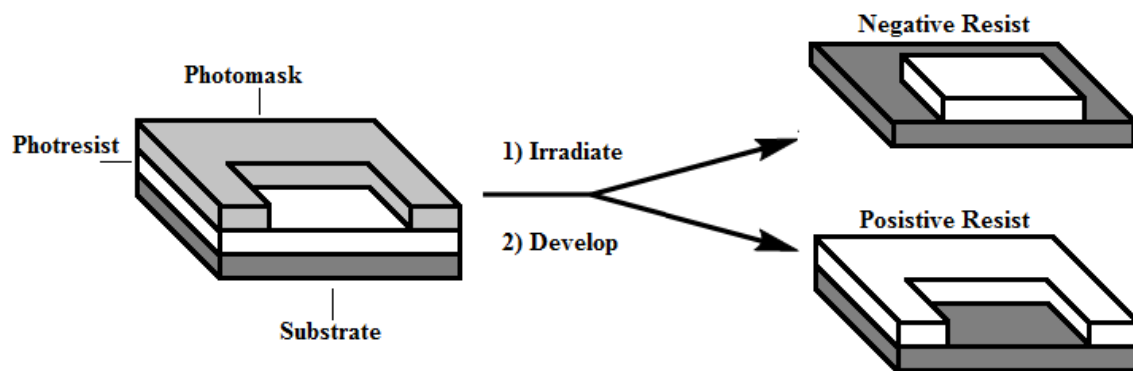


**Figure 1.3.1** Simplified procedure for the production and development of photocurable materials.

First, a thin layer of photosensitive material is deposited onto a substrate. The exact type and chemical make-up of the material varies depending on the desired outcome. Next, a light impermeable photomask is placed on top of the photoresist. Photomasks are typically glass slides with opaque patterns throughout that allows irradiation to be exposed only to certain areas of the film. The masked photoresist is then irradiated at a specific wavelength to initiate a photochemical reaction. After exposure, the substrate is washed in a developing solution to dissolve the uncrosslinked material.

Whether a photoresist is positive or negative is determined by the chemical structure of the individual polymer. Common positive photoresists take advantage of phenol-formaldehyde resins, called novolacs, and diazonaphthoquinone (DNQ).<sup>77</sup> As shown in **Figure 1.3.1**, when novolac/DNQ films are subjected to irradiation, DNQ undergoes a Wolff rearrangement, extrudes molecular nitrogen, and forms a ketene by

ring contraction.<sup>78</sup> After exposure to light, films are then developed in aqueous base for two distinct reasons. The ketenes formed after irradiation are converted to carboxylic acids. After deprotonation, the solubility of the exposed films drastically increases and the material is washed away. The remaining part of the film undergoes azo-coupling to crosslink the polymer and prevent dissolution.<sup>78</sup> This creates an image in the polymer identical to the opaque portion of the photomask, hence the designation of a positive photoresist.

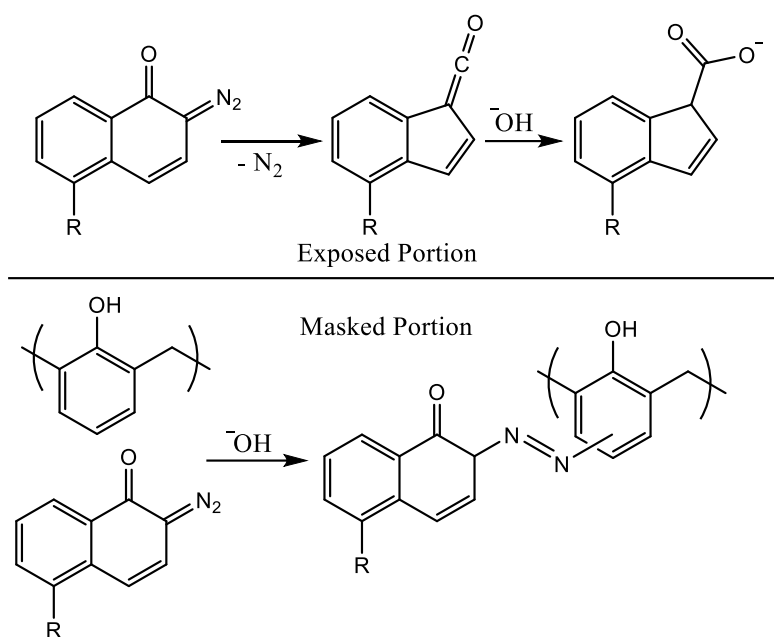


**Figure 1.3.2** Reaction scheme of both exposed and masked portions of Novolac photoresist. Where R is another unit containing a diazoketone.

This technique helped to revolutionize the semiconductor industry and is currently used in 80% of the world's integrated circuits.<sup>78</sup> However, this technique has seen little to no usage in the fabrication of bioelectrodes. More progress has been in the development of redox active negative photoresists for bioelectrode applications.

A negative photoresist makes an inverse copy of the photomask applied. When a negative photoresist is exposed to irradiation, the uncovered portion of the material

crosslinks into a cohesive polymer network. The remaining portion of the polymer is then removed by the developing solution. Some common negative photoresists used in industry and polymer research are [2+2] cycloadditions,<sup>79</sup> epoxides with photogenerated acids,<sup>80</sup> and aziridine formation from photogenerated nitrenes.<sup>81</sup> **Figure 1.3.3** gives an example of each of these reaction types.

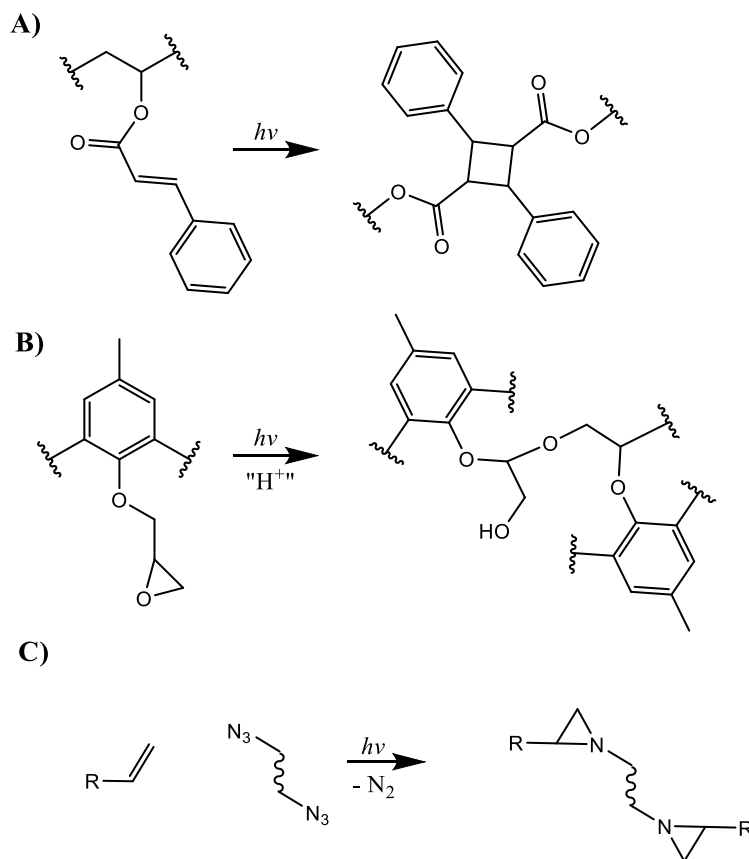


**Figure 1.3.3** Examples of common reactions used to photocrosslink negative photoresists: A) [2+2] cycloaddition, B) acid catalyzed epoxide opening, C) nitrene addition to alkenes.

While these reactions have seen development in other areas of research, as of this writing there are no published records of them being used in the immobilization of enzymes. It is not surprising that epoxides have not been used since the amino residues on the enzyme could potentially react and form unwanted crosslinks. Photogenerated

nitrenes are a common method to couple proteins together,<sup>82</sup> but there have been limited reports of this technique being used to generate enzymatic biosensors. The majority of the reported accounts that have been published involve radical polymerizations<sup>72,83</sup> and C-H insertions.<sup>69,84</sup> However, based on work previously done in our lab, we sought to incorporate photocrosslinkable moieties into the bioanode systems currently in development.

### 1.3.2 Layer-by-Layer Assembly

As the name suggests, layer-by-layer (LBL) assembly is a fabrication method where successive layers of material are built upon each other. Pioneering work done by Irving Langmuir and Katharine Blodgett in the 1930's showed that it was possible to adsorb thin films of material onto solid surfaces using solely physical methods. In the 1920's, Langmuir had been studying the dispersion of lipids on the surface of water and how they could be transferred in a uniform monolayer onto a solid surface,<sup>85</sup> but it wasn't until 1935 that Blodgett demonstrated the ability to build up successive layers of calcium stearate onto an unmodified glass slide.<sup>86</sup> These so called "Langmuir-Blodgett" films were the first widely characterized systems for self-assembly of charged small molecules onto substrate surfaces. The real breakthrough for LBL self-assembled polymer films came in 1992 when Decher, *et al.* described the process of using oppositely charged polyelectrolytes.<sup>87</sup> An example of the LBL process using polyelectrolytes is shown in **Figure 1.3.4**. First, a solid surface is modified to produce an overall cationic charge, usually through the incorporation of ammonium groups. The cationically-modified surface is then immersed in a solution containing an anionic polymer, which results in a monolayer of material being deposited. Because the concentration of the polyelectrolyte

is higher than the number of groups on the surface, the surface charge of the substrate is reversed. After rinsing to remove excess material, the substrate is next immersed into a solution of cationic polymer to restore the original surface charge. This process can be repeated until the desired number of layers is achieved.

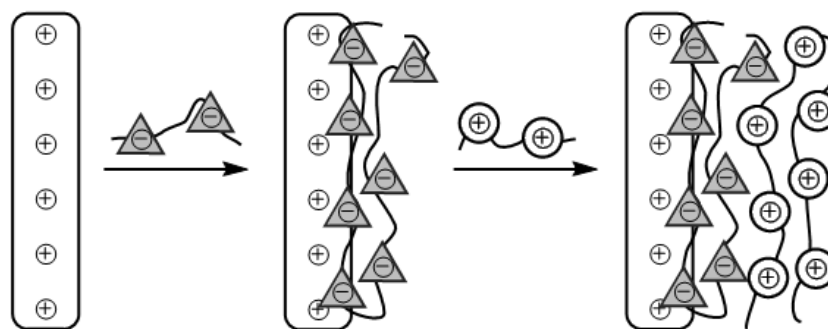


**Figure 1.3.4** Generic scheme for the layer-by-layer adsorption of polyelectrolytes onto a charged surface.

While the main force that contributes to the build-up of polyelectrolyte films is electrostatic complexation, there are other important factors that affect film fabrication. As might be expected, changes in pH can affect the development of polymer multilayer assembly.<sup>88,89</sup> Two common ionizable groups used in LBL assembly are amines and carboxylic acids. The degree to which polymers containing these moieties are charged is dependent on its various protonation states. If every repeat unit contains an ionic charge, the polymer will favor an extended chain formation due to intermolecular electrostatic repulsion. This lowers the available degrees of freedom, and can cause irregular deposition of material onto the substrate, leading to poorly defined films.<sup>88</sup> It is, therefore, often necessary to fine tune the charge density of a polyelectrolyte by altering the pH of the deposition solutions to afford optimum fabrication of films.

Another major factor in LBL assembly of polyelectrolytes is the hydrophobicity of the polymers used. In 1999 Kotov described the role of the polymer's solvation shell

and ionic atmosphere on LBL assembly.<sup>58</sup> Since LBL deposition is mainly concerned with ionically charged materials, water is typically the media used for dispersion of materials. An ion in an aqueous environment will naturally become hydrated in a solvent shell. For complexation of polyelectrolytes to occur, the ions must first release the coordinated water molecules. This increase in entropy is needed to compensate for the loss in degrees of freedom of the now bound polymer. After the expulsion of water from the polymer layers, the hydrophobic portions of the opposing polyelectrolytes will have an enhanced attraction as they are in closer proximity to each other. These short range hydrophobic interactions play a crucial role in the LBL assembly, as the adsorbed layer must be more thermodynamically preferable to being dissolved in solution. As such, there is an optimum balance between overall charge density and appropriate hydrophobic interactions. Too much charge and the polymer cannot form uniform layers, but too little charge and the opposing strands cannot complex. The complexation of the composite is then enhanced with the right amount of hydrophobicity to keep water out of the system.<sup>58</sup>

The mild conditions and aqueous media often used in LBL assembly makes it an ideal technique for the entrapment or “encapsulation” of biomaterials. LBL assembly is an attractive fabrication method for bioelectrodes because enzymes are naturally occurring polyelectrolytes which can be paired with a redox polymer containing an opposite charge. Enzymes contain amino acid residues consisting of both acidic and basic functional groups making them pH dependent weak polyelectrolytes. The isoelectric point (pI) describes the pH at which a protein has a net zero charge.<sup>90</sup> At pH below pI proteins carry a net positive charge, and above pI there is a net negative charge on the

molecule. Isoelectric points vary between proteins, but the pH can be adjusted to fine tune the LBL assembly specifically to the enzyme being used.

Early work by Lvov *et al.* demonstrated the possibility of expanding the method developed by Decher to incorporate multiple layers of protein with charged polyelectrolytes.<sup>91, 92</sup> **Figure 1.3.5** illustrates the build-up of surface material as envisioned by Lvov. This idealized method of well-defined layers has been the dominating picture associated with LBL growth, but, as will be discussed in **Chapter 3**, this may not be the case. The LBL assembly of polyelectrolytes has been widely explored in the scientific literature, and LBL assembled biosensors have been developed for the detection of glucose,<sup>93</sup> lactose,<sup>94</sup> cocaine,<sup>95</sup> cancer cells,<sup>96</sup> and a whole host of other analytes.

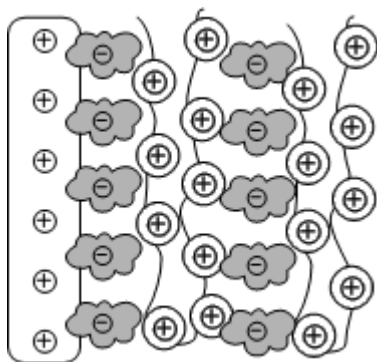


**Figure 1.3.5** Successive adsorption of charged enzymes and polyelectrolyte on a surface modified electrode.

The most common methods for determining the LBL growth of material are ellipsometry,<sup>97</sup> UV-Vis spectroscopy,<sup>92</sup> and quartz crystal microgravimetric analysis.<sup>98</sup> These techniques are exceptionally useful in quantifying the amount of material deposited and the thickness of multilayered films. Unfortunately they provide little insight into how the deposited materials are orienting when they adsorb to the surface. One possible method we thought to use to probe this physisorption phenomenon is through the usage

of electrochemical techniques. Often used simply to detect the presence of electroactive species, cyclic voltammetry can provide a wealth of information about the surface confinement of materials. By monitoring the electrochemical response of a system with regards to the increasing number of layers, we thought it should be possible to probe how the material is being deposited onto a surface.

## 1.4 Project Goals and Background

### 1.4.1 Bioelectrode Fabrication Methods

Recent work our group has shown that ferrocene-modified linear poly(ethylenimine) (Fc-C<sub>n</sub>-LPEI) can act as an efficient electron mediator for glucose oxidase.<sup>64,68,99</sup> Since then our group has made great strides in the methylation of the ferrocene moieties to lower the redox potential,<sup>100</sup> incorporation of the aforesaid polymers into a biofuel cell,<sup>101</sup> and optimization of conditions to increase power output.<sup>102</sup> All of these efforts have helped create some of the best defined bioanodes reported in the literature. One area that has received little attention up to this point is the method in which LPEI is crosslinked into a hydrogel. The method employed in these papers involves ethylene glycol diglycidyl ether (EGDGE) as a chemical crosslinker for the formation of an insoluble polymer matrix. **Figure 1.4.1** demonstrates how EGDGE can react with the nucleophilic nitrogens of the LPEI backbones of multiple polymer strands to crosslink them together into a large, macromolecular network.

This method of fabrication has been fruitful thus far, but it is not without its own problems. First, there is little control over crosslinking once the polymer and EGDGE are mixed. The reaction is widespread and will continue until all of the reactive species are gone. While this is fine for coating thin films onto planar electrodes, it makes fabrication



of more complex devices somewhat difficult. For these materials to be used in miniaturized electronics or microfluidic devices, they would need to be coated on the inside of capillaries or in a precise pattern on an interdigitated array. This would be difficult to achieve if the crosslinking reactivity cannot be controlled. Some more feasible methods would be to have the polymer only adhere to particular surfaces or to selectively crosslink the material in a desired pattern.

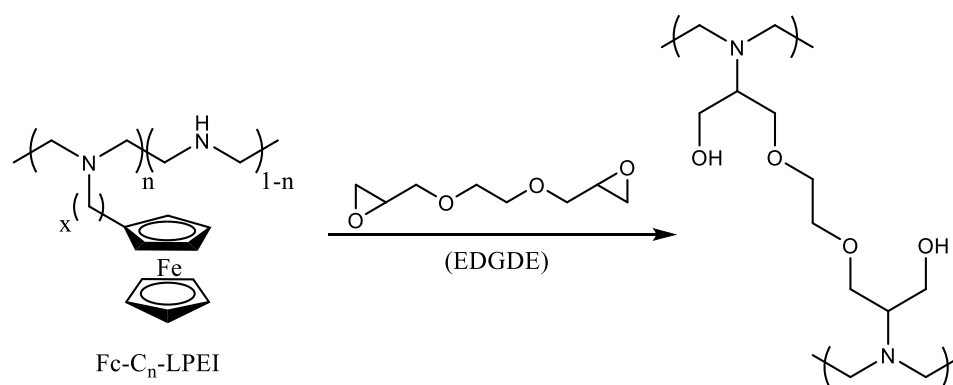


**Figure 1.4.1** Proposed reaction scheme for the crosslinking of Fc-C<sub>n</sub>-LPEI with EGDGE to form a water insoluble hydrogel. Ferrocene mediator omitted from product for clarity.

The second problem with crosslinking Fc-C<sub>n</sub>-LPEI with EGDGE is the extended curing times needed to produce suitable films. Depending on the electrode material employed, films are cured in open atmosphere for 24-48 hours. Such long reaction times are needed because the films cannot be heated due to the presence of the enzyme. The crosslinking is done at room temperature to avoid any unintentional denaturing of the enzyme. Leaving films open to the atmosphere for extended periods of time can not only cause a loss in enzyme activity but can also damage the ferrocene redox mediator. The iron complex is oxidatively sensitive and can be damaged by over exposure to atmospheric oxygen. It is evident that there is a great need to lower the assembly time associated with film curing.

The main objective of this work is to investigate various fabrication methods for the construction of Fc-C<sub>n</sub>-LPEI based bioelectrodes with the goal of lowering the overall production time. This will be achieved through photocrosslinkable polymers and by the LBL assembly of polyelectrolytes. Both of these techniques have been used in the fabrication of bioelectrodes and have precedent within our own lab.

Previous works by Hu and Kadam have shown that allyl modified LPEI (LPAEI) can be radically crosslinked by thermal or photochemical processes for usage as solid polymer electrolytes.<sup>103,104</sup> As shown in **Figure 1.4.2**, this is done through hydrogen abstraction at the allylic position, followed by radical coupling to form new covalent crosslinks between polymer strands. In both cases, the crosslinking was initiated by an external radical source: V-50 (2,2'-azobis(2-methylpropionamide) dihydrochloride) for thermal crosslinking and Li<sub>2</sub>S<sub>2</sub>O<sub>8</sub> for photochemical crosslinking. Both methods were able to produce cohesive films, but their formation still took 12 to 72 hours for the complete reaction occur. Photolithography based on LPAEI would be useful in controlling film shape, but the curing times that are currently required are not an improvement on crosslinking with EGDGE.

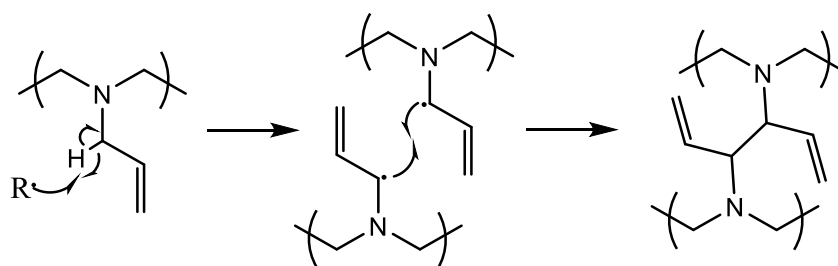


**Figure 1.4.2** One possible mechanism for the radical crosslinking of allylated LPEI. Radical shown only at secondary carbon, but some portion of the primary radical may react as well.

In **Chapter 2** of this work, we use the precedents of Hu and Kadam to produce an allylated derivative of Fc-C<sub>n</sub>-LPEI that can be used as a photocrosslinkable redox polymer, and we investigate the optimization of photoinitiator type and irradiation time on film stability. The new redox active films are also used to immobilize glucose oxidase (GOX), and we evaluate their usage as a glucose biosensor.

The other method of immobilization of interest is layer-by-layer assembly of polyelectrolytes. As mentioned above, LBL assembly using enzymes is a viable biosensor fabrication method that has seen a variety of applications. Films are constructed from an aqueous environment and do not have extended curing times to form a cohesive network. The materials are selectively adsorbed onto a modified surface and built up in a stepwise fashion. By depositing materials where needed, the film shape and location are self-assembled onto the desired substrate.

DeLuca *et al.* have recently shown that hexylferrocene-modified LPEI (Fc-C<sub>6</sub>-LPEI) can be used in the fabrication of high sensitivity, LBL assembled glucose biosensors.<sup>105</sup> Since LPEI is a polyamine, it can be protonated by water to give it a net positive charge in aqueous media. Fc-C<sub>6</sub>-LPEI can then couple with an oppositely charged polyelectrolyte to form a bilayer of material. DeLuca first constructed films using poly(acrylic acid) (PAA) and poly(glutamic acid) (PGA) as the counter polyanion to ensure Fc-C<sub>6</sub>-LPEI could participate in LBL assembly. Films assembled using this method produced anodic peak currents of ~20 μA, as evidenced in the cyclic voltammogram, when constructed with 16 bilayers of material. While these films cannot act a biosensor themselves, they provided a basis for using Fc-C<sub>6</sub>-LPEI in LBL assembly with enzymes.

Modifying gold electrodes with cystamine dihydrochloride gives the surface a net positive charge to which anionic glucose oxidase (GOX) can be adsorbed. GOX has a pI of 4.2,<sup>39</sup> which gives it a net negative charge at physiological pH. By alternating layers of GOX and Fc-C<sub>6</sub>-LPEI, DeLuca was able to assemble up to 16 bilayers onto an electrode surface. Surprisingly, assembled films with 16 bilayers were only able to generate anodic peak currents of ~0.3  $\mu\text{A}$ . This is significantly lower than PAA or PGA assembled films, and suggests that GOX has a much lower charge density than the other polyelectrolytes. While the electrochemical response was not as high as expected, the assembled films produced maximum current densities of ~0.4  $\mu\text{A}/\text{cm}^2$  in response to glucose.

The low response of the assembled Fc-C<sub>6</sub>-LPEI/GOX films is attributed to poor connectivity between the polymer and the enzyme. In an effort to increase this interaction, GOX was covalently bound to the polymer by first treating the enzyme with sodium periodate. As shown in **Figure 1.4.3**, GOX can be oxidized with sodium periodate to afford aldehyde groups on the surface of the enzyme. This periodate-oxidized GOX (p-GOX) can react with the backbone of Fc-C<sub>6</sub>-LPEI to form new covalent Schiff base crosslinks. Changing from GOX to p-GOX increased the maximum anodic peak currents to ~1.6  $\mu\text{A}$  and maximum glucose response to 220  $\mu\text{A}/\text{cm}^2$ .

In **Chapter 3** of this work, we examine the effect of mediator tether length and fabrication wash time in the preparation of LBL assembled Fc-C<sub>n</sub>-LPEI/p-GOX bioanodes. We show the viability of using electrochemical methods to elucidate the physisorption of material onto an electrode's surface, and we introduce the possibility of using layer-by-layer assembled bioanodes in a biofuel cell.



electrochemical potential of the redox mediator and reduces the overpotential between it and the enzyme, allowing for more effective electron transduction.

#### *1.4.2 Sulfur: Thermal Properties and Inverse Vulcanization*

Sulfur is a yellow, naturally occurring solid that has little industrial usage in its elemental form. It is a byproduct of the oil and gas industry, and large deposits of the material are rapidly accumulating. It has long been known that sulfur will thermally polymerize on its own, but the resulting materials revert back to the stable monomeric form in a matter of days.<sup>106,107</sup> There is a lot of interest in stabilizing the so-called “rubber phase” of sulfur, but there has only been limited success reported in the literature. Recently, there has been a push to develop stable polymers of sulfur for their usage in lithium-sulfur batteries.<sup>113</sup>

Differential scanning calorimetry (DSC) is a technique used for studying the thermal properties of materials and is a common tool used in the characterization of sulfur. DSC works by analyzing the heat flow of an unknown sample against that of a known reference. This is done by using two pans of the same material: one filled with the sample and the other left empty. The two pans are then heated at a constant rate, and a computer measures the flow of heat into and out of the sample pan. As the material in the sample pan begins to absorb or release heat, a second heater adjusts the temperature of the pan to make it match the reference. This compensating heat flow directly corresponds to the thermal properties of the sample. **Figure 1.4.4**, shows a typical thermogram for elemental sulfur.

At 114°C, the first peak on the thermogram is the solid phase conversion of orthorhombic sulfur ( $S_{\alpha}$ ) to monoclinic sulfur ( $S_{\beta}$ ). The next peak (120°C) is the sulfur

phase change from solid to liquid ( $S_\lambda$ ). Up to this point, sulfur has been in a cyclic, eight-membered ring configuration, but with further heating the ring spontaneously opens to form a diradical. These newly formed radicals will start to couple with each other which causes a drastic increase in viscosity. Given enough heat and time, the entire system will undergo polymerization which results in the third peak ( $183^\circ\text{C}$ ): the heat of polymerization to form rubber sulfur ( $S_\mu$ ).<sup>108</sup>

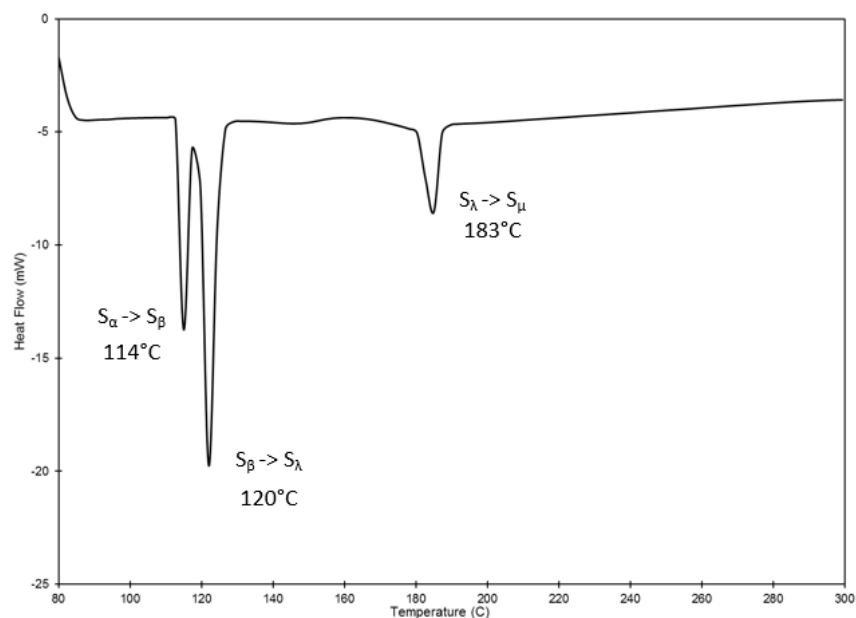


**Figure 1.4.4** DSC thermogram for elemental sulfur.

The Pyun group at the University of Arizona has recently reported the stabilization of rubber sulfur through “inverse vulcanization.”<sup>109</sup> In its traditional sense, vulcanization is the process of stabilizing natural rubber by crosslinking the polymer with small sulfur chains. Natural rubber consists mainly of poly(isoprene) which contains many allylic hydrogens. When heated in the presence of sulfur, the diradicals formed from homolytic ring opening will abstract an allylic hydrogen to form a resonance stabilized radical. These newly formed polymer radicals will couple with sulfur to form covalent crosslinks. The Pyun group’s method of inverse vulcanization is based on the

idea of stabilizing polymeric sulfur with the addition of small organic molecules that will readily accept radicals. **Figure 1.4.5** provides an example of crosslinking sulfur using diisopropenylbenzene. Inversely vulcanized sulfur can be made on the kilogram scale<sup>110</sup> and has been used for lithium-sulfur batteries<sup>111</sup> and IR transmitting materials.<sup>112</sup>

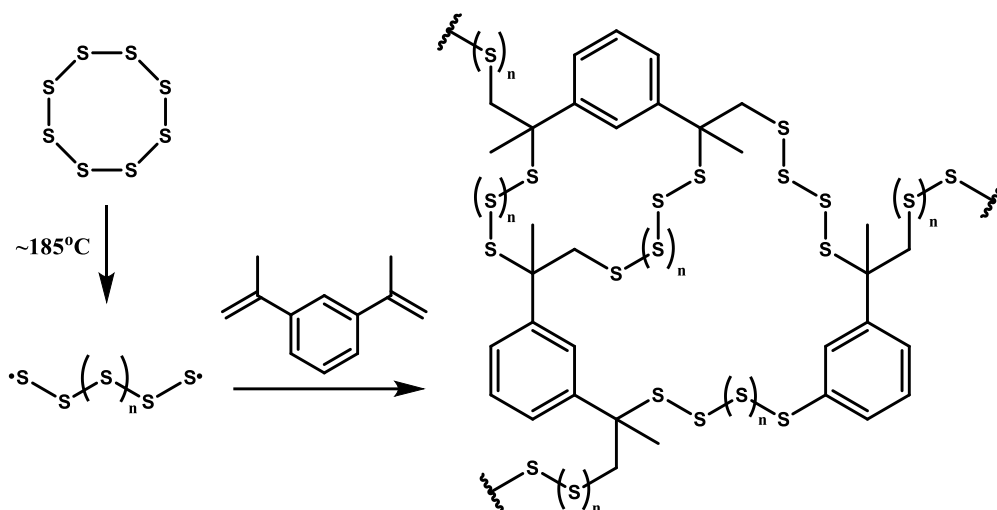


**Figure 1.4.5** Inverse vulcanization of sulfur using 1,3-diisopropenylbenzene as proposed by the Pyun group.

The final portion of this work focuses on the solvent-free polymerization of sulfur and paracyclophane copolymers (**Figure 1.4.6**) and the thermal characterization of the resulting compounds. The reaction between these two compounds can be monitored using DSC, and the reaction optimization is tuned by varying the ratio of starting materials and the incorporation of chloro-substituted paracyclophane. The materials synthesized in **Chapter 5** were designed to be used in the development of lithium sulfur batteries once full optimization of the polymerization process was completed.

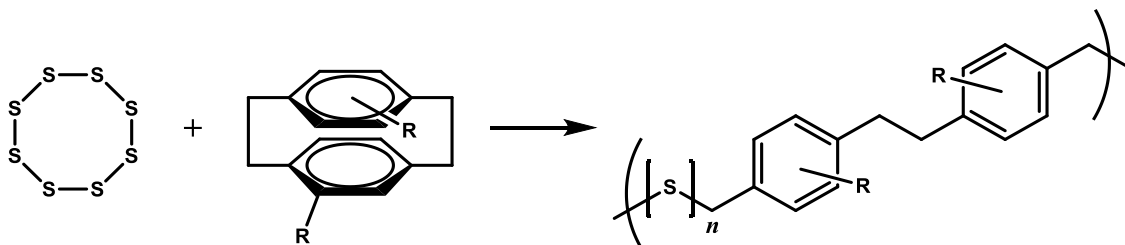


**Figure 1.4.6** Desired sulfur/paracyclophane polymer. R= H, Cl.



## 1.5 References

1. (a) May, S. W., *Current Opinion in Biotechnology* **1999**, *10* (4), 370-375; (b) May, S. W.; Padgett, S. R., *Nat Biotech* **1983**, *1* (8), 677-686.
2. Biosensor. In *Encyclopedia of Microfluidics and Nanofluidics*, Li, D., Ed. Springer US: 2008; p 106.
3. Biofuel Cell. In *Encyclopedia of Microfluidics and Nanofluidics*, Li, D., Ed. Springer US: 2008; p 66.
4. Borisov, S. M.; Wolfbeis, O. S., *Chemical Reviews* **2008**, *108* (2), 423-461.
5. Vashist, S. K.; Vashist, P., *Journal of Sensors* **2011**, *2011*, 13.
6. Danielsson, B., *Journal of Biotechnology* **1990**, *15* (3), 187-200.
7. Su, L.; Jia, W.; Hou, C.; Lei, Y., *Biosensors and Bioelectronics* **2011**, *26* (5), 1788-1799.
8. Ricci, F.; Adornetto, G.; Paleschi, G., *Electrochimica Acta* **2012**, *84* (0), 74-83.
9. Sassolas, A.; Leca-Bouvier, B. D.; Blum, L. J., *Chemical Reviews* **2008**, *108* (1), 109-139.
10. Turner, A. P. F., *Chemical Society Reviews* **2013**, *42* (8), 3184-3196.
11. Grieshaber, D.; MacKenzie, R.; Vörös, J.; Reimhult, E., *Sensors (Basel, Switzerland)* **2008**, *8* (3), 1400-1458.
12. Chaubey, A.; Malhotra, B. D., *Biosensors and Bioelectronics* **2002**, *17* (6-7), 441-456.
13. Calabrese Barton, S.; Gallaway, J.; Atanassov, P., *Chemical Reviews* **2004**, *104* (10), 4867-4886.
14. Minter, S. D.; Liaw, B. Y.; Cooney, M. J., *Current Opinion in Biotechnology* **2007**, *18* (3), 228-234.
15. Salgado, A. M.; Folly, R. O. M.; Valdman, B.; Valero, F., *Biotechnology Techniques* **1998**, *12* (4), 305-307.
16. Yoo, E.-H.; Lee, S.-Y., *Sensors* **2010**, *10* (5), 4558-4576.
17. Palmore, G. T. R.; Kim, H.-H., *Journal of Electroanalytical Chemistry* **1999**, *464* (1), 110-117.

18. Mano, N.; Kim, H.-H.; Heller, A., *The Journal of Physical Chemistry B* **2002**, *106* (34), 8842-8848.
19. Wang, J., *Chemical Reviews* **2008**, *108* (2), 814-825.
20. Willner, I.; Yan, Y. M.; Willner, B.; Tel-Vered, R., *Fuel Cells* **2009**, *9* (1), 7-24.
21. *National Diabetes Statistics Report* **2014**.
22. Polsky, R.; Brozik, S. M.; Xiao, X.; Holland, J. T.; Webster, J. G., Electrical "Wiring" of Enzymes. In *Wiley Encyclopedia of Electrical and Electronics Engineering*, John Wiley & Sons, Inc.: 1999.
23. Karyakin, A. A.; Gitelmacher, O. V.; Karyakina, E. E., *Analytical Chemistry* **1995**, *67* (14), 2419-2423.
24. Karyakin, A. A.; Kotel'nikova, E. A.; Lukachova, L. V.; Karyakina, E. E.; Wang, J., *Analytical Chemistry* **2002**, *74* (7), 1597-1603.
25. Ricci, F.; Palleschi, G., *Biosensors and Bioelectronics* **2005**, *21* (3), 389-407.
26. Schofield, C. J.; Ratcliffe, P. J., *Nat Rev Mol Cell Biol* **2004**, *5* (5), 343-354.
27. Palmisano, F.; Zambonin, P. G., *Analytical Chemistry* **1993**, *65* (19), 2690-2692.
28. Yuan, C.-J.; Hsu, C.-L.; Wang, S.-C.; Chang, K.-S., *Electroanalysis* **2005**, *17* (24), 2239-2245.
29. Rahman, M. A.; Lee, K.-S.; Park, D.-S.; Won, M.-S.; Shim, Y.-B., *Biosensors and Bioelectronics* **2008**, *23* (6), 857-864.
30. Scheller, F. W.; Schubert, F.; Neumann, B.; Pfeiffer, D.; Hintsche, R.; Dransfeld, I.; Wollenberger, U.; Renneberg, R.; Warsinke, A.; Johansson, G.; Skoog, M.; Yang, X.; Bogdanovskaya, V.; Bückmann, A.; Zaitsev, S. Y., *Biosensors and Bioelectronics* **1991**, *6* (3), 245-253.
31. Zhang, W.; Li, G., *Analytical Sciences* **2004**, *20* (4), 603-609.
32. Palmisano, F.; Zambonin, P. G.; Centonze, D.; Quinto, M., *Analytical Chemistry* **2002**, *74* (23), 5913-5918.
33. Zafar, M. N.; Safina, G.; Ludwig, R.; Gorton, L., *Analytical Biochemistry* **2012**, *425* (1), 36-42.
34. Ghindilis, A. L.; Atanasov, P.; Wilkins, E., *Electroanalysis* **1997**, *9* (9), 661-674.
35. Meredith, M. T.; Minson, M.; Hickey, D.; Artyushkova, K.; Glatzhofer, D. T.; Minter, S. D., *ACS Catalysis* **2011**, *1* (12), 1683-1690.

36. Falk, M.; Blum, Z.; Shleev, S., *Electrochimica Acta* **2012**, 82 (0), 191-202.
37. Liang, B.; Guo, X.; Fang, L.; Hu, Y.; Yang, G.; Zhu, Q.; Wei, J.; Ye, X., *Electrochemistry Communications* **2015**, 50 (0), 1-5.
38. Wu, Y.; Hu, S., *Microchim Acta* **2007**, 159 (1-2), 1-17.
39. Bankar, S. B.; Bule, M. V.; Singhal, R. S.; Ananthanarayan, L., *Biotechnology Advances* **2009**, 27 (4), 489-501.
40. Luckarift, H. R.; Ivnitski, D.; Rincón, R.; Atanassov, P.; Johnson, G. R., *Electroanalysis* **2010**, 22 (7-8), 784-792.
41. Kavanagh, P.; Leech, D., *Physical Chemistry Chemical Physics* **2013**, 15 (14), 4859-4869.
42. Marcus, R. A., *The Journal of Chemical Physics* **1956**, 24 (5), 966-978.
43. Andrieux, C. P.; Savéant, J. M., *Journal of Electroanalytical Chemistry and Interfacial Electrochemistry* **1980**, 111 (2-3), 377-381.
44. Heller, A., *Current Opinion in Chemical Biology* **2006**, 10 (6), 664-672.
45. Degani, Y.; Heller, A., *Journal of the American Chemical Society* **1989**, 111 (6), 2357-2358.
46. Cracknell, J. A.; Vincent, K. A.; Armstrong, F. A., *Chemical Reviews* **2008**, 108 (7), 2439-2461.
47. Barton, S. C.; Kim, H.-H.; Binyamin, G.; Zhang, Y.; Heller, A., *The Journal of Physical Chemistry B* **2001**, 105 (47), 11917-11921.
48. Szamocki, R.; Flexer, V.; Levin, L.; Forchiasin, F.; Calvo, E. J., *Electrochimica Acta* **2009**, 54 (7), 1970-1977.
49. Cardoso, F. P.; Aquino Neto, S.; Crepaldi, L. B.; Nikolaou, S.; Barros, V. P.; De Andrade, A. R., *Journal of The Electrochemical Society* **2014**, 161 (4), F445-F450.
50. Datta, S.; Christena, L. R.; Rajaram, Y., *3 Biotech* **2013**, 3 (1), 1-9.
51. Trevan, M. D., Enzyme Immobilization by Adsorption. In *New Protein Techniques*, Walker, J., Ed. Humana Press: 1988; Vol. 3, pp 481-489.
52. Jesionowski, T.; Zdarta, J.; Krajewska, B., *Adsorption* **2014**, 20 (5-6), 801-821.
53. Nelson, J. M.; Griffin, E. G., *Journal of the American Chemical Society* **1916**, 38 (5), 1109-1115.

54. Mateo, C.; Abian, O.; Fernandez-Lafuente, R.; Guisan, J. M., *Biotechnology and Bioengineering* **2000**, *68* (1), 98-105.
55. Zhang, S.; Wang, N.; Niu, Y.; Sun, C., *Sensors and Actuators B: Chemical* **2005**, *109* (2), 367-374.
56. Lahari, C.; Jasti, L. S.; Fadnavis, N. W.; Sontakke, K.; Ingavle, G.; Deokar, S.; Ponrathnam, S., *Langmuir* **2010**, *26* (2), 1096-1106.
57. Sammond, D. W.; Yarbrough, J. M.; Mansfield, E.; Bomble, Y. J.; Hobdey, S. E.; Decker, S. R.; Taylor, L. E.; Resch, M. G.; Bozell, J. J.; Himmel, M. E.; Vinzant, T. B.; Crowley, M. F., *Journal of Biological Chemistry* **2014**, *289* (30), 20960-20969.
58. Kotov, N. A., *Nanostructured Materials* **1999**, *12* (5-8), 789-796.
59. Trevan, M. D., Enzyme Immobilization by Covalent Bonding. In *New Protein Techniques*, Walker, J., Ed. Humana Press: 1988; Vol. 3, pp 495-510.
60. López-Gallego, F.; Betancor, L.; Mateo, C.; Hidalgo, A.; Alonso-Morales, N.; Dellamora-Ortiz, G.; Guisán, J. M.; Fernández-Lafuente, R., *Journal of Biotechnology* **2005**, *119* (1), 70-75.
61. Brena, B.; González-Pombo, P.; Batista-Viera, F., Immobilization of Enzymes: A Literature Survey. In *Immobilization of Enzymes and Cells*, Guisan, J. M., Ed. Humana Press: 2013; Vol. 1051, pp 15-31.
62. Schnapp, J.; Shalitin, Y., *Biochemical and Biophysical Research Communications* **1976**, *70* (1), 8-14.
63. Trevan, M. D., Enzyme Immobilization by Entrapment. In *New Protein Techniques*, Walker, J., Ed. Humana Press: 1988; Vol. 3, pp 491-494.
64. Merchant, S. A.; Glatzhofer, D. T.; Schmidtke, D. W., *Langmuir* **2007**, *23* (22), 11295-11302.
65. Mariani, A. M.; Natoli, M. E.; Kofinas, P., *Biotechnology and Bioengineering* **2013**, *110* (11), 2994-3002.
66. Veronese, F. M.; Mammucari, C.; Schiavon, F.; Schiavon, O.; Lora, S.; Secundo, F.; Chilin, A.; Guiotto, A., *Il Farmaco* **2001**, *56* (8), 541-547.
67. Hanson, J. A.; Duderstadt, K.; Watkins, L. P.; Bhattacharyya, S.; Brokaw, J.; Chu, J.-W.; Yang, H., *Proceedings of the National Academy of Sciences* **2007**, *104* (46), 18055-18060.
68. Merchant, S. A.; Meredith, M. T.; Tran, T. O.; Brunski, D. B.; Johnson, M. B.; Glatzhofer, D. T.; Schmidtke, D. W., *The Journal of Physical Chemistry C* **2010**, *114* (26), 11627-11634.

69. Bunte, C.; Prucker, O.; König, T.; Rühle, J., *Langmuir* **2010**, 26 (8), 6019-6027.
70. Avnir, D.; Braun, S.; Lev, O.; Ottolenghi, M., *Chemistry of Materials* **1994**, 6 (10), 1605-1614.
71. Ohara, T. J.; Rajagopalan, R.; Heller, A., *Analytical Chemistry* **1993**, 65 (23), 3512-3517.
72. Sirkar, K.; Pishko, M. V., *Analytical Chemistry* **1998**, 70 (14), 2888-2894.
73. Bickerstaff, G., Jr., Immobilization of Enzymes and Cells. In *Immobilization of Enzymes and Cells*, Bickerstaff, G., Ed. Humana Press: 1997; Vol. 1, pp 1-11.
74. Sassolas, A.; Blum, L. J.; Leca-Bouvier, B. D., *Biotechnology Advances* **2012**, 30 (3), 489-511.
75. Krajewska, B., *Enzyme and Microbial Technology* **2004**, 35 (2-3), 126-139.
76. Ariga, K.; Ji, Q.; Hill, J., Enzyme-Encapsulated Layer-by-Layer Assemblies: Current Status and Challenges Toward Ultimate Nanodevices. In *Modern Techniques for Nano- and Microreactors/-reactions*, Caruso, F., Ed. Springer Berlin Heidelberg: 2010; Vol. 229, pp 51-87.
77. Dammel, R., *Diazonaphthoquinone-Based Resists*  
SPIE - The International Society for Optical Engineering: Bellingham, Washington, 1993.
78. Reiser, A.; Huang, J. P.; He, X.; Yeh, T. F.; Jha, S.; Shih, H. Y.; Kim, M. S.; Han, Y. K.; Yan, K., *European Polymer Journal* **2002**, 38 (4), 619-629.
79. Vollenbroek, F.; Spiertz, E., Photoresist systems for microlithography. In *Electronic Applications*, Springer Berlin Heidelberg: 1988; Vol. 84, pp 85-111.
80. Ceysens, F.; Puers, R., SU-8 Photoresist. In *Encyclopedia of Nanotechnology*, Bhushan, B., Ed. Springer Netherlands: 2012; pp 2530-2543.
81. Roy, D.; Basu, P. K.; Raghunathan, P.; Eswaran, S. V., *Magnetic Resonance in Chemistry* **2003**, 41 (9), 671-678.
82. Dreiling, A.; König, S., *Rapid Communications in Mass Spectrometry* **2013**, 27 (16), 1887-1890.
83. Suraniti, E.; Studer, V.; Sojic, N.; Mano, N., *Analytical Chemistry* **2011**, 83 (7), 2824-2828.
84. Bunte, C.; Rühle, J., *Macromolecular Rapid Communications* **2009**, 30 (21), 1817-1822.

85. Langmuir, I., *Transactions of the Faraday Society* **1922**, 17 (0), 607-620.
86. Blodgett, K. B., *Journal of the American Chemical Society* **1935**, 57 (6), 1007-1022.
87. Decher, G.; Hong, J. D.; Schmitt, J., *Thin Solid Films* **1992**, 210–211, Part 2 (0), 831-835.
88. Hoogeveen, N. G.; Cohen Stuart, M. A.; Fler, G. J.; Böhmer, M. R., *Langmuir* **1996**, 12 (15), 3675-3681.
89. Sukhishvili, S. A.; Kharlampieva, E.; Izumrudov, V., *Macromolecules* **2006**, 39 (26), 8873-8881.
90. Cleaves, H., II, Isoelectric Point. In *Encyclopedia of Astrobiology*, Gargaud, M.; Amils, R.; Quintanilla, J.; Cleaves, H., II; Irvine, W.; Pinti, D.; Viso, M., Eds. Springer Berlin Heidelberg: 2011; pp 858-858.
91. Lvov, Y.; Ariga, K.; Kunitake, T., *Chemistry Letters* **1994**, 23 (12), 2323-2326.
92. Lvov, Y.; Ariga, K.; Ichinose, I.; Kunitake, T., *Journal of the American Chemical Society* **1995**, 117 (22), 6117-6123.
93. Liu, D.; Hu, N., *Sensors and Actuators B: Chemical* **2011**, 156 (2), 645-650.
94. Campos, P. P.; Moraes, M. L.; Volpati, D.; Miranda, P. B.; Oliveira, O. N.; Ferreira, M., *ACS Applied Materials & Interfaces* **2014**, 6 (14), 11657-11664.
95. Du, Y.; Chen, C.; Yin, J.; Li, B.; Zhou, M.; Dong, S.; Wang, E., *Analytical Chemistry* **2010**, 82 (4), 1556-1563.
96. Liu, J.; Qin, Y.; Li, D.; Wang, T.; Liu, Y.; Wang, J.; Wang, E., *Biosensors and Bioelectronics* **2013**, 41 (0), 436-441.
97. Arwin, H., *Thin Solid Films* **2000**, 377–378 (0), 48-56.
98. Marx, K. A., *Biomacromolecules* **2003**, 4 (5), 1099-1120.
99. Merchant, S. A.; Tran, T. O.; Meredith, M. T.; Cline, T. C.; Glatzhofer, D. T.; Schmidtke, D. W., *Langmuir* **2009**, 25 (13), 7736-7742.
100. Meredith, M. T.; Hickey, D. P.; Redemann, J. P.; Schmidtke, D. W.; Glatzhofer, D. T., *Electrochimica Acta* **2013**, 92 (0), 226-235.
101. Meredith, M. T.; Kao, D.-Y.; Hickey, D.; Schmidtke, D. W.; Glatzhofer, D. T., *Journal of The Electrochemical Society* **2011**, 158 (2), B166-B174.
102. Hickey, D. P.; Halmes, A. J.; Schmidtke, D. W.; Glatzhofer, D. T., *Electrochimica Acta* **2014**, 149 (0), 252-257.

103. Hu, L. Polyamine Based Polymer Electrolyte Modification and Performance. University of Oklahoma, 2005.
104. Kadam, R. Study of Lithium Triflate as an Electrolyte in Mixed Ether-Amine Solvents and the Use of Electron Paramagnetic Resonance Spectroscopy to Study Dielectric Properties of Materials. University of Oklahoma, 2011.
105. DeLuca, J. L.; Hickey, D. P.; Bamper, D. A.; Glatzhofer, D. T.; Johnson, M. B.; Schmidtke, D. W., *ChemPhysChem* **2013**, *14* (10), 2149-2158.
106. Fairbrother, F.; Gee, G.; Merrall, G. T., *Journal of Polymer Science* **1955**, *16* (82), 459-469.
107. Tobolsky, A. V., *Journal of Polymer Science Part C: Polymer Symposia* **1966**, *12* (1), 71-78.
108. Currell, B. R.; Williams, A. J., *Thermochimica Acta* **1974**, *9* (3), 255-259.
109. Chung, W. J.; Griebel, J. J.; Kim, E. T.; Yoon, H.; Simmonds, A. G.; Ji, H. J.; Dirlam, P. T.; Glass, R. S.; Wie, J. J.; Nguyen, N. A.; Guralnick, B. W.; Park, J.; SomogyiÁrpád; Theato, P.; Mackay, M. E.; Sung, Y.-E.; Char, K.; Pyun, J., *Nat Chem* **2013**, *5* (6), 518-524.
110. Griebel, J. J.; Li, G.; Glass, R. S.; Char, K.; Pyun, J., *Journal of Polymer Science Part A: Polymer Chemistry* **2015**, *53* (2), 173-177.
111. Simmonds, A. G.; Griebel, J. J.; Park, J.; Kim, K. R.; Chung, W. J.; Oleshko, V. P.; Kim, J.; Kim, E. T.; Glass, R. S.; Soles, C. L.; Sung, Y.-E.; Char, K.; Pyun, J., *ACS Macro Letters* **2014**, *3* (3), 229-232.
112. Griebel, J. J.; Namnabat, S.; Kim, E. T.; Himmelhuber, R.; Moronta, D. H.; Chung, W. J.; Simmonds, A. G.; Kim, K.-J.; van der Laan, J.; Nguyen, N. A.; Dereniak, E. L.; Mackay, M. E.; Char, K.; Glass, R. S.; Norwood, R. A.; Pyun, J., *Advanced Materials* **2014**, *26* (19), 3014-3018.
113. Zhang, S.S., *Journal of Power Sources* **2013**, *231* (0), 153-162.
114. Hickey, D. Ferrocene-Modified Linear Poly(ethylenimine) Bioelectrode Materials for Use in Glucose/O<sub>2</sub> Biofuel Cells. University of Oklahoma, 2014

## **Chapter 2. Photocurable Redox Polymers Based on Ferrocene-Modified Linear Poly(ethylenimine)**

---

### **2.1 Introduction**

Photolithography is a technique widely used in the construction of patternable, well defined polymer films.<sup>1,2</sup> By masking certain areas of the polymer and irradiating the exposed area, distinct patterns can be designed to fit the need of the application. These patternable materials, commonly referred to as photoresists, behave in one of two ways: (1) the exposed area of the polymer is removed upon washing (positive photoresist)<sup>3,4</sup> or (2) the exposed area of the polymer is crosslinked into an insoluble film (negative photoresist).<sup>5,6,7</sup> While photolithography has been used in a variety of applications, one function that is lacking significant study is its usage in the fabrication of enzymatic biosensors. The main setback of such a system arises from the irradiation process. Polymers must be subjected to some form of irradiation—usually UV or NIR—to allow for efficient crosslinking to occur. However, this can cause significant damage to the enzyme being employed.<sup>8,9,10,11</sup>

Since our group has interests in redox active polymers for glucose biosensors and biofuel cells,<sup>12,13,14,15</sup> being able to control the size and shape of the film is of great value. Three direct applications of photocurable redox polymers are: increasing the surface area of a film,<sup>16</sup> coating the inside of micro-channels for a ‘lab on a chip,’<sup>17</sup> and creating interdigitated arrays.<sup>18,19</sup> Having a material that could be crosslinked into a forest of micro-scaled ‘dots’ would allow for increased surface area. Since the diffusion of electrons through the film is typically faster than the diffusion of substrate into the film,<sup>20,21,22</sup> it is unlikely that a molecule of substrate would get to the interior of a film



without first being oxidized. Therefore, one can imagine the majority of the redox reactions happening at or near the surface of the film. Increasing the surface area would allow for a greater amount of substrate to be available for catalysis near the film's surface, which would, in turn, increase current output.

For a microfluidic fuel cell, microchannels for a stream of fuel to flow through are needed.<sup>23,24</sup> Fabrication of a miniaturized enzymatic biofuel cell would require coating the sides of these channels with well-defined patterns of polymer and enzyme. Chemically crosslinked films do not typically have controllable reactions that allow for the assembly of well-defined patterns. However, using a photoresist would allow for two sides of a mold to be coated with excess polymer followed by controlled crosslinking in a certain area. Masking specific areas of the deposited photoresist, irradiating the exposed area, and then washing away excess material would allow for the development of the two sides of a microchannel that could then be connected together.

The third application for such a system is the development of interdigitated arrays. In an electrochemical cell, having the electrodes separated causes an inherent drop in voltage.<sup>25,26</sup> Ions in the system must be able to freely flow for the cell to work, and as they move, there is resistance from surroundings. This added resistance, however small, will inherently result in a drop in the voltage. To overcome this problem, the electrodes should be placed as close to one another as possible. An example of such a system would be the fabrication of an interdigitated array. By coating anodic and cathodic redox polymers in close proximity, the aforementioned voltage drop can be minimized. Accomplishing this by a simple chemical crosslinker would be challenging to keep well

defined shapes. Using photolithography, it would be possible to apply a polymer, mask a defined pattern, irradiate, and wash away uncured material.

In this study, we describe the development of photocrosslinkable polymers based on ferrocene and linear poly(ethylenimine) (LPEI) and the effect of UV irradiation on the activity of glucose oxidase (GOX). The use of in depth electrochemical characterization as a tool to probe the relationship between GOX stability and electrochemical connectivity of the redox active films is discussed. The first usage of an alkylazide for the photogeneration of nitrenes for photochemical crosslinking is examined and discussed.

## **2.2 Results and Discussion**

### *2.2.1 Development of the Synthetic Methodology for Redox-Active Photoresists*

As mentioned above, there are multiple crosslinking methods that can be used for the development of negative photoresists. The two types of crosslinking that were investigated as possible methods for fabricating LPEI bioanode photoresists were [2 +2] cycloadditions of cinnamoyl functional groups, and the coupling of allyl groups based on previous research by Hu<sup>27</sup> and Kadam.<sup>28</sup>

#### *Cinnamoyl-modified LPEI*

Poly(vinylcinnamate) has long been known to crosslink upon UV exposure.<sup>29,30</sup> It was therefore envisioned that the inclusion of cinnamide groups onto the backbone of LPEI would result in a photocrosslinkable polymer for usage in bioelectrode fabrication. **Figure 2.2.1** shows the synthetic pathway for the development of cinnamoyl-modified LPEI (LPCEI).

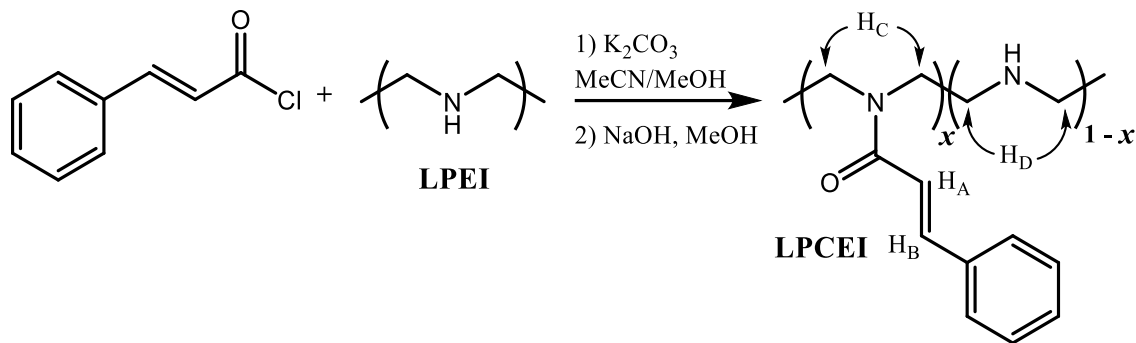


**Figure 2.2.1:** Synthetic route and structure of LPCEI.

The degree of cinnamide substitution was estimated by first setting the integration of the vinyl proton  $H_A$  ( $\delta$  6.61) to one, and the remaining peaks were integrated relatively. The four proton environments of the cinnamoyl substituted repeat units have a higher chemical shift ( $H_C$ ,  $\delta$  5.27) than the unsubstituted portion ( $H_D$ ,  $\delta$  2.95) in the  $^1\text{H-NMR}$  spectrum; therefore, the percent substitution can be determined by the equation:

$$\text{Equation 2.1: } \% \text{ cinnamide} = \frac{H_C}{H_C + H_D} * 100\%$$

Attempts to synthesize highly substituted polymers resulted in precipitation from the solution, presumably from an excess of positive charge that quickly builds up on the polymer. The addition of cinnamoyl chloride to LPEI causes an immediate reaction to occur, even at low concentrations. Even with the inclusion of potassium carbonate, LPEI could only be substituted with ~35% cinnamoyl groups. Films of LPCEI-35% were cast on glass slides, irradiated (300 and 350 nm) for increasing amounts of time, and washed with water and methanol to determine if the polymer had been rendered insoluble. Even after twenty-four hours of irradiation LPCEI films readily dissolved into solution, revealing them to be poor negative photoresists.

*Allyl- and ferrocene-modified LPEI*

The allylation and ferrocenyl-alkylation of LPEI have each been separately achieved in previous works from our group.<sup>27,13</sup> Based on the successful implementation of poly(ethylenimine-*co*-allylethylenimine) (LPAEI) as a radically crosslinkable polymer,<sup>27,28</sup> we envisioned incorporating allyl groups onto the backbone of ferrocenylpropyl-modified LPEI (Fc-C<sub>3</sub>-LPEI) for usage as a redox-active photoresist. **Figure 2.2.2** depicts the pathway developed for the synthesis of ferrocenylpropyl-modified linear poly(ethylenimine-*co*-allylethylenimine) (Fc-C<sub>3</sub>-LPAEI).

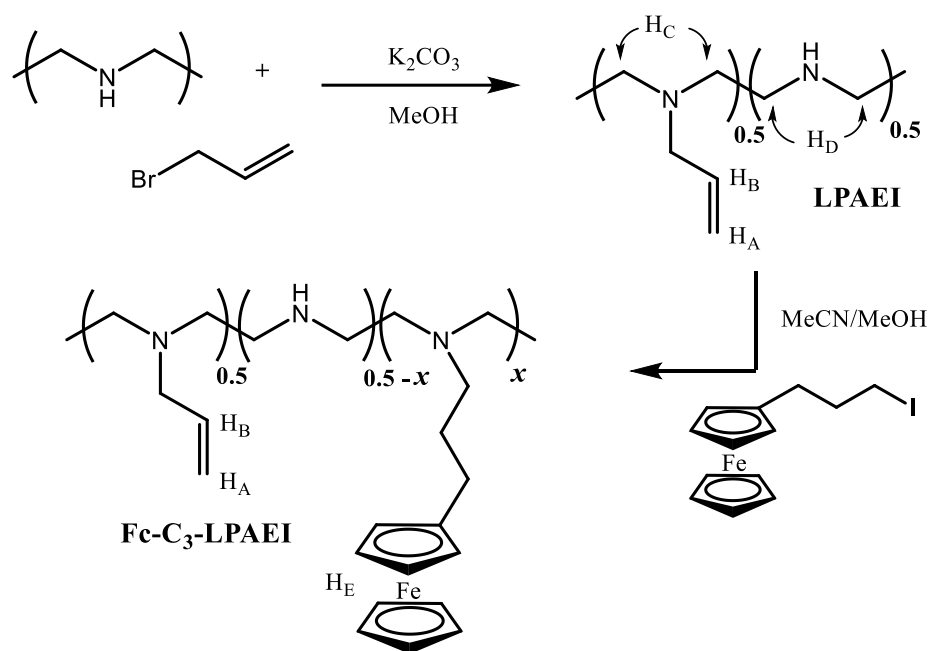


**Figure 2.2.2:** Summary of synthetic routes of LPAEI and Fc-C<sub>3</sub>-LPAEI.

The degree of allyl substitution was estimated by first setting the integration of the vinylic proton H<sub>A</sub> ( $\delta$  5.17) to two, and the remaining peaks were integrated relatively. Therefore, the substituted polymer methylene backbone signals (H<sub>C</sub>) should integrate to four in the <sup>1</sup>H-NMR. However, the chemical shifts for the protons of the substituted and unsubstituted polymer backbone overlap ( $\delta$  2.31 – 2.85) and are not readily distinguishable. Since four of the protons in the total integrated backbone signal will

always belong to the allyl substituted repeat units, the percent allyl substitution can be determined by the equation:

$$\text{Equation 2.2: } \% \text{ allylation} = \frac{4}{H_C + H_D} * 100$$

All polymers were synthesized with fifty percent of the LPEI backbone containing allyl groups. Therefore, for the remainder of this work, LPAEI will refer to LPEI that is fifty percent allylated. Further modification of LPAEI with ferrocene becomes more difficult to get an accurate percent substitution by the method previously described. Therefore, the percent substitution of ferrocene on Fc-C<sub>3</sub>-LPAEI was estimated by the ratio of ferrocene protons H<sub>E</sub> (δ 4.01 – 4.22) to the allyl vinyl protons H<sub>A</sub> (δ 5.17). The polymer LPAEI was always set relative to the triplet at δ 5.17 being integrated to two hydrogens, and the same relative peak integration was also used for Fc-C<sub>3</sub>-LPAEI. If Fc-C<sub>3</sub>-LPAEI was 50% allylated and 50% modified with ferrocene, the ratios for H<sub>B</sub> and H<sub>E</sub> would be:

$$50\% \text{ allyl} : 50\% \text{ Fc}$$

$$H_B : H_E$$

$$2 \text{ allyl-H} : 9 \text{ Fc-H}$$

However, if the polymer is less than 50% substituted with ferrocene, the integration for H<sub>E</sub> will be lower. Since all the polymers synthesized were always 50% allylated and set relative to H<sub>B</sub>, it is simple to set up an algebraic expression to solve for the percent ferrocene substitution relative to 50% substitution:

$$\frac{9 \text{ Fc-H}}{H_E} = \frac{50\% \text{ Fc}}{\% \text{ Fc}}$$

$$\text{Equation 2.3: } \text{Fc}\% = \left( \frac{50\%}{9 \text{ Fc-H}} \right) * H_E$$

Redox polymers were substituted with 20 – 25% ferrocene for the determination of tolerance of Fc-C<sub>3</sub>-LPAEI towards radicals. The radical initiators chosen were potassium persulfate (K<sub>2</sub>S<sub>2</sub>O<sub>8</sub>), benzoyl peroxide (BPO), and 2,2'-azobis(2-methylpropionamide) dihydrochloride (V50). Both K<sub>2</sub>S<sub>2</sub>O<sub>8</sub> and BPO resulted in the immediate oxidation of ferrocene as determined by the rapid change in color from orange to green. Diazo compound V50 did not immediately react with ferrocene and was chosen for further irradiation studies.

Films containing Fc-C<sub>3</sub>-LPAEI (25% ferrocene) and V50 were cast onto glass slides, irradiated for increasing amounts of time, and washed with water and methanol to determine if the polymer had been rendered insoluble. Films were inspected under a microscope, and were qualitatively determined to exhibit more swelling and less dissolution with increasing amounts of UV irradiation. However, the length of irradiation needed to achieve coherent films was 24 – 48 hours. Using UV-Vis spectroscopy, ferrocene was shown to have a much higher molar absorptivity (~325 nm) that overlapped with the very weak absorption of V50 (~375 nm). Therefore, redox polymers were substituted with five percent ferrocene to allow for a greater amount of V50 to become excited and to minimize side reactions between the photogenerated radicals and the metal center. Having a majority of the polymer substituted with photocrosslinkable groups allows for a greater chance of crosslinking rather than ferrocene degradation. Films fabricated using the new redox polymer with lower ferrocene substitution were qualitatively determined to crosslink in less than twenty-four hours. A more detailed exploration of the electrochemical properties of these materials is discussed in **Section**

**2.2.3.** For the remainder of this work, Fc-C<sub>3</sub>-LPAEI refers to the LPEI redox polymer substituted with fifty percent allyl groups and five percent ferrocene.

### 2.2.2 Proposed Mechanisms of Fc-C<sub>3</sub>-LPAEI Crosslinking

The incorporation of allyl side groups along the backbone of LPEI led us to envision two methods of crosslinking: radical coupling or aziridine formation. To investigate the viability of both methods, Fc-C<sub>3</sub>-LPAEI was irradiated for varying amounts of time in the presence of either radical initiator 2,2'-azobis(2-methylpropionamidine) dihydrochloride (V50) (**1**) or nitrene crosslinker 1,2-bis(2-azidoethoxy)ethane (TEG-N<sub>3</sub>) (**2**) (**Figure 2.2.3**). **Figure 2.2.4** shows the proposed mechanism of crosslinking associated with each system.

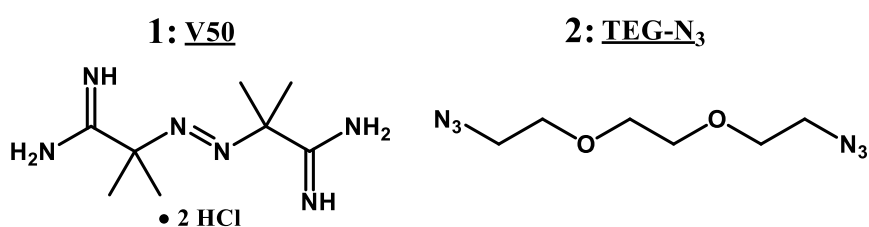


**Figure 2.2.3:** Molecular structures of V50 (**1**) and TEG-N<sub>3</sub> (**2**).

Photolysis of V50 generates two equivalent tertiary radicals that are stabilized by the adjacent imine group. Hu has previously described the radical crosslinking of LPAEI as occurring via allylic hydrogen abstraction, followed by radical coupling between polymer strands.<sup>27</sup> One possible coupling is shown in **Figure 2.2.4A** where the secondary radicals are the reactive species. The self-coupling of primary radicals or the cross-coupling of primary and secondary radicals are also feasible methods of crosslinking.

The other method of crosslinking is the photolysis of TEG-N<sub>3</sub> to generate a dinitrene species (**3**) for aziridine formation to occur (**Figure 2.2.4B**). However, it has been previously reported that alkylazides will undergo rearrangement in solution to

generate the corresponding imine (**4**) (**Figure 2.2.5**).<sup>31,32</sup> While there is debate on the existence of a nitrene intermediate in this rearrangement, crosslinking via aziridine formation would not be possible if the photolysis of TEG-N<sub>3</sub> were to result in the diimine (**4**). However, it may be possible for the films to crosslink via nucleophilic attack from the nitrogen backbones onto the imine carbons. LPEI is known to react with aldehydes,<sup>33,12</sup> so the reaction with diimine **4** is feasible.

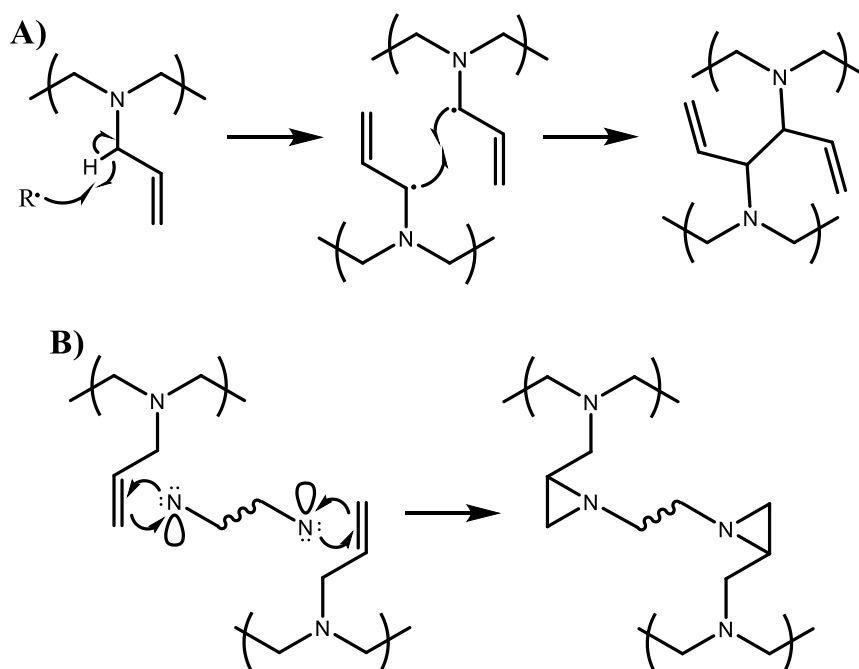


**Figure 2.2.4:** Proposed mechanisms for the crosslinking of LPAEI: (A) radical coupling, and (B) aziridine formation.

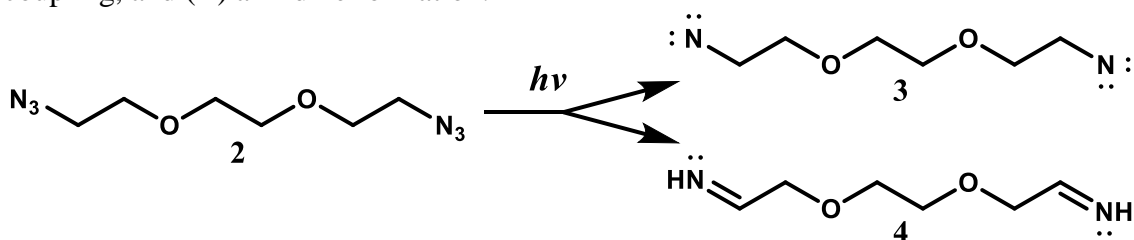


**Figure 2.2.5:** Possible products resulting from the photolysis of TEG-N<sub>3</sub>: desired dinitrene (**3**) and undesired diimine (**4**).



To determine what type of crosslinking may occur, TEG-N<sub>3</sub> (25 mol%) was mixed with both LPAEI (50% allylated) and LPEI, and films were cast onto glass plates. Films were irradiated for twenty-four hours and then rinsed with water and methanol to determine if crosslinking occurred. The LPEI/TEG-N<sub>3</sub> mixture dissolved directly into solution after irradiation, which indicates the films did not crosslink. The LPAEI/TEG-N<sub>3</sub> mixture formed a cohesive film on the surface that swelled in response to water, but did not dissolve even after several weeks immersed in water. It is evident that the allyl groups are needed for crosslinking to occur, which suggests a nitrene intermediate occurs during the photolysis of TEG-N<sub>3</sub>.

### 2.2.3 *Cyclic Voltammetric Studies of Photochemically Crosslinked Films*

Photochemical crosslinking of biosensor films is a balance between redox mediator response and enzymatic stability. The amount of irradiation required to form stable films must be juxtaposed against the loss of enzymatic activity that results from protein denaturation. An ideal system is one where maximum crosslinking is achieved from a minimum amount of irradiation. With this in mind, the mole percentage of each crosslinking agent was increased until the electrochemical response decreased under identical irradiation conditions. Fc-C<sub>3</sub>-LPAEI/GOX films were also fabricated without crosslinker to act as a control and baseline.

**Figure 2.2.6** compares the peak anodic current ( $i_{pa}$ ) from the cyclic voltammograms for Fc-C<sub>3</sub>-LPAEI/GOX films constructed in the presence and absence of an crosslinking agent as a function of irradiation time. It should first be noted that irradiation controls were obtained by coating electrodes with the same mixtures of materials and letting them sit in dark, ambient conditions for the same amount of time.

Whereas the irradiated films in **Figure 2.2.6** formed cohesive films and displayed increasing electrochemical response, the control films that were not subjected to any form of irradiation simply dissolved into solution.

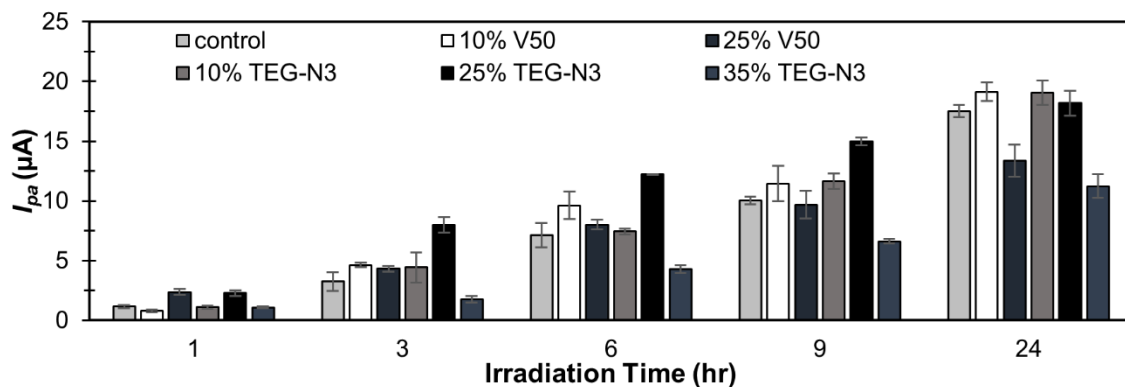


**Figure 2.2.6:** Effect of irradiation time and crosslinking agent on the anodic peak current ( $i_{pa}$ ) of Fc-C<sub>3</sub>-LPAEI/GOX films.

All electrodes were coated with the same amount of polymer to insure a consistent amount of ferrocene between samples. As seen in **Figure 2.2.6**,  $i_{pa}$  increased upon longer exposure to irradiation regardless of the amount or type of crosslinker added. This suggests that the films are becoming more sufficiently crosslinked and forming more cohesive films. As the amount of crosslinking within the film increases, the ferrocene redox units are closer together, which leads to an apparent increase in electrochemical response. Since none of the films reach a maximum peak current followed by a decrease in electrochemical response, it is fair to suggest that the variance in current between systems can be attributed to how well a system is crosslinked. If the initiator were irreversibly damaging the metal center, the film response would not continue to grow with increased irradiation. After 24 hours of irradiation, most of the films have nearly the same current which suggests the upper limit to which films can be crosslinked. While the films are becoming increasingly crosslinked with prolonged UV exposure, the half wave potential ( $E_{1/2}$ ) remained unchanged between all systems. The  $E_{1/2}$  for all films was ca.

0.21 V, which is much lower than previous accounts for chemically crosslinked Fc-C<sub>3</sub>-LPEI.

Surprisingly, the control electrodes showed an increase in electrochemical response with increased irradiation even in the absence of a crosslinking agent (**Figure 2.2.7**). The control electrodes performed nearly the same as the 25% V50 and better than the 35% TEG-N<sub>3</sub> systems (**Figure 2.2.6**). Fc-C<sub>3</sub>-LPAEI can be crosslinked without an added initiator because allylic hydrogens are well known to react with singlet oxygen. It is therefore conceivable that an allylic hydrogen atom is being abstracted by singlet oxygen generated within the photochemical reactor. This could form a terminal hydroperoxide that would homolytically cleave with increased irradiation.<sup>41</sup> Therefore, a portion of all Fc-C<sub>3</sub>-LPAEI/GOX films are being crosslinked by oxygen in the ambient atmosphere.

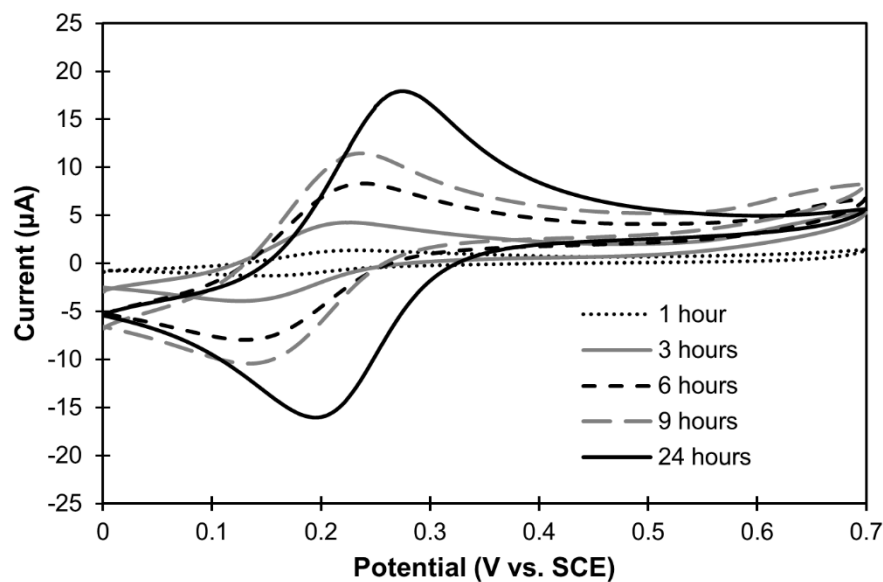


**Figure 2.2.7:** Representative CVs for Fc-C<sub>3</sub>-LPAEI/GOX control films fabricated without an added crosslinking agent. PBS pH 7.4. Scan rate = 50 mV/s.

For the radical initiator, 10% V50 is the optimum amount for successful crosslinking (**Figure 2.2.8A**). Each V50 molecule produces two radicals that will

theoretically result in 20% of the allyl groups being crosslinked; which also means that 30% of the allyl groups remain uncoupled. When the amount of V50 is increased to 25% (**Figure 2.2.8B**)—which would form one radical for every allyl group—the electrochemical response worsens over time when compared to 10% V50. Generating radicals in the presence of ferrocene could oxidize the metal before abstraction of the allylic hydrogen could occur. There are ten times the amount of allyl groups to every ferrocene to keep this possibility at a minimum, but, as the amount of V50 is increased, the probability of ferrocene oxidation occurring also increases. Another potential issue with using a radical initiator is the possibility of it damaging the enzyme. The generation of free radicals in the presence of an enzyme can cause fragmentation of the protein structure which results in a loss of activity. By increasing the amount of initiator present, there is a greater chance of damaging the enzyme instead of initiating allyl coupling. Another possible reason for the lowering in  $i_{pa}$  when changing from 10% to 25% V50 is that the increase in generated radical concentration could result in more self-coupling of V50 radicals rather than allyl hydrogen abstraction.

Even though increased amounts of radical initiator causes problems at prolonged irradiation times, it appears to not be as much of a problem early on. At one hour of irradiation, 25% V50 gives a higher response than 10%, suggesting the increased initiator loading increases the initial amount crosslinking. At three hours irradiation there is almost no difference between 10% and 25% V50, but by six hours 10% V50 is out-performing 25% V50. The difference between the two gets more disparate with further irradiation as the increased concentration of radicals leads to an increase in unwanted side reactions.

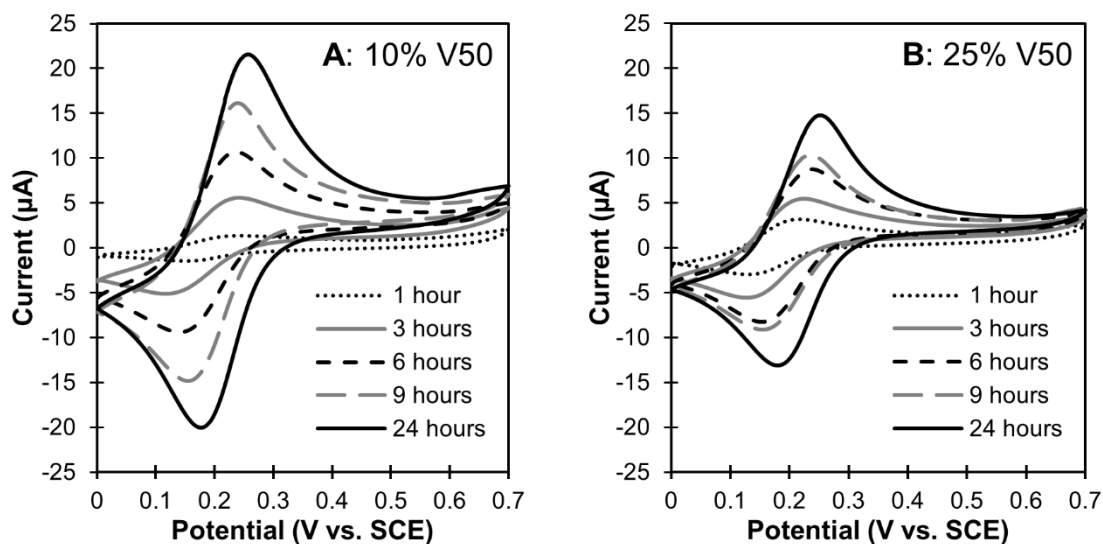


**Figure 2.2.8:** Representative CVs for Fc-C<sub>3</sub>-LPAEI/GOX films fabricated with radical initiator V50: (A) 10 mol% (B) 25 mol%. PBS pH 7.4. Scan rate = 50 mV/s.

Usage of the diazide crosslinker TEG-N<sub>3</sub> proved to be a more effective means to form redox active films than the radical initiator. While the electrochemical results for 10% TEG-N<sub>3</sub> (**Figure 2.2.9A**) were almost identical to that of 10% V50, increasing TEG-N<sub>3</sub> to 25% resulted in an increase in  $i_{pa}$  at nearly all irradiation times (**Figure 2.2.9B**). This suggests the TEG-N<sub>3</sub> crosslinking agent forms more cohesive films at a faster rate than V50. In an attempt to determine if optimal crosslinking could occur in a shorter amount of time, the percentage of TEG-N<sub>3</sub> was increased to 35%.

An increase in crosslinker up to 35% TEG-N<sub>3</sub> resulted in a rather large decrease in  $i_{pa}$  (**Figure 2.2.10**) for all irradiation times. This is likely due to only one nitrene reacting with an allyl group and leaving the other side unattached to an allyl functionality. This would decrease the overall amount of crosslinking within the film since there are more half-crosslinked TEG units around. There is also the possibility of the generated nitrenes coupling to form new diazo bonds.

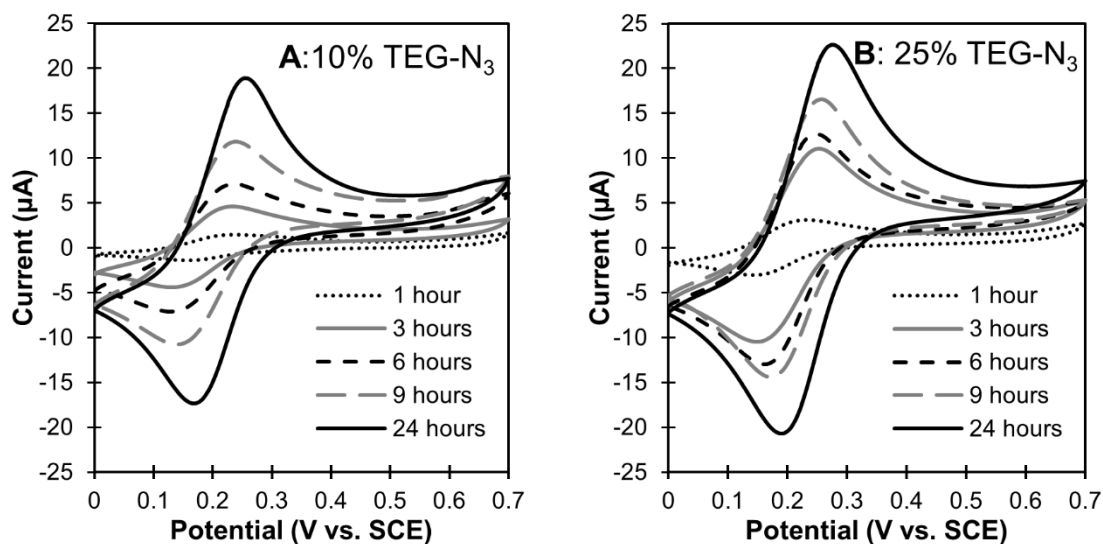


**Figure 2.2.9:** Representative CVs for Fc-C<sub>3</sub>-LPAEI/GOX films fabricated with diazide crosslinker TEG-N<sub>3</sub>: (A) 10 mol% (B) 25 mol%. PBS pH 7.4. Scan rate = 50 mV/s.

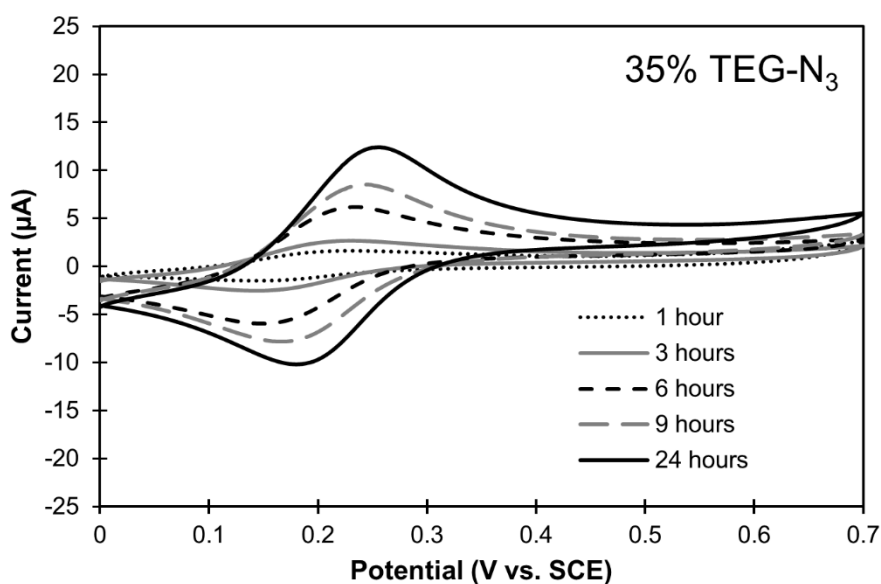


**Figure 2.2.10:** Representative CVs for Fc-C<sub>3</sub>-LPAEI/GOX films fabricated with diazide crosslinker 35 mol% TEG-N<sub>3</sub>. PBS pH 7.4. Scan rate = 50 mV/s.

Films fabricated using 25% TEG-N<sub>3</sub> almost exclusively gave the highest response out of all tested conditions. The notable exceptions were very early and very late irradiation times. At one hour of irradiation, 25% TEG-N<sub>3</sub> and 25% V50 have almost identical anodic peak currents. This again corresponds to the quick initial crosslinking

that occurs before side reactions quench the initiator. Once the films have been subjected to 24 hours of irradiation they reach a maximum similar to the control electrodes from the abundance of singlet oxygen present in the reactor.

#### 2.2.4 Effect of Photochemical Crosslinking on Electron Diffusion

We have previously reported the effect that increased crosslinking has on the relative electron diffusion ( $cD_e^{1/2}$ ) throughout a mediated film in terms of the concentration of the redox species ( $c$ ).<sup>34</sup> Using the Randles-Sevcik equation (**Equation 2.4**) it is possible to calculate the apparent  $cD_e^{1/2}$  for thin films of electroactive polymers from the peak anodic current obtained from the CV spectrum. In **Equation 2.4**,  $i_p$  is the peak anodic current,  $n$  is the number of electrons transferred in a single redox process,  $D$  is the diffusion coefficient of the electroactive species,  $c$  is the concentration of the electroactive species, and  $v$  is the potential scan rate:

$$\text{Equation 2.4: } cD_e^{1/2} = \frac{i_p}{268600n^{3/2}Av^{1/2}}$$

As the films become more tightly crosslinked, there is a higher local concentration of ferrocene per unit volume of the swollen films. Since each film is initially coated with the same amount of redox polymer, they should contain roughly equal amounts of ferrocene within the crosslinked network. An increase in  $cD_e^{1/2}$  will most likely occur if the space between redox sites decreases to such an extent to promote a more efficient flow of electrons. However if the films cannot swell to a high enough degree, the redox mediators could experience restricted motion and not interact with each other efficiently. Since there is no decrease in electrochemical response with increased irradiation, the films are still capable of swelling and effectively transferring electrons, even at maximum crosslinking.

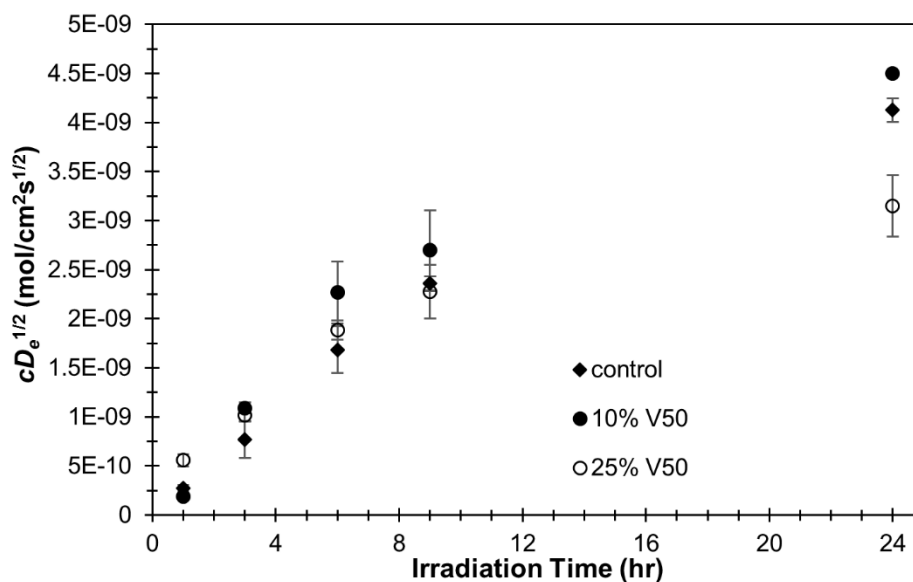


**Figure 2.2.11:** Effect of irradiation time and radical crosslinking agent V50 on  $cD_e^{1/2}$  for Fc-C<sub>3</sub>-LPAEI/GOX films.

**Figure 2.2.11** compares the effect of V50 initiator and irradiation time has on  $cD_e^{1/2}$  for Fc-C<sub>3</sub>-LPAEI/GOX films. There was a continual increase in  $cD_e^{1/2}$  with longer exposure to UV irradiation, and all films had similar electron diffusion up to 9 hours of irradiation. The relative electron diffusion rates for V50 were not drastically different from the control electrodes. In good correlation with **Section 2.2.3**, films crosslinked with 25% V50 do not perform as well as 10% V50, and at 24 hours exposure, they perform even worse than the films fabricated without an added crosslinking agent. This is most likely due to lower crosslinking associated with radical side reactions rather than an over-crosslinked network.

For films constructed using the dinitrene crosslinker, the lowest  $cD_e^{1/2}$  values are for those fabricated with 35% TEG-N<sub>3</sub> (**Figure 2.2.12**). Since these films gave the lowest electron transfer rates at every time point, this is indicative of too many unconnected TEG crosslinks. By far the highest  $cD_e^{1/2}$  values at any given irradiation were those obtained from films constructed with 25% TEG-N<sub>3</sub>. This system is able to quickly and effectively



crosslink the material to allow for increased electron flow throughout the film. These films contain an optimum amount of crosslinker to obtain high electron transfer rates at minimum amount of irradiation. This will be of great importance when looking at mediation of an enzyme.

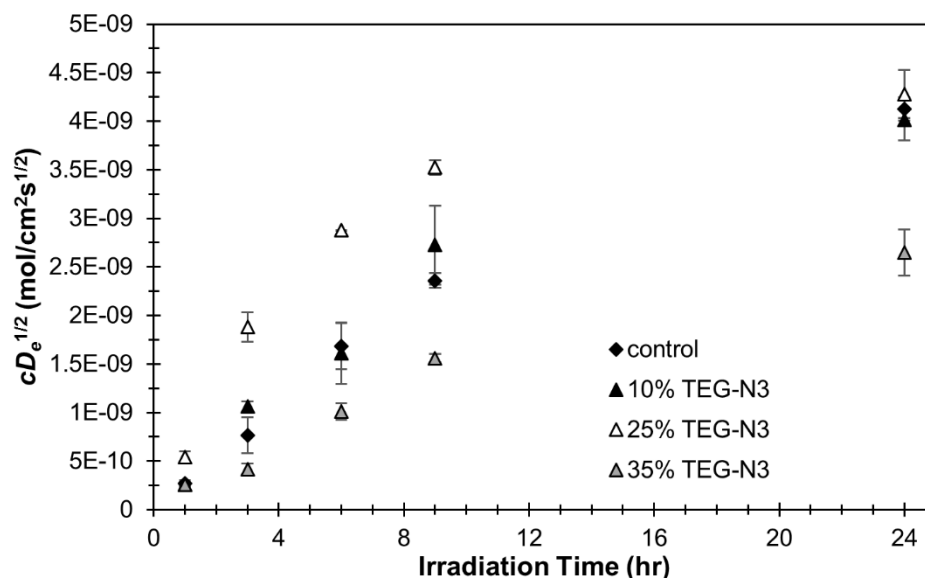


**Figure 2.2.12:** Effect of irradiation time and a quantity of diazide crosslinker TEG-N<sub>3</sub> on  $cD_e^{1/2}$  for Fc-C<sub>3</sub>-LPAEI/GOX films.

Based on the electrochemical characterization of Fc-C<sub>3</sub>-LPAEI/GOX films, the diazide does a better job of crosslinking the polymer into a cohesive film than either a radical initiator or the control. At every interval of irradiation except 24 hours, 25% TEG-N<sub>3</sub> has both a higher  $i_{pa}$  and  $cDe^{1/2}$ . However, electrochemical response of the redox polymer is not always an indication of enzymatic response in a biosensor. Therefore, it is more important to look at glucose response to evaluate how well GOX tolerates extended UV irradiation.

### 2.2.5 Enzymatic Properties of Photochemically Generated Biosensors

To investigate the viability of photocrosslinked Fc-C<sub>3</sub>-LPAEI/GOX films as bioanodes, films were poised at an oxidizing potential (0.25 V) and aliquots of concentrated glucose solution were added to the cell. **Figure 2.2.13A** shows the maximum steady-state current densities ( $J_{max}$ ) for increased irradiation times and varying crosslinkers.  $J_{max}$  is calculated from Michaelis-Menten curves with a maximum value corresponding to saturating glucose concentration (**Figure 2.2.13B**). At one hour of irradiation,  $J_{max}$  is fairly uniform between each system. This suggests the enzyme is still functioning well and small changes in the electrochemical output of the films do not affect the initial performance of the bioanodes.

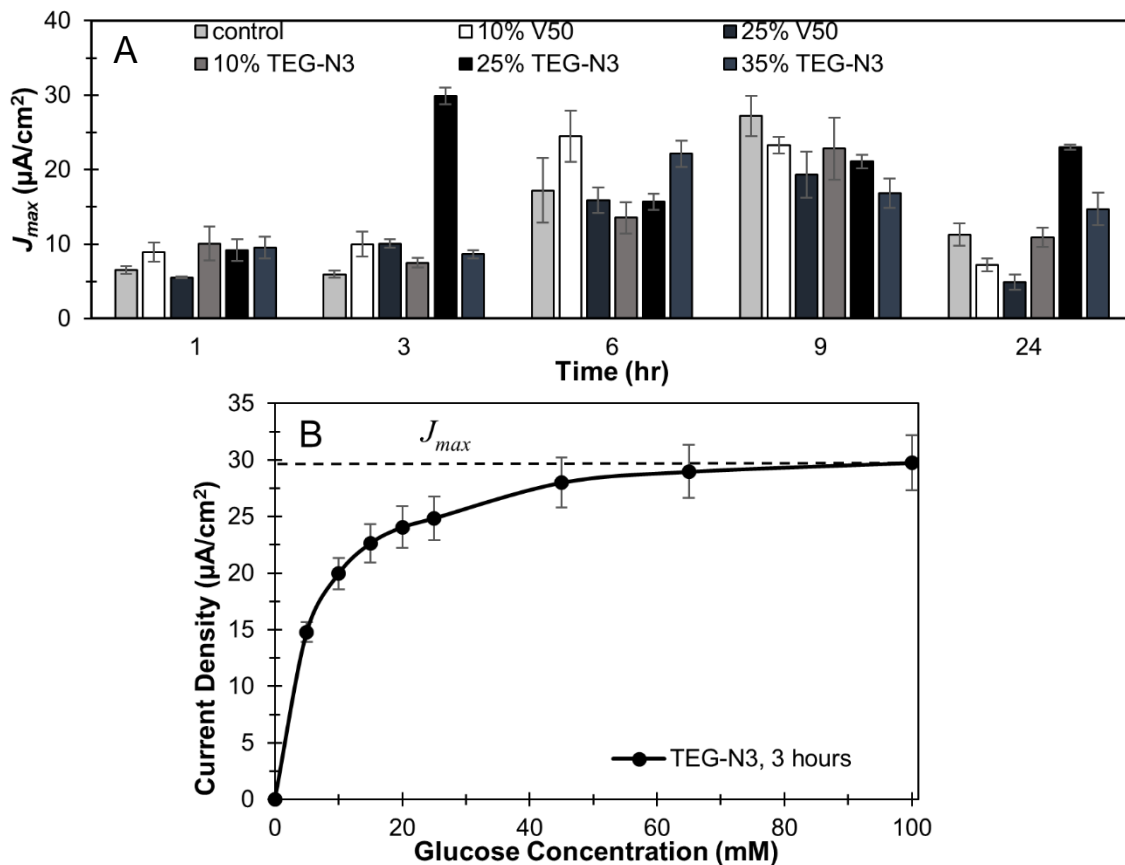


**Figure 2.2.13:** (A) Effect of irradiation time and crosslinking agent on the catalytic current density ( $J_{max}$ ) in response to glucose for Fc-C<sub>3</sub>-LPAEI/GOX films. (B) Example Michael-Menten curve for 25% TEG-N<sub>3</sub> at three hours irradiation. PBS pH 7.4.

After three hours of irradiation, 25% TEG-N<sub>3</sub> has a  $J_{max}$  of  $29.8 \pm 2.4 \mu\text{Acm}^{-2}$  which outperforms all other systems by three-fold. Not only does it give a higher response than the other systems at that time, it is the highest response for all systems—regardless of initiator choice or irradiation time—from the initial irradiation screening. Even though three hours of irradiation gives a lower electrochemical response in the CV when compared to longer UV exposure, this appears to be an ideal point of ferrocene connectivity and enzyme stability.  $J_{max}$  is a function of both how well the enzyme is working and how well electrons can diffuse through the film. If electron transfer rates through the film are high but the enzyme has been damaged by irradiation, then the overall sensor performance will decrease. Conversely, poor electronic communication between redox centers will cause result in low mediation even if the enzyme is in pristine condition.

It is also of interest that 25% TEG-N<sub>3</sub> at three hours irradiation had the highest  $i_{pa}$  and  $cD_e^{1/2}$  between all the systems tested. Having a higher electron diffusion and better crosslinking once again correlates to the higher response to glucose. Increasing the irradiation exposure to six and nine hours results in 25% TEG-N<sub>3</sub> crosslinked films no longer giving the highest response to glucose. Even though the electrochemical response in the CV continues to increase with prolonged irradiation, films fabricated with 25% TEG-N<sub>3</sub> are being outperformed enzymatically by other systems. This phenomenon could be due to two things: the optimum interstitial space between redox sites has been surpassed, or there is increased damage to GOX. Since the  $cD_e^{1/2}$  response for 25% TEG-N<sub>3</sub> continues to rise after three hours of irradiation, enzymatic damage is the most likely culprit.

At 24 hours of irradiation, 25% TEG-N<sub>3</sub> has a much higher  $J_{max}$  than the other systems. Since this system crosslinks the quickest, as evidenced by the higher  $i_{pa}$  at each irradiation point, the enzyme is kept in a more tightly bound network for a longer amount of time. Since LPEI is known to favorably interact with GOX through electrostatic interactions, the polymer strands are initially wrapped around the enzyme. As the polymer network becomes more tightly locked with increased crosslinking, the enzyme is restricted enough to better protect it from being completely denatured. Similar trends have been observed for the thermal protection of proteins by covalently binding them to a polymer.

The control electrodes showed increasing enzymatic response up to nine hours of irradiation before dropping at 24 hours. At nine hours of UV irradiation, the control electrodes had slightly higher  $J_{max}$  values than all the other systems and were within the standard deviation of 25% TEG-N<sub>3</sub> at three hours irradiation. At  $27.2 \pm 2.7 \mu\text{A}/\text{cm}^2$ , the control films have apparently reached their ideal connectivity to allow for efficient diffusion of electrons through the film. Since the enzyme is presumably being damaged with increased irradiation, this shows the importance of ferrocene communication to overall sensor efficiency. This also suggests that at nine hours the lower response from films fabricated with a photoreactive crosslinker is most likely due to enzyme damage from side reactions. Once the films reach maximum crosslinking at 24 hours, the control response drops rapidly as the enzyme is further degraded.

### 2.2.6 *Effect of Photochemical Crosslinking on Biosensor Efficiency*

The efficiency of an enzyme can be qualitatively determined by looking at changes in the Michaelis constant ( $K_M$ ), i.e. the concentration of substrate at which the

reaction rate is half of the maximum response. Irradiation of the enzyme should result in denaturation which will decrease the overall sensor response, but the activity of the active enzymes should remain relatively unaffected. Therefore, decreases in  $J_{max}$  do not necessarily reflect a decrease in enzyme efficiency, but are partially indicative of smaller active enzyme concentrations. When measuring the response of GOX using electrochemical methods, the measured  $K_M$  is a function of both the enzyme activity and the diffusion of electrons through the film. Therefore, all reported values for enzyme efficiency are actually apparent  $K_M$  values ( $K_M^*$ ). This means that changes in  $K_M^*$  can arise from three major different sources: enzyme inhibition, substrate diffusion, or changes in mediator communication. Changes in  $K_M$  that arise from enzyme inhibition are typically very large, and the value of  $K_M$  is not dependent on the concentration of the enzyme; meaning it can still be calculated even if some of it is being irreparably damaged by UV irradiation.

Assuming that  $K_M$  for GOX does not significantly change upon irradiation, then deviations in  $K_M^*$  result from substrate diffusion into the film and differences in electronic communication through the film. While changes in  $K_M^*$  resulting from electronic communication and substrate diffusion are typically much smaller and harder to separate from each other, the two factors should give different contributions to  $K_M^*$  at the extremes of UV exposure. At low levels of irradiation, the films are not crosslinked to a large degree (**Figure 2.2.6**), which is indicative of poorer electronic communication between redox active ferrocene moieties. Lower crosslinking results in larger pore sizes between polymer strands which do not hinder the diffusion of glucose into the films. After prolonged exposure to UV irradiation, the films have more cohesive electronic

communication due to a more extensively crosslinked network. Increasing the crosslinking will restrict the enzyme's mobility and stabilize its native conformation, but if it does not occur quick enough, the enzyme runs the risk of UV degradation. However, a heavily crosslinked matrix will restrict glucose diffusion into the film and could possibly hinder the conformational changes necessary for the enzyme to function.

Characterization of  $K_M^*$  is, therefore, a complicated function of multiple variables that are not easily separated, but it is still possible to obtain qualitative trends from collected data. **Figure 2.2.14** shows  $K_M^*$  data for Fc-C<sub>3</sub>-LPAEI/GOX films in relation to irradiation time and crosslinker type.

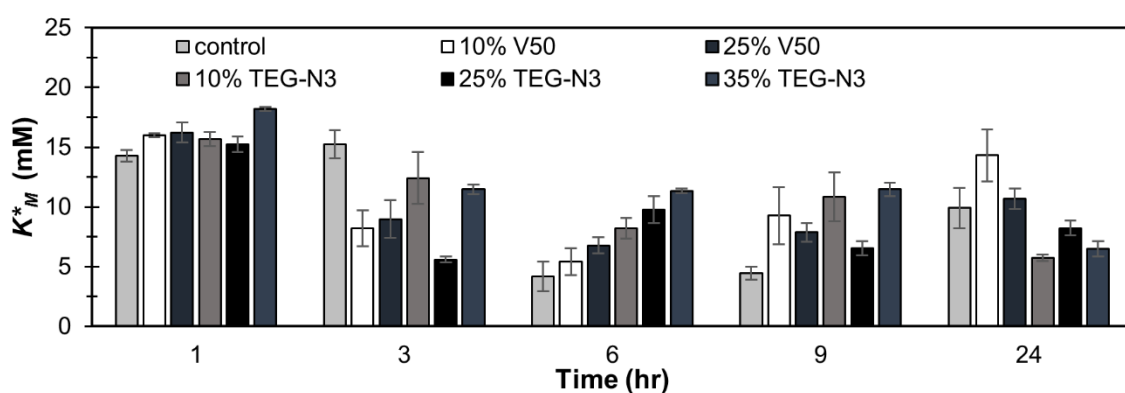


**Figure 2.2.14:** Effect of irradiation time and crosslinking agent on the apparent Michaelis constant ( $K_M^*$ ) in response to glucose for Fc-C<sub>3</sub>-LPAEI/GOX films.

In its traditional sense, a low  $K_M$  reflects a fast turnover rate and a high  $K_M$  is indicative of decreased enzyme activity. For  $K_M^*$ , however, fluctuations are more likely due to changes in electronic communication throughout the film. At one hour of irradiation,  $K_M^*$  is at its highest and is about equal for all the systems. At this point, the films are not cohesive and well connected, but the enzyme should be at its most efficient. Glucose diffusion should not be limited at this point, so the higher  $K_M^*$  is most likely a result of poorer mediator connectivity.

With increased irradiation up to three hours,  $K_M^*$  decreases for all except the control electrodes suggesting a slow crosslinking reaction in the absence of a photogenerated crosslinker. It appears that lower  $K_M^*$  is related to higher  $J_{max}$  at medium irradiation times for several reasons: 1) the enzyme has yet to be degraded by UV exposure, 2) it is being stabilized by the polymer network, and 3) the moderately crosslinked films still allow for good substrate diffusion. All of these factors work in conjunction with the increase in electronic communication from increased crosslinking to lower  $K_M^*$ .

The control electrodes have their lowest  $K_M^*$  at nine hours; which is also when they had the highest response to glucose. The higher  $K_M^*$  values for the other systems are possibly indicative of enzyme damage from the crosslinking agents. While it appears that  $J_{max}$  and  $K_M^*$  seem to relate, the correlation does not hold at extremely long irradiation times. At twenty-four hours irradiation 10% TEG-N<sub>3</sub> has the lowest  $K_M^*$ , but also the lowest  $J_{max}$ . This suggests the film has reached its maximum electronic connectivity but the concentration of active enzyme has been almost depleted.

It is impressive that the fabricated biosensors continue to work after such aggressive conditions. It has been previously reported that GOX in solution loses almost 90% of its activity after six minutes of irradiation. The fact that after twenty-four hours of UV exposure there is still a significant enzymatic response is impressive in its own right. This goes to show the extent to which immobilization of the enzyme protects it from degradation.

### 2.2.7 Optimization of 25% TEG-N<sub>3</sub> Containing Films

From the initial irradiation screening, three hours of UV exposure for 25% TEG-N<sub>3</sub> was shown to generate the most efficient glucose biosensors, as evidenced by the low  $K_M^*$  and high  $J_{max}$ . At this level of crosslinking, the electronic communication throughout the film, the diffusion of glucose, and the enzyme efficiency are at an initial optimum for maximum current response. To further fine tune the fabrication of Fc-C<sub>3</sub>-LPAEI photoresists, the irradiation time was further segmented to evaluate sensor response. **Figure 2.2.15** depicts  $i_{pa}$  with respect to irradiation time for Fc-C<sub>3</sub>-LPAEI/GOX films containing 25 mol% TEG-N<sub>3</sub>.

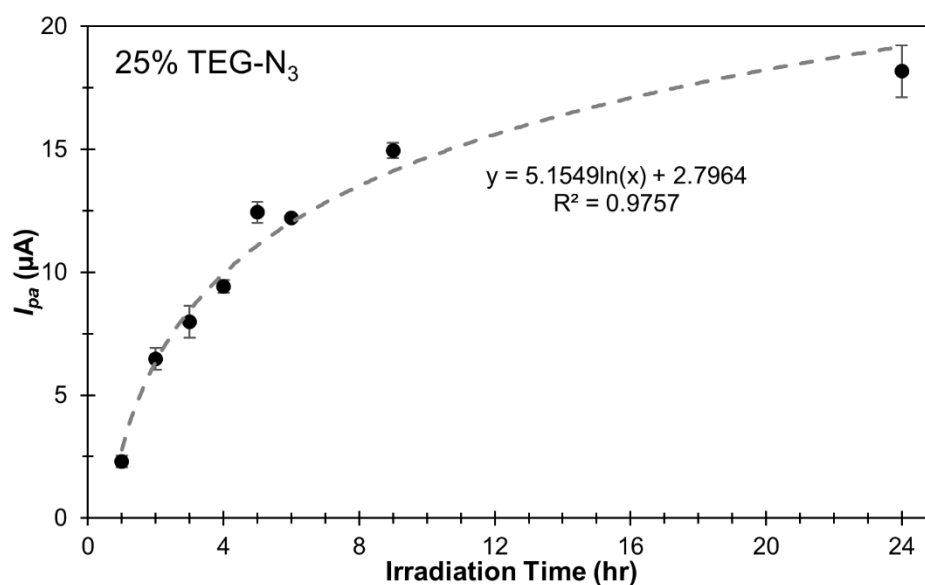


**Figure 2.2.15:** Effect of irradiation time on the anodic peak current ( $i_{pa}$ ) of Fc-C<sub>3</sub>-LPAEI/GOX films fabricated with 25 mol% TEG-N<sub>3</sub>.

With the exception of the five to six hour transition, there is a continual, near logarithmic increase in  $i_{pa}$  for Fc-C<sub>3</sub>-LPAEI/GOX films crosslinked with 25 mol% TEG-N<sub>3</sub>. This again depicts that the films are becoming increasingly crosslinked with prolonged UV exposure. However, as has been seen previously, the more important



aspect in characterization of a biosensor comes in its ability to efficiently catalyze the oxidation of glucose.

As can be seen in **Figure 2.2.16A**, Fc-C<sub>3</sub>-LPAEI/GOX films constructed with 25 mol% TEG-N<sub>3</sub> reach their highest response at five hours of irradiation giving a response of  $44.9 \pm 1.3 \mu\text{Acm}^{-2}$ . There is a continual increase in  $J_{max}$  up to three hours which is accompanied by a decrease in  $K_M^*$  (**Figure 2.2.16B**), which suggests the bulk of the enzyme population has not yet been degraded from UV exposure. The first three hours are behaving in an ideal fashion that keeps enzyme integrity intact while the films become more electronically connected from increased crosslinking. At four hours of irradiation,  $J_{max}$  is nearly identical to three hours, but the  $K_M^*$  has slightly increased. This marks the point where a portion of the enzymes within the film are starting to be affected by the UV irradiation, but the increase in crosslinking compensates by increasing the flow of electrons through the film.

The increase in  $J_{max}$  at five hours of irradiation is a result of enzyme efficiency and mediator connectivity being at a point of maximum compatibility. Since  $K_M^*$  has not changed from the four hours of irradiation, the increase in sensor response must be a result of optimum electronic connectivity between redox mediators. From **Figure 2.2.15** above, the electrochemical response for five and six hours of irradiation are almost identical. However, the increase in  $K_M^*$ , coupled with the large decrease in  $J_{max}$  at six hours, is indicative of the enzymes contained within the film being severely damaged from prolonged UV exposure. Further exposure caused slight increases in sensor performance due to increased electronic communication, but the majority of the enzymes have already been degraded.

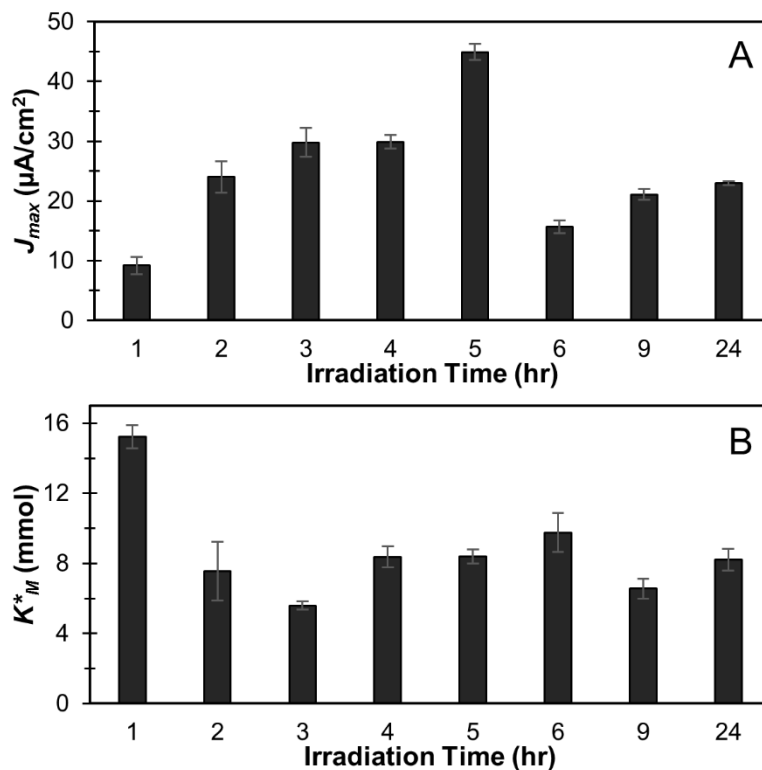


**Figure 2.2.16:** Effect of irradiation time on the (A) catalytic current density ( $J_{max}$ ) and (B) the apparent Michaelis constant ( $K_M^*$ ) in response to glucose for Fc-C<sub>3</sub>-LPAEI/GOX films fabricated with 25 mol% TEG-N<sub>3</sub>. PBS pH 7.4

### 2.2.8 Literature Comparison

There are very few examples of glucose biosensors fabricated through photolithography that have been reported in the literature. Most of these reports looked only at the linear region of the Michaelis–Menten kinetics data (0 mM - ~15mM glucose), and only a couple report or mention maximum catalytic current densities. To normalize the differences between systems, the sensitivities at 10 mM glucose for photochemically generated biosensors containing a redox mediator covalently attached to the polymer backbone were compared (Table 2.1).

The earliest example of employing a redox active photoresist was reported in 1995. This system consisted of dimethylacrylamide, azidostyrene, and vinylferrocene polymerized in the presence of GOX to form cohesive films on the surface of a rotating

disc electrode (RDE).<sup>35</sup> By using an arylazide, the researchers claim to be directly binding the polymer to the enzyme through nitrene insertion. However, the control electrodes fabricated without an enzyme present were also reported to have formed patternable hydrogels. The use of an RDE allows for increased flux of substrate to the films, which artificially increases the current response of the biosensor. However, since the rotation rate for this work was not reported, it is not a direct comparison to the work presented in this chapter.

The usage of an RDE was also employed by Bunte *et al.* in their work involving the direct coupling of a benzophenone containing polymer to the enzyme.<sup>36,37</sup> While no control experiments for the formation of hydrogels were reported, this work reports high current densities and high sensitivities in response to glucose. However, by using the Levich equation (**Equation 2.5**) it is possible to back calculate the response of the films at low rotation rates (**Equation 2.7**). In **Equation 2.5**,  $I_L$  is the Levich current,  $n$  is the number of electrons transferred in a single redox process,  $A$  is the area of the electrode,  $D$  is the diffusion coefficient of the electroactive species,  $w$  is the rotation rate,  $\nu$  is the viscosity, and  $c$  is the concentration of the electroactive species:

$$\text{Equation 2.5: } I_L = (0.620)nFAD^{2/3}w^{1/2}\nu^{-1/6}c$$

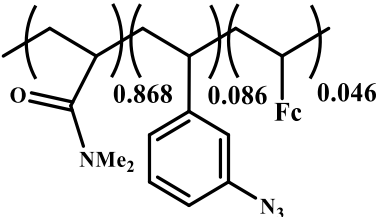
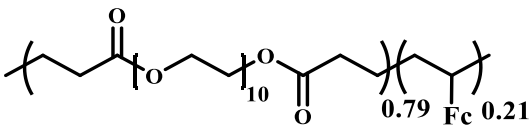
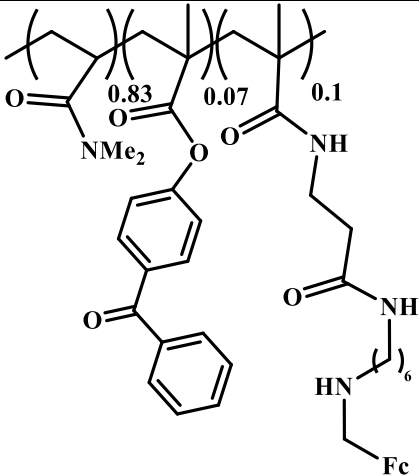
$$\text{Equation 2.6: } \frac{I_{L1}}{w_1^{1/2}} = \frac{I_{L2}}{w_2^{1/2}}$$

$$\text{Equation 2.7: } I_{L2} = \frac{I_{L1}w_2^{1/2}}{w_1^{1/2}}$$

Using **Equation 2.7**, the sensitivity to glucose response for the Bunte group's work is  $1.3 \mu\text{Acm}^{-2}\text{mM}^{-1}$  at 1 rpm, which is lower than for Fc-C<sub>3</sub>-LPAEI. This is important in that it shows the great stability afforded to GOX by the LPEI polymer.

In 1998, Sirkar and Pishko reported the copolymerization of poly(ethylene glycol) diacrylate (PEG-DA) and vinylferrocene in the presence of GOX.<sup>16</sup> These films produced very weak currents in response to glucose due to the fact that films were cast using PEG-DA as the solvent. GOX was reported to not be soluble in PEG-DA resulting in a large amount of aggregation of enzyme within the films. This poor homogeneity most likely is the result of the poor response of the fabricated biosensors.

**Table 2.2.1:** Literature summary of photochemically generated glucose biosensors

Electrode	System	Irrad. Time	Sens.* ( $\mu\text{Acm}^{-2}\text{mM}^{-1}$ )	Ref.
GC-RDE		NR	177 (rpm not reported)	35
Gold		10 s	0.56	16
GC-RDE		20 min	40 @ 1000 rpm  1.3 @ 1 rpm**	37
GC	Fc-C <sub>3</sub> -LPAEI	5 hr	2.7	This work

\* sensitivity evaluated at 10 mM glucose  
 \*\* calculate using the Levich equation  
 GC = glassy carbon; RDE = rotating disc electrode  
 NR = not reported

Glucose biosensors fabricated using Fc-C<sub>3</sub>-LPAEI are on the lower end of the reported literature values for photocrosslinkable systems. However, Meredith reported an increase in response by increasing the substitution of ferrocene from five to twenty percent for polymers constructed using a one carbon mediator spacing.<sup>38</sup> Therefore, further optimization of ferrocene and allyl content should lead to further increases in response.

### 2.3 Conclusions

We have detailed the synthesis of cinnamoyl-modified LPEI (LPCEI), and we have shown that Fc-C<sub>3</sub>-LPAEI can act as a redox active, negative photoresist capable of generating  $44.9 \pm 1.3 \mu\text{Acm}^{-2}$  in response to glucose. The electrochemical characterization of Fc-C<sub>3</sub>-LPAEI/GOX films was shown to be a complex combination of enzyme stability, glucose diffusion, and mediator connectivity. Optimization of the crosslinker percentage and irradiation time allowed for elucidation of the crosslinking process. Electrodes were still able to produce current response after exceedingly long UV exposure, which demonstrates the ability of LPEI to stabilize and protect the GOX from complete degradation.

Future work is needed to further lower the irradiation times to improve biosensor performance. This could be done through the usage of a photosensitizer to improve crosslinking of LPCEI, a technique that has been shown to enhance the crosslinking of poly(vinyl cinnamate).<sup>30</sup> This method of crosslinking would decrease the possibility of side reactions with the enzyme, and could lead to enhanced sensor response. Another possibility could be the incorporation of an arylazide crosslinking agent to minimize possible nitrene rearrangements of TEG-N<sub>3</sub>. The methylation of ferrocene could also be

employed as a method to lower its redox potential and improve electronic mediation of the enzyme.

## 2.4 Experimental

### Chemicals and Solutions

Glucose oxidase from *Aspergillus niger* (EC 1.1.3.4, type X-S, 117 units/mg solid, 75% protein) and all chemicals were purchased from Sigma–Aldrich, unless otherwise noted, and used as received. 1,2-Bis(2-azido-ethoxy)ethane was prepared by following a previously reported literature synthesis.<sup>39</sup> Stock solutions of 2 M glucose were stored at 4°C and allowed to mutarotate for 24 hours prior to usage.

### Materials

#### *Synthesis of cinnamoyl-modified linear poly(ethylenimine) (LPCEI)*

Linear poly(ethylenimine) (LPEI) was synthesized according to a previously reported protocol.<sup>40</sup> LPEI (15.6 mg, 0.36 mmol *repeat unit*) and K<sub>2</sub>CO<sub>3</sub> (12.5 mg, 0.09 mmol) were added to acetonitrile (6 mL) and heated to reflux solvent with stirring. Methanol was added dropwise to the reaction mixture until the polymer was fully dissolved (~5 drops). Cinnamoyl chloride (15.0 mg, 0.09 mmol) in acetonitrile (4 mL) was added dropwise to the stirring reaction mixture. Upon addition of cinnamoyl chloride, the reaction mixture becomes cloudy, but after two hours of refluxing the solution is clear. The reaction mixture was cooled to room temperature and the solvent was removed under reduced pressure. The residue was redissolved in methanolic NaOH (1 mL, 0.5 M) and the mixture was stirred at room temperature for one hour. After removal of methanol, the polymer was extracted with benzene and passed through a Celite

filter. Removal of benzene under reduced pressure gave neutral, 25 percent substituted LPCEI.

$^1\text{H-NMR}$  ( $\text{CDCl}_3$ )  $\delta$ (ppm): 2.95 (br s,  $-\text{CH}_2\text{CH}_2\text{NH}-$ ), 5.27 (br s,  $-\text{CH}_2\text{CH}_2\text{N}(\text{CO})-$ ), 6.61 (d,  $(\text{CO})\text{CH}=\text{CHPH}$ ), 6.95 – 7.31 (m,  $-\text{PhH}$  (*m, p*)), 7.38 (s,  $(\text{CO})\text{CH}=\text{CHPH}$ ), 7.46 (br t,  $-\text{PhH}$  (*o*))

#### *Synthesis of Fc-C<sub>3</sub>-LPAEI*

Linear poly(ethylenimine-*co*-allylethylenimine) (LPAEI) was synthesized according to a previously reported protocol.<sup>27</sup> The redox polymer (Fc-C<sub>3</sub>-LPAEI) was synthesized by coupling (3-bromopropyl)-ferrocene to LPAEI. LPAEI (400 mg, 6.34 mmol) was dissolved in a heated solution of 10:1 mixture of acetonitrile and methanol (20 mL). A solution of (3-bromopropyl)-ferrocene (97 mg, 0.32 mmol) in acetonitrile (5 mL) was added dropwise to the reaction mixture and heated to reflux solvent overnight. The solvent was removed under reduced pressure and the crude product was washed with diethyl ether to remove any ferrocenyl impurities. Removal of remaining ether under reduced pressure afforded Fc-C<sub>3</sub>-LPAEI (5% ferrocene, 50% allylated). All photocurable redox polymers were stored in the dark, under nitrogen, and at 4 °C.

$^1\text{H-NMR}$  (300 MHz,  $\text{CDCl}_3$ )  $\delta$ (ppm): 1.6-1.8 (br,  $-\text{CH}_2-$ ), 2.3-2.4 (br t,  $-\text{CH}_2\text{Fc}$ ), 2.4-2.85 (br,  $-\text{CH}_2\text{N}-$ ), 3.1 (br d,  $\text{CH}_2=\text{CH}-\text{CH}_2-$ ), 4.0-4.2 (br, Fc-**H**), 5.1 (br t,  $\text{CH}_2=\text{CH}-\text{CH}_2-$ ), 5.8 (br hx,  $\text{CH}_2=\text{CH}-\text{CH}_2-$ )

#### *Gel Preparation and Irradiation*

Solutions of Fc-C<sub>3</sub>-LPAEI were prepared by dissolving the polymer in water by the addition of a 0.1 M HCl until the final concentration of the polymer was 10 mg/mL. The pH of the polymer solution was adjusted to  $5.0 \pm 0.2$  by the addition of concentrated

HCl or NaOH. Glucose sensors were prepared in the following fashion: 14  $\mu\text{L}$  of polymer solution (10 mg/mL), 6  $\mu\text{L}$  of glucose oxidase solution (10 mg/mL), and 1  $\mu\text{L}$  of either Nanopure water or initiator (various conc.) were mixed together and 3  $\mu\text{L}$  aliquots were placed onto the glassy carbon electrode surface. The electrodes were allowed to dry in the dark to limit exposure to unwanted irradiation

Irradiation of polymer films was carried out in a Rayonet type RS model RPR-208 preparative photochemical reactor equipped with UV bulbs centered at 300 nm and 350 nm. Films coated on glassy carbon electrodes were irradiated for varying amounts of time and then immediately tested.

### **Electrochemical Measurements**

Constant potential experiments and cyclic voltammetry were performed with a CH Instruments model 832 bipotentiostat (Austin, TX). Experiments were conducted in a three-electrode cell configuration with a 3 mm glassy carbon electrode coated with redox polymer, a saturated calomel reference electrode (SCE), and a platinum wire counter electrode with phosphate buffered saline (PBS, pH 7.5) as the background electrolyte. Prior to use, all glassy carbon electrodes were polished successively on three grades of alumina (1, 0.3, and 0.05  $\mu\text{m}$ ) and washed thoroughly with Nanopure water after each polishing step.

### **2.5 References**

1. Thompson, L. F.; Kerwin, R. E., *Annual Review of Materials Science* **1976**, *6* (1), 267-301.
2. Zelentsov, S. V.; Zelentsova, N. V.; Kolesov, A. N.; Bogatyreva, L. A.; Mashtakov, I. A., *Russ Microelectron* **2007**, *36* (1), 40-48.
3. Toshio, Y.; Taro, M.; Masaru, A.; Mitsumasa, U., *Japanese Journal of Applied Physics* **1995**, *34* (11R), 6279.



4. Reiser, A.; Huang, J. P.; He, X.; Yeh, T. F.; Jha, S.; Shih, H. Y.; Kim, M. S.; Han, Y. K.; Yan, K., *European Polymer Journal* **2002**, *38* (4), 619-629.
5. Vollenbroek, F.; Spiertz, E., Photoresist systems for microlithography. In *Electronic Applications*, Springer Berlin Heidelberg: 1988; Vol. 84, pp 85-111.
6. Ceyskens, F.; Puers, R., SU-8 Photoresist. In *Encyclopedia of Nanotechnology*, Bhushan, B., Ed. Springer Netherlands: 2012; pp 2530-2543.
7. Roy, D.; Basu, P. K.; Raghunathan, P.; Eswaran, S. V., *Magnetic Resonance in Chemistry* **2003**, *41* (9), 671-678.
8. McLaren, A. D.; Luse, R. A., *Science* **1961**, *134* (3488), 1410.
9. Luse, R. A.; McLaren, A. D., *Photochemistry and Photobiology* **1963**, *2* (3), 343-360.
10. Grist, K. L.; Taylor, T.; Augenstein, L., *Radiation Research* **1965**, *26* (2), 198-210.
11. Móra, S.; Elöudi, P., *European Journal of Biochemistry* **1968**, *5* (4), 574-582.
12. Merchant, S. A.; Glatzhofer, D. T.; Schmidtke, D. W., *Langmuir* **2007**, *23* (22), 11295-11302.
13. Merchant, S. A.; Meredith, M. T.; Tran, T. O.; Brunski, D. B.; Johnson, M. B.; Glatzhofer, D. T.; Schmidtke, D. W., *The Journal of Physical Chemistry C* **2010**, *114* (26), 11627-11634.
14. Meredith, M. T.; Kao, D.-Y.; Hickey, D.; Schmidtke, D. W.; Glatzhofer, D. T., *Journal of The Electrochemical Society* **2011**, *158* (2), B166-B174.
15. Meredith, M. T.; Hickey, D. P.; Redemann, J. P.; Schmidtke, D. W.; Glatzhofer, D. T., *Electrochimica Acta* **2013**, *92* (0), 226-235.
16. Sirkar, K.; Pishko, M. V., *Analytical Chemistry* **1998**, *70* (14), 2888-2894.
17. Choi, S.; Park, J.-K., *Biomicrofluidics* **2010**, *4* (4), 046503.
18. Van Gerwen, P.; Laureyn, W.; Laureys, W.; Huyberechts, G.; Op De Beeck, M.; Baert, K.; Suls, J.; Sansen, W.; Jacobs, P.; Hermans, L.; Mertens, R., *Sensors and Actuators B: Chemical* **1998**, *49* (1-2), 73-80.
19. Montelius, L.; Heidari, B.; Graczyk, M.; Maximov, I.; Sarwe, E. L.; Ling, T. G. I., *Microelectronic Engineering* **2000**, *53* (1-4), 521-524.
20. Thévenot, D. R.; Toth, K.; Durst, R. A.; Wilson, G. S., *Biosensors and Bioelectronics* **2001**, *16* (1-2), 121-131.

21. Baronas, R.; Ivanauskas, F.; Kulys, J., *Journal of Mathematical Chemistry* **2004**, 35 (3), 199-213.
22. Kulys, J.; Baronas, R., *Sensors (Basel, Switzerland)* **2006**, 6 (11), 1513-1522.
23. Haeberle, S.; Zengerle, R., *Lab on a Chip* **2007**, 7 (9), 1094-1110.
24. Kamitani, A.; Morishita, S.; Kotaki, H.; Arscott, S., *Journal of Power Sources* **2009**, 187 (1), 148-155.
25. Scribner, L. L., *The measurement and correction of electrolyte resistance in electrochemical tests*. ASTM International: 1990; Vol. 1056.
26. Mayer, S.; Geddes, L. A.; Bourland, J. D.; Ogborn, L., *Med. Biol. Eng. Comput.* **1992**, 30 (5), 538-542.
27. Hu, L. Polyamine Based Polymer Electrolyte Modification and Performance. University of Oklahoma, 2005.
28. Kadam, R. Study of Lithium Triflate as an Electrolyte in Mized Ether-Amine Solvents and the Use of Electron Paramagnetic Resonance Spectroscopy to Study Dielectric Properties of Materials. University of Oklahoma, 2011.
29. Minsk, L. M.; Smith, J. G.; van Deusen, W. P.; Wright, J. F., *Journal of Applied Polymer Science* **1959**, 2 (6), 302-307.
30. Robertson, E. M.; van Deusen, W. P.; Minsk, L. M., *Journal of Applied Polymer Science* **1959**, 2 (6), 308-311.
31. Abramovitch, R. A.; Kyba, E. P., *Journal of the American Chemical Society* **1971**, 93 (6), 1537-1538.
32. Gritsan, N.; Platz, M., Photochemistry of Azides: The Azide/Nitrene Interface. In *Organic Azides*, John Wiley & Sons, Ltd: 2010; pp 311-372.
33. Erickson, M. J. Synthesis, Structure, and Electrochemical Performance of Poly(ethylenimine)-Based Electrolytes. University of Oklahoma, Norman, OK, 2004.
34. Hickey, D. P.; Halmes, A. J.; Schmidtke, D. W.; Glatzhofer, D. T., *Electrochimica Acta* **2014**, 149 (0), 252-257.
35. Nakayama, Y.; Zheng, Q.; Nishimura, J.; Matsuda, T., *ASAIO Journal* **1995**, 41 (3), M418-M421.
36. Bunte, C.; R uhe, J., *Macromolecular Rapid Communications* **2009**, 30 (21), 1817-1822.
37. Bunte, C.; Prucker, O.; K onig, T.; R uhe, J., *Langmuir* **2010**, 26 (8), 6019-6027.

38. Meredith, M. T. The Development of Ferrocene-Modified Linear Poly(ethylenimine) Redox Polymers and Their Application in Amperometric Glucose Biosensors and Compartment-less Biofuel Cells. University of Oklahoma, 2010.
39. Kühhorn, J.; Hübner, H.; Gmeiner, P., *Journal of Medicinal Chemistry* **2011**, *54* (13), 4896-4903.
40. York, S.; Frech, R.; Snow, A.; Glatzhofer, D., *Electrochimica Acta* **2001**, *46* (10–11), 1533-1537.
41. Prein, M. and Adam, W.; *Angewante Chemie, International Edition* **1996**, *35* (5), 477-494.

## **Chapter 3. Electrochemical Characterization of Layer-By-Layer Assembled Ferrocene-Modified Linear Poly(ethylenimine)/Enzyme Composites for Biosensor and Biofuel Cell Applications**

---

Significant portions of the chapter were completed with the help of Jared DeLuca.

### **3.1 Introduction**

Biofuel cells generate electrical currents by capturing electrons from redox processes found in nature. One method by which this is accomplished is through the immobilization of redox active enzymes and harvesting electrical current from these natural catalysts<sup>1</sup>. Glucose oxidase (GOX) is one such redox enzyme that has been extensively used for enzymatic biofuel cells<sup>2,3</sup>. There is particular interest in “wiring” GOX together with osmium<sup>4,5</sup> or ferrocene<sup>6,7</sup> based redox mediators to form cohesive bioanode films. Recent work has shown that hydrogels containing ferrocene moieties are exceptionally capable of mediating electron transfer from the GOX active site to the surface of an electrode.<sup>8,9</sup>

There are many ways to immobilize enzymes on the surface of an electrode: entrapment within a polymer matrix<sup>10</sup>, adsorption onto an electrode surface<sup>11</sup>, chemical crosslinking<sup>12,13</sup>, self-assembled monolayers<sup>14</sup>, and layer-by-layer assembly<sup>15</sup>. Due to the fast interaction times between layers, the layer-by-layer (LBL) fabrication method is a useful way to quickly assemble redox active films. LBL assembly is based on the adsorption and self-assembly of oppositely charged polyelectrolytes. By alternating layers of polyelectrolytes, thickness-tunable enzyme/polymer multilayers can be quickly generated without the need for extended curing of chemically cross-linked films. The LBL fabrication of molecular bilayers is also useful in that it allows for the construction of systems in a relatively ordered, predetermined fashion. Alternating layers of enzyme and redox polymer allows for material dispersion throughout the entire film, and

additional stability can be achieved by covalently binding the enzyme directly to the polymer.

Polyamines are one class of polymers that are useful as the cationic layer in the LBL technique. One such polyamine that has been used as a scaffold in LBL assembled biosensors is branched poly(ethylenimine) (BPEI). Sensors have been fabricated that are specific to a variety of targets, including: cocaine<sup>16</sup>, cancer cells<sup>17</sup>, thrombin and lysozymes<sup>18</sup>, lactose<sup>19,20,21</sup>, and glucose<sup>22</sup>. LBL systems using BPEI have also been fabricated using DNA as a polyelectrolyte<sup>23</sup>, made for the controlled delivery of drugs<sup>24</sup>, the oxidation of NADH<sup>25</sup>, and used to increase the growth of *E. coli*<sup>26</sup>. While BPEI has been well established as a polycation for LBL assembled biosensors, there have been very few reports using linear poly(ethylenimine) (LPEI). Our group has previously shown that ferrocene-modified LPEI produces significantly higher current densities than ferrocene-modified BPEI for solution cast, crosslinked enzymatic bioanodes<sup>27</sup>, and we have recently shown that ferrocene tethered to LPEI by a six carbon spacer (Fc-C<sub>6</sub>-LPEI) can be used in the LBL assembly of glucose biosensors<sup>28</sup>. Based on the results of these systems, we wished to further probe the use of high molecular weight LPEI as a scaffold for the LBL technique by varying structural aspects of the redox polymer derived from it, and in optimization of the LBL fabrication and characterization.

The characterization of LBL films is typically achieved through the use of ellipsometry,<sup>29</sup> UV-Vis spectroscopy,<sup>30</sup> and quartz crystal microgravimetry.<sup>31</sup> These methods are especially useful for quantifying the thickness, type, and amount of materials deposited in each layer, but these techniques give limited information about the deposition process itself. One method that is surprisingly underutilized is LBL

electrochemical characterization of multilayered polymer/enzyme films. Hodak *et al.* looked at the increase in charge with the addition of ferrocene-modified poly(allylamine) layers,<sup>7</sup> but most studies simply report the increase in sensor response with the build-up of material. Since the electrochemistry of self-assembled monolayers is well-studied,<sup>32</sup> the use of electrochemical methods to characterize LBL multilayers to study the LBL assembly process is promising.

Herein we describe how the tether length of ferrocene modified linear poly(ethylenimine) (Fc-C<sub>n</sub>-LPEI) and the wash time between bilayers effect the electrochemical and enzymatic response of LBL assembled films. The use of electrochemical methods as a tool for characterization, and the ability to use them to study the build-up of materials during the LBL assembly process, is discussed. Most LBL assembled glucose bioanodes use conductive fillers or high-surface area substrates to enhance electrochemical response, whereas our system uses planar, low-surface electrodes coated with ultra-thin conducting films. Nevertheless, the results presented here are among the most highly sensitive LBL assembled glucose bioanodes reported in the literature, and are capable of producing some of the highest current densities for LBL assembled glucose biosensors. The high current densities of the biosensors led us to demonstrate for the first time that LBL assembled films based on ferrocene redox polymers can be used as bioanodes in biofuel cells. The power densities obtained compare favorably with other LBL glucose/oxygen biofuel cells reported in the literature.

### **3.2 Results and Discussion**

Previous work by Meredith *et al.* using solution cast films crosslinked with ethylene glycol diglycidyl ether (EGDGE) has shown that the tether length by which ferrocene is

attached to LPEI affects the electrochemical and enzymatic properties of the films.<sup>6</sup> Meredith *et al.* reported that decreasing the mediator spacing between ferrocene and LPEI from six to three methylene groups increased the sensitivity, maximum enzyme response, and stability of the films. On the contrary, Mao *et al.* reported a significant increase in electron diffusion when osmium redox centers are extended further away from the polymer backbone.<sup>5</sup> Both of these works involved redox active films that were solution cast with a set polymer to enzyme ratio. For LBL assembled films, the amount of polymer and enzyme deposited onto the surface is not predetermined, so it is difficult to predict how tether length will affect the electrochemical response. To the best of our knowledge, there are no studies that investigate the effect that mediator tether length has on the response and fabrication of LBL assembled bioelectrodes. Therefore, both six and three carbon spacers (Fc-C<sub>6</sub>-LPEI, Fc-C<sub>3</sub>-LPEI) were used to probe the electrochemical and enzymatic response of multilayered polymer/enzyme films. The redox polymers Fc-C<sub>3</sub>-LPEI and Fc-C<sub>6</sub>-LPEI were synthesized (**Figure 3.2.1**) according to a previously published procedure<sup>6</sup> from LPEI,<sup>42</sup> (3-bromopropyl)ferrocene<sup>43</sup>, and (6-bromohexyl)ferrocene (Sigma-Aldrich). The ferrocene moieties present within the films provide a useful tool to examine the physisorption of material onto the electrode's surface.

While processing electrodes, it was observed that the wash time used to clean electrodes after each layer had an effect on the electrochemical and enzymatic response. We had been using a wash time of 6-8 seconds to rinse films after the deposition of material; but shortening the wash to just a quick rinse with water resulted in significant increases in response. This trend held true for both Fc-C<sub>6</sub>-LPEI and Fc-C<sub>3</sub>-LPEI.

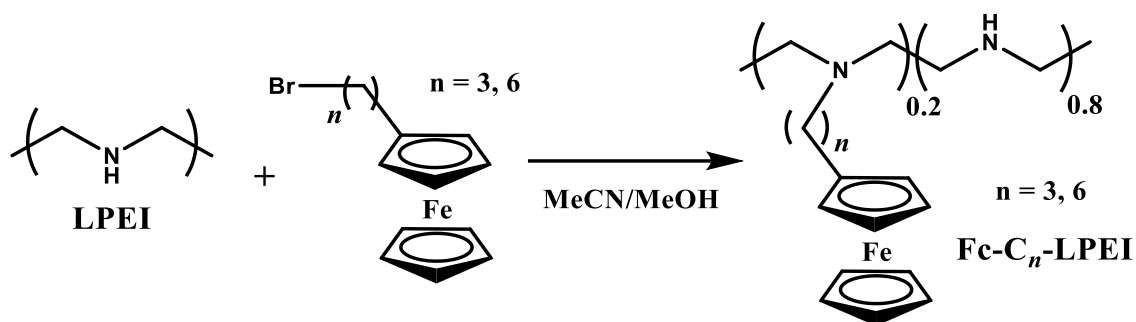


**Figure 3.2.1:** Synthetic scheme for Fc-C<sub>6</sub>-LPEI and Fc-C<sub>3</sub>-LPEI

### 3.2.1 LBL Assembly of Films

Redox polymer solutions (Fc-C<sub>6</sub>-LPEI, Fc-C<sub>3</sub>-LPEI) were prepared by dissolving them in Nanopure water until the final concentration was 10 mg/mL and the pH was adjusted to 5.0 by the addition of small aliquots of concentrated HCl and NaOH. Periodate-modified glucose oxidase (p-GOX) solution (20 μM) was prepared using a previously reported protocol.<sup>28</sup> GOX's peripheral oligosaccharides are oxidized by sodium periodate to install aldehyde functional groups (**Figure 3.2.2**). This allows for convenient sites with which to attach the enzyme to amine moieties in the polymer backbone, since Fc-C<sub>6</sub>-LPEI/GOX films assembled using purely electrostatic interactions have been shown to not be stable.<sup>28</sup>

Gold electrodes were modified with cystamine by immersing the electrode in a 20 mM solution of disulfide cystamine dihydrochloride (Cys·2HCl) for twenty minutes to give the electrodes a net positive surface charge. Electrodes were removed from solution and washed with Nanopure water to remove excess unbound material. Modified electrodes were immersed in p-GOX solution for five minutes to deposit and covalently attach enzymes to the cystamine layer. Electrodes were washed with Nanopure water by one of two methods: a long wash (6-8 sec.) or short wash (<1 sec.). The long wash procedure involved gently rinsing the sides and face of the electrode with a stream of



water from a wash bottle; whereas the short washing procedure was a quick rinse from a gentle stream of water directly onto the face or sides of the electrode. A laboratory tissue was used to carefully remove excess water from the sides of the electrode and the majority of the remaining water was removed from the electrode face using a gentle wrist flick. The electrodes were immersed in a solution of redox polymer (Fc-C<sub>6</sub>-LPEI or Fc-C<sub>3</sub>-LPEI) for five minutes, and then washed in the same manner as the previous enzyme layer. The assembly of p-GOX and Fc-C<sub>n</sub>-LPEI is considered as one bilayer and the presumed chemical attachment is shown in **Figure 3.2.2**. This process was repeated until the desired number of bilayers was achieved, and, for the remainder of this discussion, films will be identified in the following fashion: (polymer/enzyme)<sub>x</sub>, where *x* is the number of assembled bilayers.

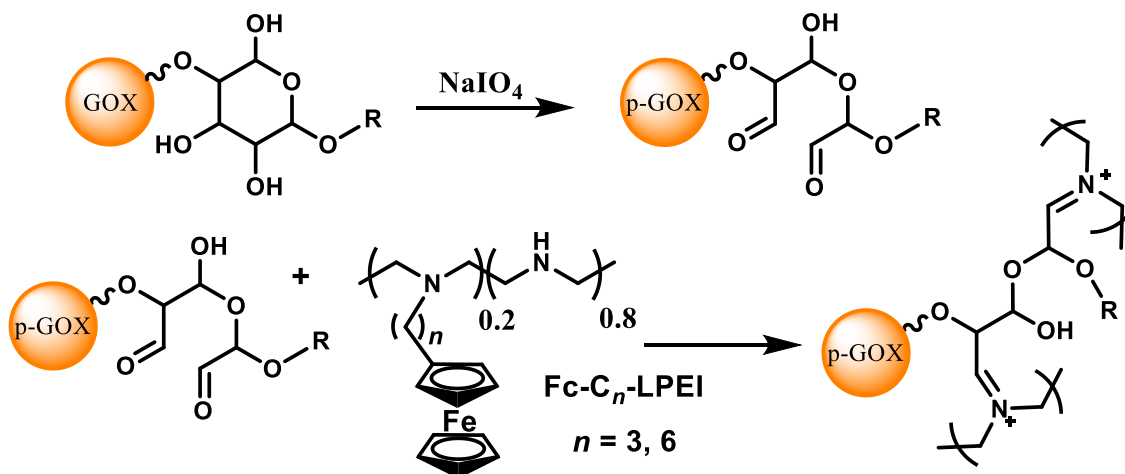


**Figure 3.2.2:** Periodate modification of glucose oxidase and presumed attachment to Fc-C<sub>n</sub>-LPEI. Ferrocene omitted in final structure for clarity.

### 3.2.2 Electrochemical Response of LBL Assembled Bioanodes

Cyclic voltammetry (CV) was used to observe the increase of ferrocene at the electrode's surface with the addition of each bilayer. As more electroactive material is

deposited, the peak current for the film should also increase. **Figure 3.2.3** compares the voltammograms (CVs) of Fc-C<sub>6</sub>-LPEI and Fc-C<sub>3</sub>-LPEI LBL films at varying numbers of bilayers using the original long wash (6-8 sec.) procedure. As shown in **Figure 3.2.3**, the peak anodic current is ca. 1.5  $\mu\text{A}$  for (Fc-C<sub>6</sub>-LPEI/p-GOX)<sub>16</sub> and ca. 9.5  $\mu\text{A}$  for (Fc-C<sub>3</sub>-LPEI/p-GOX)<sub>16</sub>: a six-fold enhancement by simply shortening the mediator spacer by three carbon units. This is likely due to the decreased steric bulk allowing for more efficient packing of material and a higher ferrocene content per unit volume. The CV also showed a characteristic decrease in the half-wave potential ( $E_{1/2}$ ) with the decrease in tether length that corresponds to previous studies.<sup>6</sup> The  $E_{1/2}$  values for Fc-C<sub>6</sub>-LPEI and Fc-C<sub>3</sub>-LPEI using the long wash were 0.33 V and 0.27 V respectively. A significant change in  $E_{1/2}$  with the number of additional bilayers was not observed.

As mentioned above, the wash time between bilayers used in the fabrication of films had a significant impact on the response. **Figure 3.2.4** shows the increase in electrochemical response for Fc-C<sub>6</sub>-LPEI and Fc-C<sub>3</sub>-LPEI films assembled with p-GOX when using a shorter wash time (<1 sec.). The peak anodic current using the short wash is ca. 2.8  $\mu\text{A}$  for (Fc-C<sub>6</sub>-LPEI/p-GOX)<sub>16</sub> and ca. 10.8  $\mu\text{A}$  for (Fc-C<sub>3</sub>-LPEI/p-GOX)<sub>16</sub>. Decreasing the wash time between each layer almost doubled the electrochemical response of Fc-C<sub>6</sub>-LPEI, but resulted in only a 10% increase for Fc-C<sub>3</sub>-LPEI. This increase in response is mostly likely due to less loosely bound material being washed away with less vigorous rinsing. The assembly of the films is attributed both to the covalent network formed from the reaction of the polymer with peripheral aldehydes on the enzyme and an attractive electrostatic interaction between the two components. Fc-C<sub>n</sub>-LPEI and p-GOX are both polyelectrolytes and a certain portion of adsorbed material

comes from this electrostatic interaction. When a new layer is deposited onto the electrostatically bound portion, and shorter, milder washing conditions are used, the excess material can form new covalent bonds and thus be incorporated into the film. Since the added steric bulk of Fc-C<sub>6</sub>-LPEI does not allow it to pack into layers as tightly as Fc-C<sub>3</sub>-LPEI, the loosely bound material is more easily washed away. This accounts for the large increase in electrochemical response for Fc-C<sub>6</sub>-LPEI but only a moderate increase for Fc-C<sub>3</sub>-LPEI.

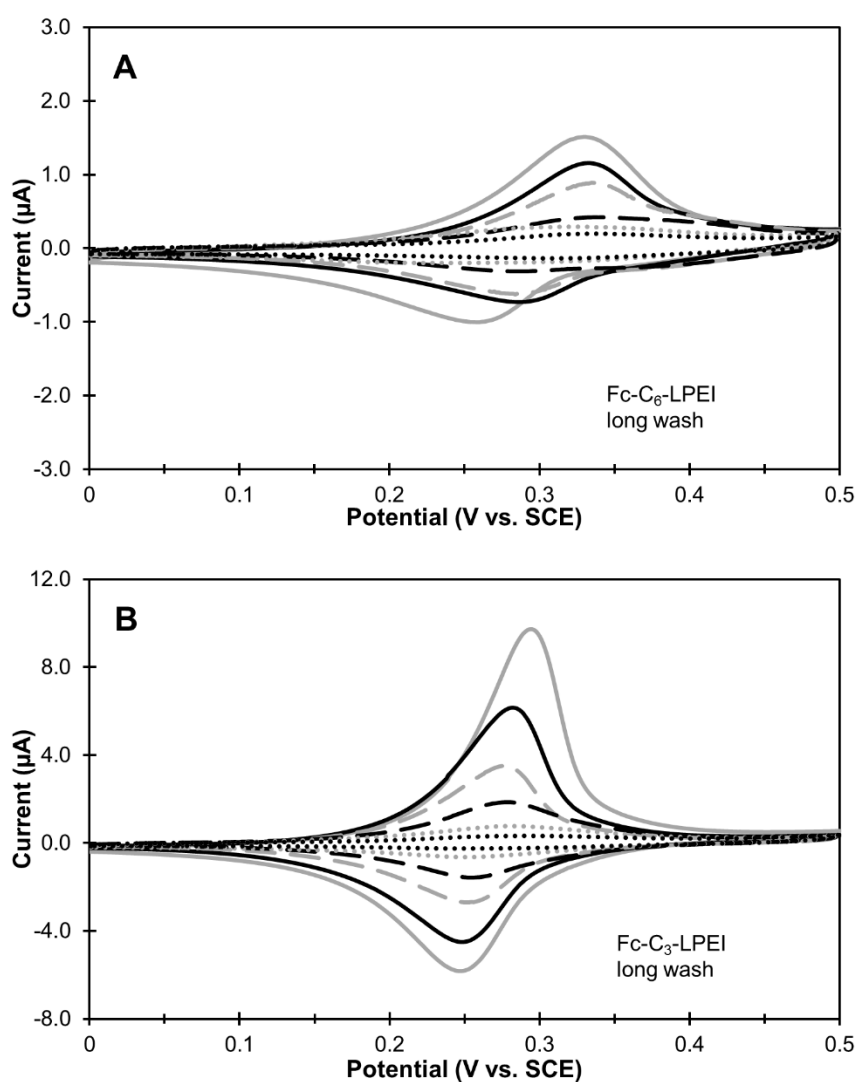


**Figure 3.2.3:** Representative CVs for  $(\text{Fc-C}_n\text{-LPEI/p-GOX})_x$  films assembled with increasing numbers of bilayers ( $x = 1, 2, 4, 8, 12, 16$ ) and the long wash method. **A)** Fc-C<sub>6</sub>-LPEI. **B)** Fc-C<sub>3</sub>-LPEI. 50 mM phosphate buffer, pH 7.0. Scan rate = 50 mV/s.

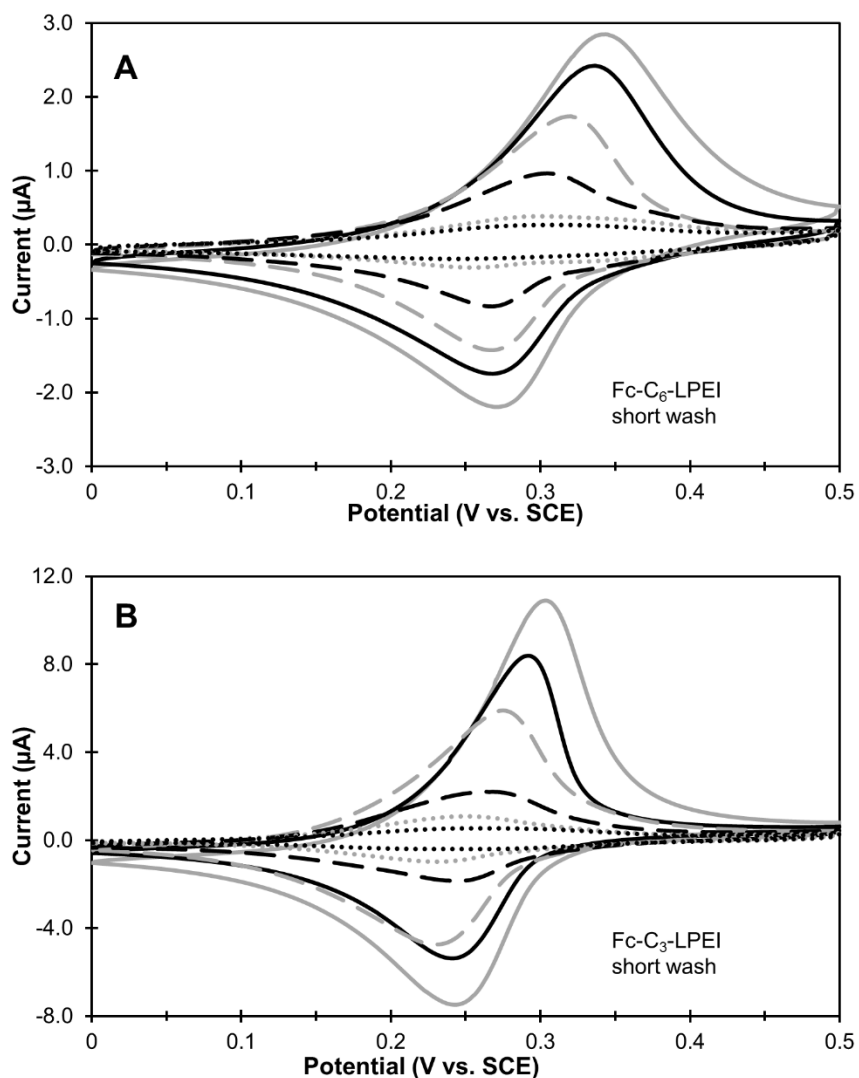


**Figure 3.2.4:** Representative CVs for  $(\text{Fc-C}_n\text{-LPEI/p-GOX})_x$  films assembled with increasing numbers of bilayers ( $x = 1, 2, 4, 8, 12, 16$ ) and the short wash method. **A)**  $\text{Fc-C}_6\text{-LPEI}$ . **B)**  $\text{Fc-C}_3\text{-LPEI}$ . 50 mM phosphate buffer, pH 7.0. Scan rate = 50 mV/s.

To probe the build-up of material, the amount of ferrocene that was deposited with the addition of polymer/enzyme bilayers was analyzed. The surface coverage of ferrocene,  $\Gamma_{\text{Fc}}$ , can be calculated from the integration under the anodic redox wave to provide the moles of redox active species on the electrode.<sup>33</sup> **Figure 3.2.5A** shows plots of  $\Gamma_{\text{Fc}}$  against the number of polymer/enzyme bilayers. Switching from a six to a three

carbon tether increased  $\Gamma_{Fc}$  by 45-85%, depending on the number of bilayers. This again suggests that longer mediator spacing interferes with the packing of the material.

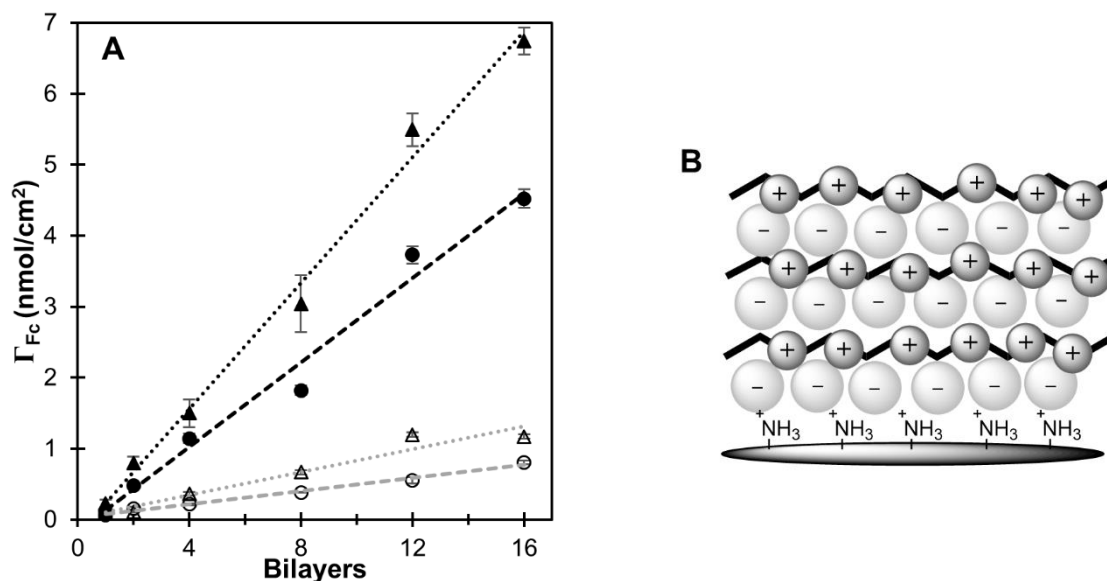


**Figure 3.2.5:** (A) Plot of ferrocene surface coverage ( $\Gamma_{Fc}$ ), obtained by integration of the anodic wave of the cyclic voltammogram, against the number of assembled bilayers. Fc-C<sub>3</sub>-LPEI, short wash (black triangle). Fc-C<sub>3</sub>-LPEI, long wash (black circle). Fc-C<sub>6</sub>-LPEI, short wash (white triangle). Fc-C<sub>6</sub>-LPEI, long wash (white circle). (B) Simplified layer-by-layer deposition of enzymes with a polyelectrolyte.

The wash time also effects the surface coverage: shortening the wash leads to an approximate 40% increase in  $\Gamma_{Fc}$  for both Fc-C<sub>6</sub>-LPEI and Fc-C<sub>3</sub>-LPEI. The relationship between  $\Gamma_{Fc}$  and number of bilayers is fairly linear, which suggests uniform distribution of ferrocene within the assembled films. However, Fc-C<sub>6</sub>-LPEI films assembled using the short wash start to plateau at 12 bilayers, which might indicate the system is reaching a distance limit by which the electroactive species can be effectively detected by electrode. Based on these results, the model for material packing seems to indicate well defined ordered layers of materials stacking on top of one another. This simple model is depicted in **Figure 3.2.5B**.

The simple model depicted in **Figure 3.2.5B**, which is a typical model proposed in the literature, does not appear to account for the possible insulating effect of the initial GOX layer. GOX does not undergo direct electron transfer,<sup>47</sup> and if an electrode were fully covered with enzyme, as depicted, it would have decreased electrochemical communication with the ferrocene moieties in the polymer. However, it has been shown in previous studies that the initial adsorption of GOX onto a surface results in patchy deposition.<sup>48,49</sup> Therefore, it is more likely that polymer fills in the gaps between enzyme clusters; which allows for electrochemical communication with the electrode. As more layers are added, the films become more like an interconnected composite rather than individually discrete layers as depicted above. To gain a better understanding of the deposition of material onto the electrode surface, electrochemical methods were used to probe the response of films constructed at increasing numbers of bilayers. Having ferrocene present in one of the deposited polyelectrolytes gives an electrochemical probe with which to further investigate the buildup of material on the surface. The peak separation ( $\Delta E$ ) in a cyclic voltammogram not only provides information about the reversibility of a reaction, but can also be used to study the relative location of the electroactive species. For a reversible, one-electron, diffusion controlled redox couple,  $\Delta E$  should be  $\sim 59$  mV, but for an ideally surface confined material  $\Delta E$  should be 0 mV.<sup>32</sup> Therefore, changes in  $\Delta E$  that arise from varying the tether length, wash time, and number of bilayers provide information about proximity and connectivity of redox centers in relation to the electrode's surface.

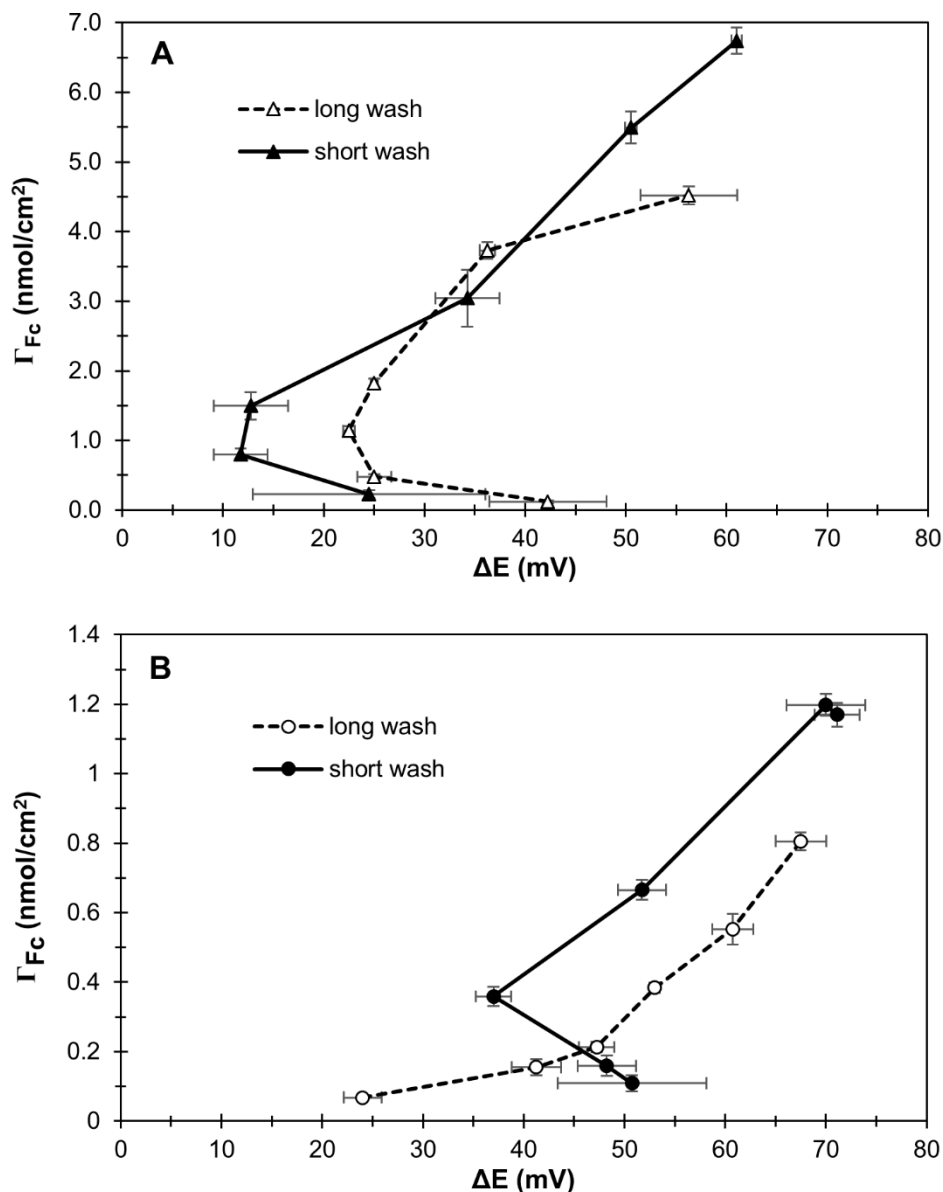


**Figure 3.2.6:** Plot of ferrocene surface coverage ( $\Gamma_{Fc}$ ), obtained by integration of the anodic wave of the CV, against the potential separation between the anodic and cathodic peaks ( $\Delta E$ ) of the CV. **(A)** Comparison of long wash (white circle) and the short wash (black circle) fabrication for Fc-C<sub>3</sub>-LPEI/p-GOX films. **(B)** Comparison of long wash (white triangle) and the short wash (black triangle) fabrication for Fc-C<sub>6</sub>-LPEI/p-GOX films.

**Figure 3.2.6A** compares  $\Delta E$  in relation to  $\Gamma_{Fc}$  for increasing numbers of bilayers for Fc-C<sub>3</sub>-LPEI films assembled using both the long and short wash washing methods. Since the initial cystamine modification of the surface is the same for all assembled films, differences in  $\Delta E$  trends between the long and short washes at least partially arise from

less enzyme and/or polymer being washed away for the short wash. By decreasing the fabrication wash time, (Fc-C<sub>3</sub>-LPEI/p-GOX)<sub>1</sub> films exhibit an increase in  $\Gamma_{\text{Fc}}$  from  $0.12 \pm 0.02$  to  $0.22 \pm 0.06$  nmolcm<sup>-2</sup> and a decrease in  $\Delta E$  from 42 to 25 mV. Under more vigorous washing condition, more material is removed from the electrode's surface which results in a less well connected film. As additional bilayers of enzyme and polymer are deposited onto the surface, there is continual increase in  $\Gamma_{\text{Fc}}$  for both the long and the short wash. The addition of bilayers also results in a decrease in  $\Delta E$  which appears to suggest that the films becoming better connected at the surface. As (Fc-C<sub>3</sub>-LPEI/p-GOX)<sub>x</sub> films reach a point of maximum connectivity at the surface, around four bilayers,  $\Delta E$  increases as the semi-surface confined films begin to act more like an ideal hydrogel.

The deposition process for (Fc-C<sub>6</sub>-LPEI/p-GOX)<sub>x</sub> films appears to be more complicated than for Fc-C<sub>3</sub>-LPEI (**Figure 3.2.6B**). The  $\Gamma_{\text{Fc}}$  for (Fc-C<sub>6</sub>-LPEI/p-GOX)<sub>1</sub> films increases from  $0.07 \pm 0.01$  to  $0.11 \pm 0.02$  nmolcm<sup>-2</sup> with the decrease in fabrication wash time due to less material being washed away. The decreased amount of electroactive ferrocene, when compared to (Fc-C<sub>3</sub>-LPEI/p-GOX)<sub>1</sub> films, is consistent with less efficient film packing due to an increase in hydrodynamic radius resulting from the increased tether length. However, there is an apparent difference in deposition process for (Fc-C<sub>6</sub>-LPEI/p-GOX)<sub>x</sub> films with regards to the washing procedure. Whereas the less vigorous washing helped to improve connectivity of the (Fc-C<sub>3</sub>-LPEI/p-GOX)<sub>1</sub> films by initially depositing more polymer onto the surface, (Fc-C<sub>6</sub>-LPEI/p-GOX)<sub>1</sub> films assembled using the short wash appear to be less cohesive than those assembled using the long wash. This is evidenced by the differences in  $\Delta E$  between the two polymers at one bilayer: 51 mV for Fc-C<sub>6</sub>-LPEI and 25 mV for Fc-C<sub>3</sub>-LPEI, both assembled using the



short wash. Since the packing of the Fc-C<sub>6</sub>-LPEI is less efficient, having more polymer present in the first bilayer leads to less electrochemical connectivity due to steric repulsions between polymer strands. Material that is deposited in subsequent bilayers is still not very well packed, but  $\Delta E$  decreases with additional bilayers as the patchy surface is filled in and the films become better connected. The (Fc-C<sub>6</sub>-LPEI/p-GOX)<sub>x</sub> films fabricated with the short wash do not become as surface confined as (Fc-C<sub>3</sub>-LPEI/p-GOX)<sub>x</sub> films, but the films reach a maximum connectivity at four bilayers before gaining more hydrogel character at higher numbers of bilayers.

There is very little electroactive polymer deposited for (Fc-C<sub>6</sub>-LPEI/p-GOX)<sub>1</sub> films fabricated with the long wash method. Since the more sterically bulky polymer does not pack as well with the enzyme, more vigorous washing removes all but the most tightly adhered material. Therefore, the small amount of adsorbed material is reasonably well connected to the surface, as evidenced by the  $\Delta E$  of 24 mV. As further bilayers build upon this patchy network, material is deposited in such a fashion that connectivity to the electrode surface does not get any better established. The further buildup of material simply increases the hydrogel characteristics of the films

The LBL deposition of material is a surprisingly complex phenomenon to characterize. Based solely on electrochemical analysis, it is possible to show that Fc-C<sub>3</sub>-LPEI forms better defined films than Fc-C<sub>6</sub>-LPEI, but the deposition of material is complicated by the interconnected electrochemical properties that arise from film thickness and redox connectivity. Together with its enhanced electrochemical response, it was likely that Fc-C<sub>3</sub>-LPEI would yield higher currents in response to glucose.

### 3.2.3 Electrochemical Stability of LBL Assembled Biosensors

To determine how mediator tether length and fabrication wash time affects the electrochemical stability of cross-linked (Fc-C<sub>n</sub>-LPEI/p-GOX)<sub>12</sub> films, the potential of the electrodes was cycled between 0.0 and 0.5 V vs. SCE. The charge of each system, as determined from the integrated area of the oxidation wave, was plotted as a function of time to quantitatively determine the electrochemical stability of LBL assembled bioanodes.

As shown in **Figure 3.2.7**, (Fc-C<sub>6</sub>-LPEI/p-GOX)<sub>12</sub> films assembled using both wash methods and (Fc-C<sub>3</sub>-LPEI/p-GOX)<sub>12</sub> films assembled using the short wash method lost over 50% of their charge within 0.5 hours, and lost over 90% of their charge within five hours. (Fc-C<sub>3</sub>-LPEI/p-GOX)<sub>12</sub> films constructed using the short wash were slightly more stable: 50 loss of charge in 0.75 hours and ~85% loss within five hours. This large loss of charge in a relatively short amount of time is most likely due to either (1) electrochemical degradation of ferrocene or (2) the loss of material into solution from a reversal of the LBL assembly process. The covalent imine linkages between Fc-C<sub>n</sub>-LPEI and p-GOX (**Figure 3.2.2**) could be reversing since the amount of material on the electrode surface is so small and the aqueous medium is in excess while films are being tested. To probe which of these factors could be playing a role in charge stability, (Fc-C<sub>3</sub>-LPEI/p-GOX)<sub>x</sub> films were constructed with varying numbers of bilayers and the potential was cycled between 0.0 and 0.5 V vs. SCE.

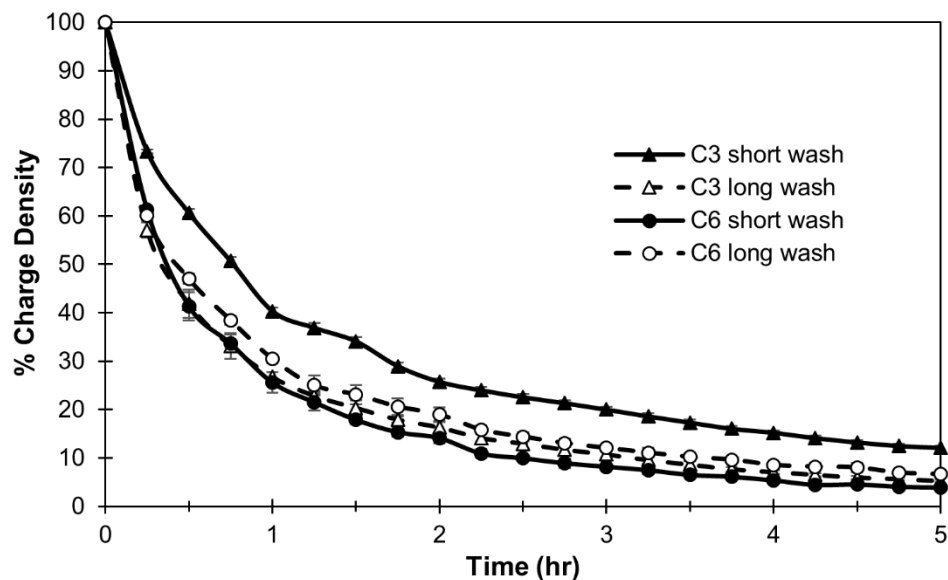


**Figure 3.2.7:** Plot of the changes in charge for LBL assembled  $(\text{Fc-C}_n\text{-LPEI/p-GOX})_{12}$  films obtained by cycling the applied potential between 0.0 and 0.5 V vs SCE. Scan rate = 50 mV/s. 50 mM phosphate buffer (pH 7.0, T = 25 °C).

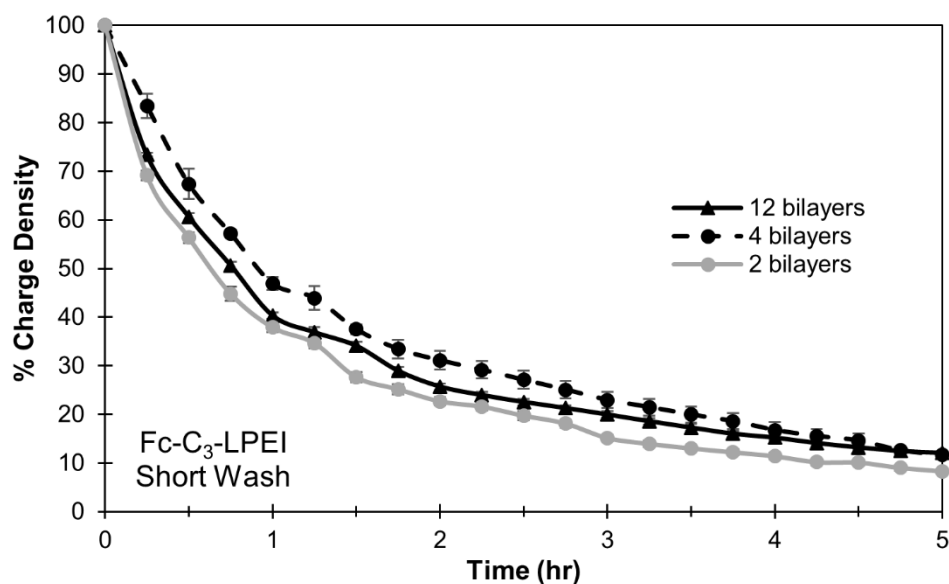


**Figure 3.2.8:** Plot of the changes in charge for LBL assembled  $(\text{Fc-C}_3\text{-LPEI/p-GOX})_x$  films obtained by cycling the applied potential between 0.0 and 0.5 V vs SCE in 50 mM phosphate buffer (pH 7.0, T = 25 °C).

**Figure 3.2.8** shows that  $(\text{Fc-C}_3\text{-LPEI/p-GOX})_x$  films experience the nearly the same percent charge decrease over time, regardless of the number of bilayers. This suggests that the loss in charge is most likely coming from electrochemical degradation rather than from loss of material into the solution. If the films were delaminating from

the electrode's surface, there should be a much larger decrease in response for the films with smaller numbers of bilayers. A loss of one layer of redox polymer for (Fc-C<sub>3</sub>-LPEI/p-GOX)<sub>2</sub> would have a much greater impact than for (Fc-C<sub>3</sub>-LPEI/p-GOX)<sub>12</sub>, assuming the delamination is occurring from the top down.

The electrochemical stability of LBL assembled (Fc-C<sub>3</sub>-LPEI/p-GOX)<sub>x</sub> films was further probed by increasing the crosslinking between films by vapor deposition of acrolein. In 2004, Erickson demonstrated that LPEI could be successfully crosslinked in solution by using acrolein.<sup>34</sup> Since acrolein is extremely volatile, it was used to further crosslink the (Fc-C<sub>3</sub>-LPEI/p-GOX)<sub>x</sub> assembled on the surface of an electrode via chemical vapor deposition. Previous work by Hickey *et al.* has demonstrated that an increase in the amount of crosslinker added to tetramethylferrocene-modified LPEI films results in an increase in E<sub>1/2</sub>.<sup>35</sup> After 15 minutes in an acrolein vapor chamber, the E<sub>1/2</sub> of (Fc-C<sub>3</sub>-LPEI/p-GOX)<sub>12</sub> films increased from 0.27 V to 0.31 V vs. SCE signifying an increase in film crosslinking.

**Figure 3.2.9** shows the effect of acrolein vapor deposition on the electrochemical stability of LBL assembled (Fc-C<sub>3</sub>-LPEI/p-GOX)<sub>x</sub> films. A significant change in response was not observed for (Fc-C<sub>3</sub>-LPEI/p-GOX)<sub>12</sub> films; however (Fc-C<sub>3</sub>-LPEI/p-GOX)<sub>2</sub> and (Fc-C<sub>3</sub>-LPEI/p-GOX)<sub>4</sub> films exhibited a faster charge degradation after acrolein vapor deposition. This further suggests that the instability of LBL assembled films results from electrochemical degradation of ferrocene rather than from the loss of material resulting from imine hydrolysis.

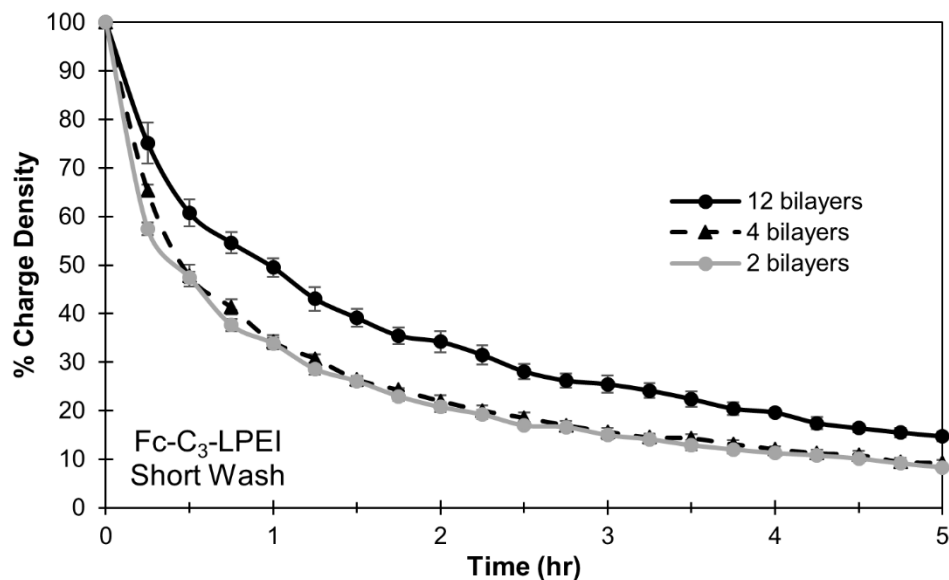


**Figure 3.2.9:** Plot of the changes in charge for LBL assembled (Fc-C<sub>3</sub>-LPEI/p-GOX)<sub>x</sub> films after acrolein vapor deposition. Obtained by cycling the applied potential between 0.0 and 0.5 V vs SCE in 50 mM phosphate buffer (pH 7.0, T = 25 °C).

#### 3.2.4 Enzymatic Response of LBL Assembled Biosensors

In order to evaluate how LBL assembled films would perform in a biosensor, glucose calibration curves for films were obtained by poisoning the electrodes at an oxidizing potential (0.5 V for Fc-C<sub>6</sub>-LPEI and 0.35 V for Fc-C<sub>3</sub>-LPEI) and adding increasing amounts of glucose into the cell. **Figure 3.2.10** shows steady-state glucose response curves for Fc-C<sub>6</sub>-LPEI/p-GOX and Fc-C<sub>3</sub>-LPEI/p-GOX films assembled using the long wash method at glucose levels between 0 and 100 mM. Decreasing the mediator tether by three carbons led to an increase in the maximum current density at saturating glucose concentration ( $J_{max}$ ). For films assembled with sixteen bilayers, switching from Fc-C<sub>6</sub>-LPEI to Fc-C<sub>3</sub>-LPEI resulted in an increase in  $J_{max}$  from  $222 \pm 19$  to  $980 \pm 51 \mu\text{Acm}^{-2}$ . As previously seen in **Figure 3.2.5A**,  $\Gamma_{\text{Fc}}$  is higher for Fc-C<sub>3</sub>-LPEI films, so the flow of electrons from the enzyme to the electrode is better mediated.

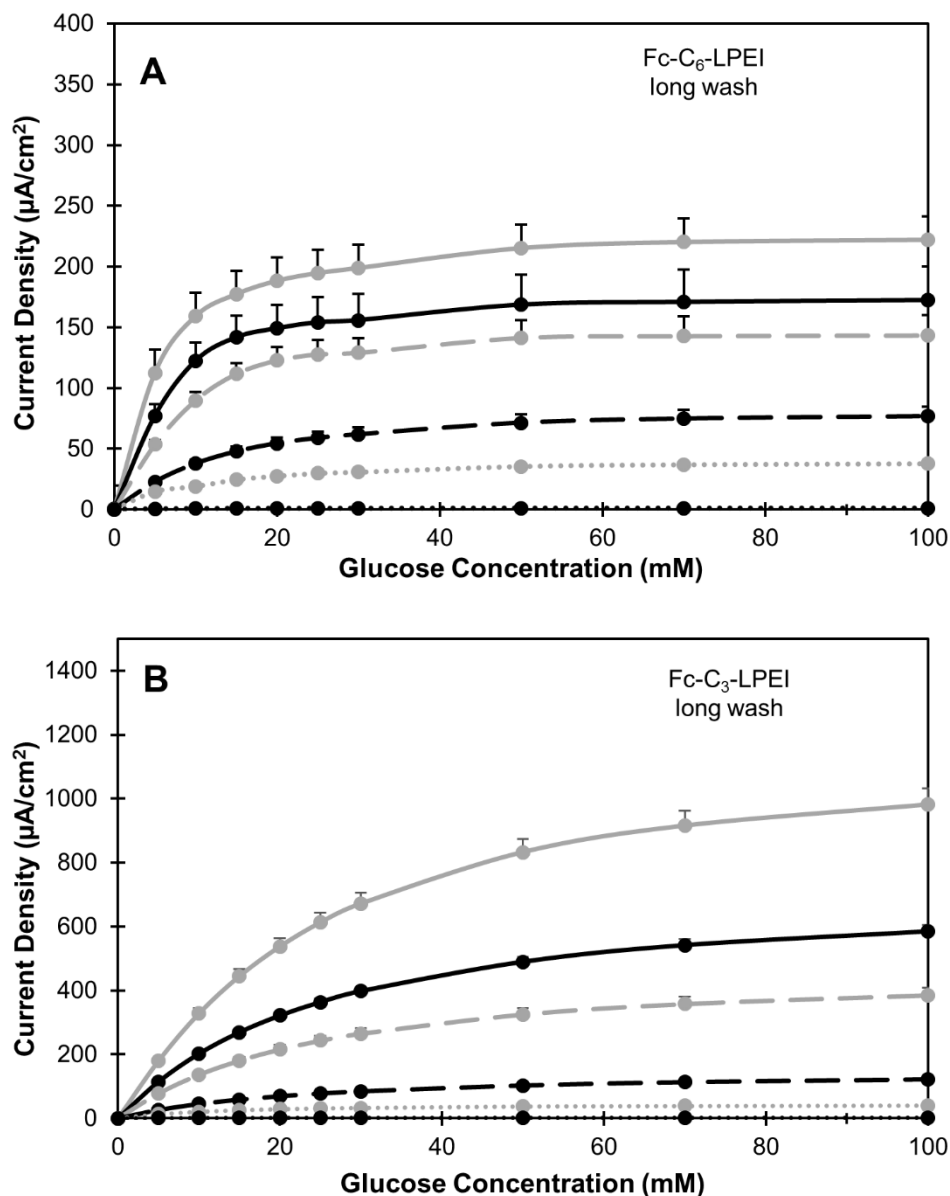


**Figure 3.2.10:** Effect of mediator tether length on glucose response for  $(\text{Fc-C}_n\text{-LPEI/p-GOX})_x$  films assembled with increasing number of bilayers ( $x = 1, 2, 4, 8, 12, 16$ ) and the long wash method. **A)**  $\text{Fc-C}_6\text{-LPEI}$ . **B)**  $\text{Fc-C}_3\text{-LPEI}$ .

The difference in wash time also had an impact on  $J_{max}$  for both redox polymers. Glucose calibration curves for LBL assembled films using the shorter wash method are shown in **Figure 3.2.11**. For  $(\text{Fc-C}_6\text{-LPEI/p-GOX})_{16}$  films (**Figure 3.2.11A**), shortening the wash time increases  $J_{max}$  from  $222 \pm 19$  to  $381 \pm 3 \mu\text{Acm}^{-2}$ , an increase of just over 70%. As seen in **Figure 3.2.11B**,  $(\text{Fc-C}_3\text{-LPEI/p-GOX})_{16}$  films assembled using the short

wash method resulted in an increase of  $J_{max}$  to  $1417 \pm 63 \mu\text{Acm}^{-2}$ , about 45% higher than for the long wash.

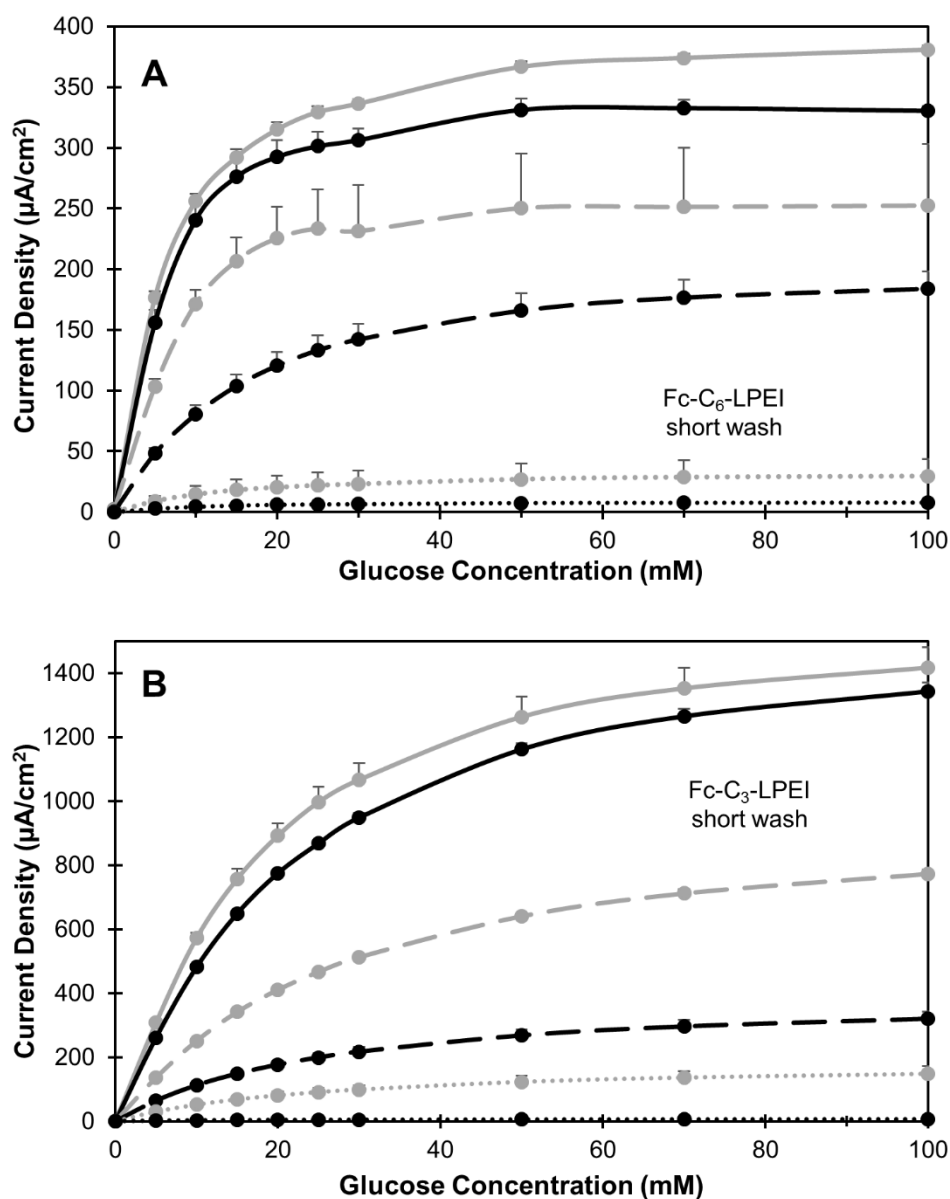


**Figure 3.2.11:** Effect of mediator tether length on glucose response for  $(\text{Fc-C}_n\text{-LPEI/p-GOX})_x$  films assembled with increasing number of bilayers ( $x = 1, 2, 4, 8, 12, 16$ ) and the short wash method. **A)** Fc-C<sub>6</sub>-LPEI. **B)** Fc-C<sub>3</sub>-LPEI.

LBL fabricated films are able to produce high current densities with minimal amounts of redox polymer. Comparing  $i_{pa}$  values from the CVs, it is clear that 16 bilayer films contain about 5-10% of the amount of electroactive ferrocene moieties found in

solution cast, crosslinked films (**Table 3.2.1**). For (Fc-C<sub>6</sub>-LPEI/p-GOX)<sub>16</sub> films,  $J_{max}$  is a third to two-thirds that of solution cast films, depending on the washing method. In contrast, LBL assembled (Fc-C<sub>3</sub>-LPEI/p-GOX)<sub>16</sub> biosensors are capable of generating as much current as solution cast films.<sup>6</sup> When using the short wash method, the films actually surpass the current output of the previously reported glucose biosensors using the same materials. This is important for two reasons: processing time and amount of material. The time needed to fabricate the LBL assembled films ranges from half an hour to four hours depending on the desired number of bilayers. This is significantly lower than the twenty-four hours of curing time currently needed for solution cast films of the same materials crosslinked with EGDGE.

**Table 3.2.1:** Effect of Fc-C<sub>n</sub>-LPEI biosensor fabrication method on electrochemical and enzymatic response.

<i>Method</i>	<i>i<sub>pa</sub></i>		<i>J<sub>max</sub></i> (μAcm <sup>-2</sup> )	
	<i>Fc-C<sub>6</sub>-LPEI</i>	<i>Fc-C<sub>3</sub>-LPEI</i>	<i>Fc-C<sub>6</sub>-LPEI</i>	<i>Fc-C<sub>3</sub>-LPEI</i>
EGDGE crosslinked <sup>6</sup>	50	95	625 ± 6	1020 ± 61
16 BL, long wash	1.3	9.2	222 ± 19	980 ± 51
16 BL, short wash	2.5	10.5	381 ± 3	1417 ± 63

It should be noted that  $J_{max}$  for (Fc-C<sub>3</sub>-LPEI/p-GOX)<sub>12</sub> and (Fc-C<sub>3</sub>-LPEI/p-GOX)<sub>16</sub> films assembled with the short wash are quite close together (**Figure 3.2.11B**). Since  $\Gamma_{Fc}$  for LBL assembled Fc-C<sub>3</sub>-LPEI never reached a plateau and are much higher than for Fc-C<sub>6</sub>-LPEI (**Figure 3.2.5A**), the films most likely have a more densely packed polymer network. This appears to hinder the diffusion of glucose through the films, as evidenced by the 5.5% increase in  $J_{max}$  relative to the 22% increase in  $\Gamma_{Fc}$  when increasing from twelve to sixteen bilayers. To better understand the possible glucose diffusion



limitations, changes in sensitivity and the Michaelis constant ( $K_M$ ), i.e. the concentration at which the reaction rate is half of the maximum response, were studied.

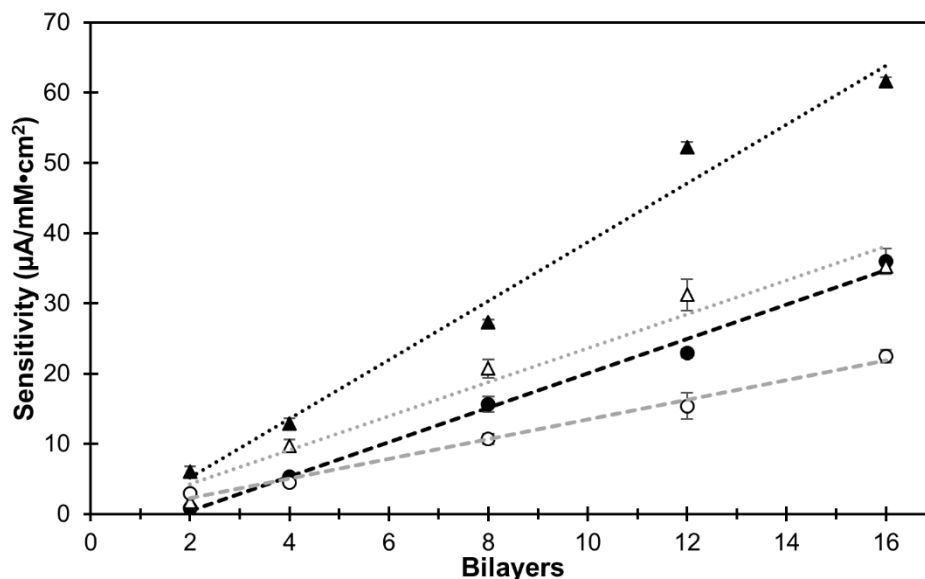


**Figure 3.2.12:** Plot of biosensor sensitivity at 5 mM glucose against the number of assembled bilayers. Fc-C<sub>3</sub>-LPEI, short wash (black triangle). Fc-C<sub>3</sub>-LPEI, long wash (black circle). Fc-C<sub>6</sub>-LPEI, short wash (white triangle). Fc-C<sub>6</sub>-LPEI, long wash (white circle).

**Figure 3.2.12** shows how ferrocene mediator spacing and the wash method effect the biosensor's sensitivity at 5 mM glucose. The decrease in tether length corresponded to an increase in sensitivity, which is consistent with previous results from solution cast films.<sup>6</sup> Decreasing the wash time also led to an increase in sensitivity for both (Fc-C<sub>6</sub>-LPEI/p-GOX)<sub>x</sub> and (Fc-C<sub>3</sub>-LPEI/p-GOX)<sub>x</sub> films. We had previously reported that the sensitivity of (Fc-C<sub>6</sub>-LPEI/p-GOX)<sub>x</sub> films assembled using the long wash procedure compared favorably with LBL films fabricated using osmium-based redox polymers, and were significantly higher than LBL films constructed using other ferrocene-based redox polymers.<sup>28</sup> The sensitivities for (Fc-C<sub>3</sub>-LPEI/p-GOX)<sub>x</sub> films are nearly triple those of (Fc-C<sub>6</sub>-LPEI/p-GOX)<sub>x</sub> films, which makes these among the most highly sensitive LBL assembled glucose biosensors currently reported in the literature.<sup>28</sup> The sensitivity of both

polymers increased at a linear rate regardless of the wash time used. This suggests an ultimately uniform dispersion of enzyme and polymer with each additional bilayer, even if the deposition of material does not initially occur in distinctly isolated layers as depicted in **Figure 3.2.5B**. Since sensitivity is not determined at saturating conditions, it is also necessary to look at changes in  $K_M$  to better understand diffusion limitations of the Fc- $C_n$ -LPEI/p-GOX films.

Since the response of p-GOX is indirectly determined using electrochemical methods, all reported  $K_M$  values are actually apparent  $K_M$  values ( $K_M^*$ ). Figure 6 shows the relationship between  $K_M^*$  and the number of Fc- $C_n$ -LPEI/p-GOX bilayers. The differences in  $K_M^*$ , with respect to the number of bilayers, can arise from changes in enzyme inhibition, substrate diffusion, or mediator communication. Enzyme inhibition often changes  $K_M$  by several orders magnitude, and all Fc- $C_n$ -LPEI/p-GOX films have good electrochemical communication with the electrode, as evidenced by the CV data. Therefore, the small changes in  $K_M^*$  shown in **Figure 3.2.113** are most likely arising from the limitation of glucose diffusion into the films. At one bilayer, the materials are close to the surface, which results in good glucose diffusion and low  $K_M^*$  values. Fc- $C_6$ -LPEI/p-GOX films assembled with both the long and short washing procedure follow the same trend: an increase in  $K_M^*$  up to four bilayers followed by a gradual decrease with the addition of more material. As the films become more compact at two and four bilayers, glucose has difficulty penetrating to the inner layers of the films and is most likely only being catalyzed near the outer surface of the film. Once greater numbers of bilayers are added, there is a larger volume near the surface of the film into which glucose can diffuse; resulting in a decrease in  $K_M^*$  that plateaus at twelve bilayers.

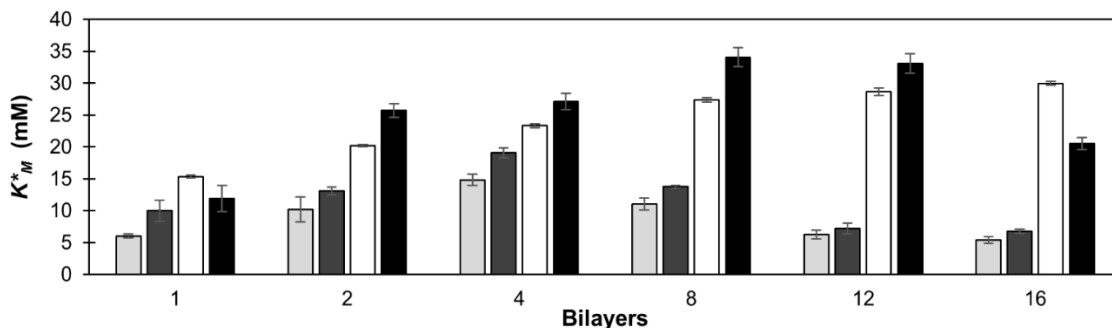


**Figure 3.2.13:** Effect of mediator tether length and fabrication wash time on  $K_M^*$  for Fc-C<sub>n</sub>-LPEI/p-GOX films assembled with increasing number of bilayers (1, 2, 4, 8, 12, 16). Fc-C<sub>6</sub>-LPEI, long wash (light gray). Fc-C<sub>6</sub>-LPEI, short wash (dark gray). Fc-C<sub>3</sub>-LPEI, long wash (white). Fc-C<sub>3</sub>-LPEI, short wash (black)

For Fc-C<sub>3</sub>-LPEI/p-GOX films assembled with the long wash there is a continual increase in  $K_M^*$  with the addition of each bilayer. Even though there are more redox active sites available in the Fc-C<sub>3</sub>-LPEI films, the tighter packing that arises from the shorter mediator spacing prevents glucose from reaching the enzyme as easily. However, Fc-C<sub>3</sub>-LPEI/p-GOX films assembled with the short wash exhibit a decrease in  $K_M^*$  from twelve to sixteen bilayers. The above observations show that Fc-C<sub>3</sub>-LPEI films require a greater amount of material to achieve the same decrease in  $K_M^*$  that was seen for Fc-C<sub>6</sub>-LPEI. It is noteworthy that  $K_M^*$  for Fc-C<sub>6</sub>-LPEI is consistently lower than Fc-C<sub>3</sub>-LPEI regardless of the number of bilayers or wash time. Because the increased steric repulsion of Fc-C<sub>6</sub>-LPEI allows for larger interstitial spaces, glucose can diffuse more freely into it.

### 3.2.5 Performance of LBL Assembled Anodes in a Biofuel Cell

The high current density response of LBL assembled (Fc-C<sub>3</sub>-LPEI/p-GOX)<sub>x</sub> films to glucose made them of interest for the construction of compartmentless-biofuel cells. Due to their maximal current density and ease of fabrication, (Fc-C<sub>3</sub>-LPEI/p-GOX)<sub>8</sub> films constructed using the short washing method were chosen as bioanodes. A commercially available, air-breathing platinum electrode was chosen as the cathode in an effort to ensure that it would not be the limiting electrode in the biofuel cell.

The (Fc-C<sub>3</sub>-LPEI/p-GOX)<sub>8</sub> bioanode and air breathing platinum cathode were allowed to equilibrate in a solution of 100 mM glucose at open circuit potential for 60 seconds before being tested. The resulting power curves are shown in **Figure 3.2.14A**. These fuel cells were able generate  $86 \pm 3 \mu\text{Wcm}^{-2}$  at ca. 132 mV with a maximum current density of  $776 \pm 3 \mu\text{Acm}^{-2}$  at pH 7.0 and 25°C. This demonstrated that LBL fabrication provides a quick and facile means to produce redox active bioanodes that can be used in effective biofuel cells.

The compartmentless fuel cells were originally run at pH 7.0 to mimic physiological conditions, but because the activity of platinum is known to be pH dependent, the fuel cells were retested at pH 5.0. The results for the fuel cell and the corresponding steady-state glucose response curves are shown in **Figures 3.2.14**. By lowering the pH two units, the power density of the fuel cell increased to  $149 \pm 7 \mu\text{Wcm}^{-2}$  at ca. 184 mV, with a maximum current density of  $930 \pm 34 \mu\text{Acm}^{-2}$  at pH 5 and 25°C. When the same bioanodes were run as a biosensor (Figure 7B),  $J_{max}$  decreased from  $773 \pm 13 \mu\text{Acm}^{-2}$  at pH 7.0 to  $355 \pm 17 \mu\text{Acm}^{-2}$  at pH 5.0. Therefore, the increased biofuel cell power results from the air breathing cathode, and shows it is the rate limiting electrode in spite of its large surface area. Raising the potential of platinum, and having a greater proton concentration that facilitates the reduction of oxygen to water, accounts for the increase in response of the fuel cell at pH 5.0. Biofuel response is expected to improve with the addition of more bilayers.

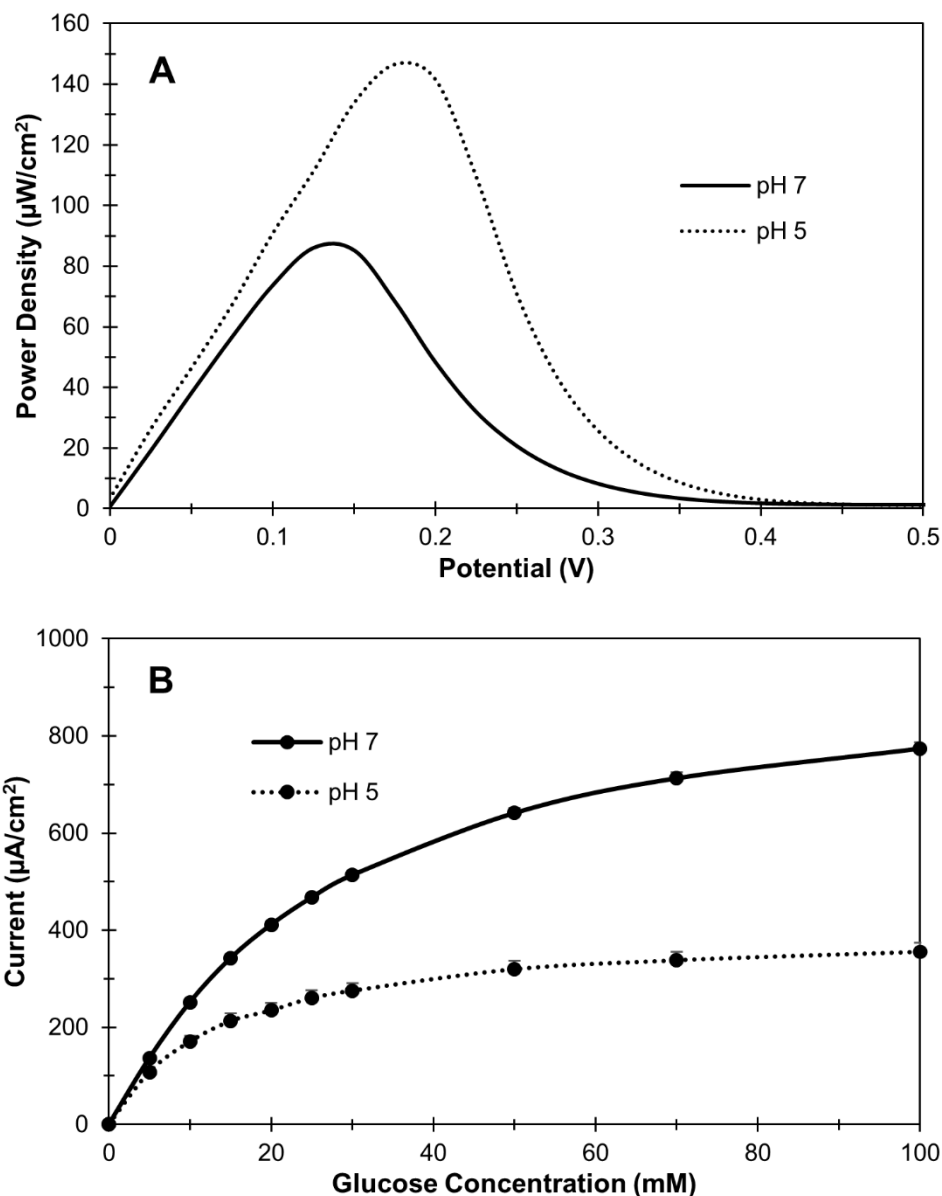


**Figure 3.2.14:** Effect of electrolyte pH on  $(\text{Fc-C}_3\text{-LPEI/p-GOX})_8$  bioanode performance: pH 7.0 (solid), pH 5.0 (dotted). (A) Representative power curves obtained by poisoning the potential against an air-breathing Pt cathode. Scan rate =  $2 \text{ mVs}^{-1}$ . (B) Constant potential, steady state glucose calibration curves.  $E = 0.35 \text{ V}$ .

The power densities for  $(\text{Fc-C}_3\text{-LPEI/p-GOX})_8/\text{Pt}$  biofuel cells compare favorably with other glucose/oxygen biofuel cells using LBL surface modified electrodes (**Table 3.2.2**).

**Table 3.2.2:** Comparison of glucose/oxygen biofuel cells fabricated using LBL assembly

Electrode	Anode	Cathode	$P_{max}$ ( $\mu\text{W}/\text{cm}^2$ )	$V_{P_{max}}$ (mV)	$pH$	$T$ ( $^{\circ}\text{C}$ )	Ref.
3DOM gold	(AuNP/GDH) <sub>5</sub>	(AuNP/laccase) <sub>5</sub>	178	226	6.0	RT	36
planar gold	(AuNP/GDH) <sub>5</sub>	(AuNP/laccase) <sub>5</sub>	12.6	360	6.0	RT	36
ITO	(MWNT/thionine/AuNP) <sub>8</sub> /GDH	(MWNT/PLL/laccase) <sub>15</sub>	329	470	6.0	RT	37
carbon paper	MWNT/(GOX/Pt-DEN) <sub>3</sub>	Pt on carbon paper*	17	NR	6.8	RT	38
glassy carbon	(SWNT/NADP <sup>+</sup> /GDH) <sub>1</sub>	SWNT/bilirubin oxidase*	23	NR	7.0	RT	39
glassy carbon	MG/(graphene/MWNT) <sub>5</sub> /GDH	SWNT/laccase*	22.5	480	6.0	RT	40
graphite	(PVI-OsOme/GOX) <sub>2</sub>	(PVI-OsCl/laccase) <sub>2</sub>	103	350	5.0	37	41
planar gold	(Fc-C <sub>3</sub> -LPEI/p-GOX) <sub>8</sub>	air-breathing Pt*	149	184	5.0	RT	This work

3DOM = three-dimensional ordered macroporous  
 AuNP = gold nanoparticle  
 GDH = glucose dehydrogenase  
 MWNT = multiwall nanotube  
 ITO = iridium tin oxide  
 PLL = poly-L-lysine  
 Pt-DEN = poly(amidoamine) dendrimer-encapsulated platinum nanoparticles  
 SWNT = single wall nanotube  
 MG = methylene green  
 PVI-OsOme = methoxypiperidyl osmium-modified poly(vinylimidazole)  
 PVI-OsCl = chloropiperidyl osmium-modified poly(vinylimidazole)  
 NR = not reported  
 RT = room temperature  
 \* not constructed using LBL assembly

All previously reported LBL assembled biofuel cells have used nanoparticles (gold<sup>36,37</sup> or platinum<sup>38</sup>), nanotubes (single<sup>39</sup> or multiwall<sup>37,38,40</sup>), graphene<sup>40</sup>, or high surface area electrodes (graphite<sup>41</sup>, carbon paper<sup>38</sup>, macroporous gold<sup>36</sup>) in their fabrication. These materials either artificially increase the electrode surface area or enhance electronic conductivity through the assembled films. The work presented herein employs planar, low-surface area gold electrodes coated with thin conducting films that accurately reflect the geometric surface in the power densities. Fc-C<sub>3</sub>-LPEI produces current via collisional electron transfer that is not enhanced by the addition of nanoparticles, which makes the obtained results even more favorable in comparison.

### **3.3 Methylated Ferrocene Polymers and Preliminary Nanotube Incorporation**

The high performance of the (Fc-C<sub>3</sub>-LPEI/p-GOX)<sub>x</sub> biofuel cells led to an investigation into the usage of methylated ferrocene polymers for LBL assembly. It has been previously shown that (dimethylferrocenyl)-propyl and tetramethylferrocenyl)-propyl modified LPEI (FcMe<sub>2</sub>-C<sub>3</sub>-LPEI and FcMe<sub>4</sub>-C<sub>3</sub>-LPEI) decrease the potential of the redox polymer and subsequently reduces the overpotential at the bioanode.<sup>9,35</sup> However, the usage of these polymers in LBL assembly with p-GOX was not possible due to the rapid oxidation of the ferrocene species in the acidic conditions used in the fabrication process. Various reducing agents (zinc, magnesium, manganese, and hydrazine) were used in an attempt to prevent oxidation in solution, but none of the materials tested provided significant protection for the amount of time needed to build a large number of bilayers. Since the oxidation of the methylated ferrocene polymers could not be inhibited for the extended amounts of time needed for the LBL assembly process,

it was thought that a high surface area electrode could maximize the amount of material that can be deposited in a minimum amount of time.

### 3.3.1 *Single Walled Nanotube Modified Glassy Carbon Electrodes*

LPEI is known to wrap around carbon nanotubes,<sup>46</sup> and it has been previously shown that Fc-C<sub>n</sub>-LPEI exhibits an increase in electrochemical response when crosslinked in the presence of single walled nanotubes (SWNT).<sup>44</sup> Glassy carbon electrodes modified with an entangled network of SWNTs (SWNT-GCE) were investigated as a viable option for the LBL assembly of LPEI based redox polymers by first constructing films with Fc-C<sub>3</sub>-LPEI and p-GOX. SWNT-GCEs were prepared as previously reported<sup>44,45</sup> by first casting 10  $\mu$ L of an aqueous suspension of SWNTs (0.4 mg/mL) and surfactant Triton X-100 (5 mg/mL) on a polished electrode's surface. SWNT-GCEs were then allowed to dry in a dessicator overnight prior to usage.

SWNT-GCEs were immersed in solution of redox polymer (Fc-C<sub>3</sub>-LPEI, FcMe<sub>2</sub>-C<sub>3</sub>-LPEI, FcMe<sub>4</sub>-C<sub>3</sub>-LPEI) for five minutes to deposit an initial layer of polymer. Electrodes were removed from solution and rinsed with Nanopure water using the short wash method described above. Care should be taken when rinsing the SWNT-GCEs so as not to delaminate the deposited nanotube film. Polymer coated electrodes were placed in a solution of p-GOX, incubated for five minutes, and then rinsed with Nanopure water. **Figure 3.3.1** shows the increase in current response for (Fc-C<sub>3</sub>-LPEI/p-GOX)<sub>1</sub> films fabricated on both planar gold electrodes and SWNT-GCEs using the short wash fabrication method.



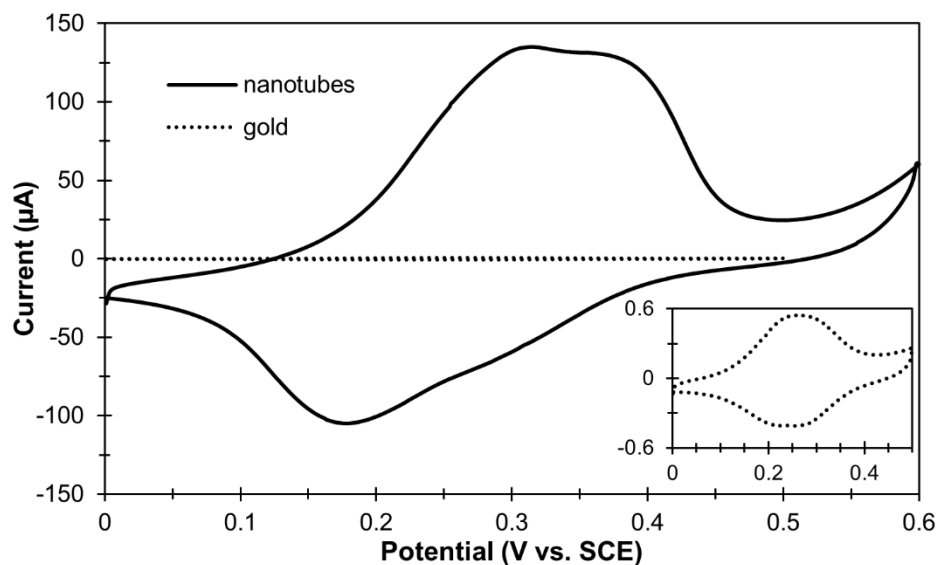


**Figure 3.3.1:** Representative CVs for  $(\text{Fc-C}_3\text{-LPEI/p-GOX})_1$  films assembled using the short wash method on both planar gold electrodes and SWNT-GCEs. Inset graph depicts the CV for gold electrodes to more accurately depict shape.

Films were fabricated using identical conditions for both of the electrode types used, and, as evidenced by the CV, there was a large increase in the amount of electroactive ferrocene deposited onto the SWNT-GCEs versus the planar gold electrodes. The CV for  $(\text{Fc-C}_3\text{-LPEI/p-GOX})_1$  films fabricated on SWNT-GCEs showed two redox peaks which suggests the ferrocene is in multiple micro-environments; most likely arising from polymer adsorbed strongly to and farther away from the SWNTs.

Glucose calibration curves for  $(\text{Fc-C}_3\text{-LPEI/p-GOX})_1$  films were obtained by poisoning the electrodes at an oxidizing potential (0.35 V for gold, 0.45 V for SWNT-GCE) and adding increasing amounts of glucose into the cell. **Figure 3.3.2** shows steady-state glucose response curves for  $(\text{Fc-C}_3\text{-LPEI/p-GOX})_1$  films constructed on both gold and SWNT-GCEs using the short wash method. Switching to a high surface area electrode increased  $J_{max}$  from  $7.2 \pm 1.4$  to  $2883 \pm 149 \mu\text{Acm}^{-2}$ , using the geometric surface area of the GCE. The response for  $(\text{Fc-C}_3\text{-LPEI/p-GOX})_1$  films constructed on SWNT-GCE is more than double the response for  $(\text{Fc-C}_3\text{-LPEI/p-GOX})_{16}$  films constructed on planar

gold electrodes. LBL films fabricated on high surface area electrodes provide a facile method to generate high current density glucose biosensors in less than fifteen minutes. Based on the extraordinary response for Fc-C<sub>3</sub>-LPEI, LBL assembled bioanodes were assembled using methylated ferrocene redox polymers

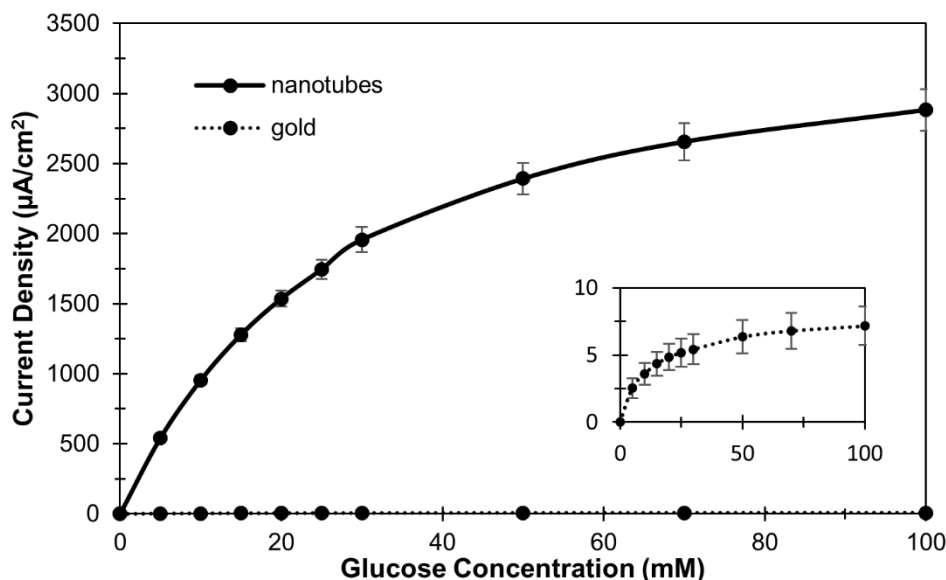


**Figure 3.3.2:** Constant amperometry glucose response curves for (Fc-C<sub>3</sub>-LPEI/p-GOX)<sub>1</sub> films assembled using the short wash method on both planar gold electrodes and SWNT-GCEs. Inset graph depicts the results for gold electrodes to more accurately depict response.

### 3.3.2 Effect of Methylation of LBL Assembled Bioanodes

Having shown that SWNT-GCEs provide a viable alternative for the LBL assembly of Fc-C<sub>3</sub>-LPEI, the usage of methylated-ferrocene redox polymers was subsequently investigated. **Figure 3.3.3** shows the electrochemical response of LBL assembled films, constructed with one bilayer, using either Fc-C<sub>3</sub>-LPEI, FcMe<sub>2</sub>-C<sub>3</sub>-LPEI, or FcMe<sub>4</sub>-C<sub>3</sub>-LPEI as the redox polymer and p-GOX. The increase in methylation resulted in a decrease in both redox potential and generated current. It has been previously shown that the added steric bulk that results from the addition of methyl groups decreases the electron transfer

rates throughout the films, which results in the lower electrochemical response. The resulting CVs for all of the redox polymers were broad and amorphous; suggesting the ferrocene groups are in multiple environments.

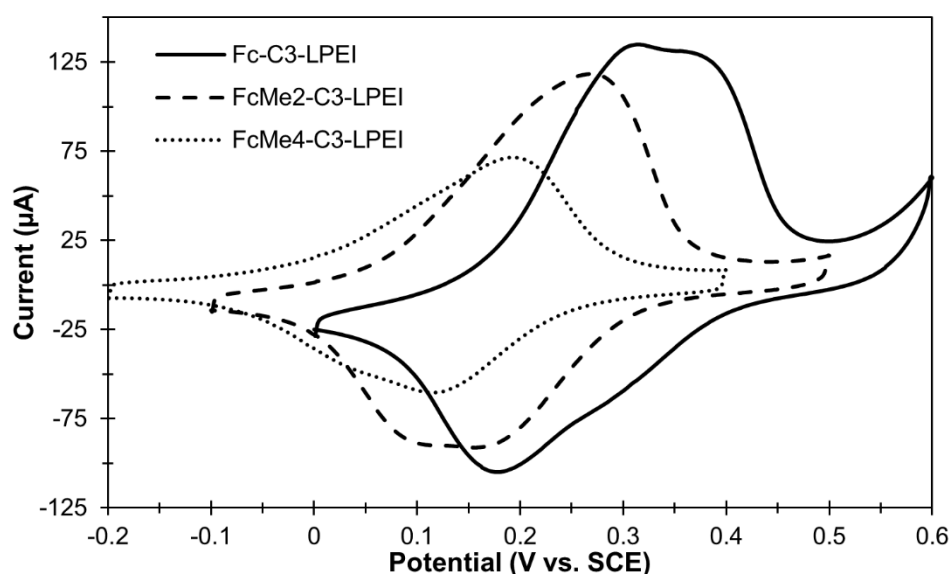


**Figure 3.3.3:** Representative CVs for  $(\text{Fc-C}_3\text{-LPEI/p-GOX})_1$ ,  $(\text{FcMe}_2\text{-C}_3\text{-LPEI/p-GOX})_1$ , and  $(\text{FcMe}_4\text{-C}_3\text{-LPEI/p-GOX})_1$  films assembled using the short wash method on SWNT-GCEs.

Glucose calibration curves for the films were obtained by poisoning the electrodes at an oxidizing potential (0.45 V for Fc-C<sub>3</sub>-LPEI, 0.35 for FcMe<sub>2</sub>-C<sub>3</sub>-LPEI, and 0.25 for FcMe<sub>4</sub>-C<sub>3</sub>-LPEI) and adding increasing amounts of glucose into the cell. **Figure 3.3.4** depicts the enzymatic response for the resulting LBL assembled films. Even though methylation of ferrocene resulted in a decrease in electrochemical response in the CV, FcMe<sub>2</sub>-C<sub>3</sub>-LPEI and FcMe<sub>4</sub>-C<sub>3</sub>-LPEI resulted in an increase in  $J_{max}$  up to  $4960 \pm 37$  and  $4063 \pm 270 \mu\text{Acm}^{-2}$ , respectively. It should be noted that these results are not entirely consistent with corresponding films crosslinked with EGDGE. The increase in  $J_{max}$  associated with FcMe<sub>2</sub>-C<sub>3</sub>-LPEI follows the same trend as EGDGE crosslinked films, but

FcMe<sub>4</sub>-C<sub>3</sub>-LPEI gives a lower response to glucose than Fc-C<sub>3</sub>-LPEI for EGDGE crosslinked films. Therefore, (FcMe<sub>4</sub>-C<sub>3</sub>-LPEI/p-GOX)<sub>x</sub> films assembled on SWNT-GCEs could prove to be an extremely useful in the fabrication of glucose/oxygen biofuel cells. This will be examined in further studies.

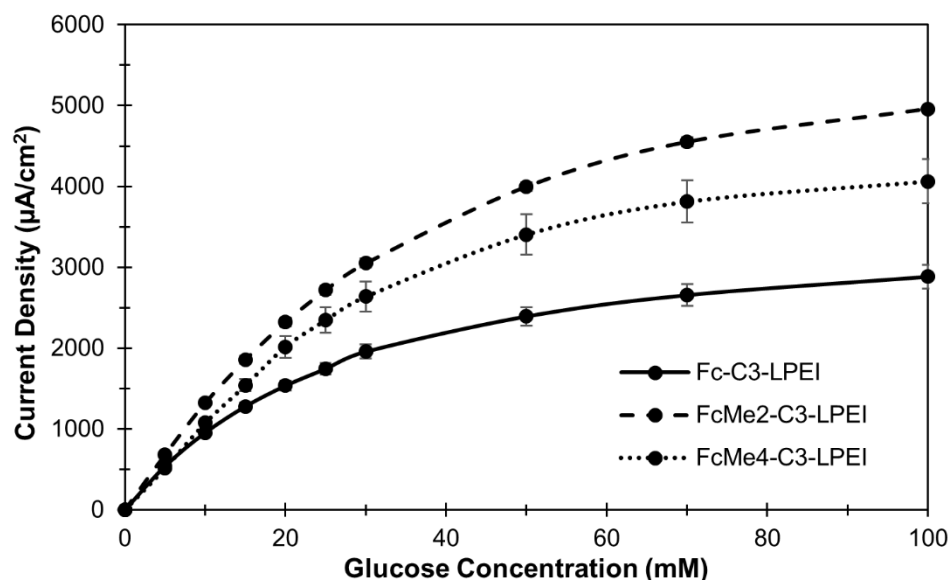


**Figure 3.3.4:** Constant amperometry glucose response curves for (Fc-C<sub>3</sub>-LPEI/p-GOX)<sub>1</sub>, (FcMe<sub>2</sub>-C<sub>3</sub>-LPEI/p-GOX)<sub>1</sub>, and (FcMe<sub>4</sub>-C<sub>3</sub>-LPEI/p-GOX)<sub>1</sub> films assembled using the short wash method on SWNT-GCEs.

### 3.4 Conclusion

We have shown that the response of layer-by-layer assembled glucose bioanodes can be greatly improved by shortening the tether length of Fc-C<sub>n</sub>-LPEI from six carbons by three carbons. We have also demonstrated that the washing procedure employed while processing electrodes is important to the overall response of the films. The combination of Fc-C<sub>3</sub>-LPEI and the short washing method account for some of the highest current densities thus far reported for LBL assembled glucose biosensors.

Electrochemical methods were used to gain a better understanding of how materials initially adsorb and then further build upon the surface of an electrode. A simplified model based on the formation of distinctly isolated layers of material was

shown to not be the best approximation for the LBL assembly of redox polymers and an enzyme, especially for the first several bilayers. Initial “patchy” deposition, followed by “filling in” of the surface in the next several bilayers, was shown to be more consistent with the experimental data. The mediator tether length and the fabrication wash time were shown to effect the packing of material onto the electrode based on the surface coverage and connectivity of polymer/enzyme composites.

When poisoning against an air-breathing Pt cathode, (Fc-C<sub>3</sub>-LPEI/p-GOX)<sub>8</sub> bioanodes (short wash) were able to reach a maximum power density of  $86 \pm 3 \mu\text{Wcm}^{-2}$  at ca. 132 mV at pH 7 and 25°C. By lowering the pH to affect the reduction potential at which the Pt electrode reduces oxygen, the maximum power density of the biofuel cells increased to  $149 \pm 7 \mu\text{Wcm}^{-2}$  at ca. 132 mV. It is conceivable that the power output could be increased if larger numbers of bilayers were used.

The use of high surface area SWNT-GCE electrodes provides a convenient method to fabricate high current density bioanodes in a very short amount of time. (Fc-C<sub>3</sub>-LPEI/p-GOX)<sub>1</sub> films were capable of generating  $2883 \pm 149 \mu\text{Acm}^{-2}$  in response to glucose. The short fabrication time allows for methylated ferrocene polymers to be used in LBL assembly to lower the redox potential and increase  $J_{max}$  of the films. (FcMe<sub>2</sub>-C<sub>3</sub>-LPEI/p-GOX)<sub>1</sub> and (FcMe<sub>4</sub>-C<sub>3</sub>-LPEI/p-GOX)<sub>1</sub> films were capable of generating  $4960 \pm 37$  and  $4063 \pm 270 \mu\text{Acm}^{-2}$ , respectively. Films assembled on SWNT-GCEs represent some of the highest current density LBL assembled glucose bioanodes reported in the literature. Further work on the optimization and characterization of the methylated ferrocene polymers in LBL still needs to be performed.

### 3.5 Experimental

#### *Chemicals and Solutions:*

Glucose oxidase (GOX) from *Aspergillus niger* (EC 1.1.3.4, type X-S, 117 units/mg solid, 75% protein), cystamine dihydrochloride, and D-glucose were purchased from Sigma-Aldrich Co. and all chemicals were used as received. The redox polymers Fc-C<sub>3</sub>-LPEI and Fc-C<sub>6</sub>-LPEI were synthesized according to a previously published procedure<sup>6</sup> from LPEI (avg. MW ca. 86 000),<sup>42</sup> (3-bromopropyl)ferrocene<sup>43</sup>, and (6-bromohexyl)ferrocene (Sigma-Aldrich). The redox polymers FcMe<sub>2</sub>-C<sub>3</sub>-LPEI and FcMe<sub>4</sub>-C<sub>3</sub>-LPEI were synthesized according to previously published procedures.<sup>9,35</sup> The polymers were found to have 17-20% of the nitrogen atoms in the polymer backbone substituted with ferrocene functional groups using NMR spectroscopy.<sup>6</sup> Sodium phosphate buffer (50 mM) was prepared by dissolving NaH<sub>2</sub>PO<sub>4</sub> in Nanopure deionized water and adding sodium hydroxide pellets with stirring to adjust the pH to 7.0. Spectra/Por molecular porous membrane tubing (Mw cutoff 12000–14 000) from Spectrum Labs and a sodium phosphate buffer (20 mM) at pH 7.4 were used for dialysis of the modified enzyme. Stock solutions of 2 M glucose were stored at 4 °C and allowed to mutatorotate for 24 hours prior to usage. Gold electrodes (2.0 mm diameter, CH instruments, Austin, TX) were polished with 1 and 0.25 μm diamond polishing paste on nylon polishing pads before being polished with 0.05 μm alumina on a microcloth pad.

#### *Electrochemical Measurements*

Constant potential experiments and cyclic voltammetry were performed with a CH Instruments biopotentiostat (CHI832, Austin, TX) in a three-electrode configuration with a platinum wire counter electrode and a saturated calomel electrode (SCE). All

experiments were conducted at room temperature (25 °C) in 100 mL of 50 mM phosphate buffer (pH 7.0 unless otherwise noted). All cyclic voltammetry experiments were performed with a scan rate of 50 mVs<sup>-1</sup>. Each experiment was performed a minimum of three times using a different fabricated electrode for each test, and the values presented are the mean ± standard error of the mean (SEM), unless otherwise stated. Constant amperometry experiments were performed by poisoning the electrodes at an oxidizing potential, and letting them equilibrate for 300 seconds. Increasing aliquots of 2 M glucose solution was then added to the bulk electrolyte to bring the final concentration up to 100 mM glucose.

#### *Biofuel Cell Construction and Testing*

Compartment-less hybrid biofuel cells were constructed using the LBL assembled bioanodes as described above, and an air-breathing Pt electrode as the cathode. The air-breathing Pt electrode (ELAT ® gas diffusion electrode, 0.5 mg/cm<sup>2</sup> Pt) was chosen to ensure that the bioanodes would be the limiting electrodes in the biofuel cell. Biofuel cells were tested using half an H-Cell with the air-breathing cathode attached to the side arm of the vessel with the anode immersed in the top opening. Glucose was added to the bulk electrolyte with magnetic stirring during the open circuit potential (OCP) measurements to bring the glucose concentration of the solution to 100 mM. Slow scan polarization (2 mV/s from the measured OCP to 1 mV) was used to obtain polarization and power curves by monitoring current as a function of potential.

### **3.6 References**

1. Sassolas, A.; Blum, L. J.; Leca-Bouvier, B. D., *Biotechnology Advances* **2012**, *30* (3), 489-511.
2. Willner, I.; Yan, Y. M.; Willner, B.; Tel-Vered, R., *Fuel Cells* **2009**, *9* (1), 7-24.

3. Cosnier, S.; Le Goff, A.; Holzinger, M., *Electrochemistry Communications* **2014**, 38 (0), 19-23.
4. Ohara, T. J.; Rajagopalan, R.; Heller, A., *Analytical Chemistry* **1993**, 65 (23), 3512-3517.
5. Mao, F.; Mano, N.; Heller, A., *Journal of the American Chemical Society* **2003**, 125 (16), 4951-4957.
6. Merchant, S. A.; Meredith, M. T.; Tran, T. O.; Brunski, D. B.; Johnson, M. B.; Glatzhofer, D. T.; Schmidtke, D. W., *The Journal of Physical Chemistry C* **2010**, 114 (26), 11627-11634.
7. Hodak, J.; Etchenique, R.; Calvo, E. J.; Singhal, K.; Bartlett, P. N., *Langmuir* **1997**, 13 (10), 2708-2716.
8. Meredith, M. T.; Kao, D.-Y.; Hickey, D.; Schmidtke, D. W.; Glatzhofer, D. T., *Journal of The Electrochemical Society* **2011**, 158 (2), B166-B174.
9. Meredith, M. T.; Hickey, D. P.; Redemann, J. P.; Schmidtke, D. W.; Glatzhofer, D. T., *Electrochimica Acta* **2013**, 92 (0), 226-235.
10. Ates, M., *Materials Science and Engineering: C* **2013**, 33 (4), 1853-1859.
11. Bonnet, C.; Andreescu, S.; Marty, J.-L., *Analytica Chimica Acta* **2003**, 481 (2), 209-211.
12. Pei, J.; Tian, F.; Thundat, T., *Analytical Chemistry* **2003**, 76 (2), 292-297.
13. Yonemori, Y.; Takahashi, E.; Ren, H.; Hayashi, T.; Endo, H., *Analytica Chimica Acta* **2009**, 633 (1), 90-96.
14. Chaki, N. K.; Vijayamohanan, K., *Biosensors and Bioelectronics* **2002**, 17 (1-2), 1-12.
15. Borges, J.; Mano, J. F., *Chemical Reviews* **2014**, 114 (18), 8883-8942.
16. Du, Y.; Chen, C.; Yin, J.; Li, B.; Zhou, M.; Dong, S.; Wang, E., *Analytical Chemistry* **2010**, 82 (4), 1556-1563.
17. Liu, J.; Qin, Y.; Li, D.; Wang, T.; Liu, Y.; Wang, J.; Wang, E., *Biosensors and Bioelectronics* **2013**, 41 (0), 436-441.
18. Du, Y.; Chen, C.; Li, B.; Zhou, M.; Wang, E.; Dong, S., *Biosensors and Bioelectronics* **2010**, 25 (8), 1902-1907.
19. Wong, D. E.; Talbert, J. N.; Goddard, J. M., *Journal of Food Science* **2013**, 78 (6), E853-E860.



20. Campos, P. P.; Moraes, M. L.; Volpati, D.; Miranda, P. B.; Oliveira, O. N.; Ferreira, M., *ACS Applied Materials & Interfaces* **2014**, *6* (14), 11657-11664.
21. Schulz, C.; Ludwig, R.; Gorton, L., *Analytical Chemistry* **2014**, *86* (9), 4256-4263.
22. Liu, D.; Hu, N., *Sensors and Actuators B: Chemical* **2011**, *156* (2), 645-650.
23. Kang, Z.; Yan, X.; Zhang, Y.; Pan, J.; Shi, J.; Zhang, X.; Liu, Y.; Choi, J. H.; Porterfield, D. M., *ACS Applied Materials & Interfaces* **2014**, *6* (6), 3784-3789.
24. Takahashi, S.; Aikawa, Y.; Kudo, T.; Ono, T.; Kashiwagi, Y.; Anzai, J.-i., *Colloid Polym Sci* **2014**, *292* (3), 771-776.
25. Abe, K.; Horiuchi, T.; Nishibayashi, Y.; Kobayashi, K.; Aburai, N., *Materials Letters* **2014**, *134* (0), 20-23.
26. Xia, B.; Shi, J.; Dong, C.; Zhang, W.; Lu, Y.; Guo, P., *Applied Surface Science* **2014**, *292* (0), 1040-1044.
27. Merchant, S. A.; Glatzhofer, D. T.; Schmidtke, D. W., *Langmuir* **2007**, *23* (22), 11295-11302.
28. DeLuca, J. L.; Hickey, D. P.; Bamper, D. A.; Glatzhofer, D. T.; Johnson, M. B.; Schmidtke, D. W., *ChemPhysChem* **2013**, *14* (10), 2149-2158.
29. Arwin, H., *Thin Solid Films* **2000**, *377-378* (0), 48-56.
30. Lvov, Y.; Ariga, K.; Ichinose, I.; Kunitake, T., *Journal of the American Chemical Society* **1995**, *117* (22), 6117-6123.
31. Marx, K. A., *Biomacromolecules* **2003**, *4* (5), 1099-1120.
32. Eckermann, A. L.; Feld, D. J.; Shaw, J. A.; Meade, T. J., *Coordination Chemistry Reviews* **2010**, *254* (15-16), 1769-1802.
33. Lillethorup, M.; Shimizu, K.; Plumeré, N.; Pedersen, S. U.; Daasbjerg, K., *Macromolecules* **2014**, *47* (15), 5081-5088.
34. Erickson, M. J. *Synthesis, Structure, and Electrochemical Performance of Poly(ethylenimine)-Based Electrolytes*. University of Oklahoma, Norman, OK, 2004.
35. Hickey, D. P.; Halmes, A. J.; Schmidtke, D. W.; Glatzhofer, D. T., *Electrochimica Acta* **2014**, *149* (0), 252-257.
36. Deng, L.; Wang, F.; Chen, H.; Shang, L.; Wang, L.; Wang, T.; Dong, S., *Biosensors and Bioelectronics* **2008**, *24* (2), 329-333.

37. Deng, L.; Shang, L.; Wang, Y.; Wang, T.; Chen, H.; Dong, S., *Electrochemistry Communications* **2008**, *10* (7), 1012-1015.
38. Zhang, J.; Zhu, Y.; Chen, C.; Yang, X.; Li, C., *Particuology* **2012**, *10* (4), 450-455.
39. Yan, Y.-M.; Yehezkeili, O.; Willner, I., *Chemistry – A European Journal* **2007**, *13* (36), 10168-10175.
40. Wang, X.; Wang, J.; Cheng, H.; Yu, P.; Ye, J.; Mao, L., *Langmuir* **2011**, *27* (17), 11180-11186.
41. Rengaraj, S.; Mani, V.; Kavanagh, P.; Rusling, J.; Leech, D., *Chemical Communications* **2011**, *47* (43), 11861-11863.
42. York, S.; Frech, R.; Snow, A.; Glatzhofer, D., *Electrochimica Acta* **2001**, *46* (10–11), 1533-1537.
43. Métay, E.; Duclos, M. C.; Pellet-Rostaing, S.; Lemaire, M.; Schulz, J.; Kannappan, R.; Bucher, C.; Saint-Aman, E.; Chaix, C., *European Journal of Organic Chemistry* **2008**, *2008* (25), 4304-4312.
44. Chen, J.; Tran, T. O.; Ray, M. T.; Brunski, D. B.; Keay, J. C.; Hickey, D.; Johnson, M. B.; Glatzhofer, D. T.; Schmidtke, D. W., *Langmuir* **2013**, *29* (33), 10586-10595.
45. Chen, J.; Bamper, D.; Glatzhofer, D. T.; Schmidtke, D. W., *Journal of The Electrochemical Society* **2015**, *162* (3), F258-F264.
46. Munoz, E.; Suh, D. S.; Collins, S.; Dalton, A. B.; Kim, B. G.; Razal, J. M.; Ussery, G.; Rinzler, A. G.; Martinez, M. T.; Baughman, R. H., *Advanced Materials* **2005**, *17* (8), 1064-1067
47. Liang, B.; Guo, X.; Fang, L.; Hu, Y.; Yang, G.; Zhu, Q.; Wei, J.; Ye, X., *Electrochemistry Communications* **2015**, *50* (0), 1-5.
48. Zhang, Y.; Li, Y.; Wu, W.; Jiang, Y.; Hu, B., *Biosensors and Bioelectronics* **2014**, *60* (0), 271-276.
49. Calvo, E. J.; Ethenique, R.; Pietrasanta, L.; Wolosiuk, A.; Danilowicz, C., *Analytical Chemistry* **2001**, *73* (6), 1161-1168.

## **Chapter 4. Development and Characterization of Layer-By-Layer Assembled Chloroferrocene-Modified Poly(ethylenimine)/Laccase Biocathodes**

---

### **4.1 Introduction**

Ferrocene is one of the most well studied organometallic complexes in the literature.<sup>1,2</sup> It is an attractive complex for study due to its low toxicity, ease of modification, and its inexpensive cost. Ferrocene has been used in many applications over the years, including, but not limited to, derivatives for cancer research,<sup>3</sup> fuel additives,<sup>4,5</sup> antioxidants,<sup>6</sup> chiral catalysts,<sup>7</sup> dyes,<sup>8,9</sup> pharmaceuticals,<sup>10,11,12</sup> and redox sensors.<sup>13,14,15,16</sup> Our group is one of many interested in the redox behavior of ferrocene, and we have particular interest in its usage as a redox mediator for enzymatic biosensors and biofuel cells.<sup>17,18,19,20,21,22</sup>

Enzymatic biofuel cells have seen a drastic increase in the current and power response in the last decade.<sup>23,24,25</sup> However, the limiting factor in many biofuel cells reported in the literature is the low current output at the cathode. The most commonly used second generation electron mediators used for enzymatic bioelectrodes are Heller-type osmium-modified redox polymers.<sup>26,27,28</sup> These polymers are popular because they can be crosslinked to form a hydrogel that allows for effective substrate diffusion and high rates of electron transfer. However, these osmium starting materials needed to prepare the redox polymers are expensive, toxic, and there is large batch-to-batch variability of the synthesized materials.

Recently our group has shown that ferrocene-modified linear poly(ethylenimine) (LPEI) is able to effectively mediate the enzymes glucose oxidase<sup>18,19,21</sup> and laccase.<sup>29</sup> The redox potential for ferrocene is between the two redox enzymes, but ferrocene's ease

of modification allows for a redox mediator with the ability to be tuned to a specific application.<sup>30,31</sup> Modification of the cyclopentadienyl rings of ferrocene is a known method to alter the electronic properties of the organometallic species. Previous work by Meredith *et al.* has shown that methylation of ferrocene decreases the electrochemical potential while still allowing for high electron transfer rates.<sup>21</sup> This allows for better electron mediation of the enzyme glucose oxidase by minimizing the induced anodic overpotential. Using a similar strategy, Hickey has shown that ferrocene can be chlorinated to raise the electrochemical potential and minimize the induced cathodic overpotential between the mediator and the enzyme laccase.<sup>29</sup>

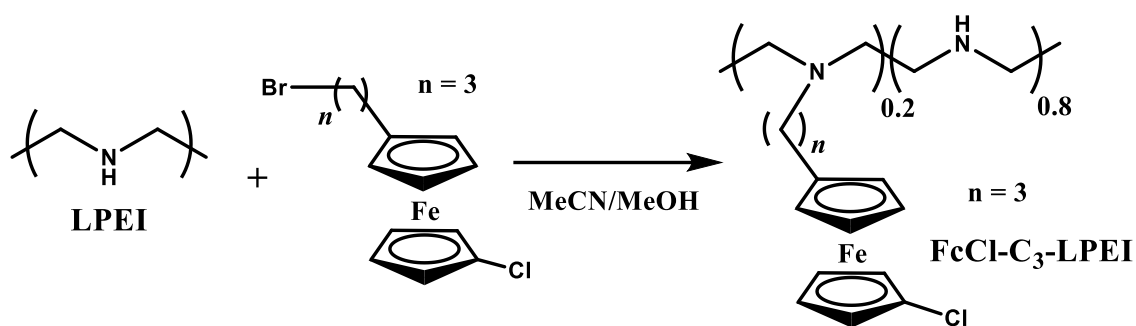


**Figure 4.1.1:** Synthesis of FcCl-C<sub>3</sub>-LPEI

The synthesis of and characterization of (chloroferrocenyl)propyl-modified LPEI (FcCl-C<sub>3</sub>-LPEI) (**Figure 4.1.1**) and its usage as a covalently crosslinked biocathode has been previously reported in David Hickey's dissertation,<sup>29</sup> and a joint manuscript over that work has been submitted to *Angew. Chem., Int. Ed.* **Figure 4.1.2** depicts a schematic for a biofuel cell recently reported by Hickey that employs tetramethylferrocene at the anode and chloroferrocene at the cathode. This chapter explores the usage of FcCl-C<sub>3</sub>-LPEI in layer-by-layer (LBL) assembled films fabricated using electrostatic complexation between the redox polymer and laccase.

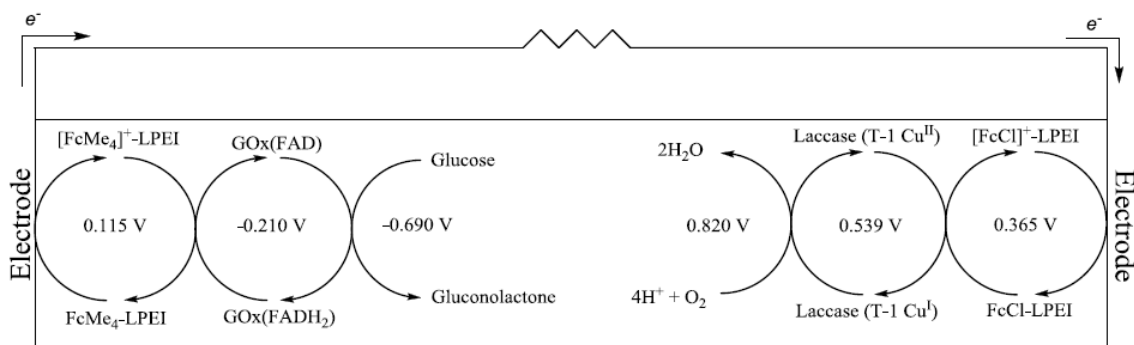


**Figure 4.1.2:** Schematic representation of a glucose/oxygen biofuel cell using tetramethylferrocene at the anode and chloroferrocene at the cathode

The long curing times associated with ethylene glycol diglycidyl ether (EGDGE) crosslinked films led us to investigate alternative fabrication methods for the construction of biocathode films. Layer-by-layer (LBL) assembly was chosen in part due to its successful implementation in the fabrication of glucose bioanodes, as detailed in **Chapter 3**. Hickey reported that a precipitate is often formed when a solution of FcCl-C<sub>3</sub>-LPEI is mixed with a solution of laccase.<sup>29</sup> This precipitate is thought to arise from the electrostatic complexation of the polymer with the enzyme. Whereas bioanodes fabricated using Fc-C<sub>n</sub>-LPEI and periodate-modified glucose oxidase required covalent attachment to improve sensor stability,<sup>32</sup> it was expected that LBL assembled biocathodes could be constructed using solely the inherent electrostatic complexation between FcCl-C<sub>3</sub>-LPEI and laccase.

## 4.2 Results and Discussion

### 4.2.1 LBL assembly of Films

Redox polymer solutions were prepared by dissolving FcCl-C<sub>3</sub>-LPEI in Nanopure water at varying concentrations and pH's by the addition of small aliquots of concentrated HCl and NaOH. Laccase solutions were dissolved in Nanopure water at varying

concentrations and placed in a centrifuge for ten minutes to remove all excess undissolved material. The supernatant was transferred via pipette for usage in LBL assembly.

The surface of the gold electrodes were modified with a negative charge by immersing the electrode in a 5 mM ethanolic solution of 11-mercaptoundecanoic acid (MUA) for 20 minutes. Electrodes were removed from solution and washed with ethanol followed by Nanopure water to remove excess unbound material. The washing was performed by gently squirting ethanol and Nanopure water onto the body and face of the electrode. A laboratory tissue was used to carefully remove excess water from the sides of the electrode and the majority of the remaining water was removed from the electrode face using a gentle wrist flick. The MUA modified electrodes were immersed in FcCl-C<sub>3</sub>-LPEI solution for five minutes to electrostatically deposit polymer onto the surface. This differs from the LBL assembly of bioanodes where the enzyme was initially deposited on the positively charge electrode surface. Polymer modified electrodes were briefly washed (<1 sec) with Nanopure water—based on the short wash method from of **Chapter 3**—and then cleaned in the same manner as above. The electrodes were immersed in a solution of laccase for five minutes, and then washed in the same manner as the previous polymer layer. The assembly of FcCl-C<sub>3</sub>-LPEI and laccase is considered as one bilayer, and this process was repeated until the desired number of bilayers was achieved, and, for the remainder of this discussion, films will be identified in the following fashion: (polymer/enzyme)<sub>x</sub>, where *x* is the number of assembled bilayers.

#### 4.2.2 *Planar Gold Electrodes: Optimization of Fabrication Parameters*

The concentrations of the polymer and the enzyme solutions were varied to determine the optimum conditions for LBL assembly. FcCl-C<sub>3</sub>-LPEI/laccase films were

constructed with four bilayers and were characterized using CV and constant potential amperometry. The enzyme and the polymer were separately dissolved into Nanopure water, and the pH was of the polymer solution was adjusted to 6.0. To understand the effects concentration has on the buildup of material, the surface coverage of chloroferrocene ( $\Gamma_{\text{FcCl}}$ ), which can be determined by integrating the area under the curve in the CV.<sup>33</sup> **Table 4.2.1** summarizes the results of FcCl-C<sub>3</sub>-LPEI and laccase concentration dependence on  $\Gamma_{\text{FcCl}}$ .

**Table 4.2.1:** Concentration dependence of  $\Gamma_{\text{FcCl}}$  (nmol/cm<sup>2</sup>) for (FcCl-C<sub>3</sub>-LPEI/laccase)<sub>4</sub>. 50 mM citrate buffer, pH 4.5.

Polymer conc. (mg/mL)	Laccase conc. (mg/mL)			
	2	4	8	16
1	.42 ± .01	.29 ± .02	.29 ± .02	.09 ± .02
2	.28 ± .03	.31 ± .02	.36 ± .04	.16 ± .03
4	.45 ± .02	.43 ± .05	.51 ± .05	.42 ± .06
8	.43 ± .04	.47 ± .05	<b>.73 ± .09</b>	.36 ± .06

The apparent trend in **Table 4.2.1** is high concentrations of laccase and low concentrations of FcCl-C<sub>3</sub>-LPEI results in  $\Gamma_{\text{FcCl}}$  being much lower. Having a high amount of laccase with a low amount of polymer could result in a thicker and more densely packed enzyme layer. This would decrease electronic communication between the polymer layers as the redox active species are now sandwiched between insulating layers of enzyme. The highest  $\Gamma_{\text{FcCl}}$  arises when both the FcCl-C<sub>3</sub>-LPEI and the laccase concentrations are 8 mg/mL. At this concentration, the polymer and the enzyme can pack in such a way that allows for good electronic communication and high chloroferrocene content. While these results show the optimum concentration conditions for polymer loading onto the surface, they do not necessarily reflect how well (FcCl-C<sub>3</sub>-

LPEI/laccase)<sub>4</sub> films will respond to oxygen. As has been shown previously, the oxygen response for EGDGE crosslinked FcCl-C<sub>3</sub>-LPEI/laccase films varies drastically with increased enzyme loading.<sup>29</sup> Therefore, having the maximum amount of FcCl-C<sub>3</sub>-LPEI as possible on the electrode may not allow for optimum enzyme response. It is therefore much more important to look at oxygen response to evaluate how well the assembled biosensors are behaving. In order to evaluate how the concentration dependence of the starting solutions would affect the performance of the biosensors, constant potential amperometry was used to determine the rate of oxygen reduction by poisoning the electrodes at a reducing potential (0.27 V vs. SCE) and monitoring the current in the presence and absence of oxygen. **Table 4.2.2** summarizes the maximum catalytic current density ( $J_{max}$ ) in response to oxygen for FcCl-C<sub>3</sub>-LPEI/laccase films at four bilayers at varying concentrations, and **Figure 4.2.1** shows a representative constant amperometry response curve.

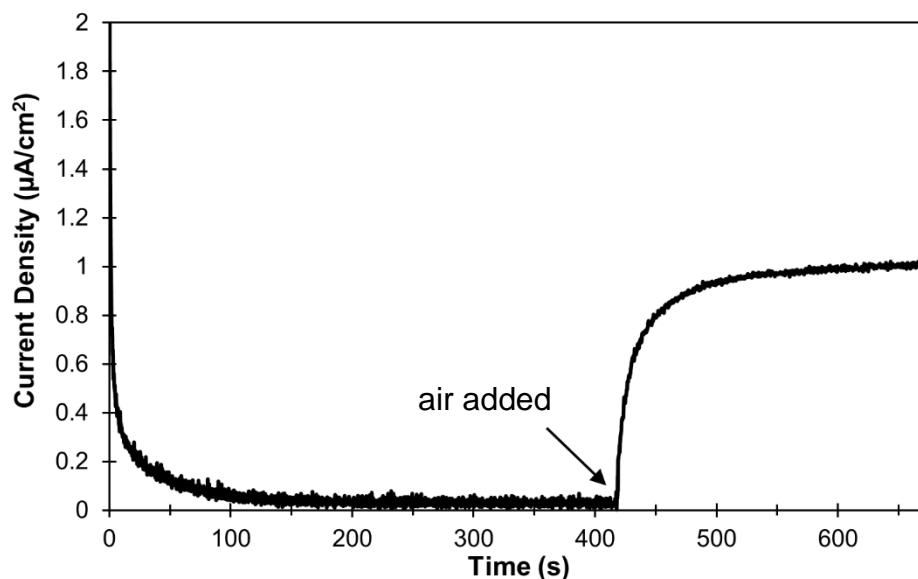


**Figure 4.2.1:** Representative amperometric response curve by (FcCl-C<sub>3</sub>-LPEI/laccase)<sub>4</sub> films to air after first purging the solution with nitrogen. 50 mM citrate buffer, pH 4.5.



Due to the nature of the LBL assembly process, performing a quantitative enzyme loading study is not feasible. However, changing the concentrations of FcCl-C<sub>3</sub>-LPEI and laccase is a way to mimic such experiments to determine the optimum conditions needed to produce maximum response. As seen in **Table 4.2.2**, the highest response to oxygen occurs when the FcCl-C<sub>3</sub>-LPEI concentration is 2 mg/mL and the laccase concentration is 4 mg/mL. This response does not correlate to the highest amount of chloroferrocene, but is instead on the lower-to-mid range of  $\Gamma_{\text{FcCl}}$ . This is consistent with previous enzyme loading experiments that showed 40% laccase to be the optimum amount for EGDGE crosslinked films.<sup>29</sup> It is theorized that higher percentages of laccase decreases the ability of the film to swell, thereby restricting the diffusion of oxygen. It appears that having less concentrated solutions of polymer and enzyme allows the assembled films to have better mediator connectivity while maintaining efficient oxygen diffusion into the films.

**Table 4.2.2:** Concentration dependence of  $J_{max}$  ( $\mu\text{A}/\text{cm}^2$ ) for (FcCl-C<sub>3</sub>-LPEI/laccase)<sub>4</sub>. 50mM citrate buffer, pH 4.5.

Polymer conc. (mg/mL)	Laccase conc. (mg/mL)			
	2	4	8	16
1	.79 ± .25	.34 ± .03	.35 ± .06	.43 ± .08
2	.49 ± .08	<b>1.08 ± .06</b>	.25 ± .04	.11 ± .02
4	.34 ± .06	.75 ± .17	.62 ± .12	.58 ± .14
8	.61 ± .08	.88 ± .19	.83 ± .08	.34 ± .05

As mentioned previously, LBL assembly of polyelectrolytes is often pH dependent when using material that do not contain permanent charges.<sup>34,35</sup> Changing pH will affect the overall charge density on the materials being deposited. Since the polymer has a greater number of ionizable groups, the pH's of the FcCl-C<sub>3</sub>-LPEI solutions were

varied from 4 to 7 to investigate the response of LBL assembled biocathodes. **Figure 4.2.2** shows how the pH of the polymer solution affects  $\Gamma_{\text{FcCl}}$  and  $J_{\text{max}}$  of (FcCl-C<sub>3</sub>-LPEI/laccase)<sub>4</sub> films.

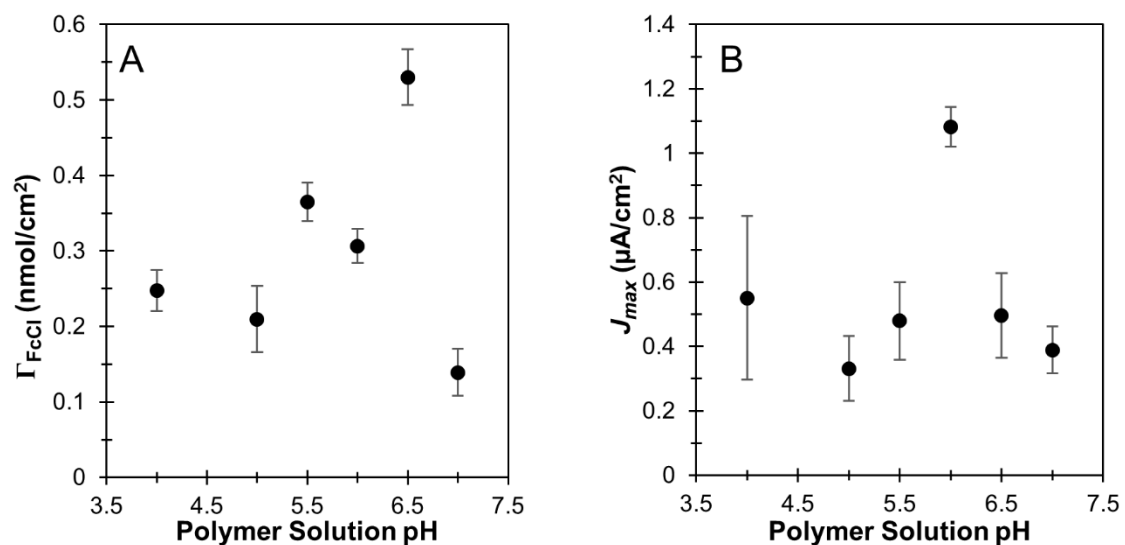


**Figure 4.2.2:** Redox polymer fabrication solution pH dependence of **A)**  $\Gamma_{\text{FcCl}}$  and **B)**  $J_{\text{max}}$  for (FcCl-C<sub>3</sub>-LPEI/laccase)<sub>4</sub>. Electrochemical experiments run in 50 mM citrate buffer, pH 4.5.

As seen in **Figure 4.2.2A**, the maximum  $\Gamma_{\text{FcCl}}$  occurs at pH 6.5. At this pH condition, FcCl-C<sub>3</sub>-LPEI and laccase have the most ideal charge matching between the two materials. The opposing charges of the polyelectrolytes are at an optimum that allows a maximum amount of polymer is able to deposit on the surface of the electrode. However, as seen in **Figure 4.2.2B**, a maximum deposition of redox polymer does not necessarily correlate to maximum sensor response. The optimum polymer solution pH that provides the highest  $J_{\text{max}}$  for (FcCl-C<sub>3</sub>-LPEI/laccase)<sub>4</sub> occurs at pH 6.0. This is in the midrange of  $\Gamma_{\text{FcCl}}$ , and again suggests that higher amounts of FcCl-C<sub>3</sub>-LPEI hinder oxygen diffusion into the film.

#### 4.2.3 Planar Gold Electrodes: Electrochemical Characterization

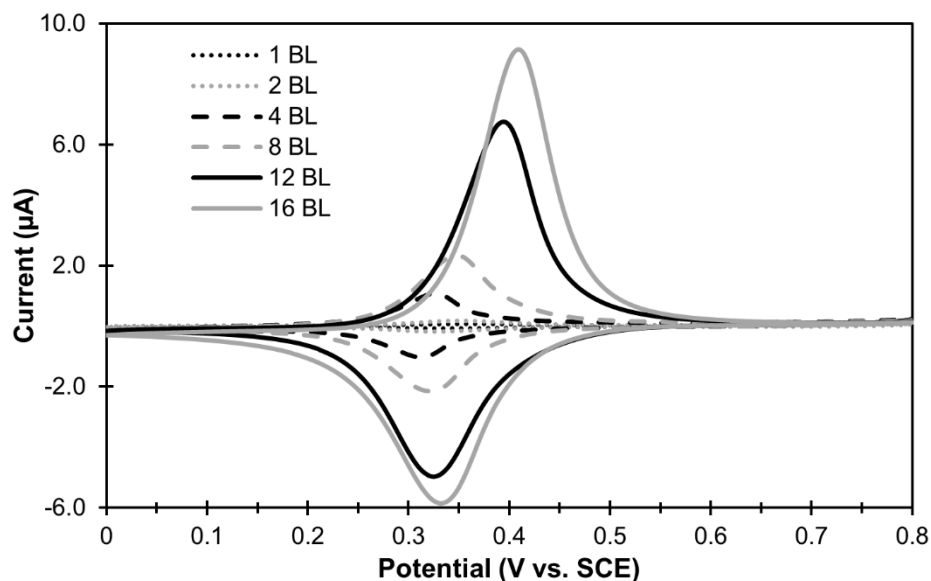


**Figure 4.2.3:** Representative CVs for  $(\text{FcCl-C}_3\text{-LPEI/laccase})_x$  films assembled on planar gold electrodes with increasing numbers of bilayers. 50 mM citrate buffer, pH 4.5. Scan rate = 0.5 mV/s.

Cyclic voltammetry (CV) was used to observe the increase of chloroferrocene at the electrode's surface with the addition of each bilayer. With the deposition of each layer of FcCl-C<sub>3</sub>-LPEI there are more redox centers at the electrode's surface which should correspond to an increase in current. **Figure 4.2.3** shows the increase in CV response for  $(\text{FcCl-C}_3\text{-LPEI/laccase})_x$  films using a short wash (<1 sec.) procedure for washing between bilayers. The peak anodic current ( $i_{pa}$ ) for  $(\text{FcCl-C}_3\text{-LPEI/laccase})_x$  films increases with the continual addition of bilayers, and  $(\text{FcCl-C}_3\text{-LPEI/laccase})_{16}$  has an  $i_{pa}$  of  $9.6 \pm 0.6 \mu\text{A}$ . This correlates well with  $(\text{Fc-C}_3\text{-LPEI/p-GOX})_{16}$  films from **Chapter 3**, and shows the strong electrostatic interactions that exist between FcCl-C<sub>3</sub>-LPEI and laccase. The half wave potential ( $E_{1/2}$ ) for  $(\text{FcCl-C}_3\text{-LPEI/laccase})_x$  films varies between 0.315 and 0.375 V, depending on the number of bilayers.

This difference in redox potential most likely arises from relative electron diffusion limitation through the films relative to the thickness and connectivity of the assembled films. This phenomenon can best be observed by looking at the change in half wave potential ( $E_{1/2}$ ) and the peak separation ( $\Delta E$ ) with respect to the number of bilayers (**Figure 4.2.4**). For a reversible, one-electron, diffusion controlled redox couple,  $\Delta E$  should be  $\sim 0.059$  V, but for an ideally surface confined material  $\Delta E$  should be 0 V. Therefore,  $\Delta E$  can be used to identify the relative location and connectivity of the electroactive species contained within the films. As seen in **Figure 4.2.4**, chloroferrocene is oxidized at a lower redox potential when the bulk of the material is well connected and closer to the surface of the electrode, i.e. at smaller  $\Delta E$  values. As the majority of the redox polymer begins to behave like an ideal hydrogel at higher numbers of bilayers, chloroferrocene becomes harder to oxidize, most likely due to electron diffusion limitations through the film.

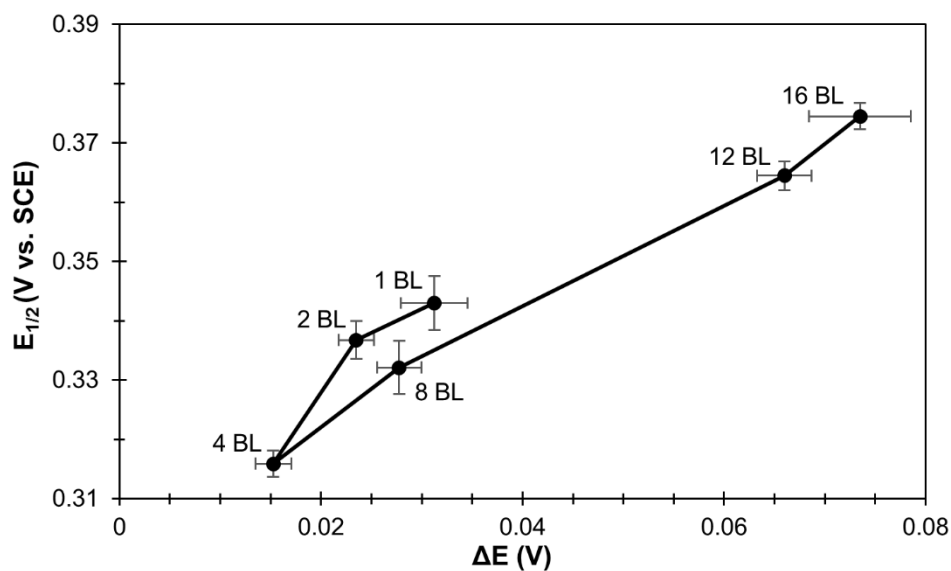


**Figure 4.2.4:** Relationship between half wave potential ( $E_{1/2}$ ) and the peak separation ( $\Delta E$ ) for  $(\text{FcCl-C}_3\text{-LPEI/laccase})_x$  films assembled on planar gold electrodes.

As seen in **Figure 4.2.4**, the build-up of bilayers does not appear to occur in discrete, well-defined layers. If that were the case, a linear correlation between  $E_{1/2}$  and  $\Delta E$  with the addition of bilayers would be expected because the films would gradually become more hydrogel-like rather than surface confined. Instead, the LBL assembly process appears to be more complicated:  $\Delta E$  starts off at 0.031 V, drops down to 0.015 V, and then steadily increases up to 0.074 V. Even though there is not a linear trend between  $E_{pa}$  and  $\Delta E$ , there is still a direct correlation between the redox potential and the relative location of the electroactive species.

A similar trend in  $\Delta E$  was seen in **Chapter 3** for LBL assembled anodes, but there is a key difference between the two systems. For LBL assembled anodes, the enzyme was adsorbed first, followed by deposition of the redox polymer, but for LBL assembled cathodes, the deposition order is reversed. The first layer of redox polymer deposited for the cathode is not dependent on the surface coverage of the enzyme, but is instead adsorbed only on the planar surface of the electrode. In the case of the LBL assembled anodes, the polymer is deposited onto a ‘rougher,’ enzyme coated electrode surface. Having the initial enzyme layer increases the effective surface area of the electrode, and allows for more redox polymer to be initially deposited. This can be seen by comparing the  $0.23 \pm 0.06 \text{ nmol}\cdot\text{cm}^{-2}$  surface coverage of ferrocene ( $\Gamma_{Fc}$ ) for  $(Fc-C_3-LPEI/p-GOX)_1$  to that of the  $0.06 \pm 0.01 \text{ nmol}\cdot\text{cm}^{-2}$  surface coverage of chloroferrocene ( $\Gamma_{FcCl}$ ) for  $(FcCl-C_3-LPEI/laccase)_1$  films assembled using the short wash procedure. This is a 74% decrease in surface coverage that arises from switching the adsorption order in the LBL deposition, and demonstrates the poor adsorption of polymer onto a planar surface.

The difference in deposition between the two systems affects the buildup of material. **Figure 4.2.5** compares the surface coverage of electroactive species relative to the number of bilayers for  $(\text{FcCl-C}_3\text{-LPEI/laccase})_x$  and  $(\text{Fc-C}_3\text{-LPEI/p-GOX})_x$  films assembled using the short wash procedure. As discussed in **Chapter 3**, LBL assembled anodes exhibit a linear increase in  $\Gamma_{\text{Fc}}$  with the addition of bilayers which suggests the deposition of material packs vertically from the surface of the electrode rather than ballooning radially outward. The deposition of  $(\text{FcCl-C}_3\text{-LPEI/laccase})_x$  cathodes occurs in a nonlinear fashion, which could indicate a more complicated growth of material.

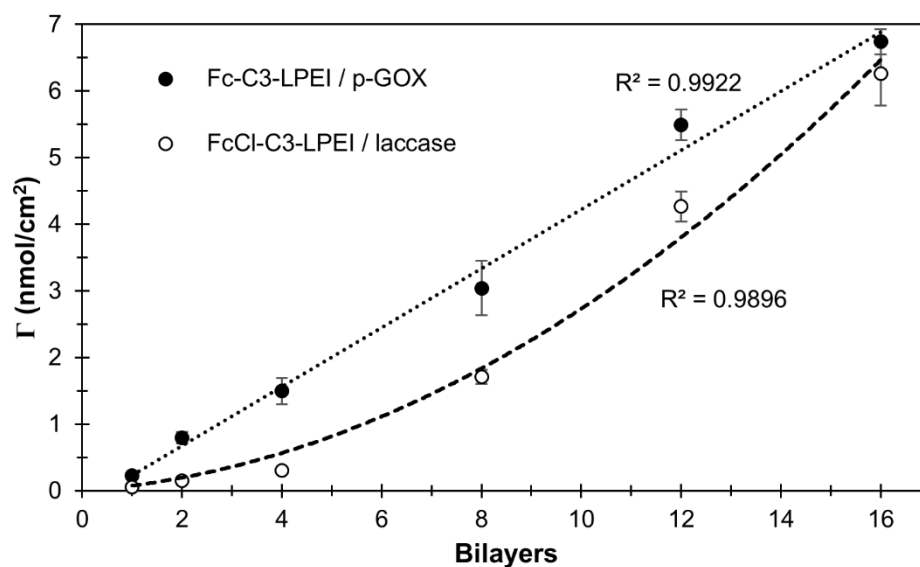


**Figure 4.2.5:** Plots of ferrocene surface coverage ( $\Gamma_{\text{Fc}}$ ) and chloroferrocene surface coverage ( $\Gamma_{\text{FcCl}}$ ), obtained by integration of the anodic wave of the cyclic voltammogram, against the number of assembled bilayers

In 2012, Xu *et al.* described the correlation of pH on whether multilayers constructed from weak polyelectrolytes experienced linear or exponential growth.<sup>36</sup> Their results showed that the LBL growth of weak polyelectrolytes was directly related to the hydrodynamic radius of polyelectrolyte complexes in solution. Varying the pH of the polymer solutions tunes the ionic charge density for weak polyelectrolytes. When the size of the polyelectrolyte complexes in solution were smaller, i.e. more tightly bound, the

LBL assembly was linear. This is due to the complexed polyelectrolytes forming more uniform, compressed layers. A decrease in charge density of the weak polyelectrolytes by altering the solution pH resulted in larger hydrodynamic radii, i.e. weakly bound polyelectrolyte complexes. This increase in hydrodynamic radius resulted in exponential LBL growth due to the deposited layers being amorphous; thereby increasing the outer surface area of the film with each additional bilayer.

Therefore, the difference in  $\Gamma$  between  $(\text{FcCl-C}_3\text{-LPEI/laccase})_x$  and  $(\text{Fc-C}_3\text{-LPEI/p-GOX})_x$  seen in **Figure 4.2.5** most likely arises from differences in charge density between the polymers and the enzymes used in the LBL assembly bioelectrodes. There are several likely possibilities contributing to the differences in LBL growth between the two systems. Assuming the difference in redox mediator does not affect the protonation of the polymer backbone for  $\text{Fc-C}_3\text{-LPEI}$  and  $\text{FcCl-C}_3\text{-LPEI}$ , the difference in polymer solution pH could result in the observed changes in multilayer growth. The ideal solution pH for  $\text{Fc-C}_3\text{-LPEI}$  was found to be 5.0 in previous work by DeLuca *et al.*,<sup>32</sup> whereas the ideal solution pH for  $\text{FcCl-C}_3\text{-LPEI}$  was found to be 6.0, as described above. This increase in pH would likely decrease the charge density of the polymer, and could result in less favorable polymer/enzyme complexation. This would result in more condensed bilayers for  $(\text{Fc-C}_3\text{-LPEI/p-GOX})_x$  and less compacted bilayers for  $(\text{FcCl-C}_3\text{-LPEI/laccase})_x$ .

The second factor that could be effecting the LBL growth is the isoelectric points (pI) of the enzymes being using. The pI is the pH at which the enzyme has an overall net-zero charge.<sup>37</sup> Using the online web-tool ExPASy ProtParam, the pI for GOX was calculated to be 4.94; whereas the pI for laccase was calculated to be 4.69. The solutions for the enzymes are kept at pH 6.8-7.0, so there is an overall negative charge for the two

enzymes. While the pI's are close fairly close together, this does not give a good indication of the charge density associated with the enzymes. The charge density of the enzyme is most likely playing a role in LBL assembly, but a comparison based only on pI does not give enough in-depth information to draw substantial conclusions.

The final factor contributing to the LBL growth is the addition of covalent linkages in (Fc-C<sub>3</sub>-LPEI/p-GOX)<sub>x</sub> from the oxidation of the oligosaccharides of GOX. This additional interaction could be more tightly binding the polymer and enzyme together which would result in more compact films. This would further support the idea of more condensed bilayers of material which lead to the linear growth for (Fc-C<sub>3</sub>-LPEI/p-GOX)<sub>x</sub> films.

To further probe the buildup of material, changes in  $\Delta E$  were plotted against  $\Gamma_{\text{FcCl}}$  for (FcCl-C<sub>3</sub>-LPEI/laccase)<sub>x</sub> films assembled using the short wash procedure. As shown in **Figure 4.2.5**, (FcCl-C<sub>3</sub>-LPEI/laccase)<sub>x</sub> biocathode films follow the same trend in  $\Delta E$  as was observed for (Fc-C<sub>3</sub>-LPEI/p-GOX)<sub>x</sub> bioanode films in **Chapter 3**. As mentioned above,  $\Delta E$  can be used to identify the relative location and connectivity of the electroactive species contained within the films. For (FcCl-C<sub>3</sub>-LPEI/laccase)<sub>x</sub> films,  $\Delta E$  starts off at 0.031 V, drops down to 0.015 V, and then steadily increases up to 0.074 V. The decrease in  $\Delta E$  with additional bilayers suggests the films are not building up in a simple, uniform fashion.

In 1996, Hoogeveen *et al.* described the effect of charge density on the adsorption of polyelectrolytes onto charged substrates.<sup>34</sup> If the charge density of a polyelectrolyte is weak, then the polymer will be loosely bound to the surface. This loosely bound polymer is not well connected to the surface, and may present difficulty for further deposition of



material. This type of model would account for the mid-range  $\Delta E$  observed for  $(\text{FcCl-C}_3\text{-LPEI/laccase})_1$  and reflects a “patchy,” ill-connected polymer/enzyme composite. Further layers of material then fill in the gaps and increase connectivity throughout the film, resulting in a decrease in  $\Delta E$ . Once a well-connected film is achieved for  $(\text{FcCl-C}_3\text{-LPEI/laccase})_4$ ,  $\Delta E$  continually increases which is consistent with a surface confined film behaving increasingly like an ideal hydrogel with the addition of more layers. At twelve and sixteen bilayers of material,  $\Delta E$  is much higher than would be expected for a diffusion controlled redox reaction. Large  $\Delta E$  values are indicative of slow electrochemical reactions and suggests limited electron diffusion from the electroactive species. With the addition of high numbers of bilayers the overall diffusion is slower as the majority of FcCl sites in FcCl-C<sub>3</sub>-LPEI become further away from the electrode.

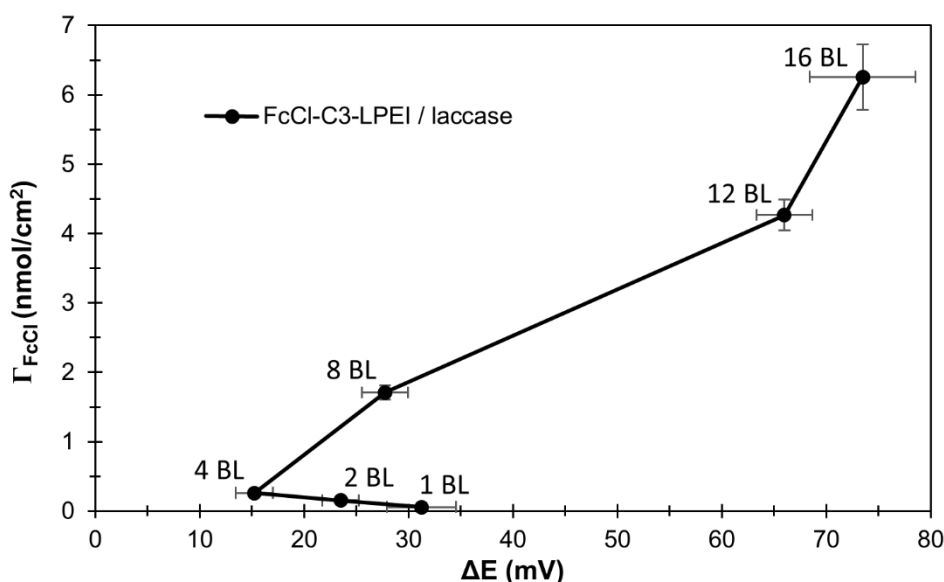


**Figure 4.2.6:** Plot of chloroferrocene surface coverage ( $\Gamma_{\text{FcCl}}$ ), obtained by integration of the anodic wave of the CV, against the potential separation between the anodic and cathodic peaks ( $\Delta E$ ) of the CV for  $(\text{FcCl-C}_3\text{-LPEI/laccase})_x$  films.

The electrochemical characterization of  $(\text{FcCl-C}_3\text{-LPEI/laccase})_x$  biocathodes, i.e.  $i_{pa}$  and  $\Gamma_{\text{FcCl}}$ , compares favorably with that of  $(\text{Fc-C}_3\text{-LPEI/p-GOX})_x$  bioanodes. Based on

the success of LBL assembled bioanodes, (FcCl-C<sub>3</sub>-LPEI/laccase)<sub>x</sub> biocathodes are expected to produce high current densities in response to oxygen.

#### 4.2.4 Planar Gold Electrodes: Enzymatic Response

In order to evaluate how LBL assembled biocathodes would perform as a biosensor, constant potential amperometry was used to determine the rate of oxygen reduction by poisoning the electrodes at a reducing potential and monitoring the  $J_{max}$  in the presence and absence of oxygen. (FcCl-C<sub>3</sub>-LPEI/laccase)<sub>16</sub> films were capable of producing  $5.75 \pm 0.14 \mu\text{Acm}^{-2}$  in response to oxygen.

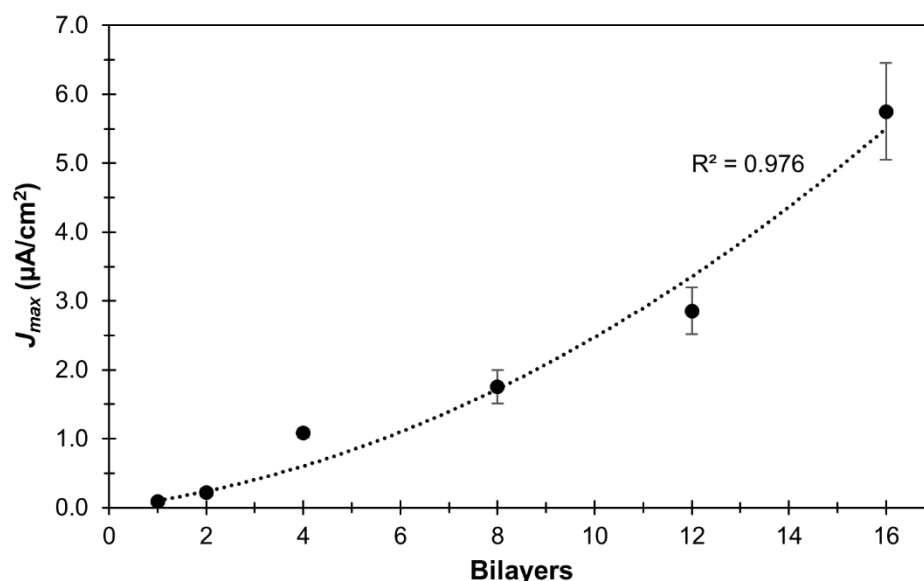


**Figure 4.2.7:** Plot of the effect of FcCl-C<sub>3</sub>-LPEI/laccase bilayers on maximum catalytic current density ( $J_{max}$ ) for films assembled on planar gold electrodes

Since  $E_{1/2}$  varies with the addition of each bilayer, the reducing potential for each biosensor was held at 0.05 V below the cathodic peak potential ( $E_{pc}$ ) for (FcCl-C<sub>3</sub>-LPEI/laccase)<sub>x</sub> films. **Figure 4.2.7** depicts the increase in  $J_{max}$  with the addition of FcCl-C<sub>3</sub>-LPEI/laccase bilayers. The non-linear increase in  $J_{max}$  is consistent with  $\Gamma_{\text{FcCl}}$ , and most likely arises for the reasons described in **Section 4.2.2**. The response of (FcCl-C<sub>3</sub>-LPEI/laccase)<sub>x</sub> cathodes is much lower than expected based on the results of (Fc-C<sub>3</sub>-

LPEI/p-GOX)<sub>x</sub> bioanodes. As discussed in **Chapter 3**, (Fc-C<sub>3</sub>-LPEI/p-GOX)<sub>16</sub> bioanodes contain about 10% the amount of electroactive ferrocene when compared to EGDGE crosslinked Fc-C<sub>3</sub>-LPEI/GOX films. Even though the LBL assembled films contain much less material, they were still capable of generating comparable current densities in response to glucose. A similar trend in the amount of electroactive species contained in the LBL biocathodes is seen by comparing the anodic peak currents ( $i_{pa}$ ) to corresponding EGDGE crosslinked films. The  $i_{pa}$  for (FcCl-C<sub>3</sub>-LPEI/laccase)<sub>16</sub> is ca. 9.5  $\mu\text{A}$  and ca. 75  $\mu\text{A}$  for EGDGE crosslinked FcCl-C<sub>3</sub>-LPEI/laccase films.<sup>29</sup> While the LBL assembled films contain about 12% of the amount of electroactive chloroferrocene, they do not produce a comparable  $J_{max}$  in response to oxygen. (FcCl-C<sub>3</sub>-LPEI/laccase)<sub>16</sub> films produced  $5.75 \pm 0.14 \mu\text{Acm}^{-2}$ , only 3% of the EGDGE crosslinked films  $J_{max}$  of  $177 \pm 40 \mu\text{Acm}^{-2}$  in response to oxygen.<sup>29</sup>

The most likely reason for the low response of the LBL assembled biocathodes is poor oxygen diffusion into the films. The ultra-thin, compact films that result from the LBL assembly of FcCl-C<sub>3</sub>-LPEI and laccase appears to be detrimental to the response of the biosensor. Because there is no feasible method of varying the complexation between the polymer and the enzyme besides the pH and concentration optimization discussed in **Section 4.2.1**, the best possible method of increasing biosensor response is through utilization of a high-surface area electrode.

#### 4.2.5 Carbon Paper Electrodes: Optimization of Fabrication Parameters

Carbon paper (CP) electrodes are a common high-surface area material used in electrochemical experiments. Due to their well-documented utility in LBL assembly of bioelectrodes and their ease of manipulation, CP electrodes were tested as a potential high

surface area material for the construction of  $(\text{FcCl-C}_3\text{-LPEI/laccase})_x$  films. Carbon fiber—the main component of CP—can be oxidized by nitric acid to introduce carbonyl, carboxylic acid, and phenolic groups on the surface of the material.<sup>38,39,40,41</sup> The addition of acidic groups onto the carbon surface is a facile means to introduce an overall anionic charge onto the electrode material for the LBL assembly of polyelectrolytes. As of this writing, the usage of nitric acid oxidized carbon paper (ox-CP) electrodes in the LBL assembly of biosensors has not been studied.

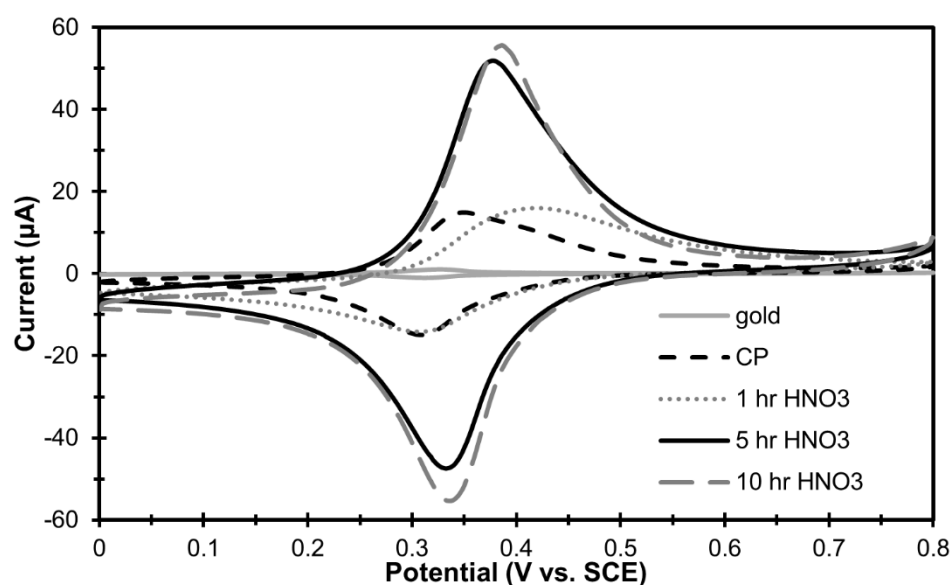


**Figure 4.2.8:** Representative CVs of  $(\text{FcCl-C}_3\text{-LPEI/laccase})_4$  films constructed on various electrode materials.

Carbon paper electrodes (unmodified and nitric acid oxidized) were immersed in  $\text{FcCl-C}_3\text{-LPEI}$  solution for five minutes to adsorb polymer to the surface. Electrodes were removed from solution, carefully rinsed with Nanopure water (<1 sec) on both faces, and the majority of the remaining water was removed using a gentle wrist flick. The polymer coated electrodes were then immersed in a laccase solution for five minutes; followed by the same washing procedure as for the first layer. The assembly of  $\text{FcCl-C}_3\text{-LPEI}$  and laccase is considered as one bilayer, and this process was repeated until the desired

number of bilayers was achieved. **Figure 4.2.8** compares the effect of nitric acid oxidation of CP electrodes on the electrochemical response of (FcCl-C<sub>3</sub>-LPEI/laccase)<sub>4</sub> films, and **Table 4.2.3** summarizes the data from the CVs.

There is nearly a 17 fold increase in the number of moles of electroactive species adsorbed, as determined by the integration of the anodic wave, when switching to the unmodified, high-surface area CP electrode. This is of particular interest due to the lack of ionizable groups on the surface of the electrode. The initial layer of material is therefore most likely adhered through weak intermolecular forces rather than through electrostatic complexation. Even lacking a net-negative surface charge, the larger surface area allows for more material to adsorb onto the electrode, which results in a higher current from the increased number of electroactive chloroferrocene moieties. Surprisingly, this large increase in response did not affect  $E_{1/2}$ , which might have been expected based on the discussion in **Section 4.2.1**. If the films assembled on CP electrodes were much thicker than those assembled on planar gold, the  $E_{1/2}$  would likely have been closer to that of EGDGE crosslinked films. The relatively unchanged  $E_{1/2}$  for CP electrodes, coupled with the relatively low  $\Delta E$ , however, would suggest that (FcCl-C<sub>3</sub>-LPEI/laccase)<sub>4</sub> films assembled on CPE are still nominally surface confined.

As seen in **Table 4.2.3**, exposure to nitric acid for one hour increased the number of electrochemically active moles of FcCl-C<sub>3</sub>-LPEI adsorbed during the LBL process. Increasing the number of anionic groups on the surface of the CP electrodes allows for a greater amount of cationic polymer to be initially deposited. This initially thick layer of redox polymer allows for a greater amount of enzyme and polymer to be deposited in subsequent multilayers. The increase in material was also accompanied by an increase in

both  $E_{1/2}$  and  $\Delta E$ , which is consistent with a thicker film behaving that is more like an ideal hydrogel.

**Table 4.2.3:** Summary of electrochemical data for  $(\text{FcCl-C}_3\text{-LPEI/laccase})_4$  films constructed on various electrode materials. 50 mM citrate buffer, pH 4.5

Electrode	FcCl (nmol) <sup>a</sup>	$E_{1/2}$ (V)	$\Delta E$ (V)
gold	$0.0096 \pm 0.0006$	0.32	0.015
carbon paper	$0.16 \pm 0.02$	0.31	0.041
1 hr HNO <sub>3</sub>	$0.25 \pm 0.03$	0.38	0.142
5 hr HNO <sub>3</sub>	$0.58 \pm 0.03$	0.36	0.048
10 hr HNO <sub>3</sub>	$0.56 \pm 0.10$	0.35	0.05

a: calculated by integrating the area under the anodic wave in the CV

Further exposure to nitric acid increases the moles of electrochemically active chloroferrocene on the surface of the ox-CP electrodes, but there does not appear to be a benefit past five hours of oxidation.  $(\text{FcCl-C}_3\text{-LPEI/laccase})_4$  films coated on ox-CP electrodes exposed to nitric acid for five hours have more than double the amount of chloroferrocene present on the surface than those exposed for only one hour. Surprisingly, this large increase in the amount of material also results in an  $E_{1/2}$  and  $\Delta E$  closer to that of films coated on the untreated CP electrodes. This indicates that the assembled films are more surface confined for the more highly oxidized CP electrodes. The increased number of anionic groups present on the ox-CP electrodes from increased nitric acid exposure not only allows for more cationic polymer to adsorb onto the surface, but results in tighter complexation of the material to the surface, as evidenced by the lowering of  $\Delta E$ . However, as has been discussed previously, an increase in the amount of material on the electrode's surface does not always correlate to an increase in biosensor response.

There is the possibility of oxygen diffusion limitations if the (FcCl-C<sub>3</sub>-LPEI/laccase)<sub>x</sub> films are too densely packed.

By poisoning the electrodes at a reducing potential, biocathodes assembled on CP and ox-CP electrodes were tested for their response to oxygen. **Figure 4.2.9** depicts the maximum catalytic current ( $I_{max}$ ) in response to oxygen obtained from (FcCl-C<sub>3</sub>-LPEI/laccase)<sub>4</sub> films constructed on various electrode support materials.  $I_{max}$  was used as an initial comparison because the exact surface area of the CP and ox-CP electrodes were unknown. As seen in **Figure 4.2.9**, there was large increase in  $I_{max}$  when switching to the high-surface area electrode material, and the ox-CP electrodes gave much higher results than the unmodified CP electrodes. This increase in enzymatic response correlates to the increase in moles of chloroferrocene on the electrode's surface, and is indicative of higher laccase loading onto the CP electrodes. Five hours of nitric acid oxidation of CP resulted in the highest response to oxygen for (FcCl-C<sub>3</sub>-LPEI/laccase)<sub>4</sub> films assembled on a variety of electrode supports. At this degree of oxidation, the amount of redox polymer and enzyme assembled on the electrodes is such to allow for high electrochemical response and high enzymatic response. There is a large amount of material adsorbed, but the bilayers are not so tightly bound together to disrupt oxygen diffusion into the films.

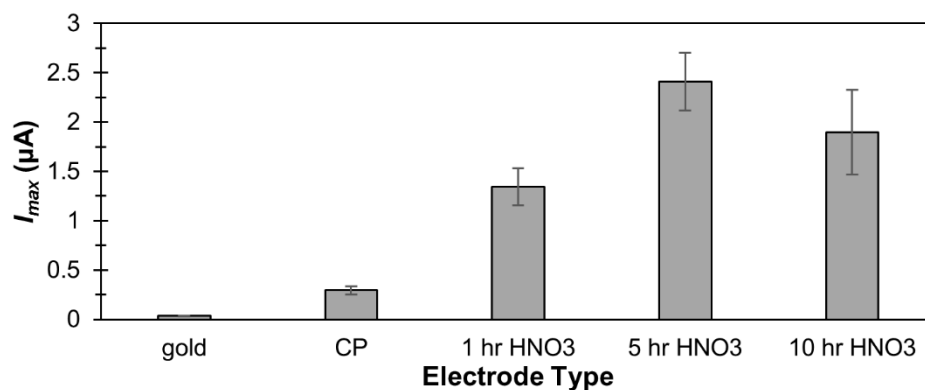


**Figure 4.2.9:** Effect of electrode material on maximum current ( $I_{max}$ ) for (FcCl-C<sub>3</sub>-LPEI/laccase)<sub>4</sub> films

The decrease in response that occurs after ten hours of oxidation could be a result of electrode damage or of decreased oxygen diffusion into the film. The CP electrode is a conjugated carbon system and too much oxidation could potentially disrupt the integrity of the electrode. Another possibility is that the increased charge density on the surface could be too high, which results in a polymer/enzyme composite that is highly compact. This would impair the ability of oxygen to diffuse into the film and would limit the rate at which it can be reduced by the enzyme. Based on the results in **Figure 4.2.9**, five hours exposure to nitric acid was used in all subsequent experiments.

#### **4.2.6** *Carbon Paper Electrodes: Electrochemically Active Surface Area*

As mentioned above, the electrochemically active surface area (EASA) of the CP electrodes is unknown. The geometric surface area of the electrodes is 0.515 cm<sup>2</sup>, but that may not accurately account for the ridges and folds on the surface of the electrodes that would increase the apparent surface area. Calculation of EASA can be achieved with cyclic voltammetry using the Randles-Sevcik equation:<sup>42</sup>

$$\text{Equation 3.1: } i_p = 268600n^{3/2}AD^{1/2}c\nu^{1/2}$$

where  $i_p$  is the peak anodic current,  $n$  is the number of electrons transferred in a single redox process,  $D$  is the diffusion coefficient of the electroactive species,  $c$  is the concentration of the electroactive species, and  $\nu$  is the potential scan rate. The comparison of two electrodes composed of similar substances can be calculated using a solution of identical electroactive species at the same concentration. Keeping  $n$ ,  $D$ ,  $c$ , and  $\nu$  as constants, the surface area comparison of two materials can be represented as the following:



$$\text{Equation 3.2: } \frac{i_{p1}}{A_1} = \frac{i_{p2}}{A_2}$$

Current is defined as the amount of charge passing in a defined amount of time, and, by using the same potential range and scan rate or both electrodes, **Equation 3.2** can be rewritten as the following to more accurately calculate an unknown EASA:

$$\text{Equation 3.3: } A_2 = \frac{A_1 q_2}{q_1}$$

where  $q$  is the anodic charge as determined by the integration of the oxidation wave from the cyclic voltammogram.

The determination of CP and ox-CP electrodes' EASA was accomplished by comparison to planar, glassy carbon (GC) electrodes with known geometric surface area. The methylchloride salt of N,N-dimethylaminomethylferrocene (**1**) was used to mimic the electroactive species used in the LBL assembly. **Figure 4.2.10** compares the CVs of GC, CP, and ox-CP (five hours) electrodes, and **Table 4.2.4** summarizes the data acquired for each electrode.

The increase in current for the high surface area CP and ox-CP electrodes is consistent with LBL assembled films discussed above. The redox potentials did not vary a significant amount between the three electrodes. The  $\Delta E$  values for the three electrodes were higher than for LBL assembled films, but this is to be expected for a redox species being diffusion controlled in solution. The  $\Delta E$  for the unmodified CP electrodes was nearly double that of the GC and ox-CP electrodes, which suggests the redox reaction is more sluggish for this electrode material. The broadening of  $\Delta E$  occurs because the current is taking more time to respond to the applied voltage for the CP electrode. This

suggests that the nitric acid oxidation not only increases the adsorption of material in the LBL assembly, but also increases the electrical conductivity of the material.

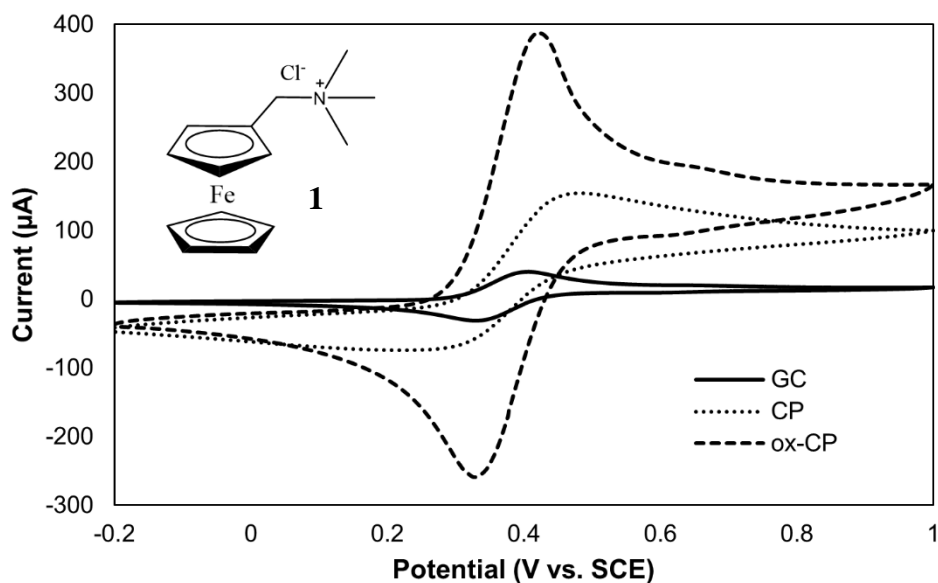


**Figure 4.2.10:** Representative CVs of compound 1 (5 mM) obtained using various carbon electrodes. PBS pH 7.4. Scan rate = 50 mV/s.

**Table 4.2.4:** Summary of calculated EASA and electrochemical measurements for various carbon electrodes.

Electrode	SA (cm <sup>2</sup> )	E <sub>1/2</sub> (V)	ΔE (V)
GC	0.07069	0.37	0.073
CP	0.388	0.37	0.162
ox-CP	0.616	0.38	0.089

Surprisingly, the EASA for unmodified CP electrodes is lower than the geometric surface area. The low EASA could in part explain the slow nature of the redox processes that seem to occur for the CP electrodes. If a portion of the electrode is not electrochemically active, then the diffusion of electrons to the bulk electrode could be slower. The increase in the EASA for ox-CP electrodes suggests the acid oxidation is either removing the non-electrochemically active portions of the surface to expose the

active material or the incorporation of acidic surface moieties increases the conductivity of the electrode.

The calculated EASA for the CP and ox-CP electrodes allows for a more direct comparison between with LBL films assembled on gold. **Table 4.2.5** compares the electrochemical and enzymatic response of (FcCl-C<sub>3</sub>-LPEI/laccase)<sub>4</sub> films constructed on various electrode supports with the surface area taken into account. When compared to planar gold electrodes, unmodified CP electrodes have a slightly higher surface coverage of chloroferrocene, but the catalytic current density in response to oxygen is about 30% lower. As mentioned above, the initial layer of redox polymer adsorbed onto the CP electrodes is achieved through weak intermolecular forces. It is therefore not surprising that the  $\Gamma_{\text{FcCl}}$  for the unmodified CP electrodes is not much higher than for the planar gold electrodes. The lower  $J_{\text{max}}$  for the CP electrodes could result from poor packing of material onto the neutral carbon surface, or from the poor electrochemical properties of the unmodified electrode.

**Table 4.2.5:** Summary of electrochemical and enzymatic data taking EASA into account

<b>Electrode</b>	<b>FcCl (nmol)</b>	<b><math>\Gamma_{\text{FcCl}}</math> (nmol/cm<sup>2</sup>)</b>	<b><math>I_{\text{max}}</math> (<math>\mu\text{A}</math>)</b>	<b><math>J_{\text{max}}</math> (<math>\mu\text{A}/\text{cm}^2</math>)</b>
gold	0.0096 $\pm$ 0.0006	0.31 $\pm$ 0.01	0.034 $\pm$ 0.002	1.08 $\pm$ 0.06
CP	0.16 $\pm$ 0.02	0.41 $\pm$ 0.06	0.29 $\pm$ 0.04	0.76 $\pm$ 0.11
ox-CP	0.58 $\pm$ 0.03	0.94 $\pm$ 0.05	2.41 $\pm$ 0.29	3.91 $\pm$ 0.48

The ox-CP electrodes have about 200% higher  $\Gamma_{\text{FcCl}}$  than either the gold or the CP electrodes. The introduction of anionic moieties from nitric acid oxidation allows for a much higher loading of redox polymer onto the surface of the ox-CP electrodes. The higher  $J_{\text{max}}$  for ox-CP electrodes, in relation to gold and unmodified CP, indicates that oxygen diffusion into the films is not being limited by the high loading of material. This

suggests that the FcCl-C<sub>3</sub>-LPEI/laccase films are not too tightly complexed onto the ox-CP electrodes and are not constricting the enzyme.

#### 4.2.7 Carbon Paper Electrodes: Electrochemical Characterization

Cyclic voltammetry (CV) was used to observe the increase of chloroferrocene at the ox-CP electrode's surface with the addition of each bilayer. With the deposition of each layer of FcCl-C<sub>3</sub>-LPEI there are more redox centers at the electrode's surface which should correspond to an increase in current. However, as seen **Figure 4.2.11**,  $i_{pa}$  for (FcCl-C<sub>3</sub>-LPEI/laccase)<sub>x</sub> films increases with the addition of bilayers up to (FcCl-C<sub>3</sub>-LPEI/laccase)<sub>8</sub>, and then decreases with subsequent bilayers of material. This is in contrast to both (FcCl-C<sub>3</sub>-LPEI/laccase)<sub>x</sub> films constructed on planar gold electrodes and (Fc-C<sub>3</sub>-LPEI/p-GOX)<sub>x</sub> films discussed in **Chapter 3**. At higher numbers of bilayers, the electroactive material is no longer being effectively detected by the electrode, or material is delaminating from the electrodes.

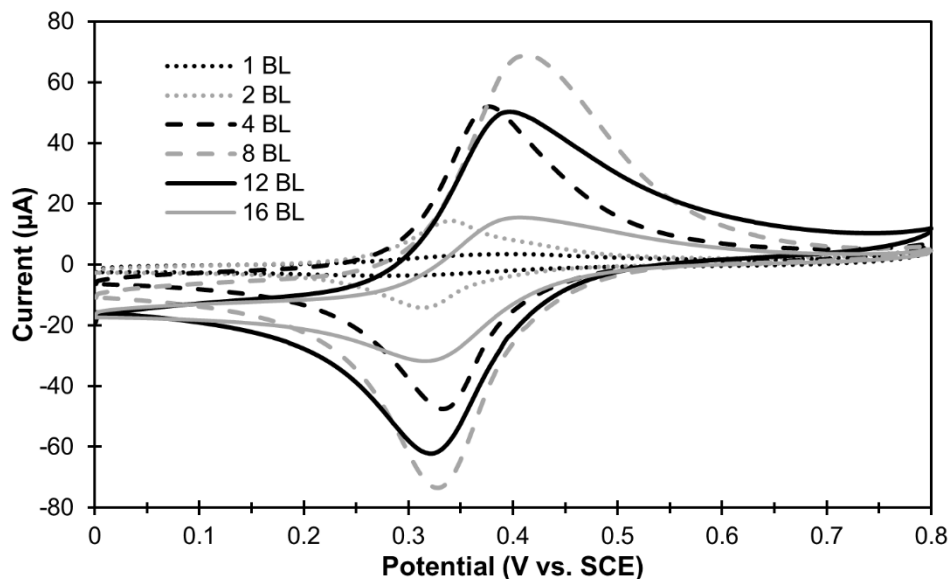


**Figure 4.2.11:** Representative CVs for (FcCl-C<sub>3</sub>-LPEI/laccase)<sub>x</sub> films assembled on planar gold electrodes with increasing numbers of bilayers. 50 mM citrate buffer, pH 4.5. Scan rate = 50 mV/s.

The decrease in electrochemical response of  $(\text{FcCl-C}_3\text{-LPEI/laccase})_x$  films assembled on ox-CP electrodes was investigated by first looking at the relationship between  $E_{1/2}$  and  $\Delta E$  (**Figure 4.2.12**). The decrease in  $\Delta E$  when changing from one to two bilayers is consistent with a disorganized, ill-connected film becoming both more cohesive at the electrode's surface. The statistically insignificant change in  $E_{1/2}$  between one and two bilayers for  $(\text{FcCl-C}_3\text{-LPEI/laccase})_x$  films, coupled with the decrease in  $\Delta E$ , suggests the films may be becoming more connected, but not becoming more surface confined.

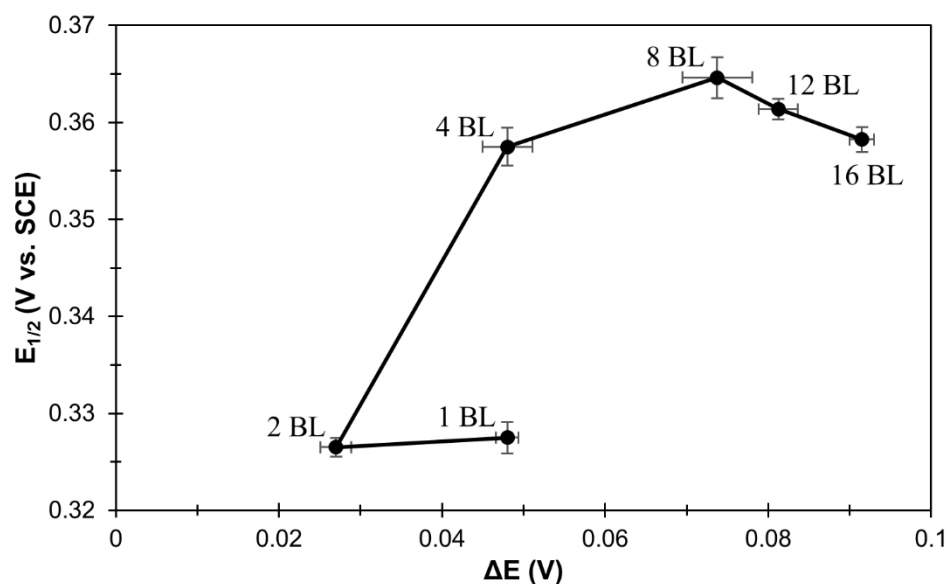


**Figure 4.2.12:** Relationship between half wave potential ( $E_{1/2}$ ) and the peak separation ( $\Delta E$ ) for  $(\text{FcCl-C}_3\text{-LPEI/laccase})_x$  films assembled on nitric acid oxidized carbon paper electrodes.

The 30 mV increase in  $E_{1/2}$  and the 20 mV increase in  $\Delta E$  when shifting from two to four bilayers indicates the films are rapidly gaining more hydrogel character. However, the addition of material beyond four bilayers does not create a large difference in hydrogel character, as evidenced by the total change in  $E_{1/2}$  from eight to sixteen bilayers is less than 7 mV. The decrease in electrochemical response for  $(\text{FcCl-C}_3\text{-LPEI/laccase})_x$  films assembled with twelve and sixteen bilayers is most likely due to inefficient

electrochemical detection rather than loss of material since the  $E_{1/2}$  and  $\Delta E$  for these films remain high. If the films were delaminating from the electrode's surface with subsequent bilayer deposition treatment, the films would get thin and  $E_{1/2}$  and  $\Delta E$  would decrease accordingly.

The continual increase in  $\Delta E$  out to 0.091 V suggests the redox process is becoming quasi-reversible, i.e. drastically slowing down. This is further evidenced by looking at changes in the apparent electron diffusion coefficient ( $D_e^{1/2}$ ) in relation to an increasing number of bilayers. The Randles-Sevcik equation (**Equation 3.1**) can be used to estimate the diffusion of electrons in an electroactive polymer films since all of the electroactive species are confined in a fixed location and not diffusing in solution. However, the concentration of redox species can be difficult to quantify in a hydrogel because the films swell and can change the volume of the film. Therefore, the relative electron diffusion ( $cD_e^{1/2}$ ) is often reported in these cases, and is determined by rearranging the Randle-Sevcik equation as follows:

$$\text{Equation 3.4: } cD_e^{1/2} = \frac{i_p}{268600n^{3/2}Av^{1/2}}$$

where  $i_p$ ,  $n$ ,  $A$ , and  $v$  are as designated above. **Figure 4.2.13** shows the changes in  $cD_e^{1/2}$  for (FcCl-C<sub>3</sub>-LPEI/laccase)<sub>x</sub> films assembled on ox-CP electrodes with respect to an increasing number of bilayers.

The  $cD_e^{1/2}$  for (FcCl-C<sub>3</sub>-LPEI/laccase)<sub>x</sub> films assembled on ox-CP decreases with the addition of material beyond eight bilayers. This suggest the films may be becoming too thick, and the kinetics of the reaction are slowing as the redox equilibrium is not being readily established. The decrease in  $cD_e^{1/2}$ , coupled with the large increase in  $\Delta E$ , gives

evidence for an effective limit for the amount of material that be efficiently detected by the electrode.

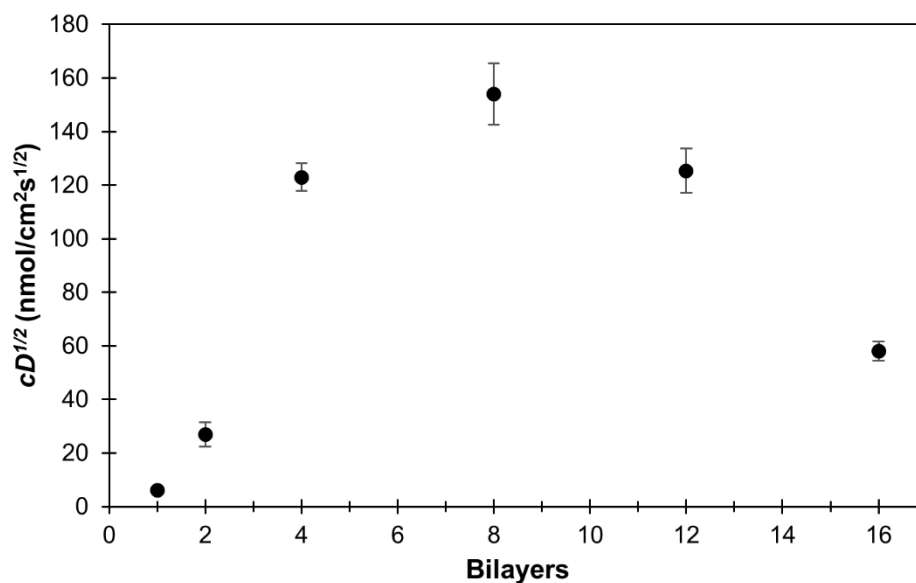


**Figure 4.2.13:** Plot of relative electron diffusion coefficient ( $cD_e^{1/2}$ ) as a function of FcCl-C<sub>3</sub>-LPEI/laccase bilayers.

To further examine the amount of material that can effectively analyzed on ox-CP electrodes, changes in  $\Gamma_{\text{FcCl}}$  were compared to planar gold electrodes with increasing number of bilayers (**Figure 4.2.14**). For systems containing up to eight bilayers, (FcCl-C<sub>3</sub>-LPEI/laccase)<sub>x</sub> films constructed on ox-CP electrodes have a higher chloroferrocene density than LBL films assembled on planar gold electrodes. There is a crossover point between eight and twelve bilayers where planar gold electrodes appear to more effectively detect deposited electroactive material than ox-CP electrodes. However, since the apparent electron diffusion for (FcCl-C<sub>3</sub>-LPEI/laccase)<sub>x</sub> films constructed on ox-CP decreases at bilayers, the redox kinetics are not equivalent between the two systems for thicker films.

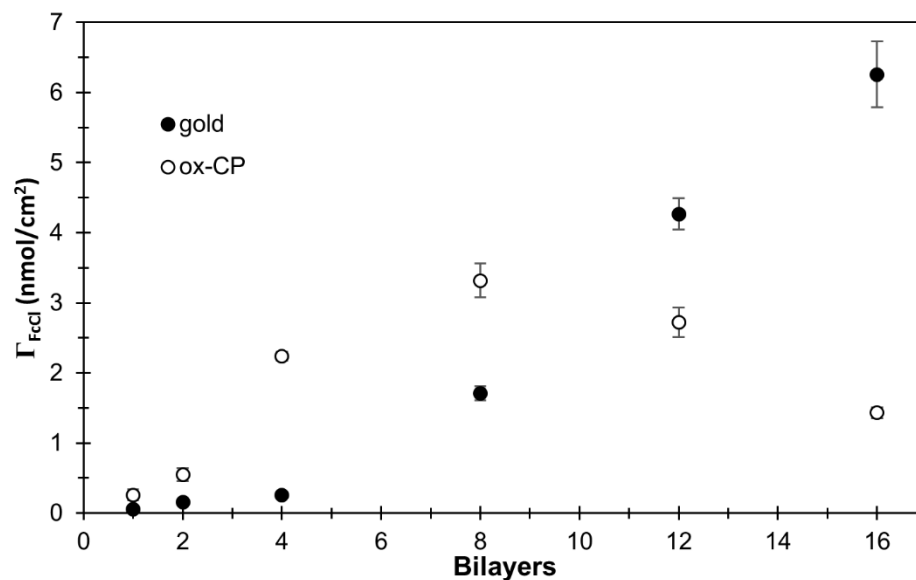


**Figure 4.2.14:** Relationship between chloroferrocene surface coverage ( $\Gamma_{\text{FcCl}}$ ) and the number of FcCl-C<sub>3</sub>-LPEI/laccase bilayers for films assembled on both gold and nitric acid oxidized carbon paper electrodes

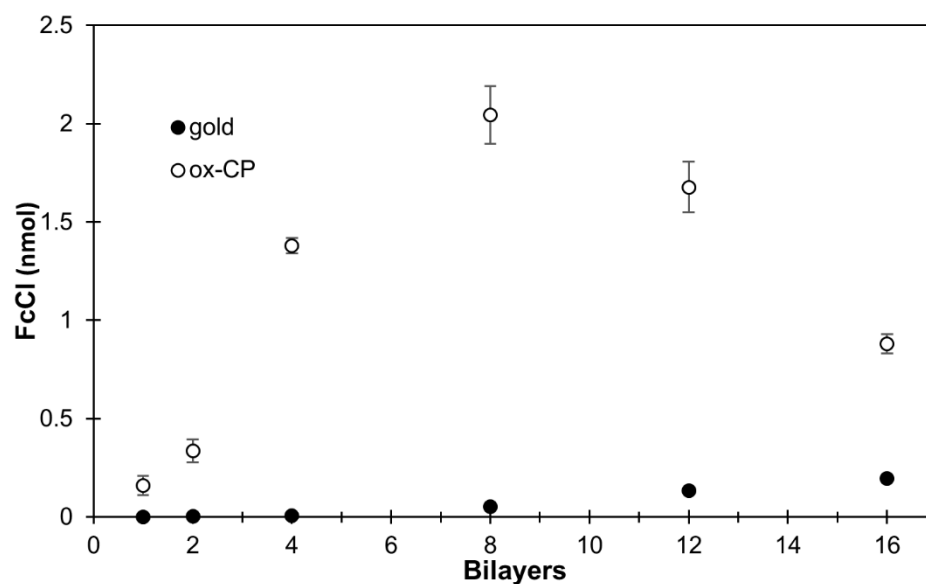


**Figure 4.2.15:** Relationship between moles of chloroferrocene and the number of FcCl-C<sub>3</sub>-LPEI/laccase bilayers for films assembled on both gold and nitric acid oxidized carbon

**Figure 4.2.15** compares the total number of moles for (FcCl-C<sub>3</sub>-LPEI/laccase)<sub>x</sub> films assembled on the different electrode supports. It is evident that there is significantly more material on the ox-CP electrodes than on the gold electrodes, and the material is initially more densely packed onto the surface, as evidenced in **Figure 4.2.14**. The films



on ox-CP become overloaded with material, and are not being effectively analyzed by the electrode. However, the addition of more laccase with each bilayer may improve sensor capabilities if oxygen diffusion is not limited in the thicker films.

#### 4.2.8 Carbon Paper Electrodes: Enzymatic Response

In order to evaluate how LBL assembled biocathodes assembled on ox-CP would perform as a biosensor, constant potential amperometry was used to determine the rate of oxygen reduction by poisoning the electrodes at a reducing potential (0.05 V below  $E_{pc}$ ) and monitoring  $J_{max}$  in the presence and absence of oxygen. **Figure 4.2.16** depicts the increase in  $J_{max}$  with the addition of FcCl-C<sub>3</sub>-LPEI/laccase bilayers. There is an initial exponential increase in oxygen response for (FcCl-C<sub>3</sub>-LPEI/laccase)<sub>x</sub> films that reaches a maximum of  $32.3 \pm 3.2 \mu\text{Acm}^{-2}$  at twelve bilayers followed by a slight decrease at sixteen bilayers. It should be noted that this increase in enzymatic response does not reflect the trend for electrochemical response discussed in the previous section. The maximum electrochemical response for (FcCl-C<sub>3</sub>-LPEI/laccase)<sub>x</sub> films occurred at eight bilayers, followed by a continual decrease in response with additional bilayers. The continued increase in  $J_{max}$  up to twelve bilayers indicates that material is still deposited onto the ox-CP electrodes even if the outer bilayers can no longer be effectively detected by cyclic voltammetry.

In the constant potential biosensor experiments, the reduction of oxygen is most likely occurring near the surface of the (FcCl-C<sub>3</sub>-LPEI/laccase)<sub>x</sub> films. This means that oxygen does not penetrate into the inner bilayers of material for the thicker films. As the chloroferrocene near the perimeter of the film is oxidized to chloroferrocenium, the chloroferrocene moieties near the electrode are able to shuttle electrons to regenerate the

active redox mediator. This process is efficient up to twelve bilayers, but the response to oxygen decreases as the films grow too thick. At  $(\text{FcCl-C}_3\text{-LPEI/laccase})_{16}$ , there is enough laccase near the surface of the films to allow for oxygen to be reduced faster than chloroferrocene can be regenerated, which leads to a decrease in  $J_{max}$ .

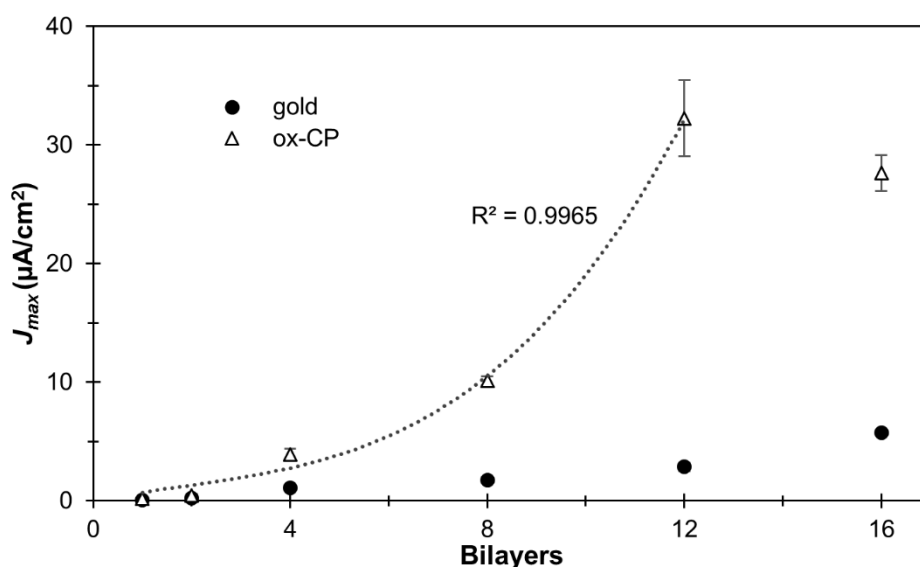


**Figure 4.2.16:** Plot of the effect of  $\text{FcCl-C}_3\text{-LPEI/laccase}$  bilayers on maximum catalytic current density ( $J_{max}$ ) for films assembled on both planar gold electrodes and nitric acid oxidized carbon paper electrodes.

As seen in **Figure 4.2.16**,  $(\text{FcCl-C}_3\text{-LPEI/laccase})_x$  films give much higher current densities when assembled on ox-CP electrodes rather than planar gold. Even though the biocathode composites are more densely packed on ox-CP (**Figure 4.2.14**), oxygen diffusion does not appear to be as big of a factor. The maximum  $J_{max}$  of  $32.3 \pm 3.2 \mu\text{Acm}^{-2}$  for  $(\text{FcCl-C}_3\text{-LPEI/laccase})_x$  films is an improvement on the films constructed on planar gold, but the response is still much lower than the  $J_{max}$  of  $177 \pm 40 \mu\text{Acm}^{-2}$  for EGDGE crosslinked films.<sup>29</sup>

#### 4.2.9 LBL Assembled Biocathode Literature Comparison

LBL assembled  $(\text{FcCl-C}_3\text{-LPEI/laccase})_{12}$  films are on the lower end of the limited number of laccase-containing LBL assembled biocathodes reported in the literature

(Table 4.2.6). The highest current density LBL biocathode currently in the literature uses a high surface area, macroporous gold electrode to artificially increase the surface area, and incorporates gold nanoparticles within the assembled structure to enhance conductivity.<sup>43</sup> Instead of using an electron mediator, this biocathode operates via direct electron transfer from the enzyme to the electrode, and the current densities were based on the geometric surface area, not the electrochemically active surface area. The lowest current density LBL laccase biocathodes use non-conducting silicon nanoparticles as a biocompatible, high surface area architecture, and cytochrome c as a direct electron transfer agent.<sup>44</sup>

**Table 4.2.6: Literature summary of LBL assembled oxygen biosensors**

Electrode	Biocathode	$J_{max}$ ( $\mu\text{Acm}^{-2}$ )	pH	Ref.
3DOM gold	(AuNP/laccase) <sub>5</sub>	795.5	6	43
gold wire	(SiNP/cyt c•laccase) <sub>6</sub>	1.316 ± 0.105	4.5	44
planar gold	(PAH-Os/laccase) <sub>7</sub> (PAH-Os)	150	4.7	45
RDE gold	(PAH-Os/laccase) <sub>6</sub> (PAH-Os)	320	4.7	46
ox-CP	(FcCl-C <sub>3</sub> -LPEI/laccase) <sub>12</sub>	32.3 ± 3.2	4.5	This work
SiNP = silicon nanoparticle cyt c•laccase = cytochrome c / laccase composite 3DOM = three-dimensional ordered macroporous AuNP = gold nanoparticle PAH-Os = [Os(bpy) <sub>2</sub> Cl(PyCOH)]Cl modified poly(allylamine) RDE = rotating disc electrode				

The two remaining reports of LBL assembled, laccase-containing biocathodes are more similar to the work presented herein. Both works come from the Calvo group, and use osmium-modified poly(allylamine) (PAH-Os) as an electron mediator for laccase. In 2009, they published the first report of an electrostatically assembled LBL biocathode

containing laccase and a redox polymer.<sup>45</sup> Films assembled on planar gold were found to be diffusion limited, so in their next work, rotating disc electrodes (RDE) were used to increase oxygen intake into the films.<sup>46</sup> The increased exposure to oxygen results in a doubling of the current, and demonstrates that, even in ultra-thin films, the limiting factor for biocathodes is often substrate diffusion. Therefore, the response of (FcCl-C<sub>3</sub>-LPEI/laccase)<sub>x</sub> would likely improve if an RDE were employed.

### 4.3 Conclusions

We have shown that FcCl-C<sub>3</sub>-LPEI can be used in the LBL construction of enzymatic biocathodes capable of generating  $32.2 \pm 3.2 \mu\text{Acm}^{-2}$  in response to oxygen. The electrochemical characterization of (FcCl-C<sub>3</sub>-LPEI/laccase)<sub>x</sub> films revealed an assembly similar to LBL bioanodes discussed in **Chapter 3**: an initial patchy deposition followed by filling in of the surface in the next several bilayers. Optimization of the assembly process demonstrated the importance of polyelectrolyte solution concentration and pH on the response of the biocathodes.

LBL assembled films were constructed on both planar gold electrodes and high surface area carbon paper. Carbon paper electrodes were characterized to determine the electrochemically active surface area so as to more accurately reflect the current density response of the assembled films. The response of (FcCl-C<sub>3</sub>-LPEI/laccase)<sub>x</sub> films fabricated on carbon paper electrodes was found to increase when the carbon paper was exposed to nitric acid before the LBL assembly process. (FcCl-C<sub>3</sub>-LPEI/laccase)<sub>x</sub> films assembled on nitric acid oxidized carbon paper electrodes were found to have a limit to the amount of electroactive material that could be efficiently detected. Electron diffusion

rates decreased after eight bilayers, but the enzymatic response of the films continued to increase up to twelve bilayers.

While the responses of the oxygen biocathodes were lower than some literature reports, the response is likely to increase with further optimization. Varying the percent substitution of chloroferrocene on the redox polymer could allow for better electron transfer through the film, and the usage of a rotating disc electrode would help to eliminate the oxygen diffusion limitations of the films.

#### **4.4 Experimental**

##### *Chemical and Materials*

Laccase from *Trametes versicolor* (EC 1.10.3.2.,  $\geq 10$  U/mg) and all chemicals were purchased from Sigma-Aldrich unless otherwise noted and used as received. Ethylene glycol diglycidyl ether (EGDGE) was purchased from Polysciences Inc., Warrington, PA. Nitric acid (70%) was purchased from Fisher Scientific. Carbon paper electrodes (Teflon treated, 0.1 mm thick, Item Number 590237) were purchased from the Fuel Cell Store. Chloroferrocene was prepared using a procedure by Nesmejanow *et al.*,<sup>47</sup> and FcCl-C<sub>3</sub>-LPEI (17 – 20% substituted) was synthesized using the procedure as described by Hickey.<sup>29</sup> Gold electrodes (2.0 mm diameter, CH instruments, Austin, TX) were polished with 1 and 0.25  $\mu\text{m}$  diamond polishing paste on nylon polishing pads before being polished with 0.05  $\mu\text{m}$  alumina on a microcloth pad.

##### *Nitric Acid Oxidation of Carbon Paper*

Carbon paper electrodes were cut into 0.5 cm x 4 cm rectangles and coated with wax except for a 0.5 cm x 0.5 cm square. Electrodes were then allowed to soak in 70% nitric acid for varying amounts of time to modify the carbon surface with carbonyls,

phenols, and carboxylic acids. Electrodes were removed from the acid, thoroughly rinsed with DI water, and dried at room temperature. Oxidized electrodes were immersed in 3.0 M NaOH for thirty minutes to ensure an overall negative charge on the surface, washed thoroughly with DI water, and dried at room temperature.

#### *Electrochemical Measurements*

Constant potential experiments and cyclic voltammetry were performed with a CH Instruments biopotentiostat (CHI832, Austin, TX) in a three-electrode configuration with a platinum wire counter electrode and a saturated calomel electrode (SCE). All experiments were conducted at room temperature (25 °C) in 100 mL of 50 mM citrate buffer (pH 4.5). Each experiment was performed a minimum of three times, and the values presented are the mean  $\pm$  standard error of the mean (SEM), unless otherwise stated.

#### **4.5 References**

1. Heinze, K.; Lang, H., *Organometallics* **2013**, *32* (20), 5623-5625.
2. Werner, H., *Angewandte Chemie International Edition* **2012**, *51* (25), 6052-6058.
3. Ornelas, C., *New Journal of Chemistry* **2011**, *35* (10), 1973-1985.
4. Kameoka, A.; Tsuchiya, K., *SAE Technical Paper* **2006**, 2006-01-3448
5. Ortiz, A.; Romero, J. L.; Cueva, I.; Jacobo, V. H.; Schouwenaars, R., *Case Studies in Engineering Failure Analysis* **2013**, *1* (2), 67-71.
6. Zhao, C.; Liu, Z.-Q., *Biochimie* **2012**, *94* (8), 1805-1811.
7. Borman, S. T. U., *Chemical & Engineering News Archive* **1996**, *74* (30), 38-40.
8. Osman, A. M.; Hassan, K. M.; Khalil, Z. H.; Turin, V. D., *Journal of Applied Chemistry and Biotechnology* **1976**, *26* (2), 71-78.
9. Wang, Z.; Tian, H.; Chen, K., *Dyes and Pigments* **2001**, *51* (2-3), 161-165.

10. Top, S.; Dauer, B.; Vaissermann, J.; Jaouen, G., *Journal of Organometallic Chemistry* **1997**, *541* (1–2), 355–361.
11. Dagani, R. O. N., *Chemical & Engineering News Archive* **2002**, *80* (37), 23–29.
12. Top, S.; Vessières, A.; Leclercq, G.; Quivy, J.; Tang, J.; Vaissermann, J.; Huché, M.; Jaouen, G., *Chemistry – A European Journal* **2003**, *9* (21), 5223–5236.
13. Valério, C.; Fillaut, J.-L.; Ruiz, J.; Guittard, J.; Blais, J.-C.; Astruc, D., *Journal of the American Chemical Society* **1997**, *119* (10), 2588–2589.
14. Nakayama, M.; Ihara, T.; Nakano, K.; Maeda, M., *Talanta* **2002**, *56* (5), 857–866.
15. Balland, V.; Lecomte, S.; Limoges, B., *Langmuir* **2009**, *25* (11), 6532–6542.
16. Saleem, M.; Yu, H.; Wang, L.; Zain ul, A.; Khalid, H.; Akram, M.; Abbasi, N. M.; Huang, J., *Analytica Chimica Acta* **2015**, *876* (0), 9–25.
17. Merchant, S. A.; Glatzhofer, D. T.; Schmidtke, D. W., *Langmuir* **2007**, *23* (22), 11295–11302.
18. Merchant, S. A.; Tran, T. O.; Meredith, M. T.; Cline, T. C.; Glatzhofer, D. T.; Schmidtke, D. W., *Langmuir* **2009**, *25* (13), 7736–7742.
19. Merchant, S. A.; Meredith, M. T.; Tran, T. O.; Brunski, D. B.; Johnson, M. B.; Glatzhofer, D. T.; Schmidtke, D. W., *The Journal of Physical Chemistry C* **2010**, *114* (26), 11627–11634.
20. Meredith, M. T.; Kao, D.-Y.; Hickey, D.; Schmidtke, D. W.; Glatzhofer, D. T., *Journal of The Electrochemical Society* **2011**, *158* (2), B166–B174.
21. Meredith, M. T.; Hickey, D. P.; Redemann, J. P.; Schmidtke, D. W.; Glatzhofer, D. T., *Electrochimica Acta* **2013**, *92* (0), 226–235.
22. Hickey, D. P.; Halmes, A. J.; Schmidtke, D. W.; Glatzhofer, D. T., *Electrochimica Acta* **2014**, *149* (0), 252–257.
23. Minter, S. D.; Liaw, B. Y.; Cooney, M. J., *Current Opinion in Biotechnology* **2007**, *18* (3), 228–234.
24. Meredith, M. T.; Minter, S. D., *Annual Review of Analytical Chemistry* **2012**, *5* (1), 157–179.
25. Luz, R. A. S.; Pereira, A. R.; de Souza, J. C. P.; Sales, F. C. P. F.; Crespilho, F. N., *ChemElectroChem* **2014**, *1* (11), 1751–1777.
26. Aoki, A.; Heller, A., *The Journal of Physical Chemistry* **1993**, *97* (42), 11014–11019.

27. Barton, S. C.; Kim, H.-H.; Binyamin, G.; Zhang, Y.; Heller, A., *The Journal of Physical Chemistry B* **2001**, *105* (47), 11917-11921.
28. Mano, N.; Kim, H.-H.; Heller, A., *The Journal of Physical Chemistry B* **2002**, *106* (34), 8842-8848.
29. Hickey, D. Ferrocene-Modified Linear Poly(ethylenimine) Bioelectrode Materials for Use in Glucose/O<sub>2</sub> Biofuel Cells. University of Oklahoma, 2014.
30. Upton, B. M.; Gipson, R. M.; Duhovic, S.; Lydon, B. R.; Matsumoto, N. M.; Maynard, H. D.; Diaconescu, P. L., *Inorganic Chemistry Frontiers* **2014**, *1* (3), 271-277.
31. Marsh, B. J.; Hampton, L.; Goggins, S.; Frost, C. G., *New Journal of Chemistry* **2014**, *38* (11), 5260-5263.
32. DeLuca, J. L.; Hickey, D. P.; Bamper, D. A.; Glatzhofer, D. T.; Johnson, M. B.; Schmidtke, D. W., *ChemPhysChem* **2013**, *14* (10), 2149-2158.
33. Lillethorup, M.; Shimizu, K.; Plumeré, N.; Pedersen, S. U.; Daasbjerg, K., *Macromolecules* **2014**, *47* (15), 5081-5088.
34. Hoogeveen, N. G.; Cohen Stuart, M. A.; Fleer, G. J.; Böhmer, M. R., *Langmuir* **1996**, *12* (15), 3675-3681.
35. Borges, J.; Mano, J. F., *Chemical Reviews* **2014**, *114* (18), 8883-8942.
36. Xu, L.; Pristiniski, D.; Zhuk, A.; Stoddart, C.; Ankner, J. F.; Sukhishvili, S. A., *Macromolecules* **2012**, *45* (9), 3892-3901.
37. Cleaves, H., II, Isoelectric Point. In *Encyclopedia of Astrobiology*, Gargaud, M.; Amils, R.; Quintanilla, J.; Cleaves, H., II; Irvine, W.; Pinti, D.; Viso, M., Eds. Springer Berlin Heidelberg: 2011; pp 858-858.
38. Wu, Z.; Pittman Jr, C. U.; Gardner, S. D., *Carbon* **1995**, *33* (5), 597-605.
39. Pittman Jr, C. U.; He, G. R.; Wu, B.; Gardner, S. D., *Carbon* **1997**, *35* (3), 317-331.
40. Tikhomirov, A. S.; Sorokina, N. E.; Avdeev, V. V., *Inorg Mater* **2011**, *47* (6), 609-613.
41. Vautard, F.; Fioux, P.; Vidal, L.; Dentzer, J.; Schultz, J.; Nardin, M.; Defoort, B., *Surface and Interface Analysis* **2013**, *45* (3), 722-741.
42. Zanello, P., Voltammetric techniques. In *Inorganic Electrochemistry: Theory, Practice and Application*, The Royal Society of Chemistry: 2003; pp 49-136.



43. Deng, L.; Wang, F.; Chen, H.; Shang, L.; Wang, L.; Wang, T.; Dong, S., *Biosensors and Bioelectronics* **2008**, *24* (2), 329-333.
44. Feifel, S. C.; Kapp, A.; Lisdat, F., *Langmuir* **2014**, *30* (19), 5363-5367.
45. Szamocki, R.; Flexer, V.; Levin, L.; Forchiasin, F.; Calvo, E. J., *Electrochimica Acta* **2009**, *54* (7), 1970-1977.
46. Scodeller, P.; Carballo, R.; Szamocki, R.; Levin, L.; Forchiassin, F.; Calvo, E. J., *Journal of the American Chemical Society* **2010**, *132* (32), 11132-11140.
47. Nesmejanow, A. N.; Ssasonowa, W. A.; Drosd, V. N., *Chemische Berichte* **1960**, *93* (11), 2717-2729.

## Chapter 5. Calorimetric Analysis of Sulfur/Paracyclophane Copolymerization

---

### 5.1 Introduction

The vast majority of polymers used in modern society are derived from the same crude oil that is also used to produce jet fuel, gasoline, kerosene, and heating oil as well as a whole host of lubricants and material feedstocks. Due to ever increasing oil prices and a growing environmental awareness, the development of polymers from alternative feedstocks is rapidly becoming a pressing need. One possible source of raw material is the elemental sulfur that is generated during the petroleum refining process.<sup>1</sup> Roughly seven million tons of excess sulfur are produced annually,<sup>2</sup> with only a small fraction of it being used in the production of various chemicals<sup>1,3</sup> and the vulcanization of rubber.<sup>4,5</sup> Sulfur (S<sub>8</sub>) will homopolymerize at temperatures above 185 °C,<sup>6</sup> but the resulting polymers have poor mechanical properties and readily depolymerize back to the monomeric rings upon cooling (**Figure 5.1.1**).<sup>1,6</sup>

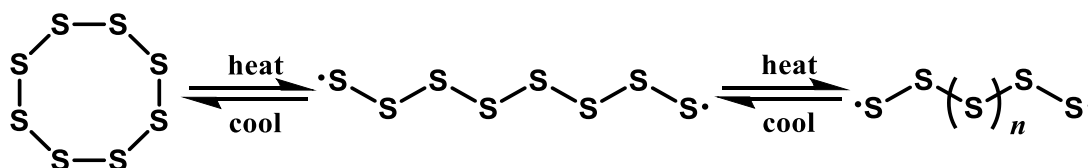


**Figure 5.1.1:** Thermal ring opening and subsequent polymerization of sulfur

The development of sulfur based polymers has long been a goal for material scientists, but most of the materials generated are brittle and crystalline.<sup>3,7</sup> Most strategies to stabilize polymeric sulfur are centered on quenching the diradicals formed from the homolytic cleavage of S<sub>8</sub> with various dienes or electron acceptors.<sup>3,8,9,10,11</sup> Some of the most recent successful advances in the stabilization of polymeric sulfur have been from the Pyun group using their method of so-called “inverse vulcanization.”<sup>12</sup> By introducing

diisopropenylbenzene directly into molten sulfur, they have been able to produce high sulfur content copolymers with a variety of applications, such as lithium-sulfur batteries<sup>13,14</sup> and high refractive index thermoplastics.<sup>15</sup>

Herein, we discuss the general strategy for using inverse vulcanization to develop a solvent-free ring opening copolymerization of S<sub>8</sub> and paracyclophane (PCP). At temperatures above 185 °C, S<sub>8</sub> will homolytically cleave to generate sulfur diradicals which can promote self-polymerization. It has also been reported that PCP will undergo spontaneous ring opening at temperatures above 200 °C.<sup>16,17</sup> Therefore, heating PCP in molten sulfur to temperature above 200 °C results in the free radical copolymerization of sulfur and PCP without the need for additional initiators or organic solvents. Sulfur/paracyclophane copolymers of varying molar ratios were synthesized and their reactions were monitored using differential scanning calorimetry (DSC). The idealized copolymerization scheme for the reaction between sulfur and PCP is shown in **Figure 5.1.2**, where the number of sulfur repeat units is dependent on the molar ratio of the two monomers.

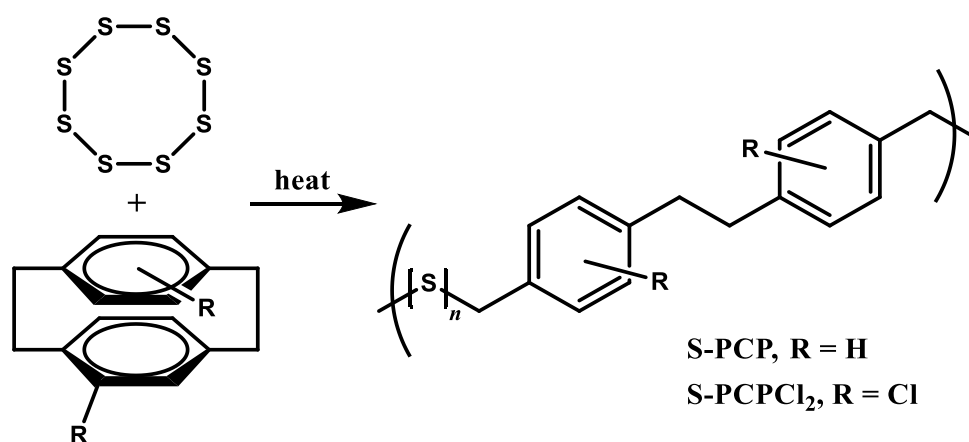


**Figure 5.1.2:** Proposed copolymerization scheme between sulfur and paracyclophane.

## 5.2 Results and Discussion

### 5.2.1 Thermal Analysis of Equal Mass Mixtures

Sulfur/PCP copolymers were milled with a stainless steel ball for 90 seconds to yield light yellow powders and samples (~6.0 mg) were placed in aluminum crucible pans. DSC was used to monitor the heat of the reaction between sulfur and PCP. **Figure 5.2.1** shows overlaid DSC thermograms for pure sulfur and pure PCP. As discussed in **Chapter 1.4.2**, the first peak on the sulfur thermogram is the solid phase conversion of orthorhombic sulfur ( $S_\alpha$ ) to monoclinic sulfur ( $S_\beta$ ), the second peak is the phase change from solid to liquid ( $S_\lambda$ ), and the third peak represents the polymerization to form rubber sulfur ( $S_\mu$ ).<sup>6</sup> There is noticeable increase in viscosity with that accompanies the polymerization of sulfur due to a large increase in molecular weight. While are no detectable thermal transition beyond the formation of  $S_\mu$ , there is large decrease in viscosity as the temperature rises beyond ca. 240 °C. This is due to the homolytic scissioning of the long polymer strands into smaller oligomers. These small chain diradicals will become important for the reaction with PCP.

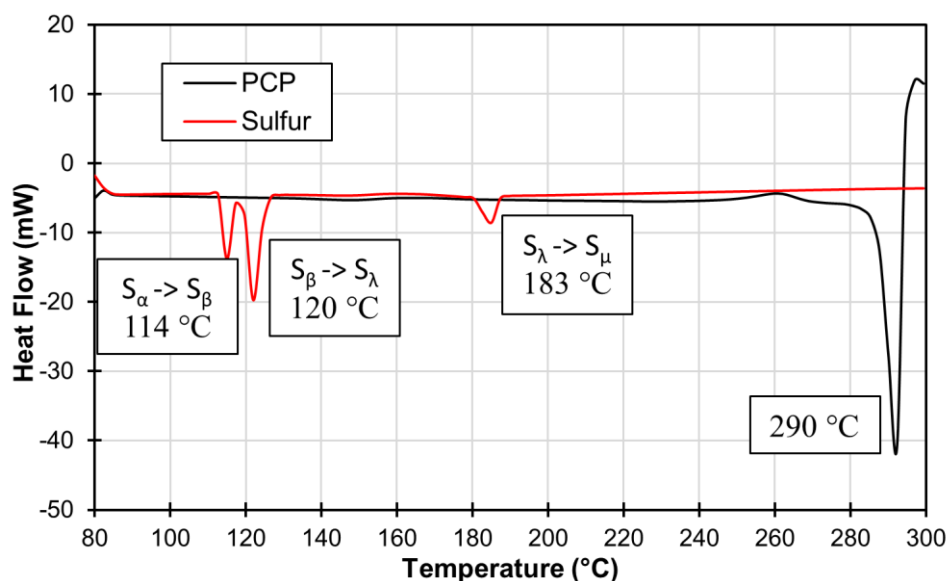


**Figure 5.2.1:** Overlaid DSC thermograms for sulfur and paracyclophane

PCP experiences no thermal changes until melting occurs around 285 °C. Initial investigations into the reaction of sulfur and PCP were run in crucibles with pierced lids, which resulted in PCP sublimating out of the pans and coating the inner furnace of the DSC. Therefore, all samples containing PCP must be run in closed crucibles, as it will readily sublime when heated above 250 °C.

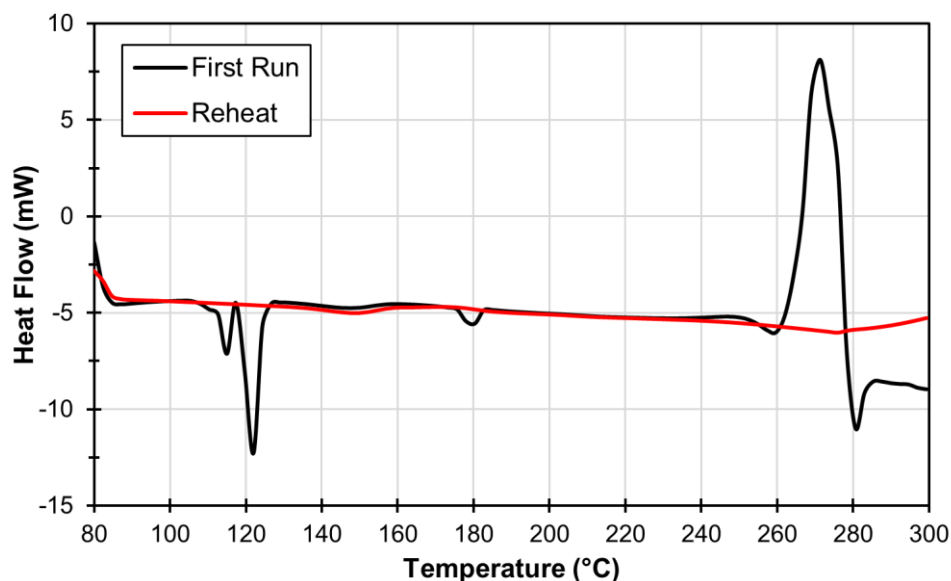


**Figure 5.2.2:** Overlaid DSC thermograms for 1:1 (weight) S:PCP, i.e. 13.3 mol% PCP, both the first run and the reheat seven days later

As can be seen in **Figure 5.2.1**, there are no detected peaks between 190 – 280 °C. However, when sulfur and PCP are mixed together, new exothermic peaks appear between 240 – 285 °C depending on the molar ratio of the two components. **Figure 5.2.2** depicts a typical thermogram for a 1:1 mixture, by weight, for sulfur ( $S_8$ ) and PCP, which corresponds to a 6.5:1 molar ratio of sulfur atoms to PCP (S:PCP), or 13.3 mol% PCP. For the remainder of the discussion, samples will be referred to as S-PCP-X, where X is the mole percent of PCP contained within the initial reaction mixture. The new exothermic peak at 270 °C for S-PCP-13.3 corresponds to the reaction between sulfur and

PCP. After the reaction had occurred, the DSC pan was opened to investigate the physical changes that had occurred. Prior to heating, the reaction mixture was a light yellow powder that was soluble in dichloromethane and carbon disulfide. After the reaction occurs, the material has become a hard, brown, and glassy solid that flexes under applied pressure before breaking. The resulting material has a few small holes throughout as if gas evolution occurred before it had solidified. The material was insoluble in benzene, hexanes, dichloromethane, carbon disulfide, acetone, water, sulfuric acid, and trifluoroacetic acid.

To probe if the polymerization of S-PCP-13.3 is an irreversible process, samples were retested in the DSC under the same conditions after seven days. As can be seen in **Figure 5.2.2**, there are no traces of residual starting materials, which indicates that all of the monomer units are incorporated into the polymer. Surprisingly, the thermogram for S-PCP-13.3 lacked a glass transition temperature ( $T_g$ ) for the polymer. If the reaction was forming linear polymers as described in **Figure 5.1.2**, there should be a  $T_g$  associated with the material. Heating out to 340 °C still did not give evidence for a  $T_g$ , and attempts to heat further were beyond the capacity of the available equipment. Attempts to get other useful spectroscopic analysis of the material was not feasible on the small scale reaction carried out in the DSC. The insolubility of the materials suggested that the samples may be forming highly crosslinked networks rather than simple alternating copolymers. To investigate optimization parameters for the copolymerization, the ratio of starting materials was systematically varied.

## 5.2.2 Variable Sulfur Content Materials

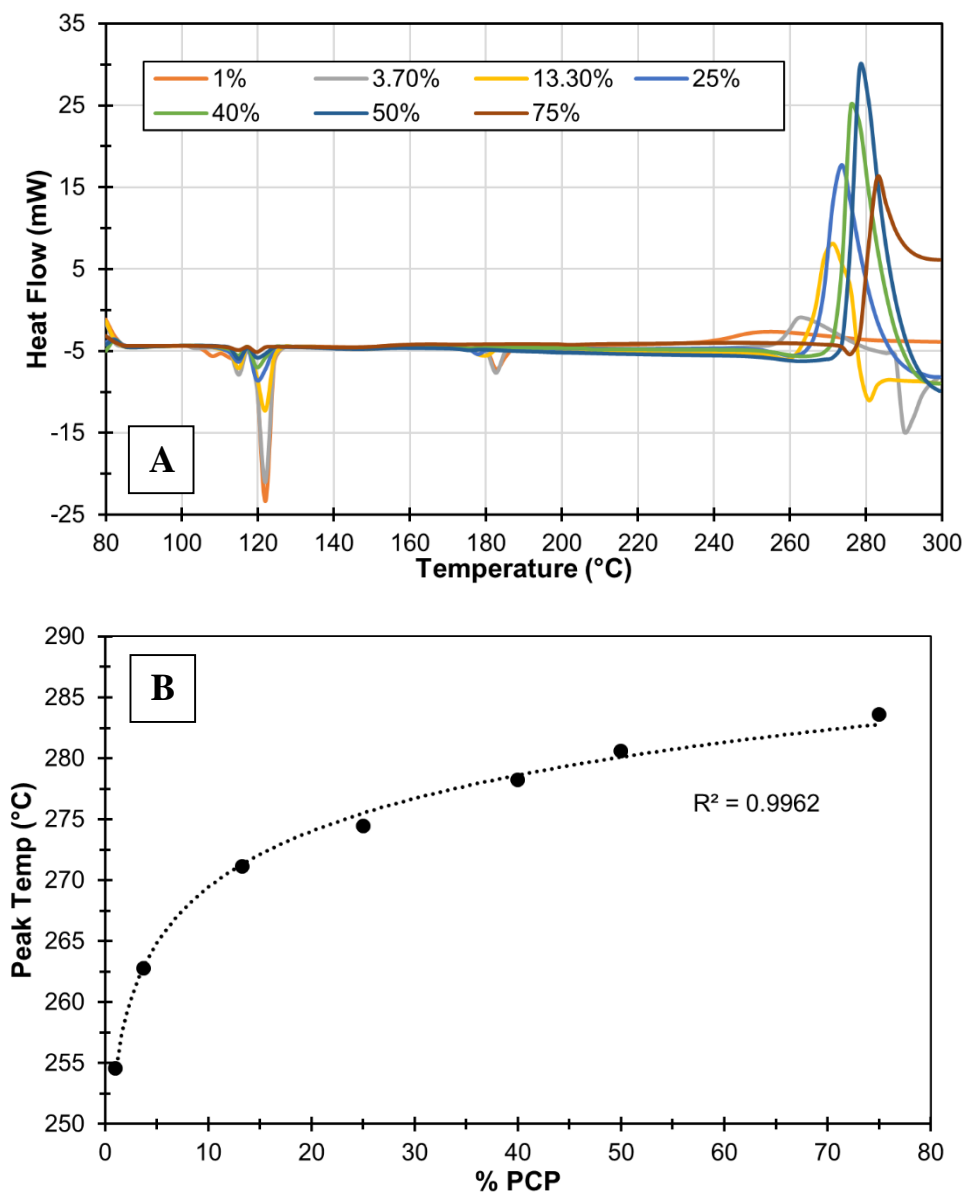


**Figure 5.2.3:** (A) Overlaid DSC thermograms for S:PCP and (B) plot of exothermic peak temperatures with relation to increasing mole percentage of PCP

DSC was used to monitor the reaction of sulfur and PCP with varying ratios of starting materials. As seen in **Figure 5.2.3A**, the endothermic peaks for sulfur decrease with the addition of increasing amounts of PCP, which is expected due to less sulfur being in the starting mixture. The magnitude of the exothermic reaction peaks increases up to 50% PCP before decreasing at 75% PCP. The maximum at S-PCP-50 would seem to

correlate to equimolar amounts of starting material reacting to give polymers with one sulfur atom to one ring-opened PCP. Interestingly, the exothermic peaks demonstrated a logarithmic increase in temperature with an increase in mole percentage of PCP (**Figure 5.2.3B**). Even though the magnitude of the exothermic peak at 70% PCP decreased, the peak temperature for the reaction followed the same increase as the rest of the series.

**Table 5.2.1** summarizes the physical characteristics of the synthesized materials after polymerization had occurred. Samples were extracted with carbon disulfide to remove any remaining starting materials, and all percentages of PCP left a large portion of insoluble material behind.

**Table 5.2.1:** Summary of physical characteristics for S:PCP with increasing amounts of PCP

mol% PCP	Color	Stiffness	Texture
75	yellow/brown	soft	sandy
50	dark orange	soft	waxy
40	dark orange	hard	glassy
25	brick red	hard	glassy
13.3	brown	hard	glassy, bubbles
3.7	brown	brittle	foam
1	orange	brittle	glassy

### 5.2.3 Polymerization Scale-Up

Larger samples were synthesized by heating the materials in flame sealed thick-walled glass reaction tubes. The first attempt at a larger polymerization resulted in the reaction tube exploding in the furnace. The dial on the furnace malfunctioned and the system was accidentally heated to ~500°C. Switching to a furnace with a more



controllable heating element allowed for further experiments to be conducted under more careful conditions.

S-PCP-50 (~250 mg) was heated up to 300 °C for various amounts of time. **Table 5.2.2** summarizes the observations of the material with increased heating while in a sealed tube, and **Figure 5.2.4** depicts the materials before and after heating. The tubes had pressure build up inside after prolonged heating, most likely due to the expulsion of hydrogen sulfide from the polymeric network. The presence of hydrogen sulfide was tested by heating a sample of S-PCP-50 in a glass vial with a short piece of tubing running from the top of the vial into a solution of cadmium chloride. Cadmium chloride has long been known to react with hydrogen sulfide to form an insoluble precipitate of cadmium sulfide.<sup>18</sup> Shortly after the sample of S-PCP-50 started bubbling, a yellow precipitate appeared in the collection vial; qualitatively signaling the presence of hydrogen sulfide.

**Table 5.2.2:** Summary of the physical characteristics of 1:1 (mol) S:PCP at increasing amounts of time at 300 °C.

<b>Time (min)</b>	<b>Description</b>
0	yellow powder
20	yellow powder
30	orange solid
40	viscous orange liquid
50	dark orange liquid, bubbling
60	dark orange solid
90	brown foam

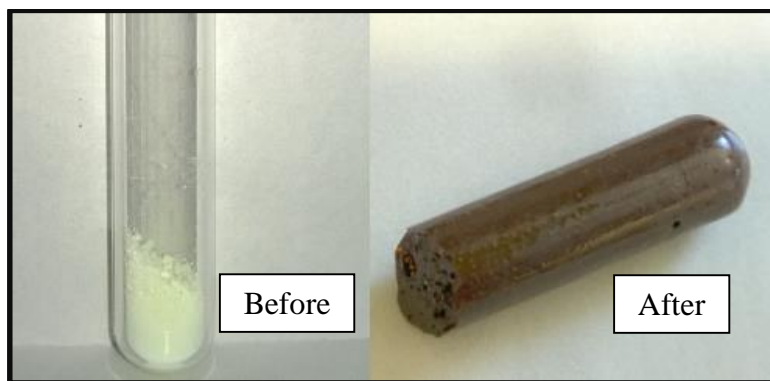


**Figure 5.2.4:** S-PCP-50 before and after heating at 300 °C for 90 minutes

The loss of hydrogen sulfide in the polymerization reaction most likely comes from the dehydrogenation of the ethylene bridge between phenyl rings. This is best demonstrated by comparing to the thermal decomposition of the model compound dibenzyl sulfide (DBS). At temperatures greater than 280 °C, DBS will decompose into a sulfur diradical and bibenzyl, which then react to form hydrogen sulfide and stilbene (**Figure 5.2.5**).<sup>19,20,21</sup> If further sulfur radicals are available, two equivalents of stilbene can further react to form tetraphenylthiophene.<sup>22,23</sup>

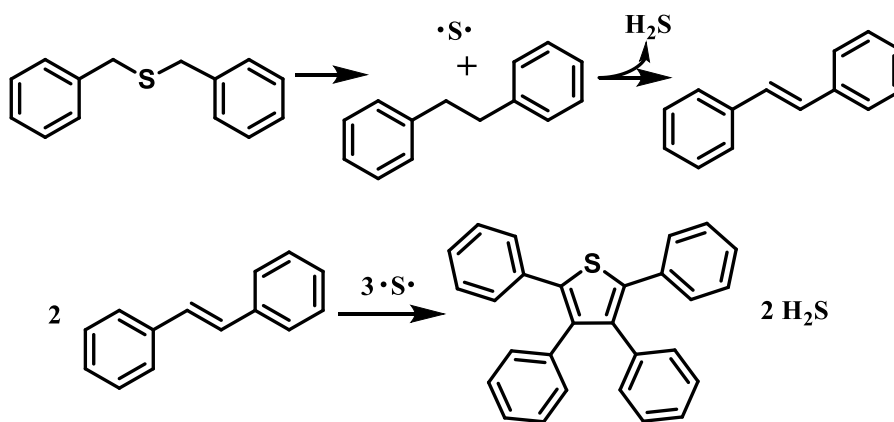


**Figure 5.2.5:** Thermal decomposition of dibenzyl sulfide into stilbene and conversion of stilbene into tetraphenylthiophene.

When PCP ring opens and couples with sulfur, the resulting polymer repeat units are similar to both bibenzyl and DBS. Heating at 300 °C could result in sulfur expulsion

to form a compound similar to poly(p-xylylene) (**Figure 5.2.6**). Therefore, there is a high probability that the system will crosslink into a covalent network bridged by thiophene units when the polymer is heated in the presence of excess sulfur. This hypothesis would help to explain the poor solubility of the synthesized material, and the foaming occurs by the evolution of hydrogen sulfide gas.

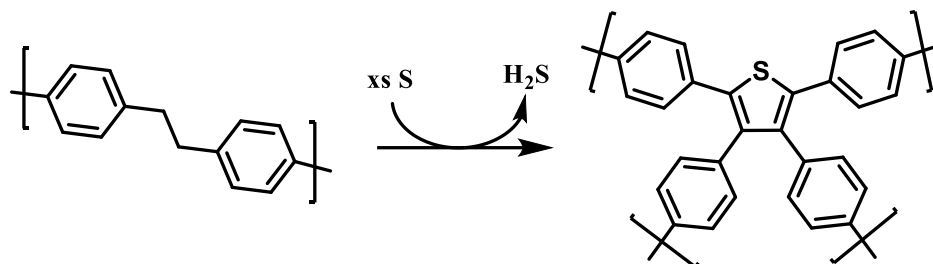


**Figure 5.2.6:** Proposed crosslinking of poly(p-xylylene) in the presence of excess sulfur.

While heating the samples in the muffle furnace allowed for high temperature control, the materials had to be continually removed for visual inspection. To gain a better visual understanding of the polymerization, samples were heated on a hot plate in a silicone cutout between two glass slides. **Figure 5.2.7** depicts the physical changes in S-PCP-50 with increased heating. The sample starts out as a homogenous yellow/white powder, but upon heating, the PCP begins to sublime and collect on the top glass slide. This separation of material results in the reaction occurring only at the interface of the two reactants.

As the S-PCP-50 continued heating, dark orange spots of molten sulfur began to appear. The liquid sulfur eventually polymerized as evidenced by the drastic increase in viscosity. With continued heating, the polymeric sulfur began to undergo scissioning, which resulted in a decrease in viscosity; this is almost immediately followed by reaction with PCP. Pockets of dark orange and dark red begin to solidify across the material, and

these spots eventually begin to bubble and turn brown. The final image in **Figure 5.2.7** shows the material after it has cooled and been removed from between the glass slides. The interior, translucent parts of the material are tough, but have a decent amount of flexibility to them. The outer portions of the material are porous and fragile like the foam created in the sealed tubes. Uniform heating and excess reaction head space appeared to be hindering the formation of uniform films.

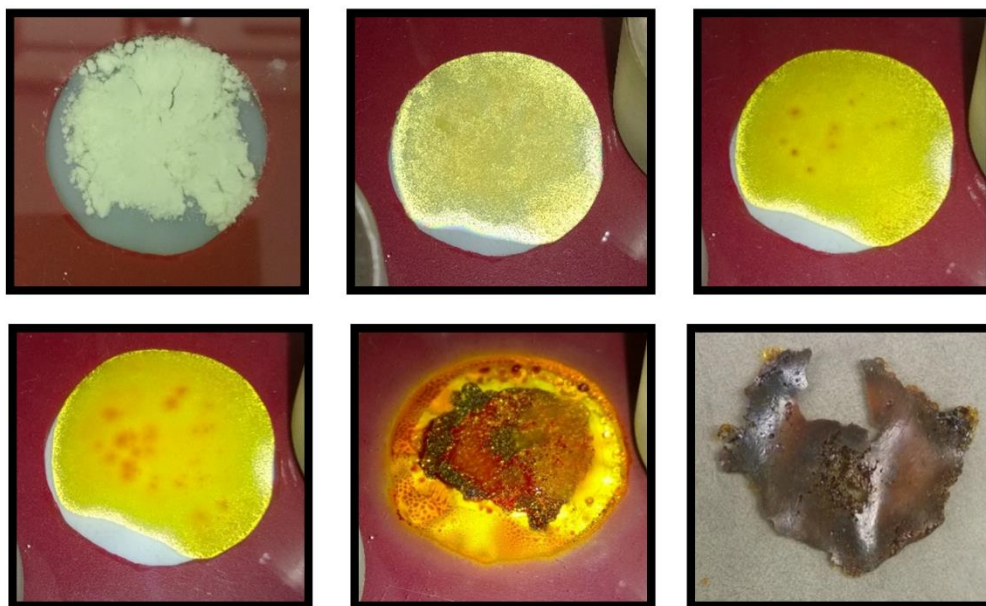


**Figure 5.2.7:** Visual depiction of S-PCP-50 with continued heating on a hot plate.

Samples of S-PCP-50 (~2.0 g) were placed in a stainless steel mold and heated in a muffle furnace to control both temperature and reaction volume. **Figure 5.2.8** depicts the S-PCP-50 sample after heating for two hours at 300 °C both before and after extraction with carbon disulfide. The material was a cohesive, orange disc that broke after mild pressure was applied to it. Soaking the disc in carbon disulfide removed ~40% of the mass which left behind a porous, fragile yellow solid. This material easily crumbled, but was also insoluble in organic solvents. Spectroscopic characterization of this material was therefore not possible.

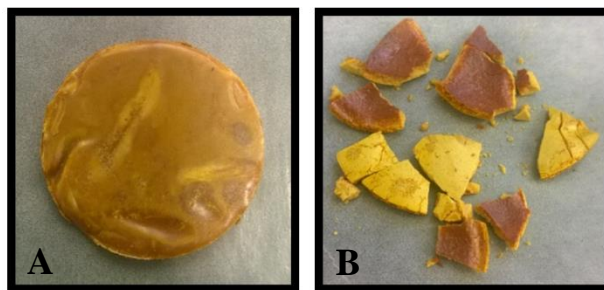


**Figure 5.2.8:** S-PCP-50 pellet after two hours heating at 300 °C in stainless steel die: (A) before and (B) after extraction with carbon disulfide.

Since a large portion of the material did not react in the initial heating, new samples were heated for longer periods of time. Even though S-PCP-50 was heated in a sealed die, the material expanded, leaked out of the die, and solidified outside of the cylinder after five hours in the furnace. As can be seen in **Figure 5.2.9**, the dark orange material expanded between the walls and came out the top rather than being contained within the die. As the viscosity of the material decreased, it was probably thin enough to flow between the piston and the walls of the die. While the sample did not remain contained as well as expected, there are several important features that can be seen from this experiment. Firstly, the copper wire surrounding the die has turned blue and formed crystals along the surface. This is most likely formed from the reaction of the copper wire with the expelled hydrogen sulfide gas. Secondly, the material that was extruded from the top of the die was porous and hollow, but it appears to have solidified before it could spread out too much. This seems to suggest the hypothesized crosslinking occurs very rapidly once the reaction sample reaches a certain temperature.

The synthesized material was a brown foam that crumbled when removed from the die (**Figure 5.2.9**). Even though the bulk material did not form a unified solid, the collected pieces were insoluble in organic solvents and were extremely hard. The large piece of material that had formed on the outside of the die was collected and heated with

a butane flame ( $\sim 1400\text{ }^{\circ}\text{C}$ ) to determine if the synthesized material would melt at temperatures beyond the capabilities of the DSC. The material did not melt after repeated heating, but instead glowed bright orange much like a metal rod will when heated. The highly crosslinked nature of the material is therefore highly heat resistant, and might have applications as a thermal insulator if the polymerization can be controlled.



**Figure 5.2.9:** S-PCP-50 heated at  $300\text{ }^{\circ}\text{C}$  furnace for five hours. Top: die immediately after removal from furnace. Bottom: foamed material remaining inside the die.

#### 5.2.4 *Dichloroparacyclophane Incorporation*

Since the melting point of PCP is very high, a halogen-substituted dichloroparacyclophane ( $\text{PCPCl}_2$ ) was used in an attempt to lower the high temperature needed for the S-PCP polymerization to occur. As seen in **Figure 5.2.10**,  $\text{PCPCl}_2$  melts at  $175\text{ }^{\circ}\text{C}$ , which is considerably lower than unsubstituted PCP. The S- $\text{PCPCl}_2$  mixtures were ball-milled in the same fashion as S-PCP; however, instead of forming a homogenous powder, S- $\text{PCPCl}_2$  formed a hard, cement-like material that had to be

chiseled out of the mixing chamber. When samples were mixed with a mortar and pestle, the two samples first formed a gel-like composition before solidifying into the cement-like material. The two solid components do not appear to have reacted, but rather are acting as a eutectic system.

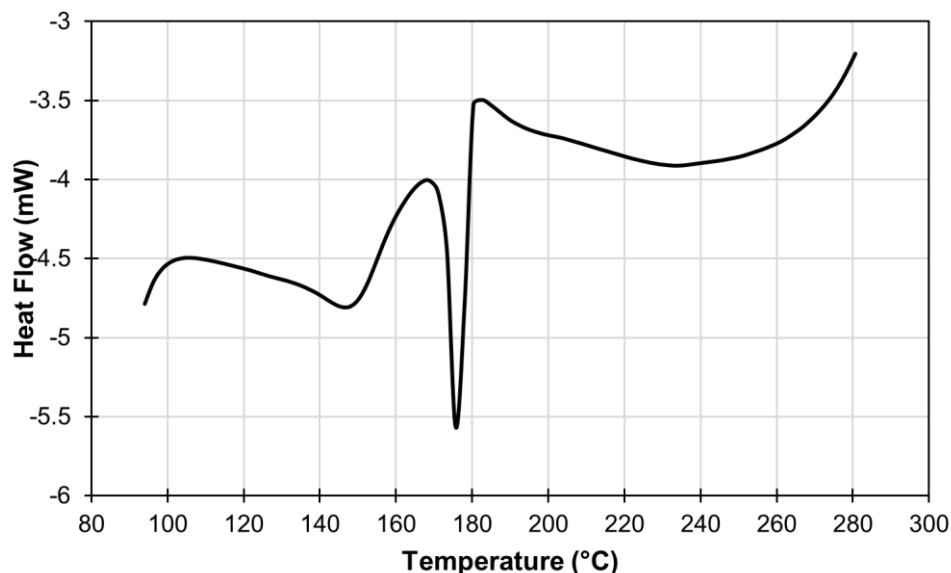


**Figure 5.2.10:** DSC thermogram for dichloroparacyclophane.

The thermal properties of S-PCPCL<sub>2</sub> were investigated using DSC, as shown in **Figure 5.2.11**. The most noticeable difference for S-PCPCL<sub>2</sub> is the lack of distinct sulfur peaks. Instead of two peaks at 114 °C and 120 °C, there is only one broad melting point at 105 °C. This melting point depression most likely arises from the blending of the two components to form a mixture with a noticeably different co-crystal structure. This hypothesis is further supported by the lack of a melting point for PCPCL<sub>2</sub>.

The exothermic reaction peaks for S-PCPCL<sub>2</sub>, seen in **Figure 5.2.11**, are about 15 °C higher than the corresponding peaks for S-PCP. Incorporation of a halogen substituted PCP had the opposite effect on the reaction. The electron withdrawing effects of the chlorine could possibly help stabilize the benzylic radicals that form from the homolytic

cleavage of PCPCl<sub>2</sub>. Therefore the incorporation of PCPCl<sub>2</sub> does not appear to aid in the copolymerization with sulfur.

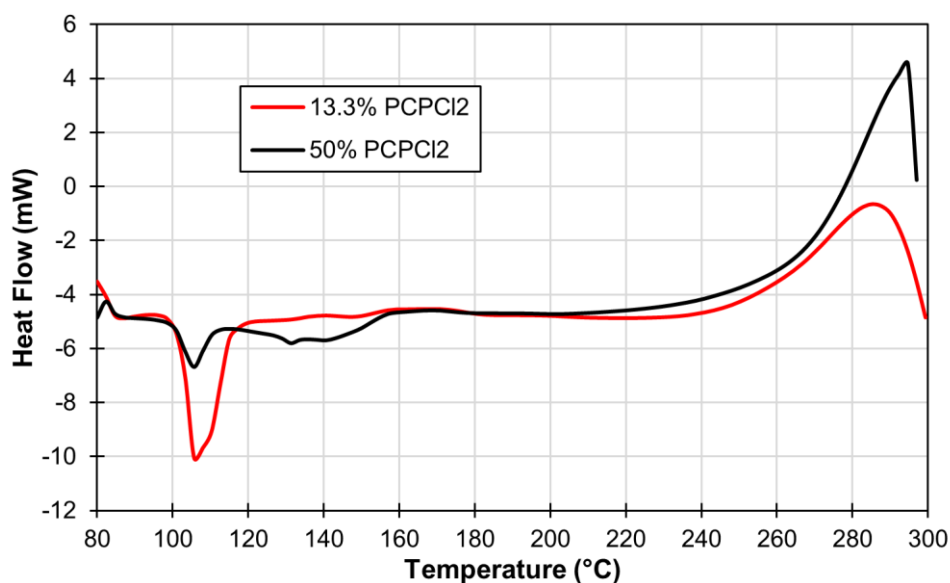


**Figure 5.2.11:** Overlaid DSC thermograms for S-PCPCl<sub>2</sub> at 13.3 and 50 mol% PCPCl<sub>2</sub>.

However, samples of S-PCPCl<sub>2</sub>-50 that were heated in seal, thick-walled reaction tubes at 300 °C did not experience the foaming issue that occurred with S-PCP-50. As seen in **Figure 5.2.12**, S-PCPCl<sub>2</sub>-50 was a viscous dark orange liquid after two hours in the furnace. Upon cooling to room temperature, S-PCPCl<sub>2</sub>-50 became a light brown solid that displayed no smell of hydrogen sulfide upon opening of the reaction tube. The resulting material was incredibly hard, and it readily dissolved into carbon disulfide and chloroform. Therefore, spectroscopic analysis of the material could be done.

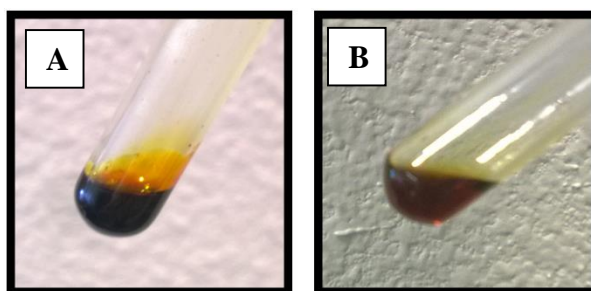


**Figure 5.2.12:** S-PCPCl<sub>2</sub>-50 after heating at 300 °C for two hours. (A) Immediately after removal from furnace and (B) after cooling to room temperature



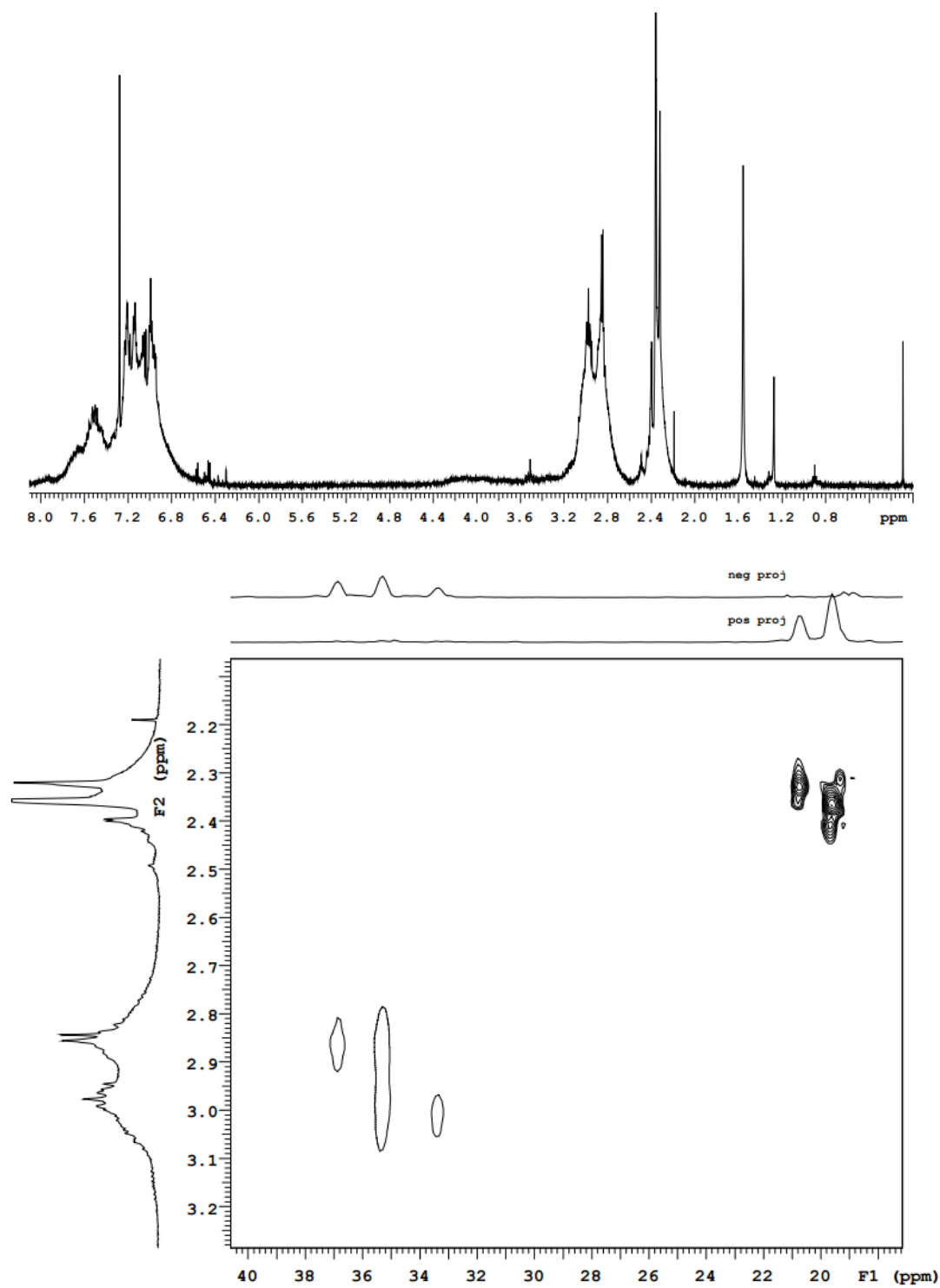


**Figure 5.2.13:** <sup>1</sup>H-NMR spectrum (top) and <sup>1</sup>H-<sup>13</sup>C HSQC spectrum (bottom) for S-PCPCl<sub>2</sub>-50.

As seen in **Figure 5.2.13A**,  $^1\text{H}$ -NMR characterization of S-PCPCl<sub>2</sub>-50 was fairly complicated due to the variety of PCPCl<sub>2</sub> isomers used in the starting material. However, there are readily apparent aromatic and alkyl peaks present in the spectrum. Because the peaks did not integrate to distinct ratios,  $^1\text{H}$ - $^{13}\text{C}$  HSQC was used to better characterize the synthesized material. The  $^1\text{H}$ - $^{13}\text{C}$  HSQC will give positive signals for carbons with an odd number of protons and a negative signals for carbons with even numbers of protons. **Figure 5.2.13B** correlates the  $^{13}\text{C}$ -NMR spectrum on the x-axis to the  $^1\text{H}$ -NMR spectrum on the y-axis for S-PCPCl<sub>2</sub>-50. The peaks at 2.3 – 2.4 ppm on the  $^1\text{H}$ -NMR spectrum correlate to only two carbons at 19 – 20 ppm in the  $^{13}\text{C}$ -NMR spectrum and result in positive peaks. This suggests the presence of a methyl group on an aromatic ring, and the peaks at 2.3 – 2.4 ppm are consistent with the peaks for the methyl group of ortho-, and meta-toluene. Bibenzyl is known to decompose into toluene from the reaction with sulfur and hydrogen sulfide, and it is therefore likely that the products formed from heating S-PCPCl<sub>2</sub>-50 are simply the ring opened PCPCl<sub>2</sub>, and possibly some short chain oligomers, rather than actual long chain polymers.

### 5.3 Conclusions

The copolymerization of elemental sulfur and PCP is a complicated reaction that results in a variety of products. The biggest challenge faced in this work was controlling the temperature to provide uniform heating and controlling the head space to prevent sublimation of PCP. The materials formed from S-PCP could not be easily characterized by spectroscopic methods, and therefore the exact structures of the synthesized materials could not be determined. However, the insolubility of the materials and the detection of hydrogen sulfide gas correspond to literature precedence for small molecule analogues

for the polymer repeat units. The materials formed are likely highly crosslinked with thiophene units to form an interconnected polymer network. The fact that the material would not melt even when subjected to a butane flame demonstrates the thermal stability of the compounds and their possible usage as a flame retardant or heat resistant coating.

The substitution of PCP for PCPCl<sub>2</sub> in the reaction mixture did not lower the reaction temperature, as evidenced by the DSC thermogram. While S-PCPCl<sub>2</sub> did not experience the foaming problem associated with S-PCP, NMR and HSQC demonstrated that the resulting material was not a long chain polymer, but rather a collection of oligomers. The usage of PCP substituted with mild electron donating groups, i.e. methyls, might allow for the reaction to occur at a lower temperature. It may also be interesting to use a blend of substituted and unsubstituted PCP molecules to try and control the foaming. Thermally resistant, light-weight materials are always of use; especially as coatings for space shuttles and satellites.

## **5.4 Experimental**

### *Chemicals*

Sulfur (S<sub>8</sub>, sublimed powder, ~100 mesh, Aldrich), carbon disulfide (Aldrich), paracyclophane (Parylene DPX-N, Specialty Coating Systems), dichloroparacyclophane (Parylene DPX-C, Specialty Coating Systems) were commercially available and used as received without further purification.

### *5.5.2 Thermal Experiments*

The thermal properties of sulfur/paracyclophane copolymers were characterized by differential scanning calorimetry (DSC). Analyses were performed under a steady

flow of nitrogen gas using a Mettler Toledo DSC 820. Bulk heating experiments were carried out using a ThermoLyne 47900 Benchtop Muffle Furnace.

### *Material Preparation*

Sulfur/paracyclophane copolymers were prepared by mixing the raw materials together in a Vivadent Silamat Model C vibrating mill. Samples were milled with a stainless steel ball for 90 seconds to yield light yellow powders. Sulfur/dicholoparacyclophane copolymers were ball-milled for DSC experiments, and mixed as dry powders without ball milling for larger polymerizations. For all DSC experiments, ca. 7 mg of each S-PCP composition were placed in aluminum crucibles (40  $\mu$ L, w/ pin and lid, DSC Consumables) and sealed prior to heating. Samples were later reheated after seven days sitting at ambient conditions.

For medium scale experiments (~250 mg), samples were flame sealed in thick-walled glass tubes under vacuum. Sample tubes were placed in a vented stainless steel crucible to act as secondary containment in case of explosion due to gas evolution. Bulk samples were heated at 300 °C for various amounts of time.

For large scale experiments (~2.0 g), samples were placed in a stainless steel die cylinder with pieces of Teflon between the plungers and the materials. The die was then kept closed with copper wire, and placed in a Pyrex dish to collect at material that leaked out. Bulk samples were heated at 300 °C for various amounts of time.

### **5.5 References**

1. Rauchfuss, T., *Nat Chem* **2011**, 3 (8), 648-648.
2. Kutney, G., *Sulfur: History, Technology, Applications & Industry*. 2nd ed.; ChemTec Publishing: 2013; p 242.

3. Meyer, B.; Kharasch, N.; Institute, S., *Elemental sulfur: chemistry and physics*. Interscience Publishers: 1965.
4. Flory, P. J., *Chemical Reviews* **1944**, 35 (1), 51-75.
5. Coran, A. Y., *Journal of Applied Polymer Science* **2003**, 87 (1), 24-30.
6. Currell, B. R.; Williams, A. J., *Thermochimica Acta* **1974**, 9 (3), 255-259.
7. B. R, C.; A. J, W.; A. J, M.; B. J, N., Plasticization of Sulfur. In *New Uses of Sulfur*, AMERICAN CHEMICAL SOCIETY: 1975; Vol. 140, pp 1-17.
8. Penczek, S.; Slazak, R.; Duda, A., *Nature* **1978**, 273 (5665), 738-739.
9. Duda, A.; Penczek, S., *Die Makromolekulare Chemie* **1980**, 181 (5), 995-1001.
10. Blight, L. B.; Currell, B. R.; Nash, B. J.; Scott, R. T. M.; Stillo, C., *British Polymer Journal* **1980**, 12 (1), 5-11.
11. Tsuda, T.; Takeda, A., *Chemical Communications* **1996**, (11), 1317-1318.
12. Chung, W. J.; Griebel, J. J.; Kim, E. T.; Yoon, H.; Simmonds, A. G.; Ji, H. J.; Dirlam, P. T.; Glass, R. S.; Wie, J. J.; Nguyen, N. A.; Guralnick, B. W.; Park, J.; SomogyiÁrpád; Theato, P.; Mackay, M. E.; Sung, Y.-E.; Char, K.; Pyun, J., *Nat Chem* **2013**, 5 (6), 518-524.
13. Simmonds, A. G.; Griebel, J. J.; Park, J.; Kim, K. R.; Chung, W. J.; Oleshko, V. P.; Kim, J.; Kim, E. T.; Glass, R. S.; Soles, C. L.; Sung, Y.-E.; Char, K.; Pyun, J., *ACS Macro Letters* **2014**, 3 (3), 229-232.
14. Griebel, J. J.; Li, G.; Glass, R. S.; Char, K.; Pyun, J., *Journal of Polymer Science Part A: Polymer Chemistry* **2015**, 53 (2), 173-177.
15. Griebel, J. J.; Namnabat, S.; Kim, E. T.; Himmelhuber, R.; Moronta, D. H.; Chung, W. J.; Simmonds, A. G.; Kim, K.-J.; van der Laan, J.; Nguyen, N. A.; Dereniak, E. L.; Mackay, M. E.; Char, K.; Glass, R. S.; Norwood, R. A.; Pyun, J., *Advanced Materials* **2014**, 26 (19), 3014-3018.
16. Reich, H. J.; Cram, D. J., *Journal of the American Chemical Society* **1967**, 89 (12), 3078-3080.
17. Reich, H. J.; Cram, D. J., *Journal of the American Chemical Society* **1969**, 91 (13), 3517-3526.
18. Lipscomb, G. F.; Hulett, G. A., *Journal of the American Chemical Society* **1916**, 38 (1), 20-27.
19. Fromm, E.; Achert, O., *Berichte der deutschen chemischen Gesellschaft* **1903**, 36 (1), 534-546.

20. Bajus, M.; Baxa, J.; Leclercq, P. A.; Rijks, J. A., *Industrial & Engineering Chemistry Product Research and Development* **1983**, 22 (2), 335-343.
21. Voronkov, M. G.; Panova, G. M.; Timokhina, L. V.; Gromkova, R. A., *Russian Journal of General Chemistry* **2004**, 74 (7), 1043-1045.
22. G. Voronkov, M.; N. Deryagina, E., *Russian Chemical Reviews* **2000**, 69 (1), 81-94.
23. Stenberg, V. I.; Hei, R. D., *The Journal of Organic Chemistry* **1985**, 50 (11), 1810-1815.

## **Chapter 6. Conclusions and Future Directions**

### **6.1 Conclusions**

The majority of this work describes new methods of constructing thin composite films consisting of a redox polymer and an oxidoreductase on the surface of an electrode for usage in biosensors and biofuel cells. The conducting thin films used were a series of redox polymers based on ferrocene-modified linear poly(ethylenimine) (LPEI). The electrochemical and enzymatic responses of the fabricated films were characterized using cyclic voltammetry and constant potential amperometry.

Allyl- and ferrocenylpropyl-modified LPEI (Fc-C<sub>3</sub>-LPAEI) was developed as a redox active, negative photoresist capable of being used in a glucose biosensor. The response of the biosensor and the efficiency of the glucose oxidase (GOX) were found to be dependent on the duration of irradiation and the type of crosslinking agent. The electrochemical response of Fc-C<sub>3</sub>-LPAEI continually increased with prolonged irradiation due to enhanced electronic connectivity resulting from increased crosslinking. The enzymatic response of the biosensor increased with irradiation up to a point before decreasing with extended irradiation due to denaturation of GOX. Fc-C<sub>3</sub>-LPAEI films were fabricated using both radical and nitrene crosslinkers. Fc-C<sub>3</sub>-LPAEI/GOX bioanodes were capable of generating  $44.9 \pm 1.3 \mu\text{Acm}^{-2}$  after five hours irradiation and crosslinking using a photogenerated dinitrene from 1,2-bis(2-azidoethoxy)ethane (TEG-N<sub>3</sub>).

Layer-by-layer (LBL) deposition of polyelectrolytes was shown to be an effective means to fabricate conducting, ultra-thin films. Varying the tether length by which ferrocene is attached to the LPEI backbone allowed for a means of probing the way

materials deposit onto an electrode's surface. Fabrication wash time between layers of material was also investigated and shown to effect the build-up of material at the electrode's surface. Ferrocenylhexyl- and ferrocenylpropyl- modified LPEI (Fc-C<sub>6</sub>-LPEI, Fc-C<sub>3</sub>-LPEI) were used with periodate modified glucose oxidase (p-GOX) in the LBL assembly of enzymatic bioanodes. (Fc-C<sub>6</sub>-LPEI/p-GOX)<sub>16</sub> and (Fc-C<sub>3</sub>-LPEI/p-GOX)<sub>16</sub> films were capable of generating up to  $222 \pm 19$  and  $980 \pm 51 \mu\text{Acm}^{-2}$ , respectively, in response to glucose. (Fc-C<sub>3</sub>-LPEI/p-GOX)<sub>8</sub> films generated  $86 \pm 3 \mu\text{Wcm}^{-2}$  at pH 7.0 and  $149 \pm 7 \mu\text{Wcm}^{-2}$  at pH 5.0 when poised against an air-breathing platinum cathode in a compartmentless biofuel cell. The deposition of material was found to be "patchy" at earlier numbers of bilayers, and then the material would fill in the gaps and form a more coherent film. This was seen by monitoring the peak separation in the cyclic voltammogram with regards to the number of bilayers of material. Electrochemical characterization of the films was shown to be an effective means to characterize the buildup of conducting thin films. The films fabricated on planar gold electrodes were capable of generating as much current as chemically crosslinked films, all while using about a tenth of the material. When films were constructed on a bed of entangled carbon nanotubes, the response to glucose was drastically increased. This made for some of the highest current density films in the literature.

LBL assembly was also used to fabricate biocathode films using (chloroferrocenyl)propyl-modified LPEI (FcCl-C<sub>3</sub>-LPEI) and the enzyme laccase. Optimization of concentration and pH of the polymer and enzyme solutions were done to determine the ideal conditions for film construction. LBL assembled biocathode films were different than bioanode films in that the redox potential was dependent on the



number of bilayers, and film growth was exponential rather than linear. It is therefore thought that FcCl-C<sub>3</sub>-LPEI/laccase films are much thinner and more compact than Fc-C<sub>3</sub>-LPEI/p-GOX films. This was also shown to be true by the rather low performance of the materials. (FcCl-C<sub>3</sub>-LPEI/laccase)<sub>16</sub> films were capable of generating  $5.75 \pm 0.17 \mu\text{Acm}^{-2}$  in response to oxygen, which is much lower than chemically crosslinked films. Fabrication of FcCl-C<sub>3</sub>-LPEI/laccase films on nitric acid oxidized carbon paper was found to improve the performance of the biocathodes. Nitric acid oxidized carbon paper was found to have a higher electrochemically active surface area when compared to the geometric surface area. Interestingly, the electrochemical response of the films reached a maximum at eight bilayers before decreasing with the addition of more bilayers. This is likely due to highly compact films that are restricting the movement of chloroferrocene in the hydrogel. However, the enzymatic response of the films increased up to twelve bilayers before a slight decrease at sixteen bilayers. This is likely due to oxygen being catalytically reduced at the outer surface of the films, and the larger surface area allows for a greater amount to be catalyzed at larger numbers of bilayers. At sixteen bilayers, it appears there is a tradeoff between increased oxygen reduction and restricted electron flow through the films. (FcCl-C<sub>3</sub>-LPEI/laccase)<sub>12</sub> films fabricated on nitric oxidized carbon paper were capable of producing  $32.2 \pm 3.2 \mu\text{Acm}^{-2}$  in response to oxygen, a 460% increase from films constructed on planar gold electrodes.

The final portion of this work involved inverse vulcanization of elemental sulfur using paracyclophane (PCP) and dichloroparacyclophane (PCPCl<sub>2</sub>). Differential scanning calorimetry (DSC) was used to monitor the small scale reaction of the starting materials. The ratio of starting materials was varied in an attempt to optimize reaction conditions.

Distinct copolymers were not isolated from the reactions due to expulsion of hydrogen sulfide gas and the likely crosslinking of the repeat units. In the case of PCPCl<sub>2</sub>, spectroscopic characterization revealed the reaction product to be mainly ring opened PCPCl<sub>2</sub> and possible some short chain oligomers, as evidenced by the presences of aryl methyl groups. However, the insoluble, crosslinked S-PCP network was found to be highly thermally resistant, and may find usage in heat resistant coatings or as a component in lithium-sulfur batteries.

## 6.2 Future Directions

The largest issue that still needs to be addressed in future photocrosslinkable biosensors based on LPEI is the irradiation time. Shortening the irradiation time needed for forming well-connected films will decrease the probability of photochemically damaging the enzyme, and increase the response of the biosensor. One possibility would be to match the light source wavelength to that of the photochemically active species used in the crosslinking reaction. The use of a light source with a discrete wavelength, i.e. a laser, or the use of filters would allow for a narrower irradiation window which might minimize extraneous, unwanted film damage.

The alkyl diazide TEG-N<sub>3</sub> yielded the best results of the crosslinking agents tested, but it would be logical to explore the use of aryl diazides to minimize the possibility of rearrangement of the photogenerated nitrene. It might also be interesting to use bis- $\alpha$ -diazoketones to generate ketenes for possible nucleophilic attack by the amine backbone of LPEI, or diazo compounds for cyclopropanation of the allyl groups in LPAEI.

There is also further work that needs to be done on the LBL assembled bioanodes with regards to the initial investigations using single walled nanotube-modified glassy carbon electrodes (SWNT-GCE). While the preliminary proof-of-concept tests were conducted with only one bilayer of polymer and p-GOX, the current densities in response to glucose for the fabricated films were some of the highest reported using ferrocene-modified LPEI. Higher numbers of bilayers should be tested to explore if additional material will improve in a similar fashion as films constructed on planar gold electrodes, or if the first bilayer has a high loading on the nanotubes followed by nominal increases with more bilayers. It will also be important to determine the electrochemically active surface area of the SWNT-GCEs to get more accurate current densities for the biosensors.

It would also be appropriate to use SWNT-GCEs as a platform for LBL assembled biocathodes. Since laccase can undergo direct electron transfer using SWNTs as a transducer, it would be interesting to assemble electrodes using both FcCl-C<sub>3</sub>-LPEI and unsubstituted LPEI to see if the presence of ferrocene is required.

There are many further explorations into the inverse vulcanization of sulfur using PCP derivatives that need to be performed. The usage of alkyl substituted PCP to lower the reaction temperature is one such possibility to optimize the reaction conditions, or to use blends of PCP and PCPCl<sub>2</sub> to yield composite materials with properties of both systems. Perhaps more important than complete reaction optimization is the usage of the fabricated materials in lithium-sulfur batteries. While the ring opening copolymerization of sulfur and PCP is a novel concept, the real world application of the synthesized compounds remains to be seen.

## Chapter 7. Appendices

### 7.1 NMR Data

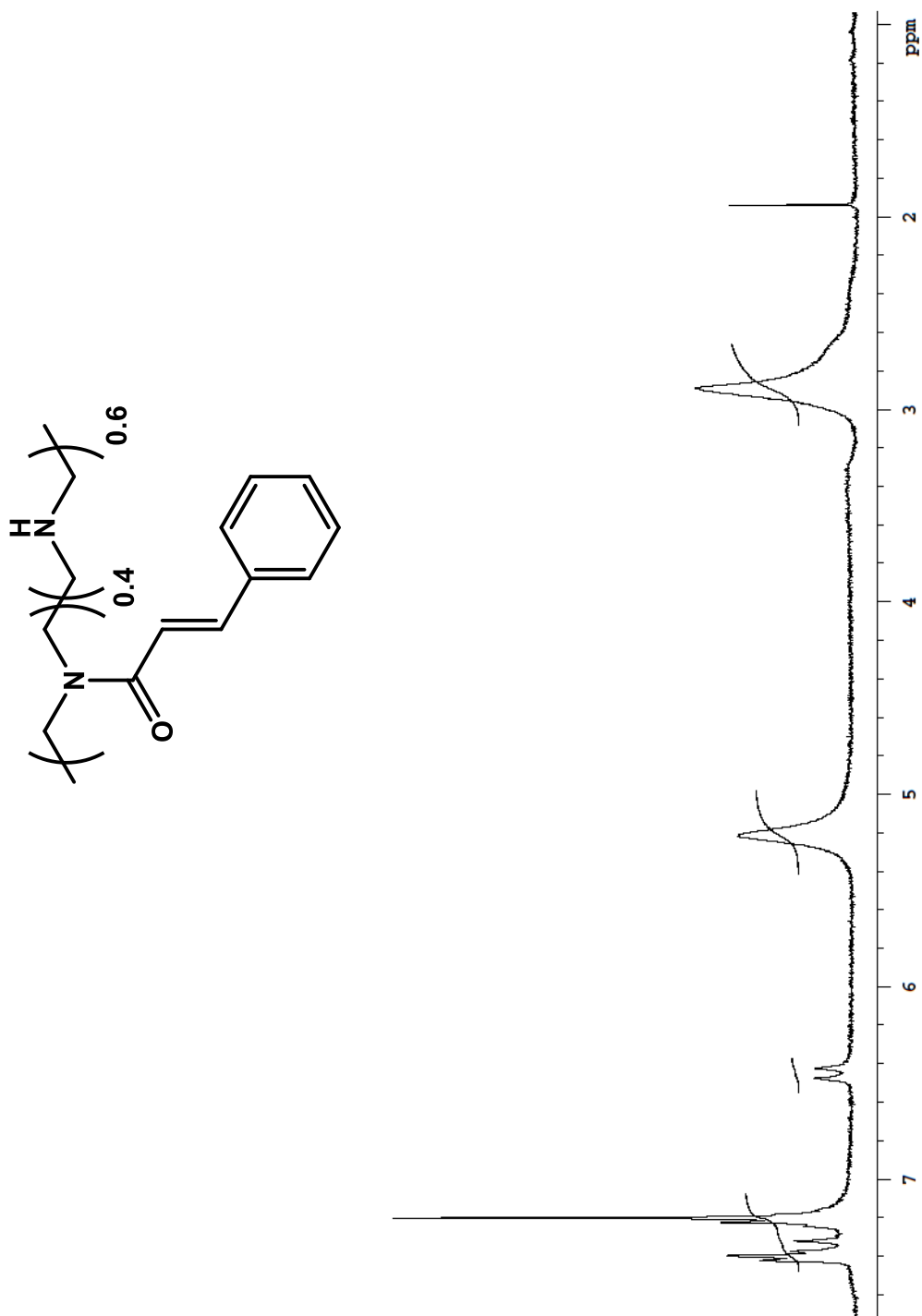


Figure 7.1.1: LPCEI

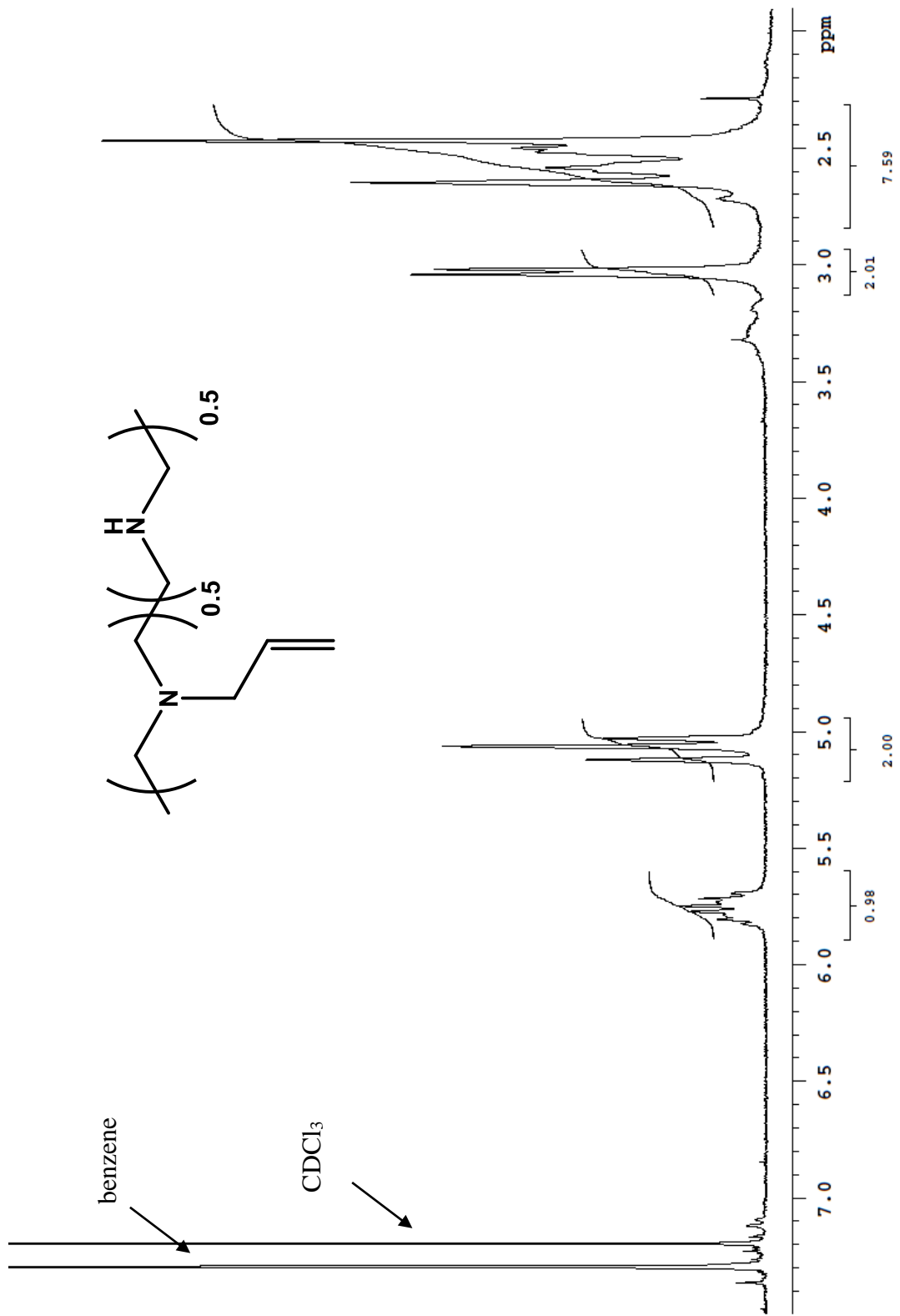
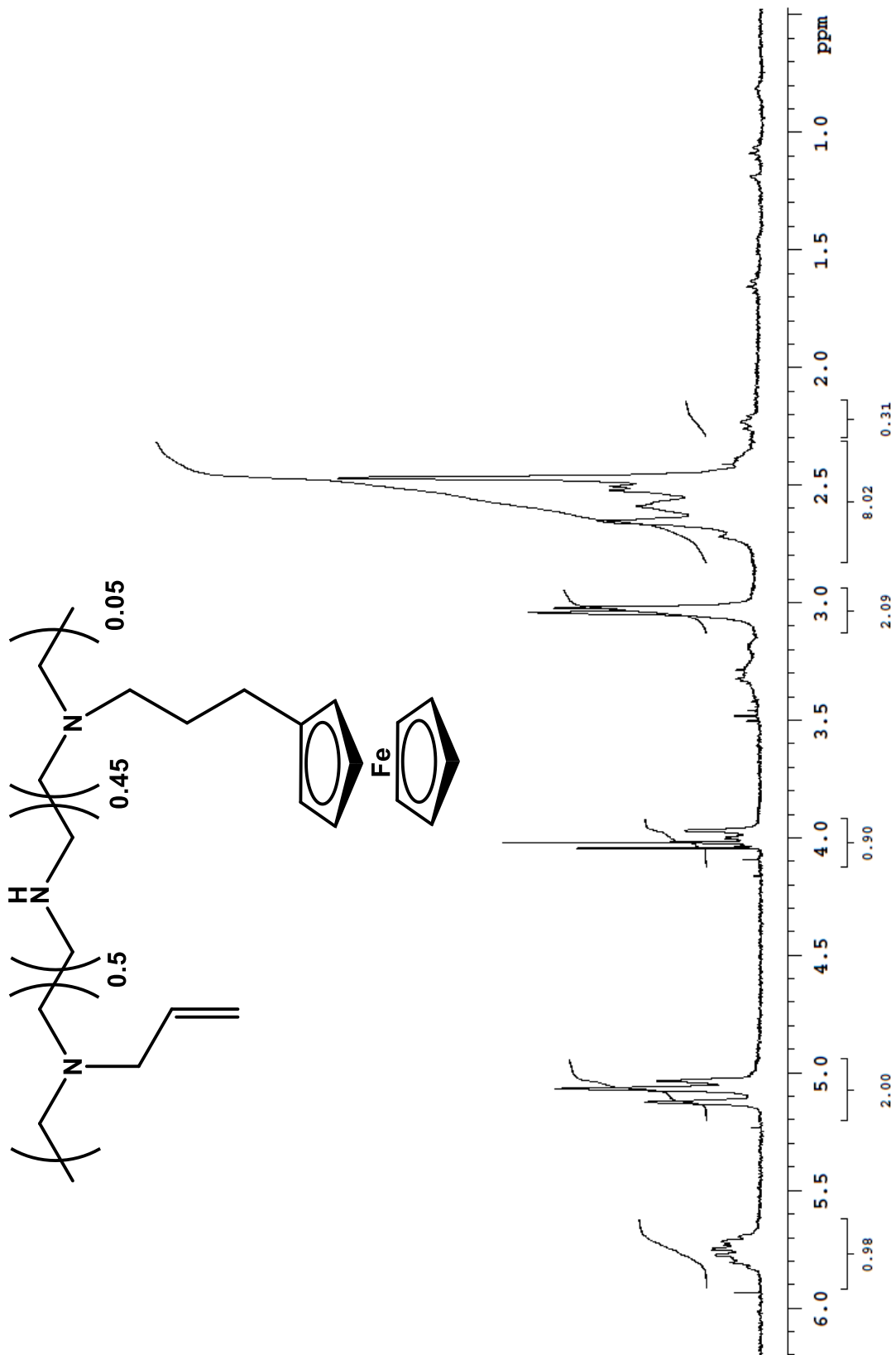
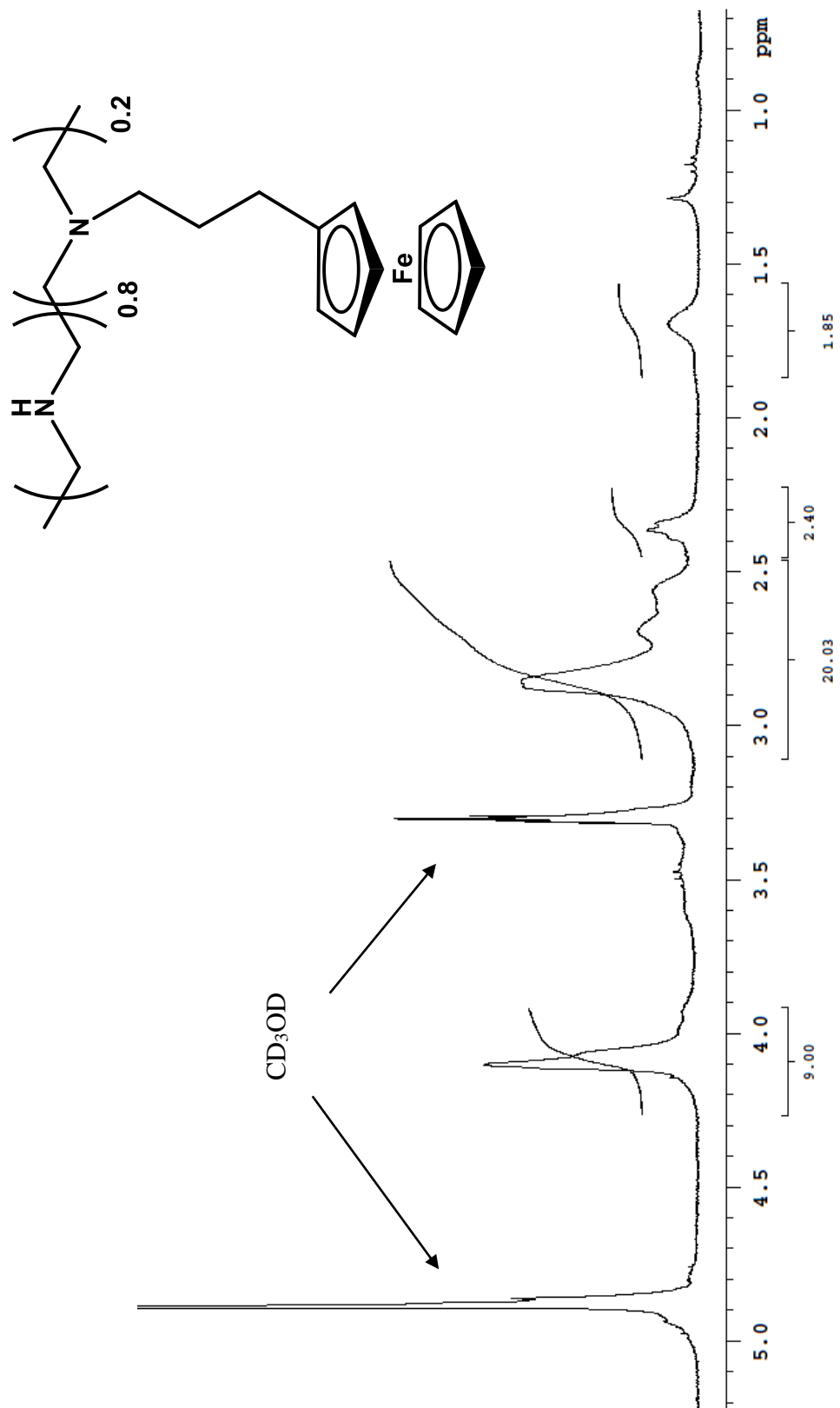


Figure 7.1.2: LPAEI



**Figure 7.1.3:** Fc-C<sub>3</sub>-LPAEI



**Figure 7.1.4:** Fc-C<sub>3</sub>-LPEI

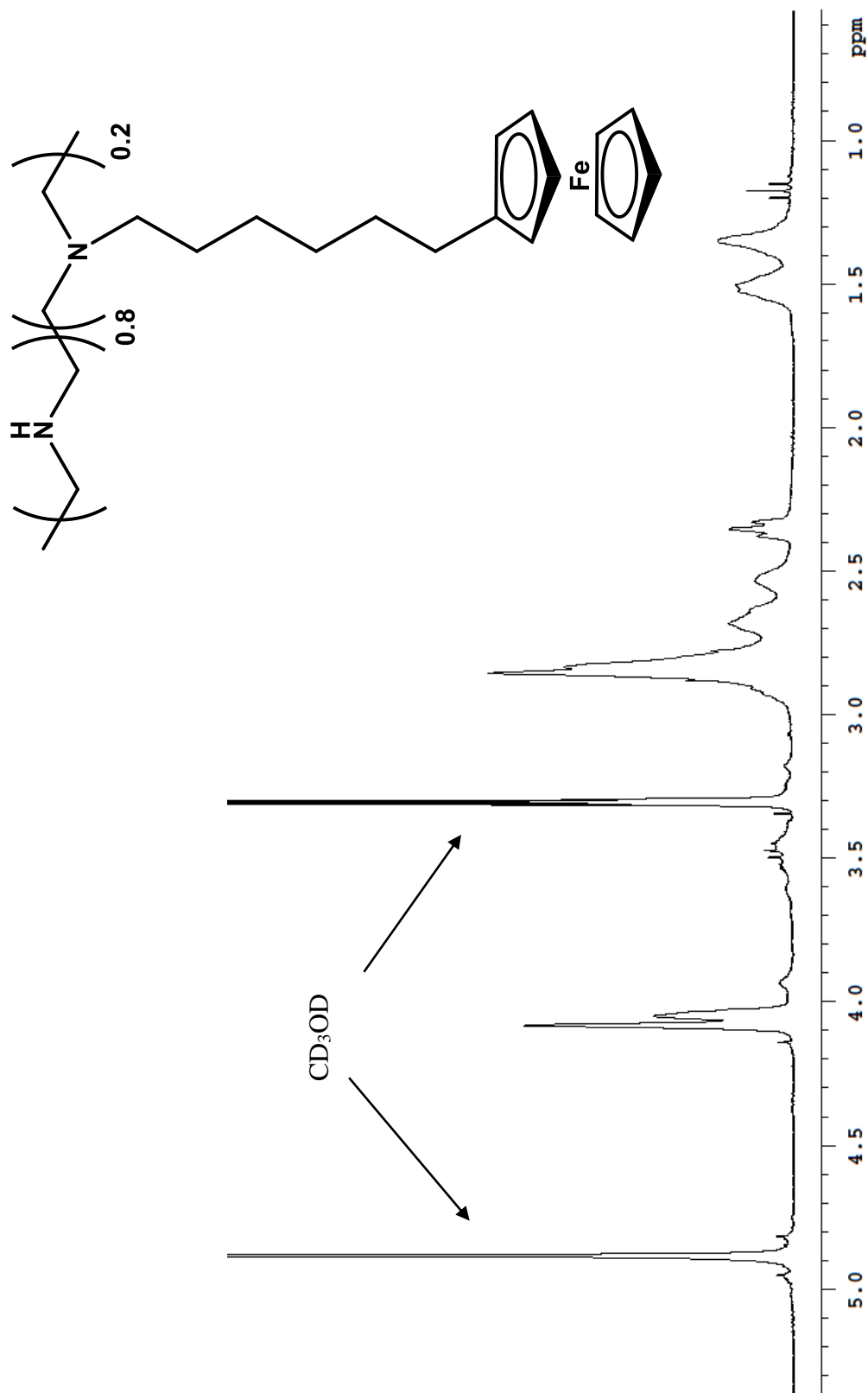


**Figure 7.1.5:** Fc-C<sub>6</sub>-LPEI



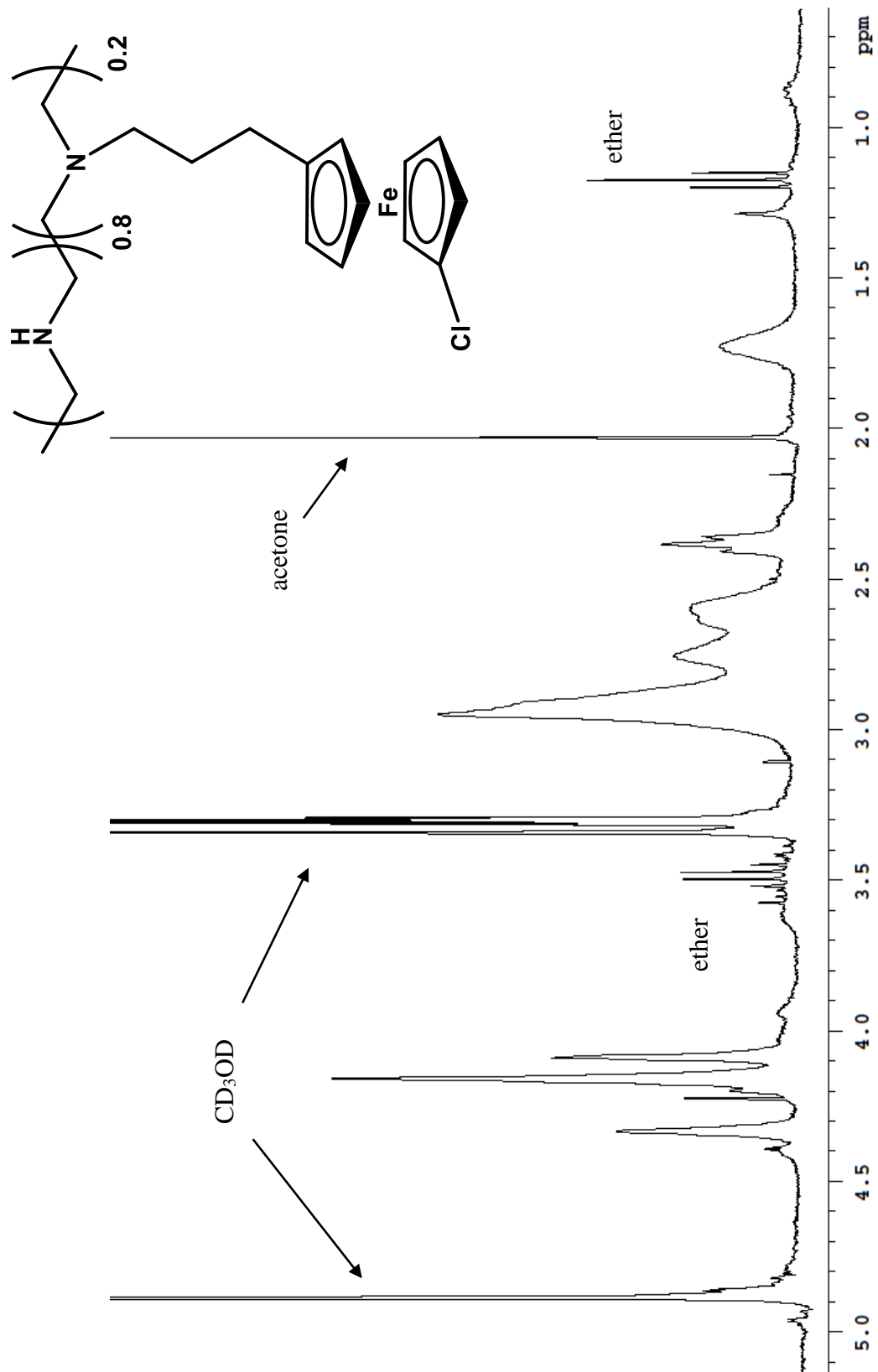


**Figure 7.1.6:** FcCl-C<sub>3</sub>-LPEI

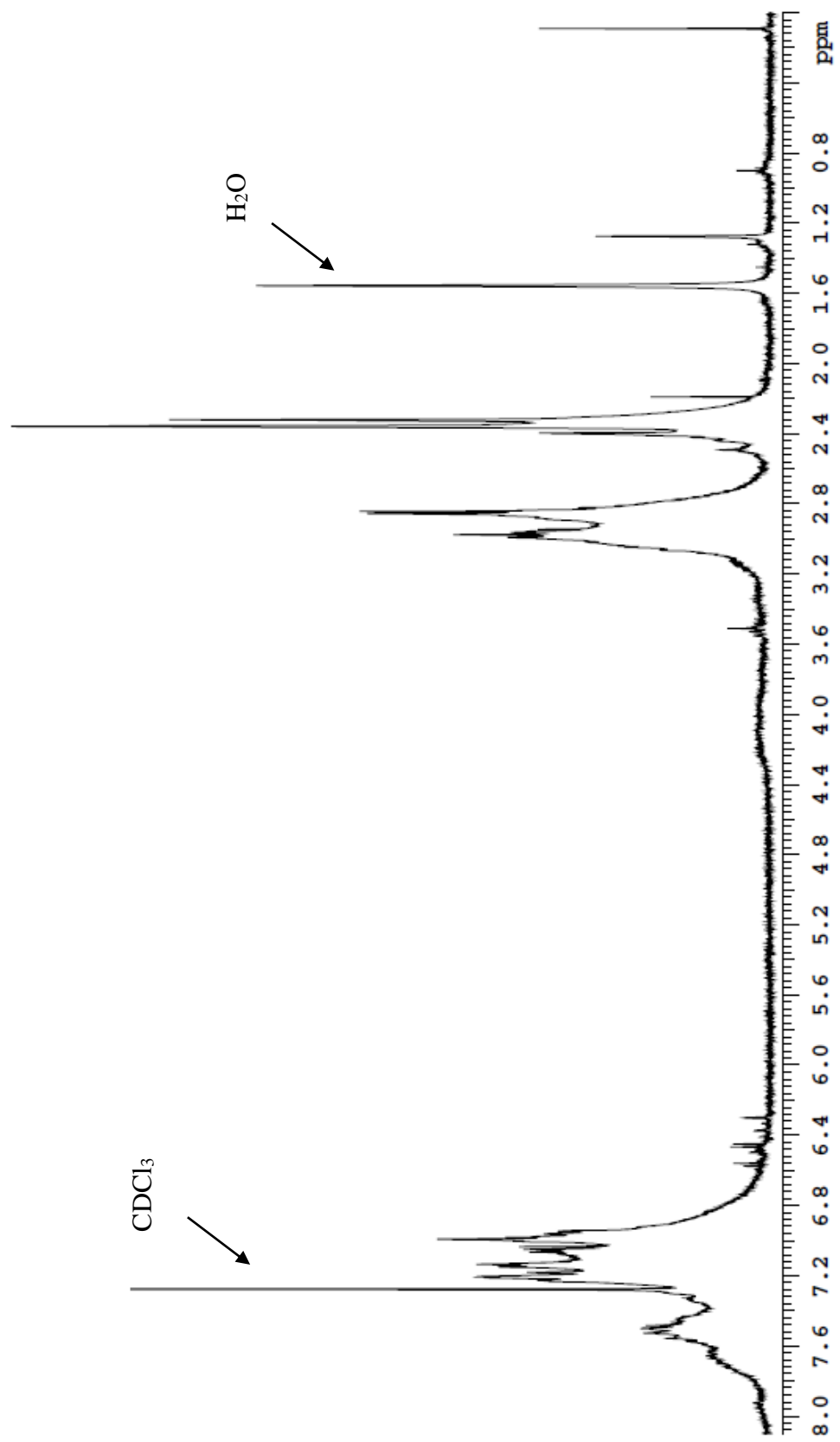


**Figure 7.1.7:** S-PCPCl<sub>2</sub>-50 after two hours heating at 300 °C

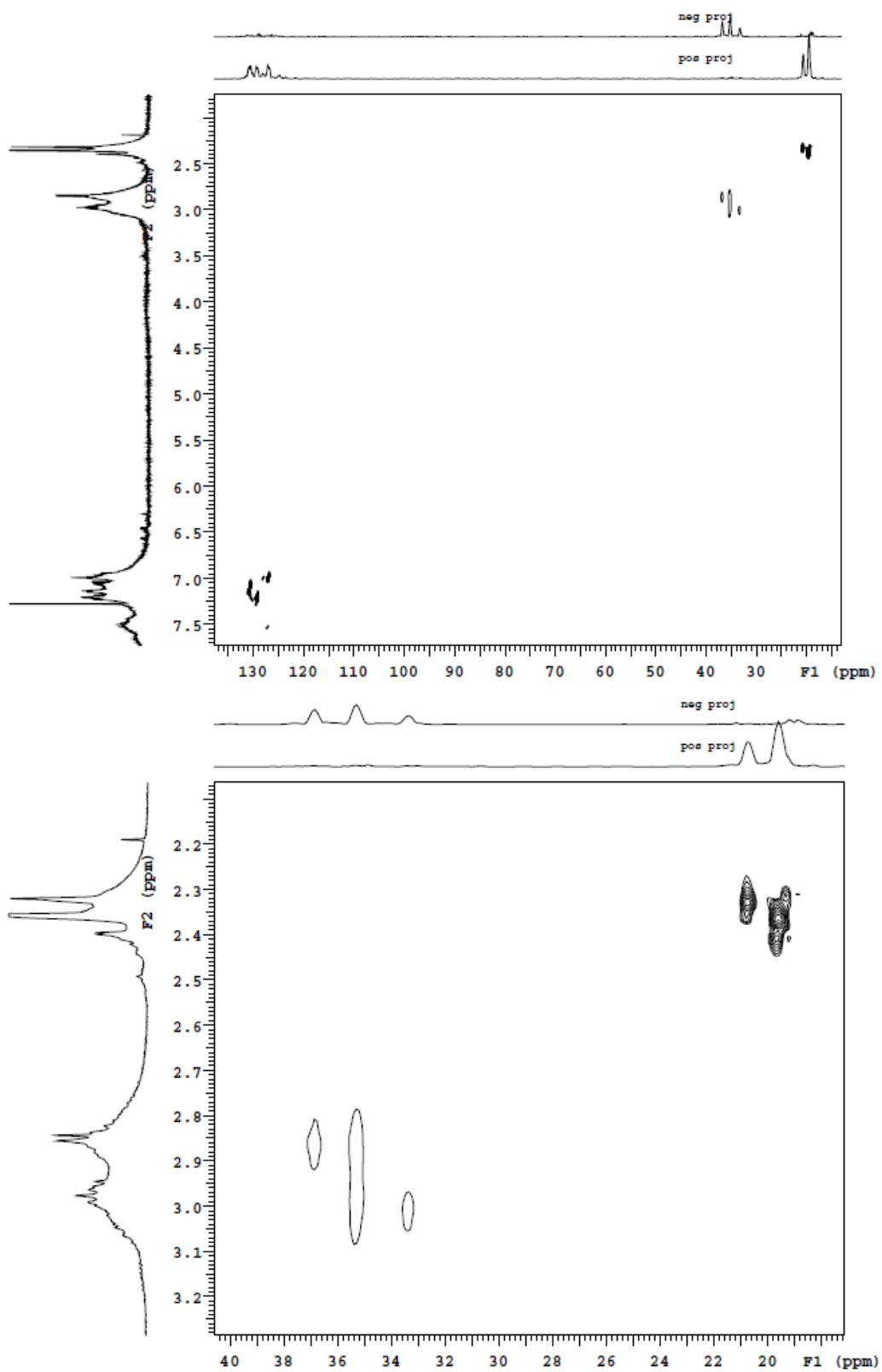


**Figure 7.1.8:** HSQC S-PCPCl<sub>2</sub>-50 after two hours heating at 300 °C

## 7.2 DSC Thermograms

